

UNIVERSITY OF OKLAHOMA

GRADUATE COLLEGE

STUDY OF LITHIUM TRIFLATE AS AN ELECTROLYTE IN MIXED ETHER-
AMINE SOLVENTS

AND

THE USE OF ELECTRON PARAMAGNETIC RESONANCE SPECTROSCOPY TO
STUDY DIELECTRIC PROPERTIES OF MATERIALS

A DISSERTATION

SUBMITTED TO THE GRADUATE FACULTY

in partial fulfillment of the requirements for the

Degree of

DOCTOR OF PHILOSOPHY

By

RAHUL SURYAKANT KADAM

Norman, Oklahoma

2011

STUDY OF LITHIUM TRIFLATE AS AN ELECTROLYTE IN MIXED ETHER-
AMINE SOLVENTS
AND
THE USE OF ELECTRON PARAMAGNETIC RESONANCE SPECTROSCOPY TO
STUDY DIELECTRIC PROPERTIES OF MATERIALS

A DISSERTATION APPROVED FOR THE
DEPARTMENT OF CHEMISTRY AND BIOCHEMISTRY

BY

Dr. Daniel T. Glatzhofer

Dr Kenneth M. Nicholas

Dr Roger Frech

Dr Charles Rice

Dr Brian Grady

© Copyright by RAHUL SURYAKANT KADAM 2011
All Rights Reserved

Acknowledgements

My journey through my PhD has been a long journey and experience and I am thankful to many people. I want to take this opportunity to thank Dr Glatzhofer, my advisor, for being the most amazing mentor and boss ever!!! I really appreciate the patience Dr Glatzhofer had with me through all these years of my learning. I still remember the Spring of 2005, when I entered Dr Glatzhofer's Lab. Being in a new country and a new academic setting left me confused and lost, but Dr Glatzhofer put me at ease and gave me time to get accustomed to the new setting. Over these years I have come a long way professionally and personally.

I would also like to thank my committee members, Dr Nicholas, Dr Frech, Dr Rice and Dr Grady for their valuable inputs and suggestions throughout my career as a PhD student at OU. I would also like to thank my colleagues in the lab, Dr Frank Yepez, Dr Matt Meredith, Farid Ismail, Sachin Chavhan, David Hickey for being good colleagues and making a enjoyable lab experience. I would also like to express my appreciation to Dr Matt Petrowsky and Dr Rachel Mason from Dr Frech's lab for helping me out with their expertise on my different projects.

I would also like to extend special thanks to Dr Susan Nimmo, the NMR lab manager, without whom my NMR project would not have been possible. Last but not the least; I am greatly indebted to my parents who made all the sacrifices in their life to be able to send me to United States to pursue my further education. Without my parents support I would not be where I stand today. Also I would like to thank my all my

friends back in India and some very special friends I made after coming to United States whose support helped me achieve my goal of pursuing a PhD.

Table of content

<i>Chapter1: Introduction</i>	1
1.1) Introduction to Batteries	1
1.2) History of Batteries	4
1.3) Battery Statistics and Future	13
1.4) How Batteries work?	17
1.5) Polymer Electrolytes	22
1.6) Poly(ethylenimine) as a polymer electrolyte matrix	30
1.7) PEO/PEI hybrids	33
1.8) Nitrogen versus oxygen in polymer electrolytes	34
1.9) Project Goals	39
<i>Chapter 2: Investigation of N vs O Heteroatom Coordination in Lithium Electrolytes</i>	
<i>Systems Using NMR and EPR as Tools</i>	46
2.1) Introduction to NMR	46
2.2) Shielding and deshielding effects	51
2.3) Chemical Shifts for NMR	51
2.4) NMR in investigation of lithium ion electrolytes	52
2.5) Lithium NMR: An overview	57
2.6) Fluorine NMR: An Overview	58
2.7) Determination of Relative ^7Li and ^{19}F NMR Shifts	59

2.8)	TEA (Triethylamine) versus DEE (Diethyl ether	63
2.9)	AC Conductivities	66
2.10)	TMEDA versus Monoglyme	77
2.11)	PFG measurements for Lithium Triflate in TMEDA and Monoglyme	85
2.12)	Master Plots for ^7Li , ^{19}F and Specific Conductivity	94
2.13)	Conclusion and Future studies	102
2.14)	Experimental	104
<i>Chapter 3: Electron Paramagnetic Resonance: A tool for studying dielectric properties of solutions</i>		108
3.1)	Introduction to Dielectric Constant	108
3.2)	Electron Paramagnetic Resonance: Theory and Concepts	115
3.3)	Relation between Electron Paramagnetic Resonance and Dielectric Constant	123
3.4)	Construction of Coaxial Assembly for Electron Paramagnetic Resonance	128
3.5)	EPR as a tool to investigate dielectric constants of unknown liquid samples	132

3.6)	EPR as as tool to investigate dielectric constant of unknown mixture of solvent samples	144
3.7)	Measurement of Errors	152
3.8)	Conclusion	156
3.9)	Experimental	157
<i>Chapter 4: Practical applications of the coaxial EPR assemblies to study dielectric properties of liquid media</i>		161
4.1)	Application to measuring % water in water/dioxane mixtures	161
4.2)	Application in studying the dielectric properties of electrolyte solutions	167
4.3)	Application in monitoring phase transitions	173
4.4)	Application to study relative kinetics for the triethylamine-allylchloride reaction	177
4.5)	Application in studying the dielectric properties of surfactant solutions	181
4.6)	Conclusions	195
4.7)	Experimental	195

<i>Chapter 5: Investigation and modification of Linear and Branched poly(ethylenimine) as Solid Polymer Electrolyte</i>	199
5.1) Introduction	199
5.2) Branched poly(ethylenimine) and Branched poly(allylethylneimine)	199
5.3) Linear poly(ethylenimine) and Linear poly(allylethylenimine)	203
5.4) Linear poly(allyl-glyme _x)ethylenimine (LPAG _x EI)	209
5.5) LPG _x EI Model Compounds	220
5.6) Branched poly(allylethylenimine) as Proton Exchange Membrane	224
5.7) Conclusion	226
5.8) Experimental	228
<i>Chapter 6: Conclusion and Future work</i>	232

Abstract

^7Li and ^{19}F Nuclear Magnetic Resonance Spectroscopy (NMR) was used to investigate of the nature of lithium triflate dissolved in mixtures of ether and amine solvents. The transport of ions in the liquid and polymer electrolytes is influenced by the presence of the heteroatoms in the polymer or the liquid. There has been considerable research reported in the literature as far as the oxygen- and nitrogen-based liquid electrolytes and solid polymer electrolytes are concerned. It is also reported in the literature that polymer electrolytes based on hybrid systems (oxygen and nitrogen heteroatoms) such as the MEEP (poly[bis(methoxyethoxyethoxy)phosphazene]) have exhibited some of the best room temperature conductivities. Another ether-amine hybrid polymer, poly(N-(2-(2-methoxyethoxy)ethyl)ethyleneimine) (LPEI-G2) was reported in the literature to show high conductivities with added lithium triflate. Analysis of the LPEI-G2 polymer electrolyte showed evidence of lithium cation coordination to oxygen but no evidence of nitrogen coordination. To study this type of mixed ether-amine system further, model compounds and their mixtures with dissolved lithium triflate were studied using ^7Li and ^{19}F NMR as an investigative probe. Conductivities, changes in dielectric constant, and self-diffusion coefficients data were measured. The ^7Li , ^{19}F , conductivity, and self-diffusion data suggest that lithium triflate does not exist as a dissociated species and mostly forms clusters or aggregates. A model is presented which reconciles the different possible species clusters/aggregates with the ^7Li , ^{19}F , conductivity, diffusion coefficient, and dielectric constant data. Application of the Nernst-Einstein equation to the self diffusion data suggests 99.99% ionic association in an amine solvent (N,N,N',N'-tetramethylethylenediamine) as compared to an ether

solvent (monoglyme) which showed 99.97% ionic association. The conductivity data supports the ionic association data derived from Nernst-Einstein equation. In amine solvents the conductivity is relatively low ($\sim 10^{-6}$ S/cm) and increases monotonically to ($\sim 10^{-4}$ S/cm) on the addition of ether solvents. Changes in the dielectric constant for samples with different fractions of nitrogen and oxygen heteroatoms suggest that the dielectric constant of the medium which dissolves the lithium triflate plays a role in the different species formed by the lithium triflate but that specific interactions of the salt with the solvent play a significant, possibly determinate role. The amine content forces formation of more or bigger clusters/aggregates that leads to lower conductivities. A chelation versus coordination effect was seen for molecules consisting of two nitrogens or oxygens compared to one nitrogen or oxygen, respectively.

In the course of this work a method to use Electron Paramagnetic Resonance (EPR) to study of dielectric properties of liquids was developed. The signal response of an EPR active species is attenuated by the medium it is in. Keeping all other parameters the same, the higher the dielectric constant of the medium, the lower the EPR signals response. This behavior is problematic in studying EPR active species in high dielectric media but can be capitalized upon to determine the dielectric constant or to monitor changes in the dielectric constant of the medium. Using a coaxial EPR cell design, the EPR signal of a stable nitroxyl radical compound (2,2,6,6-Tetramethyl-piperidin-1-oxyl radical) in a low dielectric constant solvent in the inner tube is attenuated by the solvent present between the inner and outer tubes (jacket medium). The attenuation increases monotonically with an increase in the dielectric constant of the jacket medium. Calibration curves can be constructed using jacket media of known dielectric constants

ranging from 2 to 80 and the dielectric constant of a sample used as the jacket medium can be determined by interpolation. The application of this technique to determine the dielectric constants and/or composition of mixed solvents, to monitoring the rate of a reaction, and to the study of surfactant solutions is presented.

Finally, the synthesis and modification of poly(ethyleneimine) (PEI) polymers such as branched PEI (BPEI) and linear PEI (LPEI). The modification of BPEI was done by substituting allyl groups on the nitrogens as cross-linking sites. The allyl groups were cross-linked under UV light in the absence of initiators to eliminate any interference caused by the initiators in the ionic transport phenomena. The highest ionic conductivity of the crosslinked BPAEI/lithium triflate without any initiator was measured to be 1.12×10^{-7} S/cm and was compared to the cross-linked BPAEI/lithium triflate in the presence of initiator. No significant improvement in the conductivity of the BPAEI/lithium triflate cross-linked without any initiator compared suggested that the initiators did not have a strong influence on ionic transport in the BPAEI/lithium triflate electrolyte system. Linear poly(ethyleneimine) was partially substituted with different lengths (G_x where $x = 1,2,3$) of PEO-like tethers and partially substituted with allyl groups (LPAG_xEI), cross-linked in the presence of lithium triflate as a salt, and the conductivity of the resulting cross-linked polymers was investigated. The highest conductivity for LPAG₁EI was measured to be 2.7×10^{-7} S/cm. The highest conductivity for LPAG₂EI was measured to be 4.4×10^{-6} S/cm. Comparison of the LPAG₁EI and LPAG₂EI electrolytes shows that increasing in the oxygen content in the polymers does improve the conductivity. Model compounds for LPEI- G_x polymers were synthesized and characterized using NMR.

Chapter 1

1.1 Introduction to Batteries

“Electricity” is the one of the major utilities which benefits mankind in enormous ways. Thermal, hydro and nuclear are some of the important ways to generate electricity. Another way of generating electricity is electrochemically¹. Electricity can be produced electrochemically by the conversion of chemical energy into electrical energy and the reverse process is referred to as recharging. These processes are generally carried out using electrochemical cells known as batteries^{2,3,4}. The global battery market is more than 50 billion dollars, out of which roughly 5.5 billion dollars is allocated to rechargeable (secondary) batteries⁵. The growth of the battery industry is estimated to be 6% annually. In the future it is predicted that countries like China, India, Brazil and South Korea will record some of the highest market gains as far as the battery market is concerned.

With the supply of the fossil fuels running out, making breakthrough research in the development of renewable energy sources (solar, wind, etc.) has become one of the important agenda items for research scientists. Since the last decade, tremendous effort has been made to develop efficient methods to convert renewable energy to electricity for use in applications which are dependent on fossil fuels now. Renewable energy could be a solution to the threatening problems of:

1. Securing energy and resources,
2. Steady economic growth, and

3. Preservation of the natural environment.

Although renewable energy is long lasting, it is also unstable. For example, the sun does not shine all the time and the wind blows hard sometimes or not at all^{6,10}. Therefore storage of energy is necessary so that it can be used when required. Batteries are one way to store renewable energy, making use of these resources practical.

A battery is an electrochemical cell that consists of an electrolyte which separates two electrodes, the anode and the cathode^{7,8}. All the three components, the electrolyte, the cathode and the anode have been the subject of a tremendous amount of research over the past 30 years. In an attempt to make batteries more reliable and durable, the battery electrolyte is one of the most studied and researched components of a battery. A “*battery electrolyte*” is the medium in the battery through which the flow of electric current takes place by ion migration. Battery electrolytes can be classified in different categories known as liquid, gel and solid polymer electrolytes^{8,9}. Commercially available batteries mostly use liquid electrolytes. These liquid electrolytes are commonly solutions of acids, bases, or salts. The disadvantages of liquid electrolytes include leakage of the electrolyte, low energy density, and low physical durability and reliability. Solid polymer electrolytes could be a solution to these liquid electrolyte problems as will be discussed later in this chapter. However, in all kinds of electrolytes (liquid, gel or solid polymer electrolytes) one factor remains common, ion transport in the electrolyte medium⁹.

For a battery the effectiveness depends on its conductivity, which in turn depends on effective ion transport in the battery electrolyte. Ion transport depends on a

lot of factors. The most important factor is the medium (electrolyte) through which the ions are transported. Regardless of nature of electrolytes (solid or liquid), heteroatoms play an important role in ion transport mechanism since heteroatoms such as nitrogen and oxygen have the capability to coordinate to metal cations. To study the effect of the heteroatoms, it would be easier to study liquid model compounds, rather than the corresponding solid polymer electrolyte, eliminating morphological issues caused by the bulky, long polymer chains.

The research presented in this thesis involves a detailed study of ^7Li and ^{19}F NMR spectroscopy of lithium triflate in liquid electrolyte media with mixtures of two different heteroatom (nitrogen and oxygen) solvents that represent solid polymers with nitrogen and oxygen heteroatoms. Changes in the chemical shift of ^7Li and ^{19}F NMR for different mixtures of nitrogen and oxygen containing solvents will be investigated. The effects on the conductivity of the different electrolyte mixtures with different ratios of nitrogen and oxygen containing solvents will also be investigated.

The change in the dielectric constant of the electrolyte mixtures with different ratios of nitrogen and oxygen containing solvents will also be investigated using EPR (Electron Paramagnetic Resonance) spectroscopy. The application of this EPR technique to measure dielectric constant of solvents, mixtures of solvents, and study different dielectric constant-related properties is also discussed in this dissertation. The observations made in the liquid model compounds will be useful of application in developing new solid polymer electrolytes involving nitrogen and oxygen in the same polymer.

In this chapter, a brief history of batteries and statistics involving battery use will be followed by an introduction to liquid, as well as polymer, electrolytes. The role of solvent heteroatoms in ion transport in electrolytes and a detailed account of the competition for coordination between nitrogen and oxygen will be discussed.

1.2 History of Batteries

The first use of batteries dates to almost 2000 years ago¹¹. In 1936 archaeologists discovered a set of terracotta jars with an iron rod in it. It is speculated that these were ancient galvanic cells. It is also believed that common food acids like vinegar were used as electrolytes in these cells.

The first recorded reports of the invention of a battery date back to the 1700's. In the year 1749 Benjamin Franklin was the first person to use the term "battery"¹². He referred to a set of capacitors he linked to perform an experiment with electricity as a battery. The capacitors were panels of glass coated with metals on both the surfaces. The capacitors were charged using a generator and discharged by contacting it with a metal electrode.

In 1800 Volta invented the first true battery (*Figure 1.1*)^{12,13,20}. The cell was known as a Voltaic pile. A Voltaic pile consisted of copper and zinc disc plates stacked on top of each other. Each pair of copper and zinc plates was separated by cloth soaked in a brine solution which acted as the electrolyte. This battery produced a continuous and stable current. Volta experimented with a lot of metals as electrodes and found out that zinc and silver worked the best. Although these batteries gave stable and continuous currents, they had some disadvantages such as leakage of electrolyte, short

circuit due to compression between the two electrodes, and bubbles of flammable hydrogen from the electrolyte being electrolyzed on the copper, which also increased the internal resistance of the battery.

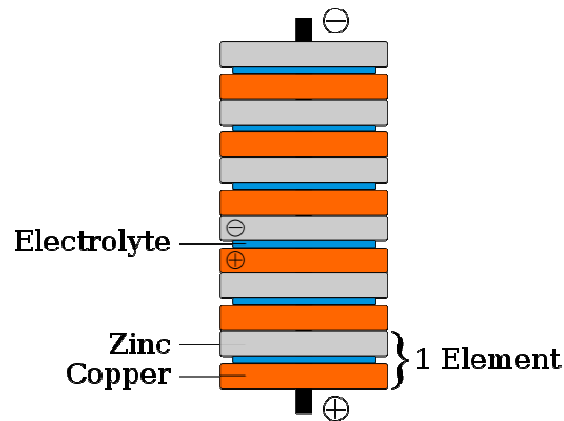


Figure 1.1 Representation of Voltaic Cell (Figure reproduced from http://en.wikipedia.org/wiki/History_of_the_battery)

The Voltaic pile, though with some disadvantages, was the first ever “wet battery” invented. This battery is the reference for all batteries made since then. Due to his important contribution to mankind, the term “Volt” that represents the potential needed to drive 1 ampere of current through a resistive load of 1 ohm is named after him. After the invention of Voltaic pile, a lot of effort was put into research to overcome the problems faced by these batteries. William Cruickshank overcame the problems of electrolyte leakage and short circuit faced by the voltaic pile^{14,20}. He put the copper and zinc plates horizontally rather than stacking them one over the other. This was known as a “trough battery” (*Figure 1.2*).

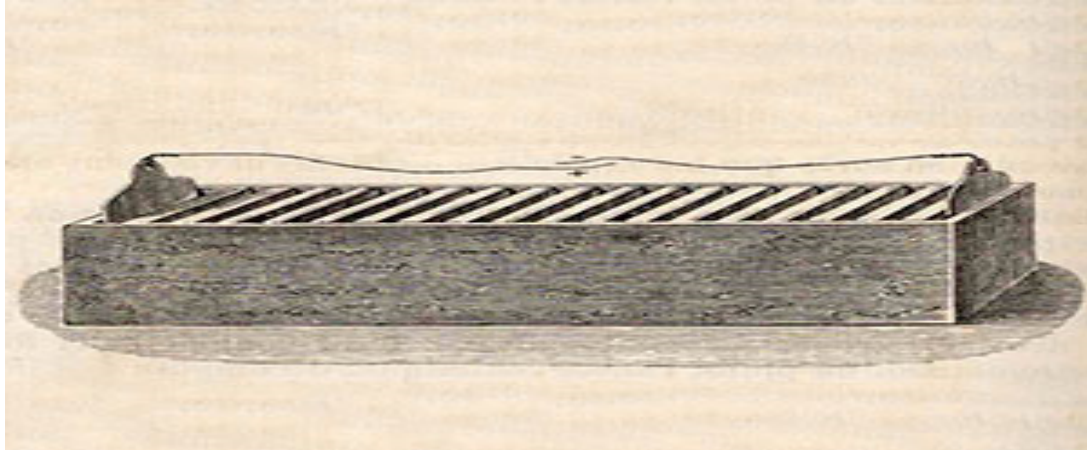


Figure 1.2 Representation of Trough Battery (Figure reproduced from http://en.wikipedia.org/wiki/History_of_the_battery)

In 1836, a British chemist named John Fredric Daniell came up with a battery which eliminated the problem of hydrogen bubble formation in Voltaic pile batteries^{15,20,47} (Figure 1.3).

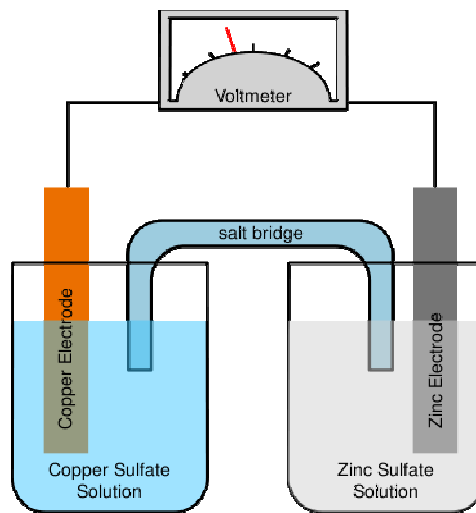


Figure 1.3 Modern representation of Daniell Cell. (Figure reproduced from http://en.wikipedia.org/wiki/Daniell_cell)

The battery consisted of a copper pot with copper sulfate solution. Another earthen pot was immersed in the copper sulfate solution with zinc sulfate and a zinc electrode in it. The earthen pot is porous enough for the ions to pass through but the two solutions do not get mixed. Shown above is a modern version of Daniell Cell which is used in laboratories to display Daniell cells. The Daniell cell puts out a voltage of approximately 1.1 Volts.

William Robert Grove invented the Grove cell in the year 1844.^{16,20} In this cell the anode was a zinc electrode dipped in sulfuric acid and a platinum cathode dipped in nitric acid. The cathode and the anode were separated by porous earthenware. It was advancement over the Daniell cell in that it gave high currents and nearly two times the voltage of the Daniell cell. This cell was a favorite at the time for the American telegraph services. However, this cell had some disadvantages like evolution of toxic nitric oxide gas. Another disadvantage was that platinum was expensive.

Until the year 1859, all the batteries discussed were permanently dead after the chemical reaction was spent.²⁰ A major breakthrough came in the year 1859 when Gaston Plante invented the first rechargeable batteries.



Figure 1.4 Lead-Acid Cell (Figure reproduced from http://en.wikipedia.org/wiki/History_of_the_battery)

The first rechargeable battery was the lead-acid cell. It was the first battery that could be recharged by passing a reverse current through the cell. The lead acid cell consisted of a lead anode and a lead oxide cathode separated by rubber sheets. The cathode and anode were dipped in sulfuric acid. The Plante's lead acid battery was a pretty large and bulky battery. Nonetheless, the lead acid battery is still being used today in the automotive industry and is used most of the time in places where the weight or size of the battery does not matter^{17,20}.

In 1866 Georges LeClanche (*Figure 1.5*) invented a battery which had a zinc anode and a manganese dioxide/carbon cathode which was wrapped in the porous membrane. The electrolyte solution used in the cell was ammonium chloride. It provided voltage up to 1.6 volts. It became a huge success in powering telephones before telephones would power themselves from the telephone line. One disadvantage

was short lifetime, so that long conversations could not be had on the telephone using this battery.^{18,16,20}

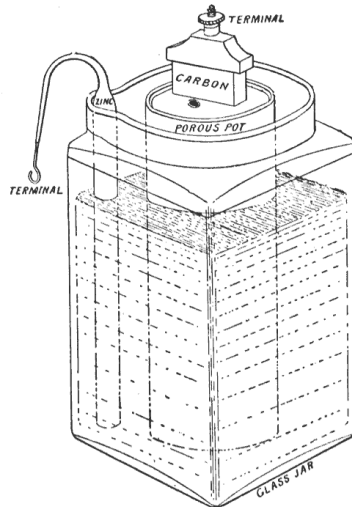


Figure 1.5 LeClanche Cell (Figure reproduced from

http://en.wikipedia.org/wiki/History_of_the_battery)

The year 1887 was very important as far as historic events go in battery research.^{19,20} It was the year the first “dry” battery was introduced. Carl Gassner modified the LeClanche cell to have an electrolyte that was a solid rather than a liquid. The electrolyte consisted of an ammonium chloride - plaster of paris mixture to make it into a paste. Manganese dioxide, which acts as a cathode, was put in this paste and packed in zinc containers that operated as the anode. This battery used a “dry” electrolyte, thus avoiding leakage problems, and could be used in any orientation. It provided a voltage of 1.5 volts. A modified version of Gassner cell where the plaster of paris was replaced with cardboard was first mass-produced in 1897. The cell was called a “Columbia dry cell” and was marketed by the National Carbon Company. The modification allowed more room for the cathode and was easy to build. This battery

was used in portable devices. The modification of the Columbia cell that uses a zinc container as an anode and a carbon rod as a cathode is called the Zinc-Carbon Battery.^{20,48} The cathode in the Zinc-Carbon Battery is dipped in a mixture of manganese dioxide and carbon powder. Zinc chloride and ammonium chloride is used as electrolyte in the Zinc-Carbon battery. Zinc-Carbon batteries were widely used primary batteries and are still popular today.

In the year 1899, the first rechargeable alkaline battery was introduced. It was called the Nickel-Cadmium battery²⁰. It had nickel and cadmium as electrodes and a potassium hydroxide electrolyte. It was the first time in battery history an alkaline electrolyte was used. These batteries were commercialized in United States in 1946. These batteries were robust and could be used to replace Lead-acid batteries.

Up until 1955 Zinc-Carbon batteries were the popular primary batteries. At that time an engineer at Eveready (now Energizer), Lewis Urry, was given the task to improve the life of zinc-carbon batteries^{20,49}. He thought that developing a new battery would be more cost efficient than improving older ones. That's when he invented an alkaline battery. These batteries used a manganese dioxide cathode and a zinc powder anode with an alkaline electrolyte. His alkaline battery had several times durability and longer life than the Zinc-Carbon battery. The batteries were mass produced in the year 1959 and have been popular since.

During the span 1970-1980 a lot of research was done on nickel chemistry and the application of nickel in batteries^{20,21,22}. During this period new battery chemistries evolved using Ni-Cd (Nickel-cadmium) and NiM-H (Nickel-metal hydride). Since

cadmium is harmful to the environment, Ni-Cd batteries have their limitations. These batteries were used for energy storage in commercial communication satellites.

The next generation of batteries was that of lithium batteries. Pioneering work was done by G. N. Lewis in 1912. But it was not until the 1970's that the first non-rechargeable lithium battery was introduced. Lithium batteries are non-rechargeable batteries which involve lithium metal or lithium compounds as the anode. Lithium metal is the lightest metal and therefore has a large energy density by weight. Lithium batteries are therefore extremely light and are of great demand in electronic and defense applications²⁰. Lithium batteries have replaced primary alkaline batteries in many applications. The first lithium ion battery was marketed by Sony Corporation in the 1980's²⁰. Since the introduction of the lithium ion battery, the market for lithium ion batteries has been growing exponentially as compared to other battery chemistries. Japan is the major producer of lithium ion batteries. In 1991 Sony introduced the first secondary (rechargeable) lithium ion battery⁵⁰. Secondary lithium ion batteries have been used in a lot of applications such as powering cellular phones, electronic cameras, minidisk players, etc. The lithium battery has a cathode, an anode, and a porous, inert polymer separator soaked in a lithium salt liquid electrolyte. The simple sketch of a lithium ion battery is shown in *Figure 1.6*.⁹

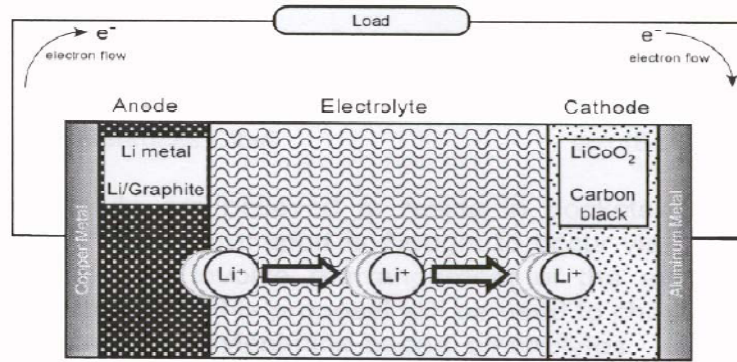
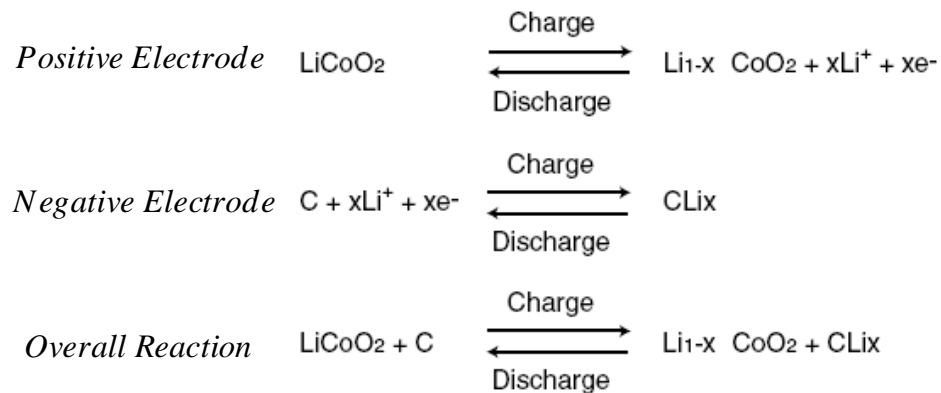


Figure 1.6 (Figure reproduced from Hu, L. PhD Dissertation 2005, University of Oklahoma)

The figure above shows the discharging process in a lithium ion battery. In the secondary lithium ion batteries the reverse process is the charging process. The chemical reactions taking place at the cathode (positive electrode) and anode (negative electrode) are shown in *Equation 1.1*.



Equation 1.1 Overall reaction for Lithium ion battery during charging and discharging. Equation 1.1 is reproduced from Ref. 51.

The electrolyte poses a leakage problem and it is also difficult to make the electrolyte thin enough to provide high energy densities. These problems with lithium

ion batteries could be, in principal, solved by designing “solid state lithium ion batteries”.

Solid state lithium ion batteries have the solid state polymer separator which serves a dual purpose. The separator separates the cathode and anode as well as being a transport medium for the lithium ions. Research on solid polymer electrolytes has now been going on for more than 20 years and there is still a lot to be discovered in this relatively new field of battery electrolytes.

1.3 Battery statistics and future

Devices such as i-pods, calculators, digital cameras, camera phones, and portable computing devices are driving growth and research in the battery field. As seen in *Figure 1.7*, batteries are a part of everyday life²³.

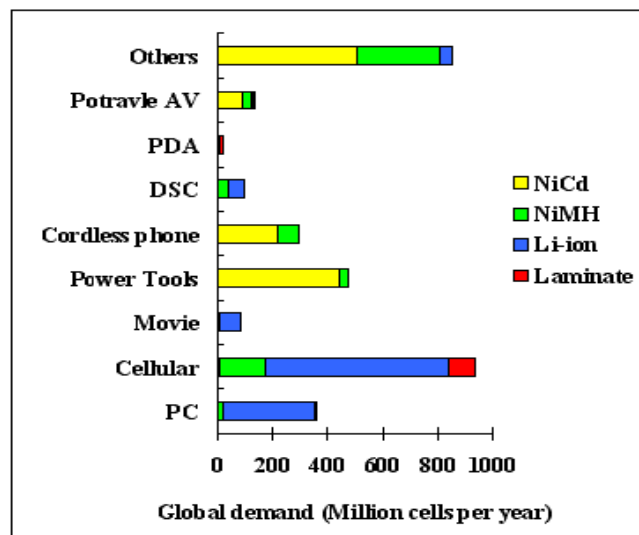


Figure 1.7 (Figure reproduced from <http://batteryuniversity.com/parttwo-55.htm>)

Batteries can be classified as two different types, primary batteries and secondary batteries.⁵ A primary battery is a battery which cannot be recharged when completely discharged; whereas a secondary battery can be recharged.

In 2007 it was estimated that the demand for primary and secondary batteries by the year 2012 would be worth over 15 billion dollars in the United States of America alone (*Figure: 1.8*). Every new incremental improvement in battery performance opens up the possibility of new applications.⁵

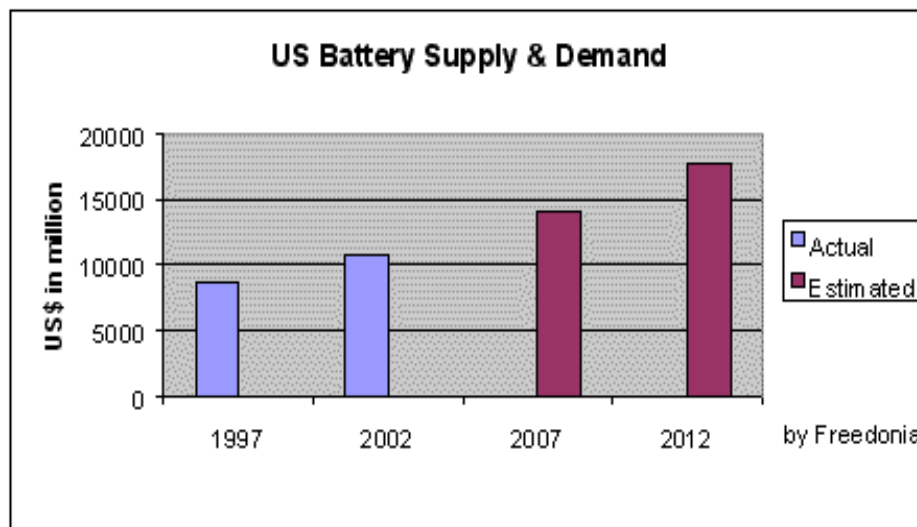


Figure 1.8 (Data reproduced from http://www.li-ion-battery.com/Knowledge/Battery_statistics.htm)

The demand for primary batteries is always higher than for secondary batteries. Primary batteries can have storage lives over 10 years. Primary batteries also have higher energy densities than secondary batteries. Among primary batteries, alkaline batteries are in higher demand than any other primary battery. Some of the other

primary batteries used are lithium and zinc. *Figure 1.9* gives a good statistical projection of future demand.

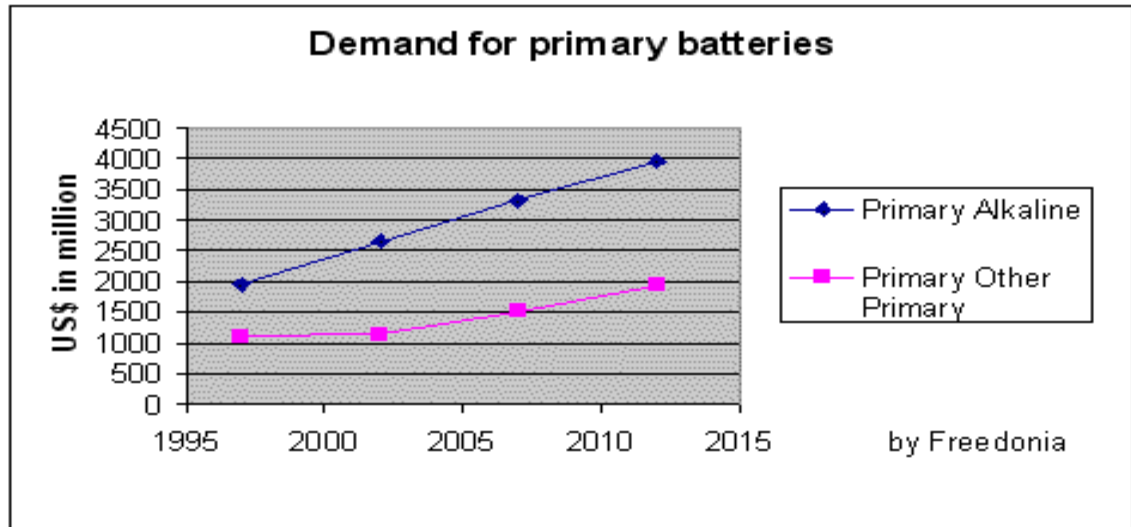


Figure 1.9 (Data reproduced from http://www.li-ion-battery.com/Knowledge/Battery_statistics.htm)

As seen in *Figure 1.9*, the demand for primary alkaline batteries is worth 4000 million dollars, whereas the demand for any other primary battery is almost 50 % less. Alkaline batteries will continue to dominate the primary battery business⁵.

Among the secondary (rechargeable) batteries, lead acid batteries have and will continue to dominate the secondary battery business (*Figure 1.10*). However, lithium rechargeable batteries are closing the gap.

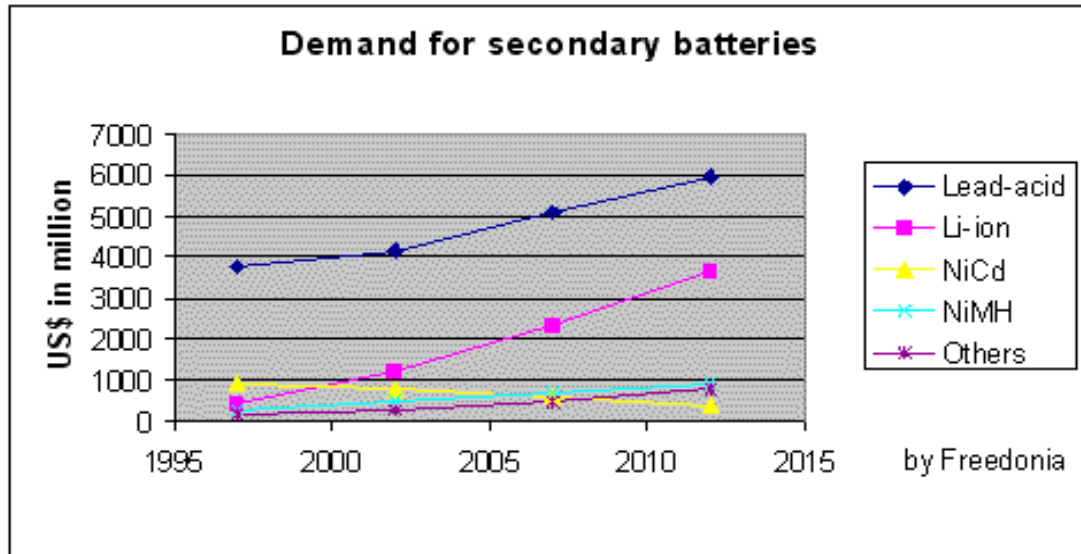


Figure 1.10 (Data reproduced from http://www.li-ion-battery.com/Knowledge/Battery_statistics.htm)

The lead acid battery is generally used for automotive and back-up purposes. The lead acid battery has a low production cost and is greatly dependable in the worst weather conditions. The demand for lead acid batteries depends mainly on the production of vehicles. A tremendous amount of effort in battery research has decreased the rate of battery replacement in automobiles⁵.

Hybrid vehicles currently require a high voltage of more than 200 volts to function⁵². This voltage is achieved using nickel-metal hydride (Ni-H) cells connected in series. Manufacturers generally give 8-10 year warranties with these batteries because if these batteries fail they are very expensive to be replaced.

Among secondary batteries, lithium ion batteries show the best scope of applications after the lead acid batteries. By the year 2012, it is predicted that the demand for lithium ion batteries will be worth 4 billion dollars and the demand will keep on rising in the coming future⁵. Again, the popularity of lithium metal in battery

applications is because of its light weight, great electrochemical potential, and large energy density by weight.

1.4 How Batteries Work

A battery is device that stores chemical energy and converts it into electrical energy. The process can be separated into two parts, electrical and chemical. The electrical process takes place outside the cell whereas the chemical process takes place inside the cell by ionic conduction in an electrolyte, driven by a chemical potential. An elementary battery consists of four different parts: an anode (negative electrode), a cathode (positive electrode), an electrolyte and a load. This basic set up is known as a galvanic cell. (Figure: 1.11)²⁴

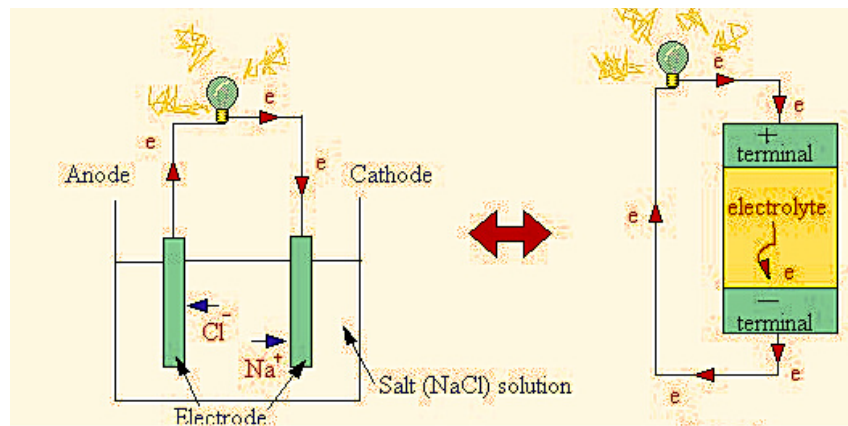


Figure 1.11 (Schematic of a simple battery; Picture reproduced from <http://sciencewithalice.blogspot.com/2009/08/how-battery-works.html>⁵³)

In the cell shown above, when the electrons flow from the anode to the cathode through the load the process is known as discharging. The reverse process, when the electrons flow from cathode to the anode is called recharging and involves storing the chemical

energy. The cell voltage (theoretical), E° , is directly proportional to the free energy change (ΔG°) of the electrochemical reaction taking place in the cell (*Equation 1.2*).

$$\Delta G^\circ = nFE^\circ \quad (\text{Equation 1.2})^{24}$$

In equation 1.2, n = number of electrons flowing through one electrode to the other and F = Faraday's constant.

A battery can be classified by the physical state of electrolyte employed in it. Batteries can be classified as wet (liquid electrolyte) batteries, dry batteries, or solid state polymer batteries.

A good example of a wet (liquid electrolyte) rechargeable battery would be the lead acid cell. The lead acid cell uses sulfuric acid as an electrolyte. Lead metal is used as the anode and lead oxide as the cathode. The half (discharging) reaction is given in *equation 1.3*²⁵



(Equation 1.3)

At the anode, the lead metal reacts with the ionized sulfuric acid to give lead sulfate, protons and two excess electrons. At the cathode, the lead oxide reacts with the ionized sulfuric acid, the protons, and the excess electrons transferred through the load to give lead sulfate and water. While charging, the flow of the electrons is reversed against the electrochemical potential of the reactions. During the charging process, the lead sulfate

is turned back into the lead and lead oxide on the electrodes and the sulfuric acid is restored in the solution. Since sulfuric acid is a dense liquid, the density of the solution increases during charging and decreases during discharging. Thus density or specific gravity can be used to gauge the charging and the discharging process. Lead acid batteries have some disadvantages. Since a lead-acid battery has a liquid electrolyte, it poses the risk of leakage of the caustic electrolyte. The orientation and placement also play an important role in the proper function of this battery. These batteries are therefore used for non-portable applications.

To overcome the problem of leakage of the liquid electrolyte, “dry” electrolyte batteries were introduced. A good example of a dry battery was introduced by Carl Gassner and was an improvement over the LeClanche battery. This cell was known as the Zinc-Carbon battery⁹. The electrolyte, ammonium chloride, was mixed with plaster of paris, making it into a paste that could not leak and could be used in any placement and orientation. The cell uses zinc metal as the anode and manganese dioxide as the cathode. At the anode, the zinc metal is oxidized to give Zn^{2+} . At the cathode, the manganese dioxide, which has an oxidation state of 4+, reduces to an oxidation state of 3+ to give manganese oxide and form hydroxide ions⁹. There are some side reactions involved in this cell. The hydroxide ions react with ammonium chloride to give ammonium hydroxide which dissociates to form ammonia and water. The overall reaction of the cell can be given as follows (equation 1.3). The battery stops functioning when all the manganese dioxide is used up in the reaction.



(Equation 1.4)

Dry batteries usually have a higher density than that of the wet batteries. Due to their high energy density, these batteries are generally small in size and can be used in portable devices such as toys, radios, flashlights, etc. Due to side reactions these batteries show some internal resistance that causes a voltage decrease in the battery over a period of time^{19,24,9}. Although these batteries are an improvement from their predecessors, the use of liquid electrolyte is not totally eliminated and these batteries too, pose a problem of leakage after some time.

Scientists all around the globe are working to develop a battery that will be free of the electrolyte leakage problem. Solid-state batteries could be the solution to most of the disadvantages faced by liquid electrolyte batteries. Since solid-state batteries have solid electrolytes, the electrolyte leakage problem is eliminated. The temperature at which the batteries function can have a wider range with solid-state batteries. In liquid state batteries, the functional temperature range of the battery can be a limitation because the electrolyte may freeze or evaporate at certain temperatures. This is not a problem with solid-state electrolytes. The solid electrolyte takes less space than a liquid electrolyte, thus making it possible to make batteries thinner and more space efficient. High energy density and low internal resistance due to fewer side reactions are some of the specifications of a solid state battery^{24,26}. In order to have a proper functional

battery, the ionic conductivity of the solid state electrolyte should be considerably high but should have no electronic conductivity to have a long shelf life⁹.

Various different chemistries have been applied to make a solid state battery. By the 19th century scientists had realized some solid-state materials have ionic conductivities. With the increasing number of solids which can conduct ionically, these materials started gaining worldwide interest. However, it is in the last 30 years with the discovery of many solid electrolytes with high chemical stability and high ionic conductivity at room temperature that the application of these solid electrolyte materials increased. One example of such solid electrolyte material developed into a commercial product is oxygen ion conducting, stabilized solid zirconium dioxide (ZrO₂). The zirconium dioxide solid electrolyte is applicable in the automotive industry. Sodium- β/β' -alumina has also been used as a solid electrolyte in sodium/sulfur and sodium/nickel chloride batteries also known as the zebra batteries. Other examples of such solids include α -AgI, Ag₄RbI₅ and LiAlCl₄.²⁷

Ionic transport in these solids mainly occurs due to atomic disorder in the crystal lattice of these ions or compounds. Defects in the crystal lattice like vacancies (missing ions) or interstitial ions (additional ions) are responsible for ionic conductivities in the crystalline phase²⁷. Large numbers of these available sites (defects in a crystal), with a low enthalpy for hopping processes for the ions to move from one site to another is responsible for high ionic conductivity in these materials at room temperature and above. In a few cases, solid ionic conductivities are comparable to those of liquid electrolytes as well as electronic conductivities of some of the semiconductors. Although these solid-state materials have shown promising properties they still have

their share of disadvantages. One of the biggest disadvantages faced by these solid state materials is the electrode interfacial resistance during the charging and discharging cycles.

Right now there is great interest in the application of solid electrolytes in secondary lithium ion batteries. Lithium is the lightest metal known. Lithium metal also has half cell potential of -3 V which is lower than any other metal. Lithium has low density and has high energy density by weight. These advantages shown by the lithium metal and its compounds have already led to commercialized applications such as pacemaker batteries which provide high energy density and reliability²⁷.

1.5 Polymer electrolytes

Another class of electrolytes that is of interest is the polymer electrolytes. Polymers were relative late-comers in the field of solid state ionics. It was in the year 1973 that the potential for use of polymers in solid state batteries was realized. Polyethylene oxide - salt complex systems were the first to be measured for its ionic conductivity by Wright and his co-workers²⁶. The importance of these electrolytes was at first overlooked, but once recognized, a rapid growth in the research and development of other polyether - salt systems took place.

According to “The Handbook of Batteries”, the term “polymer electrolyte” can be classified into several different families of ion conducting materials²⁶:

- 1) A system consisting of metal salts dissolved in a polar, high molecular weight polymer matrix,

- 2) A gel electrolyte formed by dissolving metal salts in a polar solvent and an inactive polymer added to give mechanical strength and stability,
- 3) A plasticized electrolyte involving a polymer electrolyte doped with a small amount of liquid with high dielectric constant to improve conductivity.
- 4) An ionic rubber that consists of mixtures of low temperature molten salts with high molecular weight polymers. These systems were first discovered in 1993 and are still in the early stages of development, and
- 5) A polyelectrolyte with inert backbone like “Nafion”. They are doped with plasticizers like water to improve the conductivity. These kinds of electrolytes are known for their proton conduction and used in solid-state polymer electrolyte fuel cells²⁶.

This research thesis is mainly concerned with systems where a lithium salt is dissolved in a highly polar, high molecular weight polymer matrix. Lithium salts are mainly employed in polymer electrolytes for the reasons mentioned earlier. Polymer electrolyte lithium batteries were first introduced in North America and Europe in 1980. Due to uneven plating (dendrite formation) on recharging, and safety issues associated with the use of lithium metal anodes, there has been a strong barrier to commercialization of secondary lithium batteries with liquid electrolytes²⁸. However, under optimum conditions one could eliminate the problem of dendrite formation on the anode has led to a new excitement among researchers.

The polymer being employed in a polymer electrolyte must have a certain properties. Firstly, the polymer should have coordinating groups because the solvation enthalpy for the salt depends on the coordination strength between the coordinating groups and the cation of the salt. For example, poly(ethylene oxide) (PEO, $[-\text{CH}_2-\text{CH}_2-\text{O}]_n$) is a polymer which contains “oxygen” heteroatoms as coordinating groups²⁶. The polymer should have facile segmental motion, which is possible if the energy of rotation around the bonds is low. The spacing between the coordinating groups should also be optimum for solvation. PEO provides the optimal spacing compared to other polyethers such as $[-\text{CH}_2-\text{O}]_n$ and $[-\text{CH}_2-\text{CH}_2-\text{CH}_2-\text{O}]_n$. Last, but not least, the polymer employed for polymer electrolyte should be thermally, mechanically, chemically and electrochemically stable²⁶.

Polyether-based, solvent free systems with lithium salts are the most studied polymer electrolytes for secondary lithium batteries. They are simple to make and they have unique mechanical as well as physical properties. The mechanism by which the ionic conductivity occurs in these materials is reasonably well understood. It is believed that the lithium cation is supported by the multiple coordination sites in the polymer, such as the heteroatoms, forming transient bonds to the cation²⁶. Thus, the lithium ion resides in a pocket coordinated to various coordination sites (*Figure 1.12*). Ion transport happens by ion jumps from one pocket to another pocket involving transient bond breaking and transient forming process. It could be viewed that the cation “hops” from one site to another²⁹.

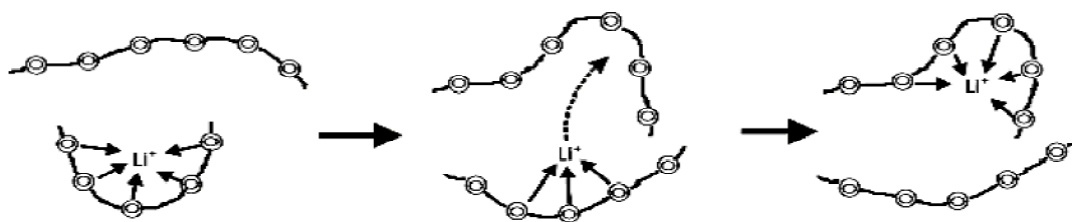


Figure 1.12 Lithium ion jumps from one site to another. (Figure reproduced from Lieyu Hu's Thesis)⁹

Entropy and enthalpy are both important factors as far as dissolution of the salt in the polymer is concerned. Generally, the dissolution of salts has negative entropy in polymer electrolytes. The negative entropy for dissolution can be attributed to the low dielectric constant of the polymer matrix. The low dielectric constant causes less dissociation of the salts and affects ionic conductivity. For better ionic conductivity, ionic dissociation is necessary for which the free energy of dissolution should be negative. When dissolved, ion pairs of the lithium salt need to dissociate and solvate with the solvent molecules to give the “hopping” transport of the lithium cations described earlier. Ion pairs of the salt will not yield ionic conductivity if not dissociated^{30,26}.

As mentioned earlier, the “hopping” mechanism of the lithium cation from one pocket of the polymer to another leads to ionic conductivity, which in turn is measured as electrical current produced by the transportation of ions. Ionic conductivity is the measure of transport of the ions through the polymer. Ionic conductivity can be quantitatively stated by the Kohlrausch summation (Equation 1.4)³¹.

$$\sigma_{(T,P)} = n e \mu \quad (\text{Equation 1.5})$$

In the Kohlrausch equation the ionic conductivity (σ) is a function of temperature and pressure and is directly related to:

- 1) The number of each charge carrying species (n),
- 2) The charge that each species actually carries (e), and
- 3) The mobility of the charge carriers (μ).

For example, when dissolved in a polymer (solvent), lithium triflate could completely dissociate as “free” lithium cation (Li^+) and “free” triflate anion (CF_3SO_3^-). The application of the Kohlrausch equation³¹ would be easy to apply to this specific sample since the exact number of charge carrying species (lithium cation and triflate anion) is known. Ionic conductivity can be easily calculated if the actual charge and mobility of these charge carrying species is known. However, it is well known that lithium triflate, when dissolved in the polymer (solvent), does not simply dissociate into lithium cation and triflate anion. There are other species formed when lithium triflate is dissolved in the polymer (solvent) as shown in *Figure 1.13*.³²

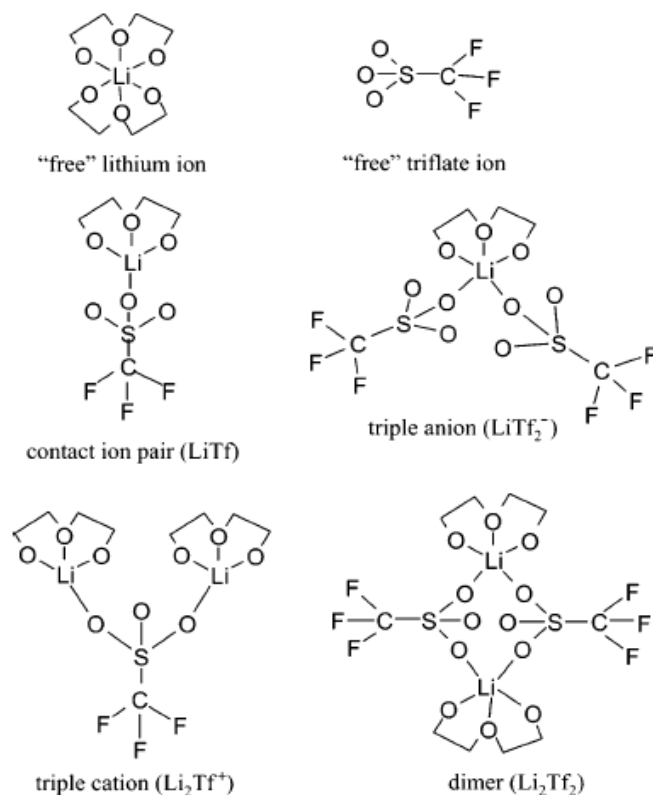


Figure 1.13 Different speciations of lithium triflate with PEO polymer³²

As seen from Figure 1.13, there are at least four other recognized species when lithium triflate is dissolved in the polymer. These species are bigger than the “free” lithium cation and “free” triflate anion species. Theoretically, any charged species should be able to carry charge in a polymer electrolyte. Generally the smaller the charge carrier, the greater its mobility in the polymer electrolyte, resulting in greater ionic conductivity. Application of the Kohlrausch equation becomes more complicated since the number of charge carrying species cannot be exactly determined and the mobility of each species will be different.

Along with the speciation of the lithium salt, self-diffusion of the ions through the polymer plays an important role as far as the ion mobility is concerned in polymer

electrolytes. Self-diffusion coefficients are the measure of the diffusion of the ions through the polymer or solvent matrix without the application of any electric field on the system. On the other hand, ionic mobility is the measure of mobility of the ions through the polymer matrix or solvent under the influence of a field. The diffusion can be related to the polymer matrix by the following equation (*Equation 1.6*)⁹

$$\boxed{D \propto 1/M^2} \quad (\text{Equation 1.6})$$

In the above equation, D = diffusion coefficient and M = molecular weight of the polymer.

According to Equation 1.6, the higher the molecular weight of the polymer, the lower the diffusion coefficient. This observation holds only up to a certain molecular weight. Structure and morphology also play an important role in a polymer electrolyte's ionic conductivity. Ion mobility in the polymer electrolyte depends on the crystallinity of the polymer and/or the polymer/salt mixture. An increase in the crystallinity of the polymer increases the ordering of the polymer and restricts the movement (segmental motion) of the polymer around the bonds as mentioned earlier²⁶. Theoretically, an amorphous polymer above its glass transition temperature (T_g) would be perfect to act as a polymer electrolyte because amorphous polymers have a large degree of freedom as far as segmental motion of the polymer is concerned. It is known from the literature that ion transport in a polymer electrolyte occurs through the amorphous phase of the polymer²⁶. Although the amorphous phase of a polymer/salt mixture above T_g gives a perfect morphological condition for ion transport, it does not give the required physical and mechanical stability for a solid polymer electrolyte^{9,26}. So a balance between

crystallinity and disorder in the polymer/salt mixture is must for the balance between ion transport and good mechanical and physical stability.

The glass transition temperature (T_g) of a polymer/salt mixture is another important factor for the ion transport in polymer electrolyte. The glass transition temperature is the temperature above which the polymer becomes rubbery and the onset of polymeric segmental motion improves ion mobility. Therefore the glass transition temperature of the polymer should be below use temperature to achieve good ionic conductivity⁹. Cross-linking increases the glass transition temperature of the polymer, making it rigid (less flexible), but in turn also increases the physical and mechanical stability of the polymer. A lot of effort has been put into finding an optimum balance between polymer T_g and degree of cross-linking to achieve both flexibility and physical and mechanical stability in solid polymer electrolytes^{9,26}.

As mentioned earlier, PEO was the first polymer to be studied as a solid polymer electrolyte matrix. Since then a lot of different polymers and their modifications have been extensively studied for their potential application in solid polymer electrolytes. After the electrolyte properties of PEO with lithium salts were recognized, *Armand et al* applied PEO with lithium salts to make batteries^{33,34}. Although PEO is a good solvent for alkali metal salts due to its solvating properties, its crystallinity is a drawback for electrochemical applications. PEO-lithium triflate systems show low room temperature conductivity ($\sim 10^{-8}$ S/cm). Conductivity on the order of approximately 10^{-4} S/cm is required to make it applicable in practical batteries. The low conductivity restricts the application of PEO/Li salt mixtures as electrolytes at room temperature for battery purposes²⁶.

Concerns about the crystallinity of PEO polymer electrolytes at room temperature and its adverse effects on conductivity eventually led to the synthesis and study of MEEP Poly[bis(methoxyethoxyethoxide)phosphazene] (*Figure 1.14*) as a polymer electrolyte system, which is amorphous at room temperature.³⁵

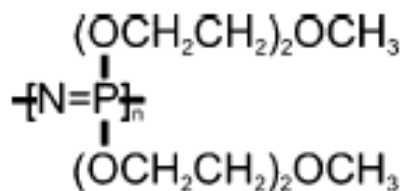


Figure 1.14 Structure of MEEP

MEEP with lithium salts dissolved in it as a polymer electrolyte system was first studied by Shriver and Allcock, *et al.* A MEEP monomer unit consists of a phosphorus-nitrogen backbone with two ethylene oxide side chains that has the sites to coordinate to lithium ions. MEEP polymer electrolyte systems are amorphous over a large range of temperatures (-100 – 100 °C) and has reportedly shown high conductivity ($\sim 2.7 \times 10^{-5}$ S/cm) at room temperature. However MEEP electrolyte systems are glutinous materials with tendencies to flow under mild compression and cannot be cast into free standing films.³⁵

1.6 Poly(ethylenimine) as a polymer electrolyte matrix

Poly(ethylenimine) has been studied for application as a solid polymer electrolyte matrix. Two types of poly(ethylenimine) polymers are known (*Figure 1.15*)^{36,37,9}:

- 1) Linear poly(ethylenimine) (LPEI) and

2) Branched poly(ethylenimine) (BPEI).

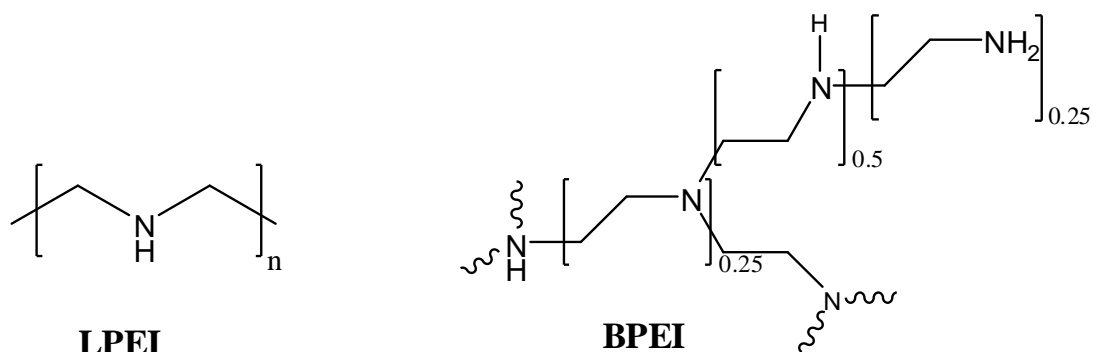


Figure: 1.15 Structure of LPEI and BPEI

PEO as a polymer is difficult to chemically modify but structurally similar LPEI can be easily modified through the amine functional groups. The LPEI repeat unit has secondary nitrogens instead of oxygens in the PEO repeat unit. The secondary nitrogen allows for modifications such as crosslinking or attaching side chains to eliminate the problems seen in PEO as a polymer electrolyte matrix. The synthesis of LPEI was first reported by Saegusa et al³⁸, followed by Tanaka³⁹ using a different synthetic route. In 2001 our group synthesized LPEI via acidic hydrolysis of poly(2-ethyl-2-oxazoline), which is commercially available^{40,37}.

Conductivity studies on LPEI showed that its mixtures with salts have relatively low conductivities ($\sim 10^{-9}$ S/cm@20:1 N:Li ratio - 10^{-7} S/cm@5:1 N:Li ratio)³⁶ at room temperature as compared to MEEP systems which show conductivity on the order of 10^{-5} S/cm³⁵. The relatively low conductivity of the LPEI systems is attributed to its high crystallinity and high degree of hydrogen bonding in the system. One way to reduce or eliminate hydrogen bonding is to N-alkylate the LPEI. The synthesis of linear

poly(methylethyleneimine) (LPMEI) from LPEI is done by Eshweiler-Clark methylation which was first reported by Tanaka, *et al.* The LPMEI-lithium triflate polymer electrolyte system shows better room temperature conductivity ($\sim 1 \times 10^{-5}$ S/cm) than LPEI-lithium triflate polymer electrolyte system at a 20:1 nitrogen:lithium ratio. The LPMEI-lithium triflate system has potential as a polymer electrolyte system, however the physical properties are poor as the system is viscous and cannot form free standing films³⁷.

Branched poly(ethyleneimine) (BPEI) as shown in Figure 1.15 has 1:2:1 ratio of primary, secondary, and tertiary nitrogens, respectively. BPEI can be easily be synthesized by a ring opening polymerization of aziridine. BPEI and its modified versions will be discussed in some of the future chapters in this dissertation. Due to the complicated nature of BPEI with three different kinds of nitrogens, it is complicated to use BPEI for fundamental studies of PEI as a polymer electrolyte. Since LPEI has all secondary nitrogens, it is less complicated to study as a solid polymer electrolyte matrix⁹.

LPEI and BPEI can be modified to make these polymers more effective and useful as solid polymer electrolytes matrices. Cross-linking of LPEI and BPEI makes robust elastomeric films with good physical and mechanical properties. Dr. Lieyu Hu substituted BPEI with allyl groups, which could be easily cross-linked using radical initiators⁹. Though these films were strong and robust, their conductivity was not sufficient. One concern was whether by-products from the radical initiators were interfering with the conductivity. This problem can be dealt with by avoiding radical

initiators in the system and cross-linking the polymer using ultra-violet (UV) light. This study was done in detail and will be discussed later.

1.7 PEO/PEI hybrids

As discussed earlier, LPEI-based polymers did not have high enough conductivities (10^{-9} S/cm) at room temperature. The highest room temperature conductivity for a solid phase polymer electrolyte system was seen in a MEEP-lithium triflate system (2.7×10^{-5} S/cm @24:1 O:Li ratio). The ethylene oxide side-chains are of interest because these side chains mimic the desirable features of PEO. Therefore adding $[-CH_2-CH_2-O-]_x$ side-chains to PEI was a strategy to increase conductivity of the polymer electrolyte.

In 2003 Dr. Albert Snow modified LPEI by reductive alkylation to form linear poly(N-(2-(2-methoxyethoxy)ethyl)ethyleneimine) (LPEI-G2) (*Figure 1.16*). Modification of LPEI backbone using tethered ethoxy ($-CH_2CH_2-O-$) side chains gives the new polymer some PEO-like structure properties^{41,37}.

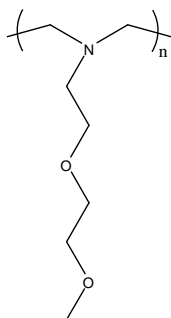


Figure 1.16 Schematic presentation of LPEI-G2.

The LPEI-G2 system with lithium triflate as an electrolyte with a 20:1=O:Li ratio has conductivity of 5×10^{-6} S/cm at 25°C which is lower than, but close to that of MEEP-lithium triflate (2.7×10^{-5} S/cm) at room temperature^{41,37}.

Fourier Transform infrared spectroscopy (FTIR) was used as a tool to analyze the LPEI-G2–lithium triflate system. Lithium triflate was chosen as the salt because the triflate anion shows absorption bands in distinct regions in the IR spectra that are diagnostic of ionic speciation. Two such regions are the CF_3 symmetric deformation ($\sim 760 \text{ cm}^{-1} - 751 \text{ cm}^{-1}$) and SO_3 symmetric stretch ($\sim 1100 \text{ cm}^{-1} - 1000 \text{ cm}^{-1}$). Band assignments can be made for three ionic species, free ion (solvent separated ion), contact ion pair, and aggregate species e.g. $(\text{Li}_2\text{Tf})^+$ which contribute to the conductivity of the polymer electrolyte system.

LPEI-G2 shows the best room temperature ionic conductivity among the PEI based electrolyte systems. Comparison of the LPEI-G2 bands in the region ($1000 \text{ cm}^{-1} - 800 \text{ cm}^{-1}$) to the bands from diglyme-lithium triflate suggested a similarity in the coordination of the lithium to the oxygen of the diglyme (a model compound for PEO polymer) (*Figure 1.17*) and the tethered side chains in LPEI-G2.

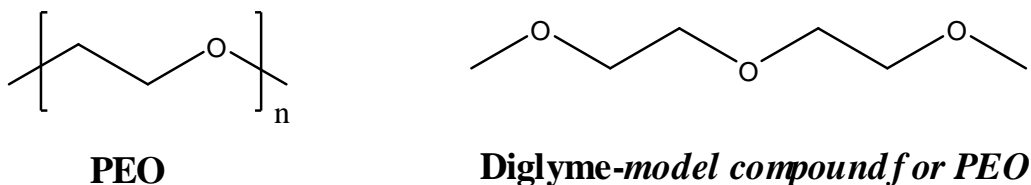


Figure 1.17

Dr. Snow did not report strong and unambiguous spectral proof in the FTIR data for any coordination of the lithium to the backbone “nitrogens”. When compared to MEEP-lithium triflate system, the IR data showed similar interaction of the lithium cation with the tethered PEO like side chains in both the systems (LPEI-G2 and MEEP)^{41,37}.

1.8 Nitrogen versus oxygen in polymer electrolytes (heteroatom’s competition)

As described earlier, although MEEP and LPEI-G2 with lithium triflate show lithium cation coordination to the oxygens in the tethered chain, evidence has not been given concerning whether lithium cations coordinate to nitrogen in the backbone. These observations give rise to a critical question. Is there any nitrogen coordination effect which cannot be studied using FTIR spectroscopy?

Since the heteroatom plays a major role in the transport of the ions it becomes a crucial factor in designing a polymer electrolyte. The heteroatom in the polymer which functions as a coordinating site to the cation to help ion transport should coordinate to the cation with optimum strength. In other words, the coordination to the cation from the heteroatom should not be too tight or too loose. In both cases it will impact the conductivity in a negative manner. Generally lithium salts are chosen for these polymer electrolytes for the advantages they have as discussed earlier in this chapter. Nitrogen and oxygen are both compatible with the lithium cation as described in inexhaustible literature on solid polymer electrolytes^{36,37,39,9}. However, still one question remains unanswered, which heteroatom (oxygen or nitrogen) is more compatible (coordinates better) to the lithium cation?

The above questions would be easily answered if the theory of “*Hard and soft acids and bases*” (HSAB) is taken into consideration. The HSAB theory is based on three postulates:⁴²

- 1) A majority of the chemical reactions can be considered to be simple acid-base type reactions and compounds as Lewis acids and Lewis bases,
- 2) The compounds involved in the reaction can be classified as hard, soft and intermediate compounds, and
- 3) The chemical reactions take place in such a way that hard acids preferentially coordinate to hard bases and soft acids preferentially coordinate to soft bases. Intermediate acids and bases can be coordinated either way (hard or soft) depending on special considerations.

Figure 1.18 shows some relative trends established by Pearson as far as hardness and softness of elements are concerned;⁴²

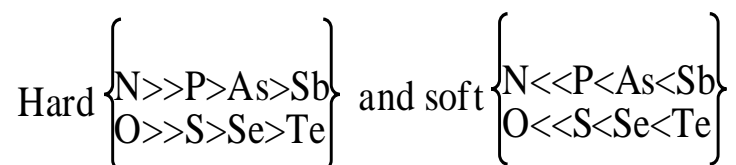
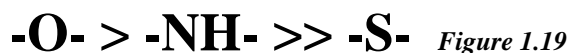


*Figure 1.18 Comparison of Hardness and Softness of Elements*⁴²

Yatsimirskii⁴³ gave another classification which showed that lithium cation as a strong and hard acceptor. According to the above classification since both oxygen and nitrogen are hard bases and lithium cation is a hard acid, both nitrogen and oxygen should coordinate well. For a polyether, such as PEO, the strongest solvation is with a hard cation like Li^+ followed by Na^+ , Mg^{2+} and Ca^{2+} . Similarly, according to the HSAB

theory, the ranking for the best donors for the lewis acids could be given by the relative negative charge on the heteroatom²⁶ (*Figure 1.19*).



When competition arises between nitrogen and oxygen to coordinate to the lithium cation the lithium cation prefers to coordinate to the oxygen over the nitrogen. According to the HSAB theory oxygen is harder than nitrogen because oxygen is more electronegative than nitrogen. A good example for this issue is morpholine (*Figure 1.20*) which is discussed by *Garnovskii* in his review over HSAB⁴⁴.

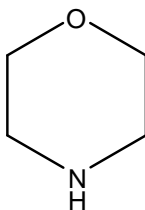


Figure 1.20 Morpholine

Morpholine, as seen in *Figure 1.20* contains identically hybridized oxygen and nitrogen. As mentioned earlier, the oxygen is harder than nitrogen since oxygen is more electronegative than nitrogen. It was observed that when a softer cation like Ag^+ (AgI) is added to morpholine, the location of the coordinate bond between the heteroatom and the cation is at the nitrogen. Thus, the silver ion being softer prefers to coordinate to the relatively softer nitrogen over the oxygen. These conclusions are in complete agreement with the HSAB theory⁴⁴.

However, there are some discrepancies with the HSAB theory. For example, in 1967 Greenwood and Robinson observed that in N'-alkyl (aryl) substituted ureas, boron trifluoride coordinates to the nitrogen instead of the oxygen (*Figure 1.21*)⁴⁵.

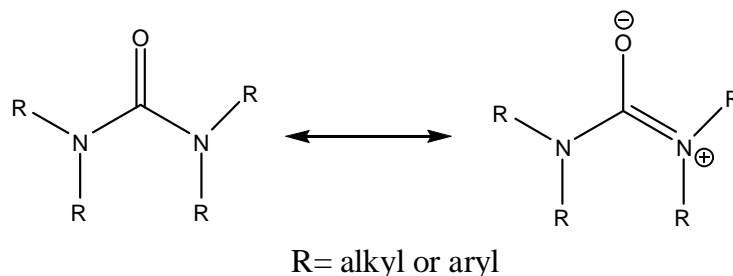


Figure: 1.21 : Resonance contribution of N'-alkyl (aryl) substituted urea

According to HSAB theory, boron in BF_3 is hard acid and it should prefer to coordinate to the more electronegative oxygen over the nitrogen. However, the boron prefers to coordinate to the nitrogen over the oxygen. The authors suggested that HSAB theory should be applied with a great caution.

Another example which shows a deviation from the HSAB theory was noted by Cram and Wilson⁴⁶. They were studying the effects of solvents, temperatures and reagents on the stereospecific synthesis of 2,3-diphenyl-2,3-butanediols from substituted α -hydroxyketones with alkyl or aryl lithium reagents. They observed that when TMEDA (N,N,N',N'-tetramethylethylenediamine) was added to the pot as a solvent instead of pentane (non-polar solvent), the stereospecificity of the reaction decreased. They proposed two models for the reaction mechanism of the reaction, with and without TMEDA (*Figure 1.22*).

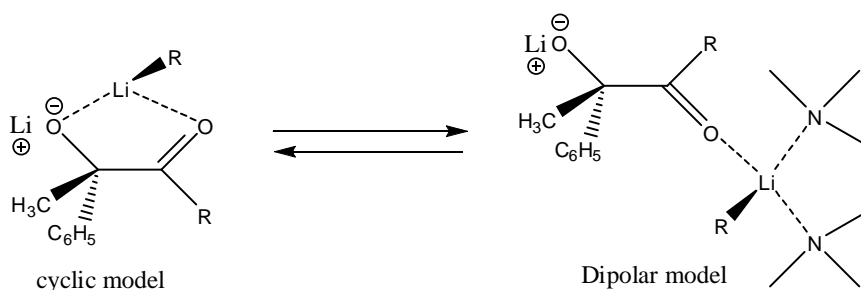


Figure: 1.22: cyclic model without TMEDA and dipolar model with TMEDA

The lowering of the stereospecificity with the addition of TMEDA suggests that there is competition between the nitrogens of the TMEDA and the oxygens of the substrate to coordinate to the lithium of the alkyl (aryl) lithium reagent⁴⁶.

As seen from the examples above, claims which support the HSAB theory and claims which deviate from the HSAB theory have both been made. As mentioned earlier, this issue (nitrogen or oxygen coordination of lithium) becomes very important in designing a solid polymer electrolyte. Since research our group is involved in modification of PEI-based polymers to make them more durable (good physical and mechanical strength) and more conducting over a large range of temperature (25°C-120°C), the question of heteroatom coordination to lithium cation becomes crucial.

1.9 Project Goals

The goals of this research project can be separated into three different parts:

- 1) A study of the heteroatom competition (oxygen versus nitrogen) for the coordination to the lithium cation using ⁷Li and ¹⁹F NMR (nuclear magnetic resonance) and ionic conductivity as an investigative tool.
- 2) Investigation of the dielectric constant of mixed ether-amine electrolyte systems.

- 3) Modification of LPEI and BPEI by substitution with different tethers and cross-linking of these polymers with lithium triflate present.

The fundamental issue of heteroatom competition will be addressed first. ^7Li and ^{19}F NMR were used in an attempt to solve the problem. To carry out these studies, different model compounds that representing the PEI (nitrogen containing polymer), PEO (oxygen containing polymer), and PEO/PEI hybrids were either bought or synthesized. Working with model compounds simplified the studies, since for NMR working in the liquid state is much less complicated than working the solid state. Although NMR data gives insight into the heteroatom coordination, dielectric constants of the solutions were another factor which needed to be considered when analyzing the data from the NMR. The dielectric properties affect ion pairing and dissociation of the salt in the solution. The dielectric constant effect of these solvent mixtures containing nitrogen and oxygen with lithium salts was studied using Electron Paramagnetic Resonance spectroscopy (EPR) as an investigative tool. With the intention of investigating the salt systems with different solvents, it was realized that EPR could be used as tool to study the dielectric constant of an unknown liquid by using a very simple set-up. A detailed explanation of this EPR technique for studying dielectric properties will be given in Chapters 3 and 4. The EPR technique was also applied to studying dielectric properties of different types of materials.

The latter half of this thesis involves the radical cross-linking of a partially allylated and partially G1, G2, G3 substituted respectively (*Figure 1.23*). The parameters for cross-linking the polymers and the concentrations of salt used were the same as that described by Dr. Lieyu Hu in his dissertation. These polymers are of great interest since they have

mixture of heteroatoms which can be correlated to the previous model compounds and imitate MEEP. These compounds were studied for their ionic conductivity.

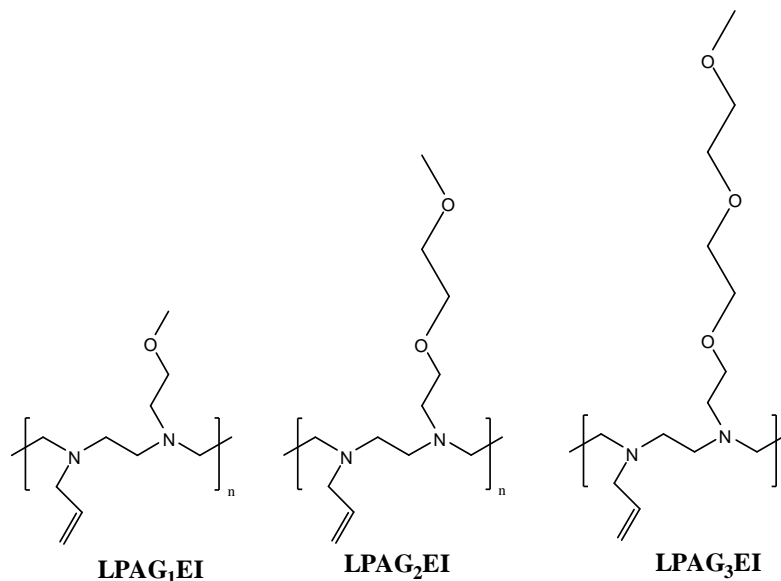


Figure 1.23

This research also included a detailed study of partially allylated BPEI (BPAEI) cross-linked without a radical initiator and its comparison to BPAEI systems cross-linked with initiators as studied by Dr. Lieyu Hu. The intention of studying this system was to investigate the effect of the radical initiator in the system on the ionic conductivity of the polymer electrolyte. Data on BPAEI and linear poly(N-allylethyleneimine-co-N-(2-(2-(methoxyethoxy)ethyl)ethyl)ethyleneimine) (LPAG₂EI) is taken from Dr. Lieyu Hu's dissertation.

References:

- 1: Jones, D.A. *Proceedings of the IEEE: Science, Measurement and Technology* **2006**, 138, 1-10.

- 2: Huggins, R.A. *Advanced Batteries: Material Science Aspects* **2009**, p 1-23.
- 3: Ehrlich, G.M. *Handbook of Batteries* **2002**, Chapter 35, p 35.1- 35.94.
- 4: Besenhard, J.O. *Handbook of Battery Materials* **1999**: Part 1 Fundamentals and General Aspects of Electrochemical Power Sources.
- 5: *Battery Statistics*; URL: http://www.li-ion-battery.com/Knowledge/Battery_statistics.htm
- 6: “*Why is alternative energy important*”, URL: <http://www.alternative-energy-engineering.com/energy-sources.htm>
- 7: “*Batteries in Fact and Fiction*”, URL: <http://www.chem.hawaii.edu/uham/bat.html>
- 8: Tarascon, J.M.; Armand, M. *Nature* **2001**, 414, 359-367.
- 9: Hu, Lieyu. PhD Dissertation, The University of Oklahoma 2005.
- 10: Dresselhaus, M.S.; Thomas, I.L. *Nature* 2001, 414, 332-337.
- 11: Corder, G.W. *Virginia Journal of Science Education*, 1, 33-36.
- 12: Bellis, Mary. “*History of Electric Battery*”, URL: About.com
- 13: “*Origin of Electric Power*” URL: <http://americanhistory.si.edu/powering/past/prehist.htm>
- 14: “*Trough Battery*” URL: <http://brunelleschi.imss.fi.it/museum/esim.asp?c=100497>

- 15: Carboni, G. Experiments in Electrochemistry, URL:
http://www.funsci.com/fun3_en/electro/electro.htm
- 16: Calvert, J.B. “The Electromagnetic Telegraph”, URL:
<http://mysite.du.edu/~jcalvert/tel/morse/morse.htm#HB>
- 17: “Gaston Plante” URL: <http://www.corrosion-doctors.org/Biographies/PlantelBio.htm>
- 18: “Georges Lelanche” URL:
<http://www.batteryfacts.co.uk/BatteryHistory/Leclanche.html>
- 19: “The Columbia Dry Cell Battery”, American Chemical Society, URL:
<http://acswebcontent.acs.org/landmarks/drycell/columbia.html>
- 20: “History of batteries”: en.wikipedia.org.
- 21: Dunlop, J.D. Stockel, J.F. *J.Energy* , 6, 28.
- 22: Bush, D.M. *Aerospace and Electronic Systems Magazine, IEEE* **1990**, 5, 27-30.
- 23: Buchmann, I. URL: <http://batteryuniversity.com/parttwo-55.htm>
- 24: Vincent, C.A.; Scrosati, B. *Modern Batteries, An Introduction to Electrochemical Power Sources*; Wiley and Sons; New York, **1997**.
- 25: Bode, H. *Lead Acid Batteries*; Wiley and Sons: New York, **1977**.
- 26: Gray, F.M. Armand, M. *Polymer Electrolytes*; Handbook of Battery Materials; Wiley-VCH Verlag **1999**.

- 27: Birke, P.; Weppner, W. *Solid Electrolytes*, Handbook of Battery Materials; Wiley-VCH Verlag **1999**.
- 28: Nazri, G.; Pistoia, G. *Lithium batteries*; Science and Technology (Eds).
- 29: Ratner, M.A.; Shriver, D.F. *Chemical Reviews* **1988**, 88-109.
- 30: Shriver, D.F.; Bruce, P.G. *Solid State Electrochemistry* Cambridge University Press: New York, 1995.
- 31: Atkins, P. *Physical Chemistry, Sixth Edition* WH. Freeman and Company: New York, 1998.
- 32: Petrowsky, M.; Frech, R.; Suarez, S.N.; Jayakody, J.R.P.; Greenbaum, S. *The Journal of Physical Chemistry: B* **2006**, 110, 23012-23021.
- 33: Berthier, C.; Gorecki, W.; Minier, M.; Armand, M.B.; Chabagno, J.M.; Rigaud, P. *Solid State Ionics* **1983**, 11, 91-95.
- 34: Bouridah, A.; Dalard, F.; Deroo, D.; Armand, M.B. *Journal of Applied Electrochemistry* **1987**, 17, 625-634.
- 35: Blonsky, P.M.; Shriver, D.F.; Austin, P.; Allcock, H.R. *Solid State Ionics* **1986**, 18 and 19, 258-264.
- 36: Tanaka, R.; Fujita, T.; Nishibayashi, H.; Saito, S.; *Solid State Ionics* **1993**, 60, 119-123.
- 37: Snow, A. PhD Dissertation, The University of Oklahoma 2002.

- 38: Saegusa, T.; Ikeda, H.; Fujii, H. *Macromolecules: Communications to the Editor* **1971**, 108.
- 39: R. Tanaka, I. Ueoka, Y. Takaki, K. Kataoka, S. Saito, *Macromolecules* **1983**, 16, 849.
- 40: York, S.; Frech, R.; Snow, A.; Glatzhofer, D.T. *Electrochimica Acta* **2001**, 46, 1533-1537.
- 41: Snow, A.; Sanders, R.; Frech, R.; Glatzhofer, D.T. *Electrochimica Acta* **2003**, 48, 2065-2069.
- 42: Pearson, R.G. *Hard and Soft Acids and Bases, HSAB, Part 1*, Fundamental Principles.
- 43: Yatsimirskii, K.B. *Theoretical and Experimental Chemistry* **1970**, 6, 376-380.
- 44: Garnovskii, A.D. *Russian Chemical Reviews* **1972**, 41, 341.
- 45: Greenwood, N.N.; Robinson, B.H. *Journal of Chemical Society (A)* **1967**, 511-517.
- 46: Cram, D.J.; Wilson, D.R. *Journal of American Chemical Society* **1963**, 85, 1245-1249.
- 47: “Daniell Cell”, URL: http://en.wikipedia.org/wiki/Daniell_cell
- 48: “Zinc-Carbon Battery”, URL: http://en.wikipedia.org/wiki/Zinc-carbon_battery
- 49: “Lewis Urry”, URL: http://en.wikipedia.org/wiki/Lewis_Urry
- 50: Nishi, Y. *Journal of Power Sources* **2001**, 100, 101-106.
- 51: *Overview: Lithium ion Batteries*, URL: <http://industrial.panasonic.com/www-data/pdf/ACA4000/ACA4000PE3.pdf>
- 52: *The Hybrid Car Battery: A definitive guide*, URL: <http://www.hybridcars.com/hybrid-car-battery>

53: “How battery works”, URL: <http://sciencewithalice.blogspot.com/2009/08/how-battery-works.html>

Chapter 2

Investigation of N vs O Heteroatom Coordination in Lithium Electrolytes Systems

Using NMR and EPR as Tools

2.1 Introduction to NMR^{1,2,3}

Nuclear magnetic resonance (NMR) is a widely used tool in the field of chemistry. As the name itself suggests, the technique involves the absorption of electromagnetic radiation of a specific frequency by an *atomic nucleus* that is placed in a *magnetic field*. Over the past fifty years nuclear magnetic resonance (NMR) has become an eminent technique for structure determination, kinetic studies, quantitative analysis, and examination of dynamic processes. Although a larger amount of sample is needed for NMR than some of the spectroscopic methods, good data can be obtained with modern instruments and less than a milligram of sample. To use NMR as an investigative tool it is necessary to understand the physical principles on which the NMR technique is based.

The principle of “Nuclear Magnetic Resonance” involves two sequential steps. The first step involves the aligning of the nuclear spin with the magnetic field of the external constant magnetic field (H_0). The second step involves the “perturbation” of the above alignment of the nuclear magnetic spins by an electro-magnetic, radio frequency (RF) pulse. The frequency of the electromagnetic radiation applied depends on the static magnetic field (H_0) and the nuclei under observation.

The two fields, the constant magnetic field (H_0) and the electromagnetic radio frequency radiation, are generally perpendicular to each other as it maximizes the NMR

signal strength. The phenomenon of total magnetization (M) of the nuclear spins due to both the applied fields (constant magnetic field and electromagnetic radiofrequency radiation) is exploited in NMR spectroscopy. NMR spectroscopy uses strong applied magnetic fields (H_0) in order to achieve high stability and deliver good spectral resolution.

All nuclei have charges on them. In some of the nuclei, the charge present on the nuclei spins around the nuclear axis. The circulation of nuclear charge generates a magnetic dipole along the axis. The angular momentum created by the spinning charge can be represented by its spin number (I). The nuclei of different elements have a characteristic spin (I). Some nuclei have an integral spin (e.g. $I = 1, 2, 3$), some have fractional spin (e.g. $I = 1/2, 3/2, 5/2$) and some have no spin at all where $I = 0$ (e.g. ^{12}C , ^{16}O , ^{32}S etc). The spin number can be determined from the atomic number and atomic mass as shown in table 2.1.

Table 2.1^{1,2,3}.

(I)	Atomic mass	Atomic number	Example nuclei
Half integer	Odd	Odd	^1H , ^3H , ^{15}N , ^{19}F , ^{31}P
Half Integer	Odd	Even	^{13}C , ^{17}O , ^{29}Si
Integer	Even	Odd	^2H , ^{14}N , ^{10}B
Zero	Even	Even	^{12}C , ^{16}O , ^{34}S

Nuclei such as ^1H , ^3H , ^{15}N , ^{19}F , ^{31}P , ^{13}C , ^{17}O , ^{29}Si have a spin number of $1/2$ and a uniform spherical charge distribution and their spectra can be readily obtained. The

most widely observed nuclei are ^1H and ^{13}C . Nuclei with spin number 1 and higher have non-spherical charge distributions. This asymmetry is caused by electrical quadrupole moments which affect the line width and coupling with the neighboring nuclei.

A non-zero spin is always associated with a non-zero magnetic moment (μ) by the relation

$$\mu = \gamma \mathbf{I} \quad (\text{Equation 2.1})$$

Where γ is the gyromagnetic ratio.

It is the magnetic moment that leads to NMR absorption spectra resulting from transitions between nuclear spin levels. The nuclei with even numbers of protons and even numbers of neutrons have zero magnetic moment and also have zero magnetic dipole. Therefore, nuclei with an even number of protons and an even number of neutrons do not show NMR absorption.

Consider nuclei with $\frac{1}{2}$ spin, like ^1H , ^{13}C or ^{19}F . The nucleus has two possible spin states; $m = (+) \frac{1}{2}$ and $m = (-) \frac{1}{2}$. The spin states are also referred to as spin up and spin down, or α and β spin states, respectively. These states are degenerate, which means they have same energy. Thus the number of atoms in these two degenerate states will be equal at equilibrium. When the nucleus is placed in an external magnetic field (B_0), there is interaction between the nuclear magnetic moment and the external magnetic field which means that two states have no longer the same energy (Figure 2.1).

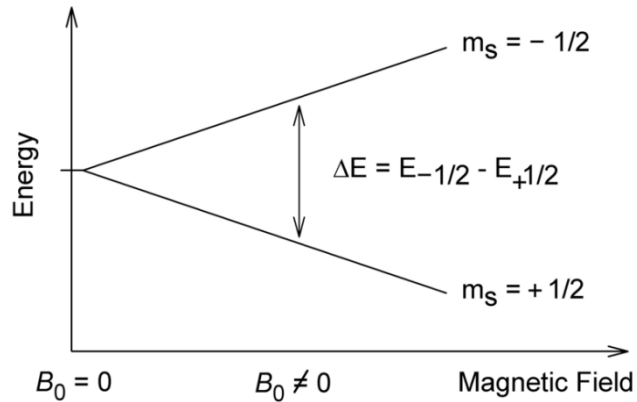


Figure 2.1 Splitting of nuclei spin states when placed in an external magnetic field B_0 .

The energy of the magnetic moment when in an external magnetic field is given by

$$\mathbf{E} = -\boldsymbol{\mu} \cdot \mathbf{B}_0 = -\gamma \mathbf{m} \mathbf{h} \mathbf{B}_0. \quad (\text{Equation 2.2})$$

Where m = magnetic quantum number (can take values from $+I$ and $-I$, in integer steps).

h = Planck's constant,

γ = gyromagnetic ratio,

B_0 = external magnetic field, and

m = magnetic moment of the nuclei,

As a result, the different nuclear spin states have different energies in a non-zero magnetic field. The two spin states of spin $\frac{1}{2}$ can be seen as aligned with or against the magnetic field. If γ is positive, which is true for most of the isotopes, then $m = \frac{1}{2}$ should be the lower energy state. The difference in the energy is given by

$$\Delta E = \gamma \mathbf{h} \mathbf{B}_0. \quad (\text{Equation 2.3})$$

The difference in the energy always results in a small population skewed towards the lower energy state. The difference in the energy (ΔE) between the lower and higher energy states depends on the strength of the applied magnetic field (B_0) (Figure: 2.1).

When a sample placed in the external magnetic field is subjected to a pulse of radiation that corresponds to the energy difference between the lower spin and higher spin states, nuclei in the lower energy spin state are promoted to the higher energy spin state. The transition is called “flipping” of the spin. With magnets currently available, the energy difference between the lower energy spin state and the higher energy state is so small that only a small amount of energy is required to flip the nuclei. The radiation generally used to supply this energy is radio frequency (*rf*) radiation of the electromagnetic spectrum. When the nuclei absorb the radio frequency radiation, a spin flip occurs which generate signals whose frequency depends on the difference in energy (ΔE) between the lower and the higher energy spin states. The NMR spectrometer detects the radiation given off and thus gives a plot of signal frequency versus intensity which is the NMR spectrum. The nuclei are said to be in resonance with the radio frequency radiation. Thus, the spectroscopic technique is called “Nuclear Magnetic Resonance”. In this context, resonance refers to the flipping of the electrons back and forth between the lower energy state and the higher energy state. As mentioned earlier, the energy difference (ΔE) depends on the external magnetic field, Therefore, as seen from Figure: 2.1, stronger magnetic fields require higher energies of radio frequency radiation. NMR spectrometers are equipped with electromagnetic radiation sources that can be tuned to different frequencies to obtain NMR spectra of different nuclei^{4,5}.

2.2 Shielding and deshielding effects

The frequency of an NMR signal depends on the external magnetic field felt by the nucleus. If all the nuclei present in the compound were to experience the same magnetic field, then just one single peak would be seen in an NMR spectrum. But every nucleus is surrounded by a different cloud of electrons which shields the nucleus from the external magnetic field^{4,5}. Fortunately for chemists, the shielding by the electron cloud is different for different nuclei within the molecule. The electrons revolve around the nuclei to create a local magnetic field that acts against the external applied magnetic field and subtracts from the external applied magnetic field. The effective magnetic field actually felt by the nucleus is smaller than that of the applied magnetic field. The effective magnetic field felt by the nucleus is given by

$$\mathbf{B}_{\text{effective}} = \mathbf{B}_{\text{applied}} - \mathbf{B}_{\text{local}} \quad (\text{Equation 2.4})$$

Therefore, the greater the electron density around the nucleus, the greater is the B_{local} and therefore $B_{\text{effective}}$ is smaller. The smaller the $B_{\text{effective}}$, the lower the frequency required to get the nucleus in resonance, i.e. to flip the spin of the nucleus, as the ΔE is smaller (Figure 2.1). Nuclei which are in an electron poor environment will require higher frequency radiation to bring the nucleus into resonance^{4,5}.

2.3 Chemical shifts

In an NMR spectrum, the energy-axis is generally given by a scale in ppm (parts per million). The position where the NMR peak occurs on this scale is called the chemical shift (δ). The chemical shift is given by Equation 2.5.

$$\delta = \text{chemical shift (ppm)} = \frac{\text{Distance downfield from reference (TMS)(Hz)}}{\text{Operating frequency of the spectrometer (MHz)}} \quad (\text{Equation: 2.5})$$

The equation above shows that the chemical shift directly depends on the frequency at which the nuclei resonate. As mentioned earlier, nuclei with electron poor environments require higher frequency radiation and therefore appear at higher chemical shifts. Similarly, electron rich nuclei require lower frequency radiation and therefore appear at relatively lower chemical shifts. Tetramethylsilane (TMS) is usually used as the reference in NMR spectroscopy. All the 12 hydrogens are equivalent in TMS and they absorb at a lower magnetic field than any protons usually seen in normal organic compounds²². TMS is also inert to most chemicals and soluble in most organic solvents. Any signal at higher frequency from the reference signal is referred as downfield from the reference. Any signal relatively to the left (higher frequency) on the scale is referred to as “downfield” and any signal relatively to the right as “upfield”⁵.

2.4 NMR in investigation of lithium ion electrolytes

The NMR technique was used by Siekierski *et al* to investigate lithium ion transport in different lithium salt electrolytes^{6,7,23}. Siekierski used the ⁷Li and ¹⁹F NMR signals as an investigative tool to study the ionic association and ionic conductivity of different concentrations of lithium triflate in various ethers like glyme, diglyme and mixtures of monoglyme and dioxane. Siekierski used the ¹⁹F NMR shifts to quantify the different species formed from lithium triflate with oxygen containing solvents and mixtures of different oxygen containing solvents. Using this paper as a reference, we thought ⁷Li and ¹⁹F NMR would be an appropriate tool to investigate the speciation of lithium triflate for liquid electrolytes involving mixtures of solvents containing nitrogen

and oxygen. The study of lithium ion transport is very important in lithium salt electrolytes because of their importance in lithium ion batteries. The transport mechanism of the lithium ion in an electrolyte solution was discussed in Chapter 1. Nuclear magnetic resonance is a potentially important tool in the investigation of solvation of the lithium ion as shown by Siekierski et al^{7,23}. Lithium ions coordinate to the heteroatoms of the solvent. Ionic conduction occurs by the transient jumping of lithium ion from one heteroatom pocket to another. The coordination number of the lithium ion with the heteroatoms depends on lot of factors like the type of solvent, the type of heteroatom, and also the atoms surrounding the heteroatom. Therefore, under different circumstances different lithium ion-heteroatom coordination is observed. Different coordination will result in different electron densities around the lithium ion, which will cause a change in the ⁷Li NMR chemical shift. Depending on the solvent, the counterion for the lithium ion will also show varying behavior. Thus, it becomes very important to monitor the counter ion (¹⁹F in triflate as anion) as well^{6,7}. Together, the lithium ion spectra and the counterion spectra can give insight into the behavior of different heteroatom solvents and different lithium salts, which can in turn give insight into lithium ion conduction in different electrolytes.

The purpose of this chapter is to investigate competition between oxygen and nitrogen containing solvents in coordination to the lithium cation. This study was done using model compound solvents which are small model compounds for nitrogen and oxygen based polymers used in SPE's (Solid Polymer Electrolyte). The investigation of the nitrogen versus oxygen issue is important for polymers which have both oxygen and nitrogen (PEO/PEI hybrids) heteroatoms and also to understand the transport

mechanism of the lithium ion in these polymers as discussed in Chapter 1. Some of the questions which arose for the polymers discussed in Chapter 1 are listed below.

- ❖ **If LPEI-G2 shows same interaction of lithium cation with the side chains as in MEEP lithium triflate system, why is LPEI-G2 lithium triflate system less conducting than MEEP lithium triflate²⁵?**
- ❖ **If LPEI-G2 shows interaction with the ethylene oxide side chains with no proof of backbone nitrogen interaction, why is the LPEI-G2:LiTf less conducting than PEO:LiTf at elevated temperatures^{24, 25}?**
- ❖ **Is there a role played by the back-bone nitrogen in LPEI-G2 lithium triflate system which cannot be diagnosed by IR?**

These above questions are very important for the understanding and development of LPEI-G_x systems.

Lithium triflate was the salt used in NMR investigations into the above mentioned questions. Since lithium triflate was used as the salt in various different solvents, ⁷Li and ¹⁹F nuclei were monitored using the NMR spectroscopy. NMR spectroscopy allows for monitoring the lithium and fluorine nuclei directly and thus should give a direct indication of the electronic environment of lithium and triflate in the sample.

Different nitrogen and oxygen containing solvents were mixed in different mole fractions of the two solvents with lithium triflate as a salt in the ratio of 80:1 heteroatoms to lithium. The dilute concentration of lithium triflate was used to

minimize the number of species that may form and to give more “solvent isolated” species. The different solvent systems used are shown below.

- ❖ Diethylether (DEE) vs triethylamine (TEA). (1 O vs 1 N)
- ❖ Monoglyme (MG) vs tetramethylethylenediamine (TMEDA). (2 O vs 2 N)
- ❖ Monoglyme (MG) vs triethylamine (TEA). (2 O vs 1 N)
- ❖ Diethylether (DEE) vs tetramethylethylenediamine (TMEDA). (1 O vs 2 N)
- ❖ 2-methoxy-N,N-dimethylethanamine (G1) vs monoglyme (MG).
- ❖ 2-methoxy-N,N-dimethylethanamine (G1) vs TMEDA.

Figure: 2.2 shows the chemical structure for different solvents used in the investigation.

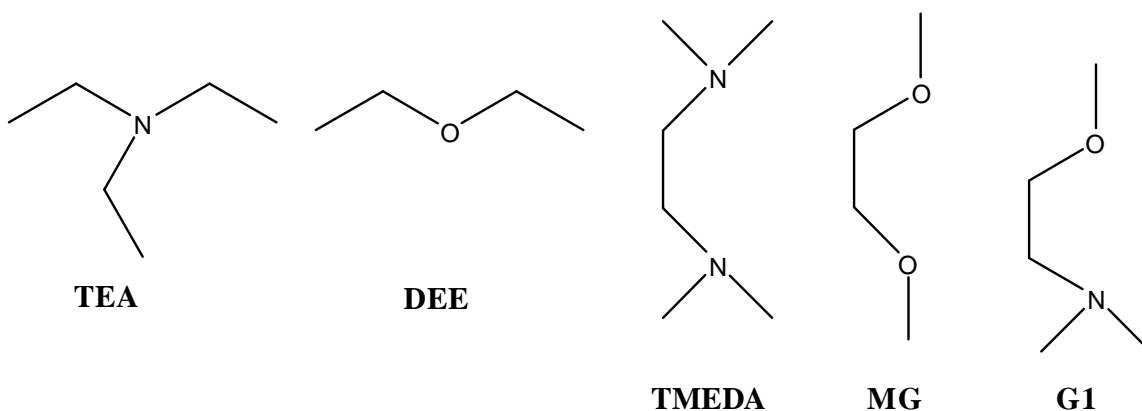


Figure 2.2 Chemical structures for different solvents under investigation..

The different mole fraction mixtures of the two solvents in a system (as mentioned above) with lithium triflate were expected to show different chemical shifts for each sample in a system. The chemical shift of lithium and fluorine for a sample in a

system is an average of each fraction of species formed by the lithium cations with the heteroatoms and the triflate anions respectively. Theoretically, different mole fractions of the two solvents should show different chemical shifts for lithium as the concentration of oxygen and nitrogen atoms changes with each sample and thus the coordination of the lithium to the heteroatom changes too.

Along with the coordination effect of the lithium to the heteroatom there is another change which needs to be monitored, the change in the dielectric constant of the sample (salt solution). Since different samples involve different mole fractions of the two solvents containing nitrogen and oxygen, the dielectric constant of the sample changes. Each solvent mentioned above has different a dielectric constant and therefore a change in the dielectric constant is expected. Ion separation (dissociation) of the lithium triflate partly depends on the dielectric constant of the solvent it is dissolved in. It therefore is very important to have an assurance that changes in the chemical shift in the ^7Li and the ^{19}F NMR spectra are not simply due to changes in the dielectric constant, which might cause the lithium triflate to either associate or dissociate, and is due to the coordination effect of the ions to the heteroatoms. The change in the dielectric constant could also change the dissociation of the salt in the solution, which could be reflected in the NMR spectra. Thus it becomes a very important to monitor changes in the dielectric constant.

The monitoring of the dielectric constant for different salt solution samples was done using an EPR technique developed in our laboratory that will be discussed in detail Chapter 3 and Chapter 4. The dielectric properties of the salt solutions were

measured using the EPR technique to investigate the change in trend of dielectric constant as the mole fraction of heteroatoms changes in a given system.

2.5 Lithium NMR: An overview ^{8,9}

The element lithium was discovered in 1817 by Johan August Arfwedson in a Swedish mineral called pelatite. Lithium metal has an atomic number of 3 and atomic weight of 6.94. Lithium mainly exists in two isotopic forms, ⁶Li and ⁷Li. Detailed information about ⁶Li and ⁷Li is presented in Table 2.2. As seen from the table, ⁷Li has a higher abundance (93%) and larger quadrupole and gyromagnetic moments^{8,9}. However, ⁶Li has a spin number of 1 and ⁷Li has a spin number of 3/2. The range of chemical shifts for lithium NMR are small, and therefore it is not possible to resolve the resonance of different lithium nuclei environments based solely on the chemical shift interaction. The resolution can sometimes be improved by using higher field strength, extracting some chemical data from the spectra. As far as the research in this thesis is presented, only ⁷Li was used as a tool for investigation.

Table 2.2

	Natural abundance <i>N</i> (%)	Spin (<i>I</i>)	Magnetic Moment μ (μN)	Magnetogyric Ratio γ (10^7 rad T ⁻¹ s ⁻¹)	Quadrupole Moment Q (10^{-28} m ²)	Resonance frequency ν (MHz)
⁶ Li	7.42	1	1.1624	3.9371	-6.4X10 ⁻⁴	58.868
⁷ Li	92.58	3/2	4.2035	10.3976	-3.7X10 ⁻²	155.464

2.6 Fluorine NMR: An Overview¹⁰

Aside from carbon and hydrogen, the fluorine nucleus is the most studied. The reason for this is the importance of molecules containing fluorine and the fluorine nuclei itself. To obtain a fluorine NMR spectrum, one must of course have access to a spectrometer with a probe which can observe fluorine nuclei. Fortunately, most of the high field NMR spectrometers available have this ability. The most commonly used NMR spectrometers to obtain fluorine spectra operate at 300 or 400 MHz.

The ^{19}F nucleus has a natural abundance of 100% that partly makes the NMR spectra easy to obtain. It also has a high magnetogyric ratio, about 0.94 greater than for ^1H . The chemical shift range of ^{19}F NMR is greater than 350 ppm. Therefore, the resonances obtained in fluorine spectra for different F-containing species are well separated. The nuclear spin quantum number for fluorine is 1/2 and the relaxation times are sufficiently large for ^{19}F nuclei.

Fluorotrichloromethane (CFCl_3) is the most commonly used internal reference for the measurement of ^{19}F NMR spectra and it is assigned as a chemical shift of zero (0). Signals shift upfield from zero are assigned a negative value, whereas signals that shift downfield of zero are assigned positive values. Reports of ^{19}F NMR chemical shifts should be always reported in reference to CFCl_3 . ^{19}F NMR spectra are very different than proton NMR spectra. For example, the effects of anisotropic magnetic fields, such as those created by the ring currents, are much less important than for proton NMR spectra. This effect gives a complete overlap of vinylic and aromatic fluorine chemical shifts¹⁰.

2.7 Determination of Relative ^7Li and ^{19}F NMR Chemical Shifts for “More Paired” and “Less Paired” Ions

The determination of the relative upfield and downfield chemical shifts for “more paired” and “less paired” ions containing ^7Li and ^{19}F , relative to the references, was essential before investigating systems with nitrogen and oxygen heteroatoms. A system with carbon tetrachloride and diethyl ether as solvents was investigated. Different mixtures of carbon tetrachloride and diethyl ether were made with an 80:1 (heteroatom:Li) ratio of lithium triflate. The reference used for ^7Li NMR was lithium triflate in D_2O . The chemical shift for lithium triflate in D_2O was set at 0 ppm and the ^7Li NMR chemical shifts for different solvent mixtures with lithium triflate were measured relative to it. The reference used for ^{19}F NMR was CFCl_3 and the chemical shift was set at 0 ppm for this reference.

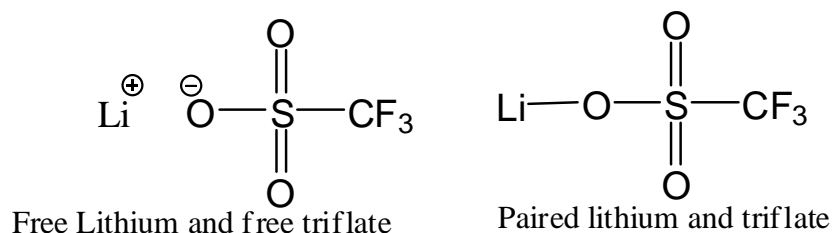


Figure 2.3 Free and paired lithium triflate

The assumption is made that addition of carbon tetrachloride to diethyl ether will force ion pairing in the lithium triflate. This assumption can be justified on the basis that carbon tetrachloride has no strong coordinating heteroatom and also the dielectric constant of carbon tetrachloride is relatively low ($\epsilon = 2.24$). Addition of carbon tetrachloride, with a relatively lower dielectric constant to diethylether ($\epsilon = 4.8$)

forces pairing of the lithium cation and triflate anion of the lithium triflate salt in the salt solution²⁸. The chemical shift for the less-paired lithium cation and less-paired fluorine of the triflate anion should be different from the more-paired lithium and the fluorine of the more-paired triflate anion.

The trend in ⁷Li chemical shifts for different mole fractions of diethyl ether with carbon tetrachloride is shown in Figure 2.4.

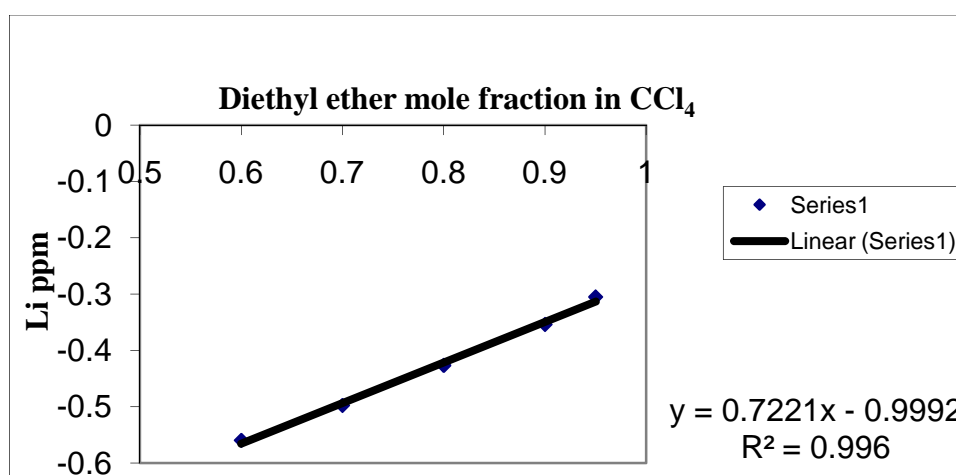


Figure 2.4 Plot of diethyl ether mole fraction with carbon tetrachloride versus ⁷Li chemical shift. (Samples made with lithium triflate as salt with 80:1 heteroatom:Li ratio and measured at 25°C)

As seen from Figure 2.4, the chemical shift trends toward more negative values on the addition of carbon tetrachloride to the diethyl ether. The chemical shift moves upfield on the addition of carbon tetrachloride to diethyl ether. The upfield shift suggests that the lithium cation becomes more shielded on the addition of carbon tetrachloride to diethyl ether, which in turn suggests that more electron density is present around the lithium cation on the addition of carbon tetrachloride to diethyl ether. When the lithium cation is more paired, the positive charge is smaller as there is greater

donation of electrons from the triflate ion and the lithium ion should be shielded, thus showing a signal upfield in relation to the more paired lithium cation.

Based on the above observation, an upfield shift of the chemical shift correlates to more coordination around the lithium cation or more pairing of lithium cation with triflate and downfield shift correlate with less coordination around the lithium or less paired lithium cation (Figure 2.5). It should be noted that the change in ^7Li NMR chemical shifts for addition of carbon tetrachloride to diethyl ether appears to be linear.

^7Li NMR

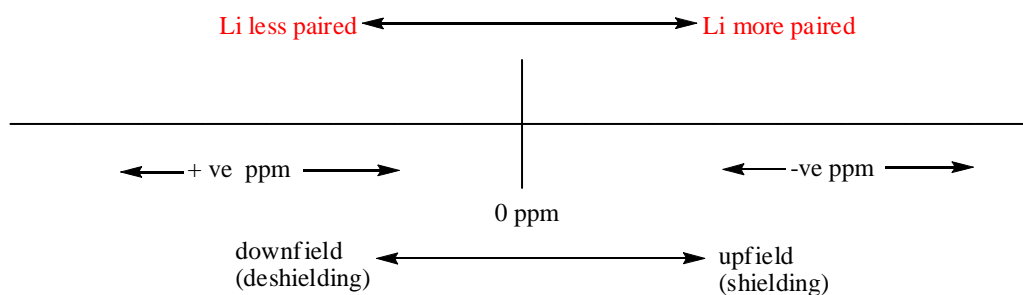


Figure: 2.5 ^7Li NMR chemical shift: upfield and downfield assignments

The ^{19}F chemical shift trend for lithium triflate in different mole fractions of diethyl ether with carbon tetrachloride is shown in Figure 2.6.

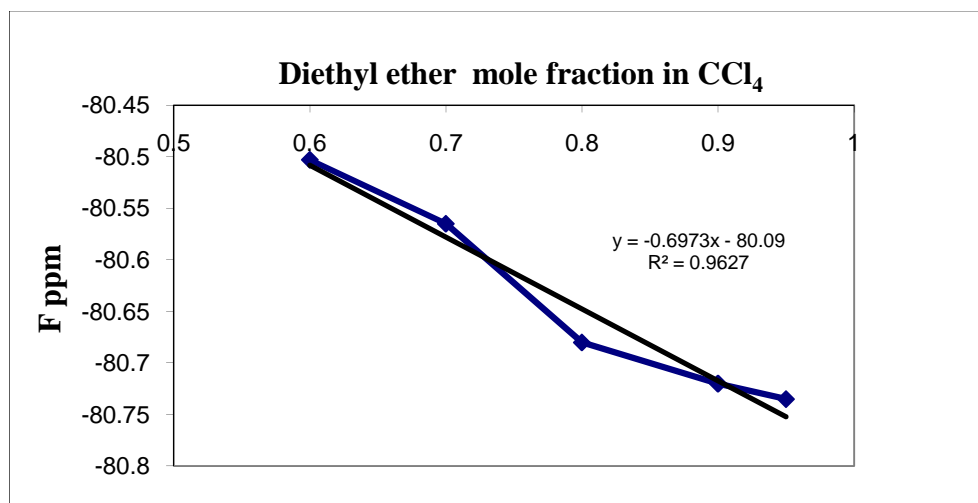


Figure 2.6 Plot of diethyl ether mole fraction with carbon tetrachloride versus ¹⁹F chemical shift. (Samples made with lithium triflate as salt with 80:1 heteroatom:Li ratio and measured at 25°C)

From the plot of mole fraction of CCl₄ ($\epsilon = 2.24$) in diethyl ether ($\epsilon = 4.8$) and ¹⁹F NMR chemical shift for the fluorine nuclei in the triflate anion, it can be seen that on the addition of carbon tetrachloride to diethyl ether the chemical shift shifts in the less negative direction, that is, downfield. Therefore, on the addition of carbon tetrachloride to the diethyl ether, the fluorine is deshielded. This means that on the addition of carbon tetrachloride to diethyl ether, less electron density is present around the fluorine. This behavior is expected as the triflate ion, when more-paired, shares more electron density with the lithium cation and thus less electron density is felt by the fluorine in the triflate, resulting in a signal that is relatively downfield. When less-paired triflate is present in the solution, the negative charge on the oxygens is less shared by the lithium cation and thus the fluorine in the triflate anion feels more electron density. Therefore less-paired triflate should appear relatively upfield on the ¹⁹F NMR scale when compared to more-paired triflate. It should be noted that the

change in ^{19}F NMR chemical shifts for addition of carbon tetrachloride to diethyl ether appears to be linear.

The relative assignment of shifts for more-free triflate and more-paired triflate anion can be made as shown in Figure: 2.7.

F^{19} NMR

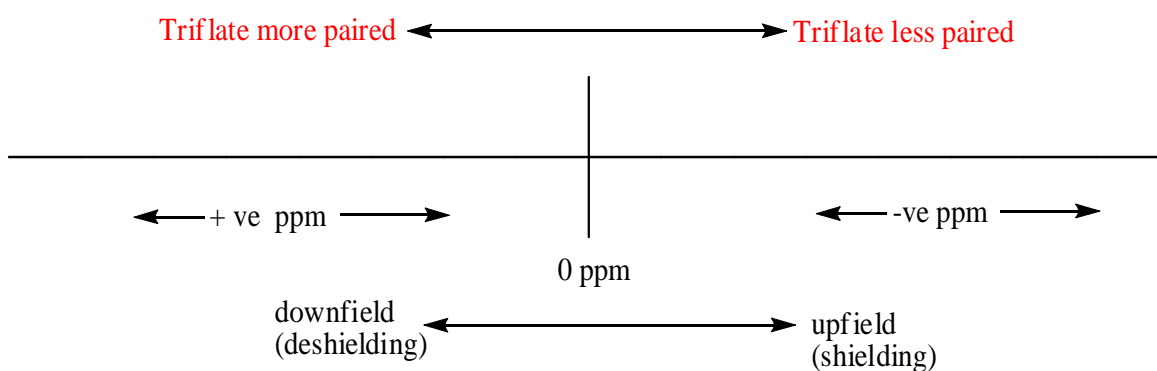


Figure: 2.7 ^{19}F NMR chemical shift: upfield and downfield assignments

The conclusion is that the ^7Li and ^{19}F NMR data for lithium triflate in diethyl ether and carbon tetrachloride mixtures is consistent with the assumptions made for ion pairing.

Having established basic parameters for ^7Li and ^{19}F NMR shifts, the investigation of systems that mimic PEO/PEI solid electrolytes will be discussed in the following sections.

2.8 TEA (Triethylamine) versus DEE (Diethyl ether)- 1 Nitrogen versus 1 Oxygen

The first system that is an obvious choice for investigation is 1 nitrogen and 1 oxygen system, i.e. diethyl ether and triethylamine. Triethylamine has a dielectric

constant of 3.2 whereas diethyl ether has a dielectric constant of 4.8. The expectation was to see effects similar to those observed with the addition of carbon tetrachloride ($\epsilon = 2.24$) to diethyl ether ($\epsilon = 4.8$), due to the closeness of dielectric constant for carbon tetrachloride ($\epsilon = 2.24$) and triethylamine ($\epsilon = 3.2$), if there are no specific interactions involved. Recall that a linear change in the chemical shift was seen with the ^7Li NMR data for the diethyl ether and carbon tetrachloride and would be expected in the ^7Li NMR data for diethyl ether and triethylamine if changes in dielectric constant were the only factor responsible for changes in the chemical shift with the addition of triethylamine to diethyl ether.

The plot for the mole fraction of triethylamine in diethyl ether versus ^7Li NMR chemical shift is shown in Figure 2.8.

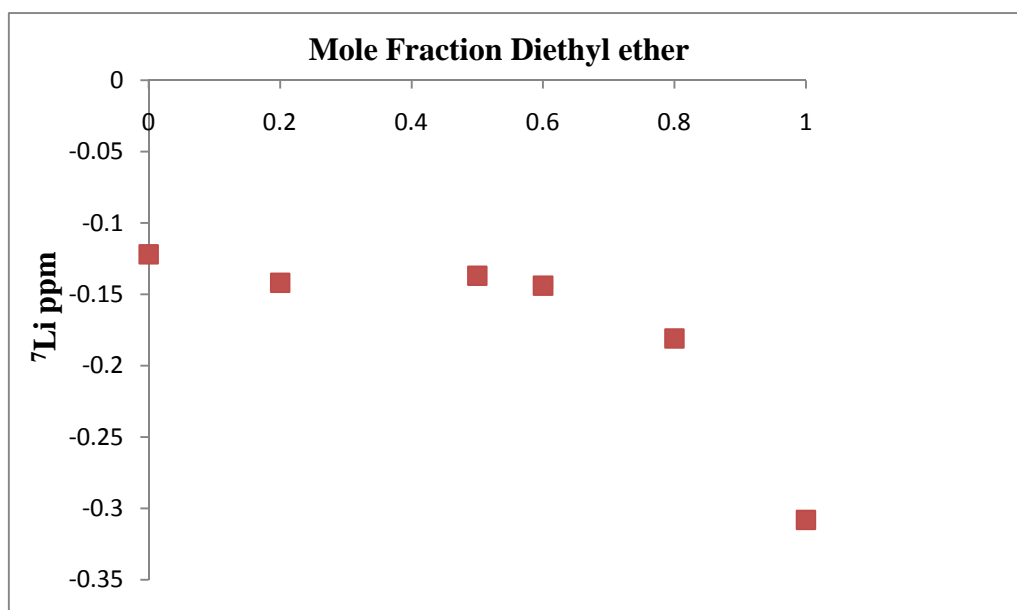


Figure 2.8 Plot of Mole fraction of diethyl ether in triethylamine and ^7Li NMR chemical shift.

(Samples made with lithium triflate as salt with 80:1 heteroatom:Li ratio and measured at 25°C)

As seen from the plot, with the addition of triethylamine to diethyl ether in the presence of lithium triflate as a salt, the chemical shift of the signal shifts upfield. The most important thing to be noticed here is the difference between the carbon tetrachloride-diethyl ether ^7Li chemical shift trend and the triethylamine-diethyl ether ^7Li chemical shift trend. Contrary to the carbon tetrachloride-diethyl ether system, the addition of triethylamine to diethyl ether shifts the ^7Li chemical shift downfield. This suggests that the lithium cation is deshielded on the addition of triethylamine to diethyl ether, which means less electron density around the lithium cation on the addition of triethylamine to diethyl ether. This, in turn, suggests that lithium cation gets less paired as we add more triethylamine to diethyl ether. This observation is completely opposite to the observation made for the ^7Li NMR data for diethyl ether and carbon tetrachloride. On an absolute scale the chemical shift shifts from -0.325 ppm for 100% diethylether to -0.125 ppm for 100% triethylamine. The change in the trend for the ^7Li chemical shift for the diethyl ether-triethylamine mixtures is not linear as would be expected from the diethyl ether-carbon tetrachloride mixtures. Initially a small addition of triethylamine to diethyl ether causes a fast change in the chemical shift up to the 80% diethyl ether point. After the 80% diethyl ether point, the further addition of triethylamine does not cause significant change in the chemical shift in the ^7Li NMR. This observation suggests the possibility that the nitrogen heteroatom from the triethylamine interacts with the lithium more strongly than that of the oxygen of the diethyl ether. The non-linear curve initially suggests that equilibrium favors the coordination of lithium to nitrogen over oxygen.

If lithium cation becomes less paired, it was expected that the addition of triethylamine to diethyl ether would give higher conductivities. To investigate if the conductivity is in agreement with the ^7Li NMR data, AC conductivities were done on the diethyl ether-triethylamine mixtures. Before discussing the data for the conductivities, a brief introduction to AC conductivity measurements and the cell used will be discussed in the following section.

2.9 AC conductivities

Conductivity is the measure of the ability of the electrolytic solution to conduct electricity. Conductivity measurements are widely applied in industry, often to measure the concentration of ionic contaminants in water. The units for conductivity are Siemens/cm (S/cm). Siemens in older texts is given as Mhos, which represents that it is the reciprocal of resistivity in Ohms.

All the mixed systems containing nitrogen and oxygen mentioned earlier have been studied with regard to their AC conductivities. AC conductivity methods are preferred in measuring ionic conductivity over DC methods because in DC conductivity measurement techniques electrode polarization occurs. A special cell was constructed in the laboratory. Using inverted T-shaped polyethylene tube with two stainless steel electrodes at the end of the cell. A schematic sketch of the cell with electrodes is shown in Figure 2.9.

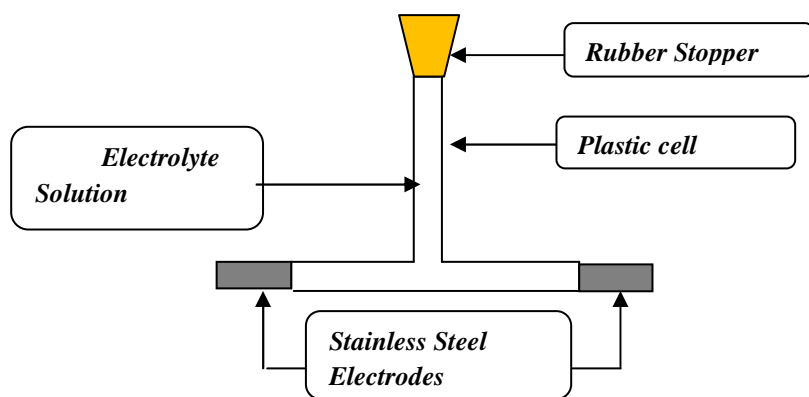


Figure 2.9 Schematic sketch of the Conductivity Cell

The cell shown in Figure 2.9 was connected to a frequency generator as the current source with an ammeter in series. The AC current was measured on the ammeter, varying the frequency over a large range (10 Hz- 10^5 Hz). A voltmeter is connected in parallel and the potential drop across the two electrodes is measured. A schematic representation of the complete conductivity set up is shown in Figure 2.10.

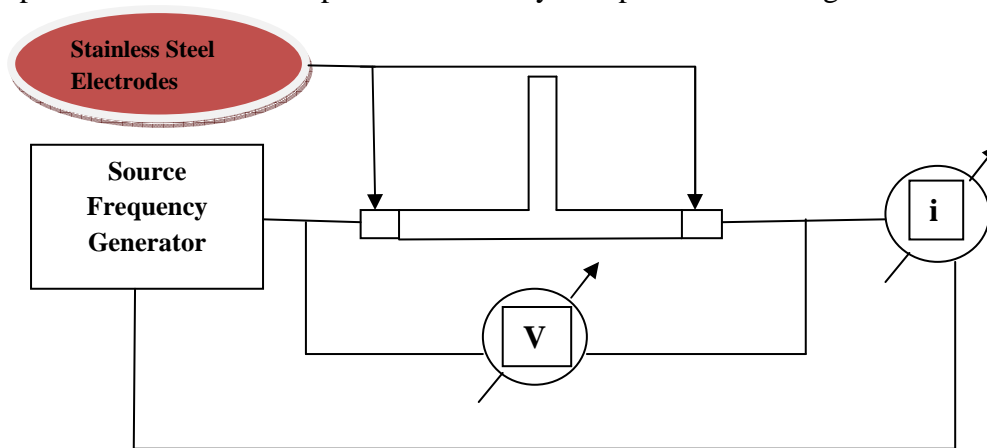


Figure 2.10 Schematic sketch for measuring AC conductivity.

The conductivity cell was tested for conductivity with a solution of KCl whose conductivity is known in the literature. The voltage (V) and current (I) were measured for the system over a large range of frequencies. The resistance (impedance for AC measurements) is calculated from the voltage and the current.

$$R = V/I$$

Equation 2.6

A plot of resistance versus logarithm of frequency is plotted as shown in Figure 2.11.

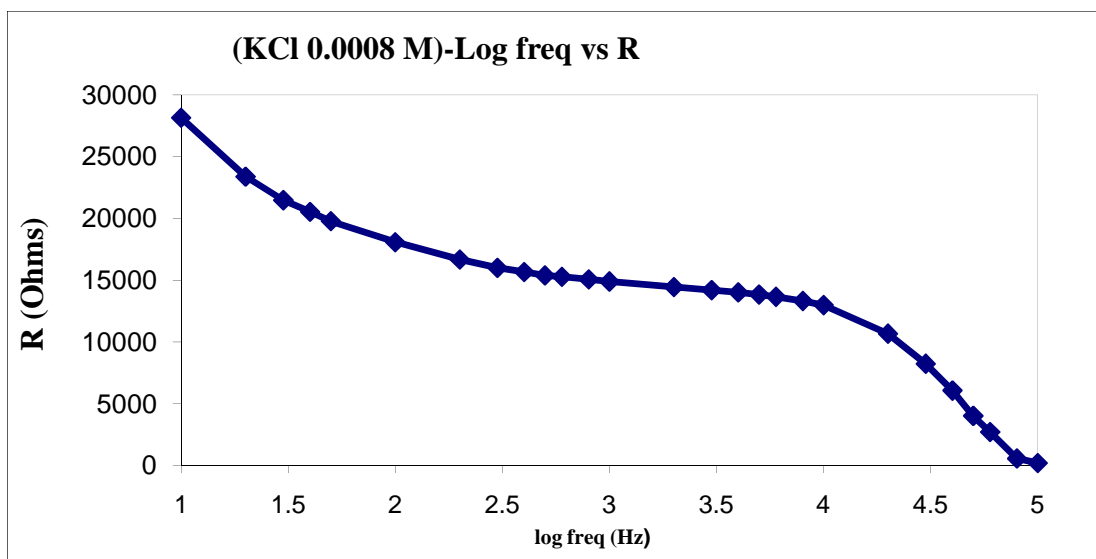


Figure 2.11 (Plot for aqueous KCl 0.0008 M at 25°C) - Log Frequency versus Resistance.

It can be seen from the plot above that resistance is relatively independent of the frequency around 1000 Hertz. The conductivity is measured at 1000 Hertz as the change in the slope for the resistance is minimal at 1000 Hertz. At higher frequency, the conductivity increases with increase in frequency as explained by the Debye-Falkenhagen effect²⁶. The specific conductivity (σ_s) can be calculated from the equation 2.6^{12,13}.

$$\sigma_s = C * \text{Cell constant.} \quad (\text{Equation 2.6})$$

Where C = conductance (1/ohms=Siemens) is simply the inverse of resistance.

The cell constant is dependent on the dimensions of the conductivity cell^{12,13,20}.

$$\text{Cell constant} = \frac{\text{Length or distance between the electrodes}}{\text{Area of the electrodes}} \quad (\text{Equation:2.7})$$

The unit for specific conductivity (σ_s) is 1/(ohms*cm), which can be written as (Siemens/cm).

The specific conductivity (σ_s) for the 0.0008 M KCl solution was measured 1.40×10^{-4} S/cm, which is close to the literature value $(1.18 \times 10^{-4} \text{ S/cm})^{21}$. The specific conductivity for 0.0008 M KCl gave a confirmation that the cell was of satisfactory design and could be used for specific conductivity measurements of the lithium salt solutions.

Having described the parameters for conductivity measurements and the construction of the cell, conductivity data for diethyl ether-triethylamine system can be discussed.

The conductivity data for the diethyl ether-triethylamine system is shown in Figure 2.12.

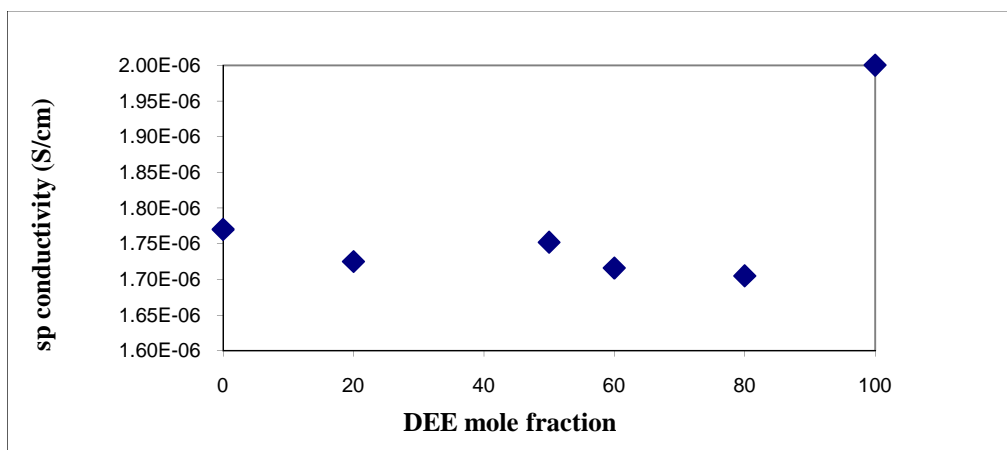


Figure 2.12 Plot of Diethyl ether mole fraction versus Specific conductivity. (Samples made with lithium triflate as salt with 80:1 heteroatom:Li ratio and measured at 25°C)

The conductivity, which is already fairly low in diethyl ether, appears to decrease abruptly with the addition of triethylamine. The change in the conductivity is not linear, and conductivity decreases sharply up to the 80% diethyl ether and 20% triethylamine point. Although a change from 1.7×10^{-6} to 2.0×10^{-6} S/cm is not a significant conductivity change, a sudden jump of specific conductivity is clear at 80% diethyl ether: 20% triethylamine. After that point, the conductivity more or less levels off. This appears to be contradictory to the interpretation of the ^7Li NMR data observed for the diethyl ether-triethylamine mixtures. If the lithium cation tends to be more free in triethylamine, the conductivity should increase with the addition of triethylamine to diethyl ether, but an opposite trend is seen as far as conductivity is concerned. Of course, conductivity also depends on the anion (triflate anion) of the salt. Therefore it was decided to investigate the NMR shifts of the fluorine of the triflate anion.

^{19}F NMR spectra were taken for the diethyl ether-triethylamine mixtures. The ^{19}F NMR data is shown in Figure 2.13.

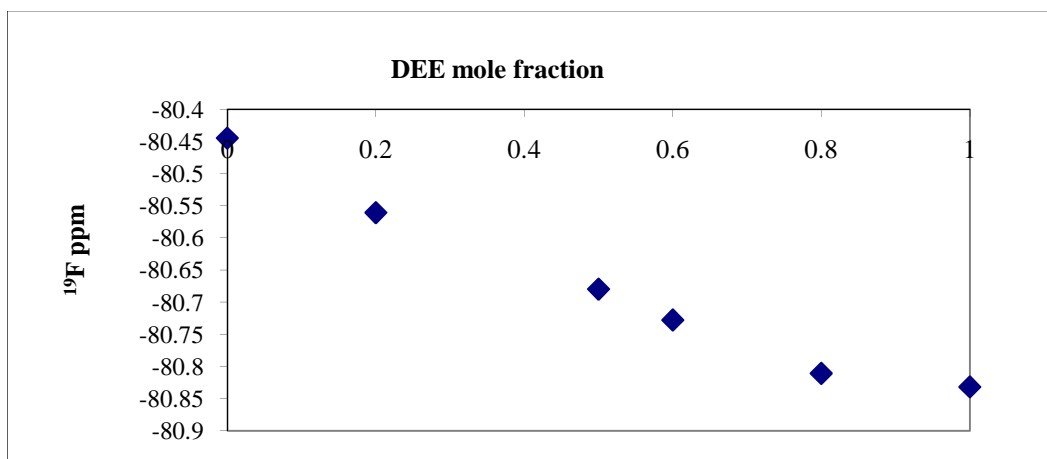


Figure 2.13 ^{19}F NMR data for TEA/DEE system. (Samples made with lithium triflate as salt with 80:1 heteroatom:Li ratio and measured at 25°C)

The ^{19}F data shows that with the addition of triethylamine to diethyl ether there is downfield shift in the chemical shift. This suggests that on the addition of triethylamine to diethyl ether the fluorine is deshielded as electron density decreases around the fluorine. The ^{19}F data suggests that the triflate gets more paired on the addition of the triethylamine to diethyl ether. The ^{19}F data is in agreement with the conductivity data where the conductivity decreases with more pairing of the triflate. One interesting feature of the ^{19}F plot occurs upon initial addition of triethylamine to diethyl ether. From the 100% diethyl ether to 80% diethyl ether-20% triethylamine point there is a downfield shift in the chemical shift but not as prominent as after the 80% diethyl ether-20% triethylamine point. An abrupt change in the chemical shift at 80% diethyl ether-20% triethylamine was seen with the ^7Li NMR chemical shifts. A similar break around 80% diethyl ether-20% triethylamine was also seen in the conductivity data.

Comparing the trends for ^7Li and ^{19}F NMR data, the ^7Li NMR data is in contradiction with the conductivity and the ^{19}F NMR data. A possible explanation for

these observations is that speciation does not result in discrete ion pairs or solvent-separated ions but rather in poorly defined aggregate species. Aggregates are species involving more than one lithium and one triflate clustered together. The aggregate speciation of the lithium and triflate complicates interpretation. Aggregates are well known to be present in oxygen and nitrogen containing solvents, but their exact structural nature is not well known understood and is likely highly variable¹¹. Further, a computational study done by Farid Ismail in our research group shows the formation of aggregates from lithium triflate in both amine- and ether-based solvents and also in mixtures of amine- and ether-based solvents. He has also showed that with changing nitrogen to oxygen ratios, the nature of the aggregates change. Considering the complexity of the species formed in these mixtures, two different general types of aggregate can be hypothesized to give a simplified explanation for the data observed for lithium triflate in the diethyl ether and triethylamine mixtures. The two different aggregate types are discussed below.

1) Lithium rich aggregates: The numbers of lithium cations in the aggregates are greater than the number of triflate anions (Figure 2.14). Thus the numbers of more-free triflate are higher and the chemical shift for ^7Li would trend toward more-paired lithium cation chemical shifts. Similarly, the chemical shift for ^{19}F for triflate anion would trend toward more-free triflate.

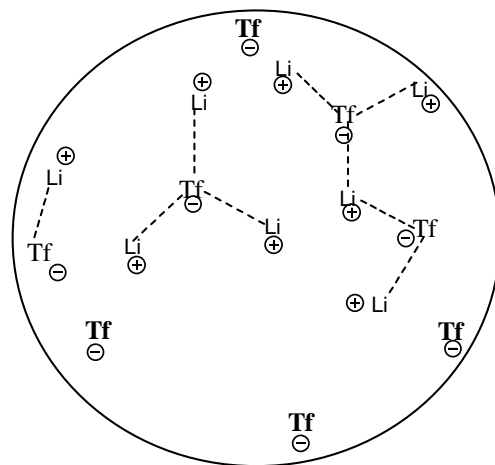


Figure 2.14 Lithium rich aggregate species

2) Triflate rich aggregates: The numbers of triflate anions in the aggregate are higher than the number of lithium cations (Figure 2.15). Thus the number of free lithium cations is higher and the chemical shift would trend toward more-free lithium cation chemical shifts. Similarly, the ^{19}F NMR chemical shift for the triflate would appear to trend toward more-paired triflate ion chemical shifts.

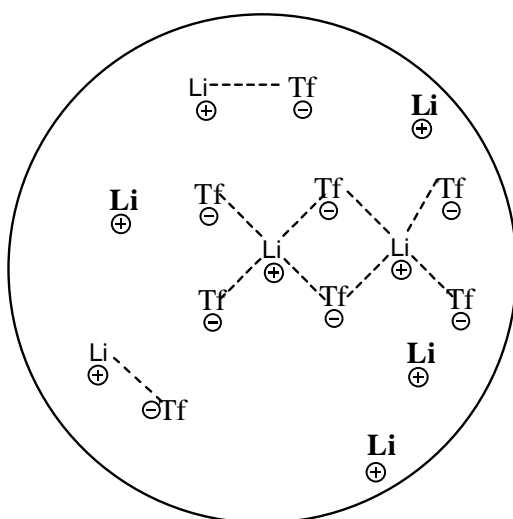


Figure 2.15 Triflate rich species of lithium triflate

It is important to note the number of “free” lithium cations and “free” triflate anions in the triflate rich aggregates and lithium rich aggregates, respectively. In the lithium rich aggregates, statistically, a number of more-free triflates are present. The more-free triflate would mean most of the lithium cations are more-paired and the lithium NMR chemical shift will show up relatively upfield as per the discussion earlier. On the contrary, in the triflate rich aggregates, statistically, a number of less-paired lithium ions are present. Thus the ^7Li NMR chemical shift will show up relatively downfield. The conversion from lithium rich species to triflate rich species or vice versa should go through a de-aggregated state of the lithium and triflate.

It is rather difficult to predict what the exact speciation is at a given point in time because of the limitations of the NMR technique as the observed chemical shift is a weighted average of all the species formed in the sample. Looking at the macroscopic picture of the solution, we could have the presence of lithium rich aggregates or the triflate rich aggregates present in the electrolyte solution. Dynamics of the electrolyte solution can complicate explanation further as these species are constantly exchanging with each other.

Nonetheless, the contradictory trends in the ^7Li NMR, conductivity and ^{19}F NMR data allow for a putative model to be put forth for lithium triflate in the diethyl ether-triethylamine mixtures. In 100% diethyl ether, if there are any aggregates present, the CCl_4 -diethyl ether data suggests the presence of triflate rich aggregates (lithium cation is less-paired). On the addition of small amounts of triethylamine to diethyl ether, ^7Li NMR data suggests the lithium cation to be less-paired, but the triflate becomes more-paired and the conductivity decreases. All these observations suggest that there

could be more formation of triflate rich aggregates on the addition of triethylamine. As the triflate rich aggregates are formed, the triflate gets more paired as observed in the ^{19}F NMR. Since the ^7Li NMR data suggest that the lithium get less paired on the addition of triethylamine to diethyl ether, the formation of triflate rich species can explain that observation too. Since more triflate rich aggregates are formed, the lithium cation tends to be less-paired in the aggregates, which can be seen in the ^7Li NMR shifts. On addition of more triethylamine to diethyl ether, there could be increase in the number or the size of the triflate rich aggregates. The increase in the number or the size of the triflate rich aggregates would be consistent with the decrease in the conductivity, as it is a known fact that aggregates contribute less to conductivity²⁷. After a certain point, (70% diethyl ether and 30% triethylamine) the triflate rich aggregates have mostly formed as most triflates are already engaged in the aggregates. This results in no further decrease in the conductivity and the ^7Li NMR chemical shift after adding ca. 30% triethylamine to diethyl ether.

The above explanation does not include any specific interactions with the solvents and the argument is solely based on the lithium and triflate aggregation. It is well known that dielectric constant of the solvent often can have a significant effect on the speciation of a salt in a solvent²⁷. To investigate if the nitrogen and oxygen of the triethylamine and diethyl ether respectively has any specific interaction with the lithium triflate that would facilitate the aggregation in these mixtures, changes in the trend of dielectric constant of these mixtures were measured using an EPR technique which will be discussed in detail in Chapter 3. Since there will be a lot of mention to the EPR technique to measure the change in the dielectric constant in this chapter, it is important

to establish the basic relationship between the EPR signal intensity and dielectric constant. The EPR signal intensity decreases with increase in the dielectric constant of the solvent or salt solution.

The aggregation phenomenon described could be attributed simply to the decreasing the dielectric constant of the solvent mixtures, which decreases linearly from 4.8 for diethyl ether to 3.2 for triethylamine (*vide infra*). However, the dielectric constant data trend for the lithium triflate solutions studied by the EPR technique is shown in Figure 2.16.

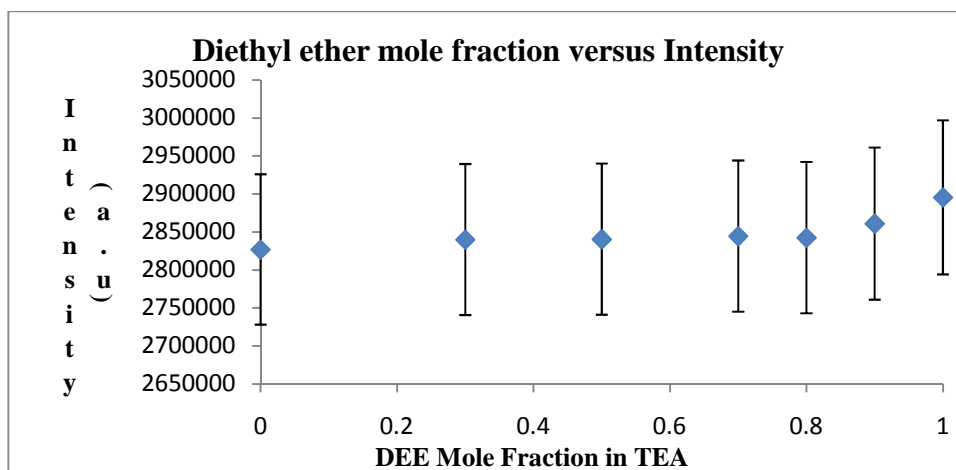


Figure 2.16 Plot of DEE/TEA mole fraction versus EPR signal intensity (a.u.). (Samples made with lithium triflate as salt with 80:1 heteroatom:Li ratio and error bars represent 3.5% error)

The EPR data for the diethyl ether-triethylamine with lithium triflate system shows little change in the EPR signal intensity (from 2820000 to 2890000) with increasing the mole fraction of diethyl ether. The error bars on the data represent a 3.93 % error in measurement of the signal intensity using this technique. The dielectric constant of the salt solutions is constant within experimental error. There is a slight increase in the intensity after the 80% diethyl ether point to the 100% diethyl ether point

is observed. If correct this was unexpected since the EPR signal intensity of the mixtures on the addition diethyl ether to triethylamine without any lithium triflate should decrease. The ^7Li and ^{19}F data suggests that on the addition of triethylamine to diethylether, there is formation of triflate rich aggregates. The EPR data suggests that the triflate rich aggregates formed are somewhat more polarizable and therefore the intensity decreases which means the dielectric constant increases. The increase in dielectric constant is seen up to 80% diethyl ether point, after which there is not a significant change in the speciation, causing the EPR signal intensity to stay constant, which suggests that the dielectric constant stays constant. The EPR data fits with the conductivity and the spectroscopic data. Detailed explanation of the dielectric constant effect in these mixtures for diethyl ether and triethylamine is complicated due to the aggregate formation. It is difficult to determine exactly how an aggregate (triflate rich or lithium rich) would affect the dielectric constant of the electrolyte solution.

2.10 TMEDA (N,N,N',N'-tetramethylethylenediamine) versus MG (Monoglyme) - 2 Nitrogens versus 2 Oxygens

Although diethyl ether and triethylamine represent the heteroatoms present in the PEO/PEI hybrid polymer, the diethylether-triethylamine system would not mimic the PEO/PEI hybrid solid polymer electrolyte very closely. To investigate further and choose a system that would much more closely represent PEO/PEI hybrid polymers, monoglyme and TMEDA were chosen as the nitrogen and oxygen based solvents. With these solvents, the chelating effects from having heteroatoms in close spatial proximity will be observed, which is expected in the PEO/PEI hybrid solid polymer electrolytes. The ^7Li NMR data for monoglyme and TMEDA is shown in Figure 2.17.



Figure 2.17 Plot for monoglyme mole fraction versus ^7Li ppm. (Samples made with lithium triflate as salt with 80:1 heteroatom:Li ratio and measured at 25°C)

The ^7Li NMR chemical shift for TMEDA/Monoglyme with lithium triflate covers a broader range when compared to the DEE/TEA system. The range of the chemical shift for the ^7Li NMR goes from 0.4 ppm to -0.75 ppm. The trend seen for the system is similar to the TEA/DEE system. The ^7Li NMR shows a shift in the chemical shift from upfield to downfield, which suggests that the lithium cation is becoming deshielded on the addition of TMEDA to monoglyme. Thus, the lithium cation appears to be less-paired on the addition of TMEDA to monoglyme. When compared to the diethyl ether-carbon tetrachloride mixtures, the change in the ^7Li chemical shift is not linear as seen for the diethyl ether-carbon tetrachloride mixtures. It again appears from the plot (similar to the diethyl ether/triethylamine mixtures) that the nitrogen holds on to the lithium tightly and the equilibrium lies in favor of the effect of the nitrogens of TMEDA more than the oxygens of monoglyme.

Since the ^7Li NMR did not explain the phenomena in detail, AC conductivities were done on the monoglyme and TMEDA mixtures. The plot of mole fraction of TMEDA in monoglyme vs specific conductivity is shown in Figure 2.18.

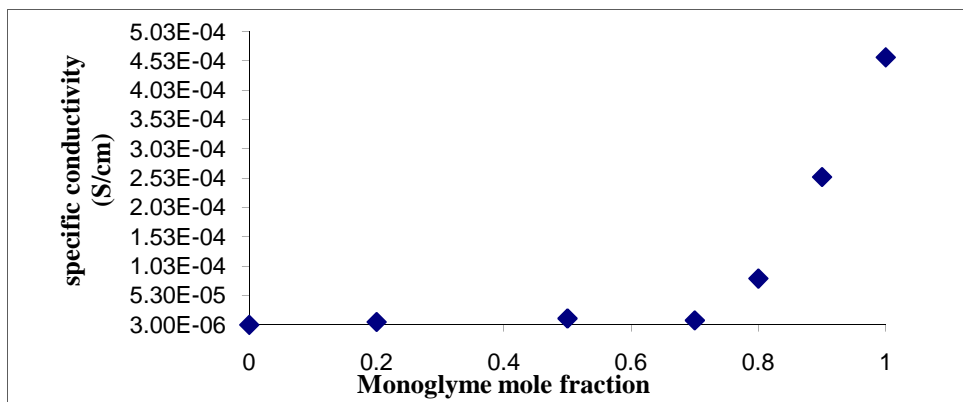


Figure 2.18 Plot of Monoglyme Mole Fraction in TMEDA versus specific conductivity. (Samples made with lithium triflate as salt with 80:1 heteroatom:Li ratio and measured at 25°C)

The specific conductivity data was surprising. Although the trend for the specific conductivity looks similar to the TEA/DEE system, the specific conductivity covered a much larger range than that of the TEA/DEE system. The specific conductivity shows higher values at the higher mole fractions of monoglyme. The specific conductivity for 100% TMEDA is approximately 3×10^{-6} S/cm and reaches all the way up to 4.5×10^{-4} S/cm for 100% monoglyme. The most interesting part of the trend is the region in which the specific conductivity decreases with increasing mole fraction of TMEDA. The specific conductivity drops significantly until the 70% Monoglyme - 30% TMEDA point, after which further addition of TMEDA does not cause a significant change in the specific conductivity. Again, this was a contradiction to the ^7Li NMR data where the lithium cation appears to get less paired with the addition of TMEDA to the monoglyme whereas the conductivity decreases with the addition of TMEDA to monoglyme.

Certainly, it appears that the formation of aggregates also plays a significant role in the monoglyme and TMEDA mixtures. To add evidence for aggregate formation again, monitoring of the triflate anion in the monoglyme and TMEDA mixtures with the ^{19}F NMR was done and is shown in Figure 2.19.

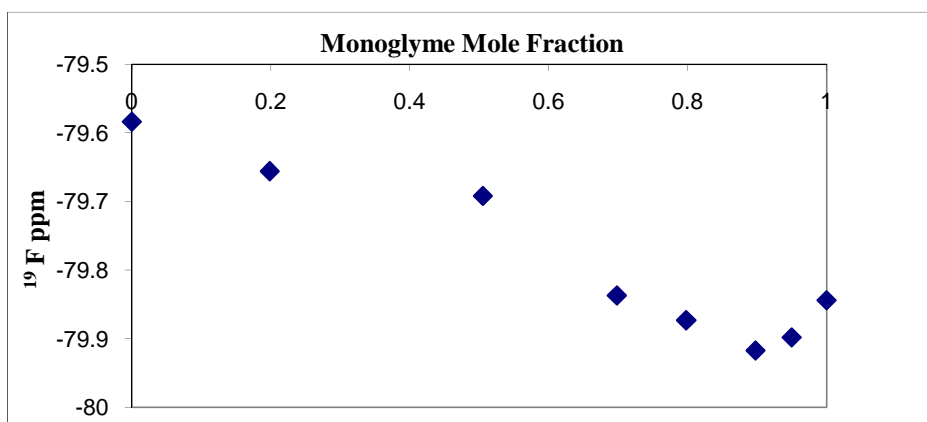


Figure 2.19 Plot for Monoglyme mole fraction in TMEDA versus ^{19}F NMR chemical shift. (Samples made with lithium triflate as salt with 80:1 heteroatom:Li ratio and measured at 25°C)

The ^{19}F NMR chemical shift for TMEDA/Monoglyme system shows behavior similar to that seen for the DEE/TEA system except for the small downfield shift seen at 90% monoglyme-10% TMEDA. On the addition of small amount of TMEDA to monoglyme, the chemical shift shifts upfield, which suggests that the triflate becomes less-paired. Further addition of the TMEDA to monoglyme shifts the chemical shift downfield, which suggests that the triflate starts becomes more-paired. Again, this behavior was surprising and not expected. The triflate data mostly fits with the conductivity data where the triflate starts to get more paired the conductivity starts to decrease. But the initial upfield shift of the triflate does contradict the conductivity data. This behavior can again be explained by the formation of aggregate species. Though the exact nature of these aggregates is difficult to predict based just on the data obtained, a

speculation can be made about the aggregate formation based on the data observed. On an absolute scale, the ^{19}F NMR chemical shift does not show a big shift. For ^{19}F NMR a shift of approximately 0.4 ppm is small when compared to the range covered in the ^{19}F NMR (approximately 350 ppm). This suggests that the interactions taking place in these solutions is not as large enough to create a big change in the chemical shift. Another important observation to be made here is that relative to the ^{19}F NMR chemical shift range for the TEA/DEE system, the ^{19}F chemical shift range for TMEDA/Monoglyme system is relatively downfield. This shows that the triflate is more paired over the entire range than is seen in the TEA/DEE system.

From the ^7Li NMR, conductivity, and ^{19}F NMR data, speculation can be made that on the addition of TMEDA to monoglyme there is formation of triflate rich aggregates. The initial dip in the ^{19}F NMR where the triflate appears to move upfield, suggesting that the triflate gets less-paired, is difficult to explain but could be due to subtle changes in the aggregate speciation and this area may be worthy of further study. After the dip on the ^{19}F data, everything seems to fit the ^7Li , conductivity, and ^{19}F NMR data to suggest that the triflate rich aggregates are formed. Similar to the diethyl ether and triethylamine mixtures, assuming that the triflate rich aggregates are formed which will make the lithium appear less-paired and the triflate more-paired. On the addition of more TMEDA to monoglyme, the formation of triflate rich aggregates can grow in size or number, which shifts the ^7Li NMR chemical shift downfield and shift the ^{19}F downfield. Further addition of TMEDA to monoglyme does not cause any significant change in the triflate rich aggregates, which causes the ^7Li NMR chemical shift and the conductivity to change insignificantly.

The above explanation for the triflate rich aggregates does not include any specific interactions of the solvents (monoglyme and TMEDA) with lithium triflate and only deals with aggregate formation between lithium and triflate. To investigate the solvent interaction with lithium triflate, monoglyme-TMEDA salt mixtures were also measured for changes in dielectric constant. Before measuring the lithium triflate salt solution of monoglyme and TMEDA mixtures, monoglyme and TMEDA mixtures without the salt were measured (Figure: 2.20) for reference to compare it with the dielectric constant trend of the monoglyme and TMEDA mixtures with lithium triflate. All the measurements were done using the EPR technique mentioned earlier and discussed in detail in Chapter 3.

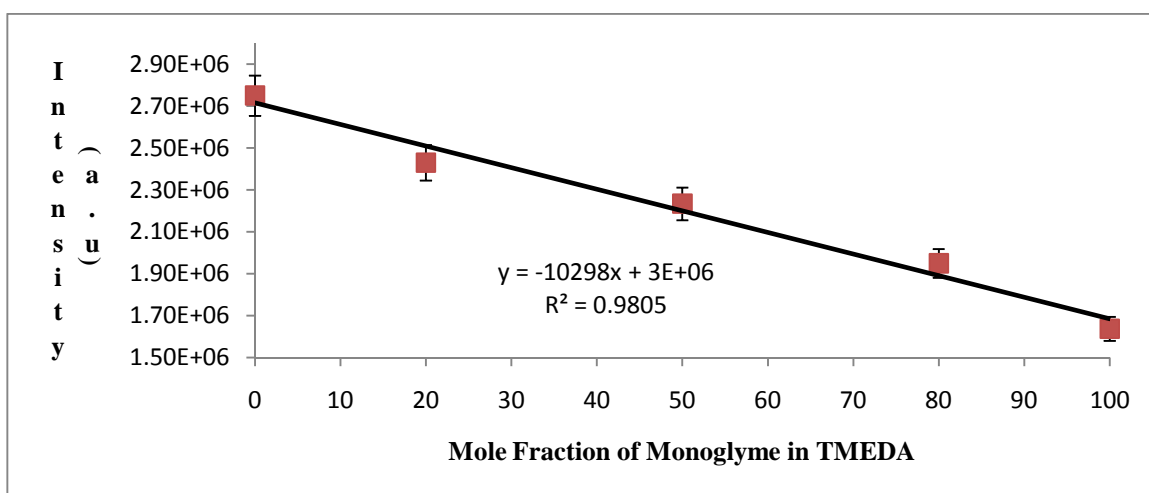


Figure 2.20 Plot of Mole fraction of monoglyme in TMEDA (without lithium triflate) vs EPR Intensity (a.u). Error bars represent 3.5% error in the intensity.

As seen in Figure 2.20, the EPR signal intensity changes linearly for different monoglyme and TMEDA mixtures. The dielectric constant for pure TMEDA is 2.8 whereas the dielectric constant for pure monoglyme is 7.2. With the addition of TMEDA to monoglyme without any salt, the change in the dielectric constant is linear

for monoglyme - TMEDA mixtures. The data for the change in the dielectric constant for different monoglyme-TMEDA mixtures with lithium triflate is given in Figure 2.21.

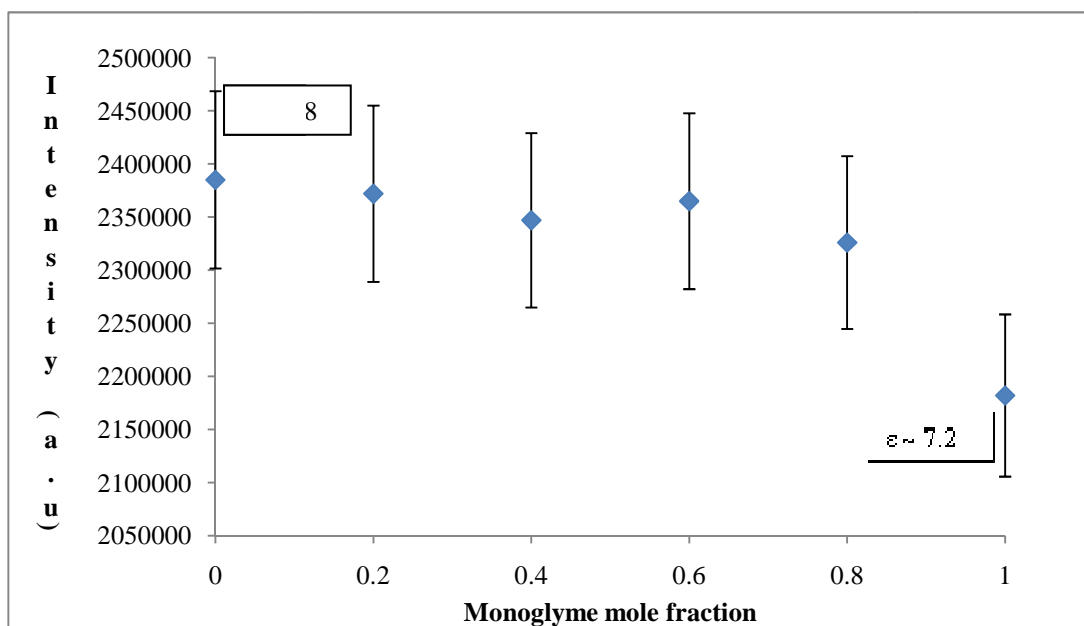


Figure 2.21 Plot of EPR intensity versus Mole fraction of TMEDA in Monoglyme. (Samples made with lithium triflate as salt with 80:1 heteroatom:Li ratio) Error bars represent an error of 3.5%.

As seen from Figure 2.21, from 100% TMEDA-lithium triflate to 100% monoglyme-lithium triflate, the intensity changes from 2170000 to 2370000 with an error of 2% for every measurement. This change in the EPR signal intensity is more significant than the one seen in TEA-DEE system. The more important issue is the change in the trend seen in the plot. The plot shows a nonlinear trend for the change in the dielectric constant for TMEDA-Monoglyme system with lithium triflate as salt. The comparison of the two plots, with and without salt, suggest that there is a specific interaction of the solvent with the salt which affects the dielectric constant of the mixed

systems. However, it is difficult to draw conclusions about the exact kind of interactions the solvents have with the salt with the data presented.

In Figure 2.21, the trend again shows a break at the 80% Monoglyme-20% TMEDA point. The observation supports the data seen in ^7Li NMR data and follows the same trend as seen for ^7Li NMR chemical shift. As seen from the EPR data, the change in the dielectric constant of the system is significant (intensity range from 2170000 a.u to 2370000 a.u). At the 100% TMEDA point, it shows a relatively higher intensity which in turn means a lower dielectric constant. The ^7Li , ^{19}F and specific conductivity data suggest that with the increase in the TMEDA fraction, the triflate rich aggregates increase in size or number. As we add a fraction of TMEDA to the monoglyme an increase in the intensity is seen which suggests that there is a decrease in the dielectric constant. This observation suggests that the species (not aggregates necessarily) formed in 100% monoglyme are more polarizable on the application of the electric field. On the addition of TMEDA, with the formation of triflate rich aggregates, the polarizability of these aggregates is low and therefore the dielectric constant decreases. After the 80% monoglyme-20% TMEDA point, we speculate that insignificant amounts of aggregate formation continues, which is reflected in the dielectric constant plot showing minimal changes in EPR signal intensity (dielectric constant) of the mixtures. Although unlikely, the change in the dielectric constant could also be a result of the changing volume fraction of the solvent and a change in the concentration of the lithium triflate in the sample. More investigation is needed in this case to come to a strong conclusion.

Since the dielectric constant measurements showed that the solvents do have specific interactions with the salts, it was decided to study the lithium triflate salt

mixtures of monoglyme and TMEDA without any applied electric field. The self diffusion coefficient for these monoglyme-TMEDA mixtures with lithium triflate were measured using Pulse Field Gradient (PFG) techniques on both the ^7Li and ^{19}F . A brief discussion of the theory behind PFG techniques will be discussed in the following section, after which the PFG results for the monoglyme-TMEDA mixtures with lithium triflate will be given. The self diffusion results will also be related to the conductivity results for the monoglyme-TMEDA mixtures with lithium triflate.

2.11 Pulse Field Gradient NMR measurements for Lithium Triflate in the TMEDA-monoglyme system ^{14,15,16,19}

To investigate the TMEDA-monoglyme system in more detail, self-diffusion coefficient studies were carried out on lithium triflate in different mole fractions of monoglyme in TMEDA using pulse field gradient NMR techniques. Self diffusion coefficients measure the self diffusivity of the cation and the anion in the solution without the application of any external field.

Self diffusion is a measure of the translational motion of molecules or ions due to the internal kinetic energy of the system. Self diffusion is an important phenomenon in a system as it is responsible for the collision of the molecules when a reaction between two molecules occurs. Diffusion depends on the molecular size of the diffusing species and is expressed by Stokes-Einstein equation (Equation 2.8).

$$\mathbf{D} = \mathbf{kT}/f \qquad \qquad \qquad (\text{Equation 2.8})$$

Where D = diffusion coefficient, k = Boltzman constant, T = Temperature in $^{\circ}\text{K}$, and f = friction coefficient.

The friction coefficient (f) can be given as

$$f = 6\pi\eta r_s$$

where η = viscosity of the solution and r_s = Stokes radius of the species diffusing. From the latter equation it can be seen that diffusion of the cation or anion depends on the viscosity and as the viscosity increases the diffusivity decreases.

Diffusion coefficients can also be related to specific conductivity by the Nernst Einstein equation (Equation 2.9).^{17,18,19}

$$\sigma = \frac{nq^2}{kT} [D(Li^+) + D(CF_3SO_3^-)] \quad (\text{Equation 2.9})$$

where σ = ionic conductivity, D = Diffusion coefficient, q = charge on the species, n = number of charge carriers per unit volume, k = Boltzman constant, and T = temperature in °K.

The above-mentioned Nernst-Einstein equation can be applied to calculate ionic conductivity of the electrolyte solution. When the above equation is applied to the system, an assumption is made that the salt is completely dissociated. Generally, ionic conductivity values calculated using the Nernst-Einstein equation are higher than measured ionic conductivity values due to the different ionic species formed in the electrolyte solution, especially those which do contribute to the diffusion coefficient and not to the ionic conductivity.

Since the scope of this thesis is limited to understanding transport of the lithium cation and the triflate anion in mixed solvent systems containing nitrogen and oxygen as heteroatoms, explanation of the Pulse field gradient technique will be limited to a

qualitative explanation of the theory behind the experiment. In a pulse field gradient experiment, a coil of wire is placed around the x-axis which will provide additional magnetic field in addition to the static magnetic field (B_0) along the z-axis. Figure 2.22 shows a schematic diagram of pulse sequence set up to measure the diffusion coefficients of the samples^{15,19}.

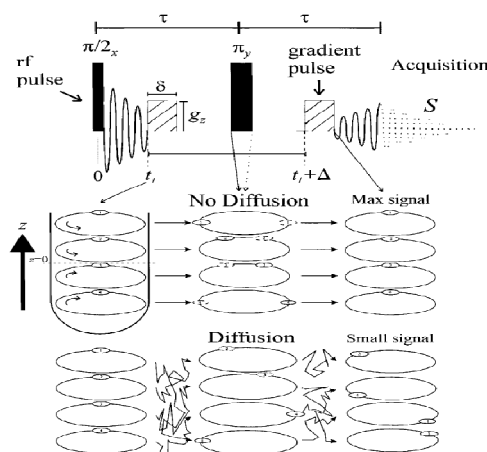


Figure 2.22 Schematic of the pulse sequence^{15,19}.

Consider a collection of spins diffusing at thermal equilibrium so that the net magnetization is along the z-axis. A 90° radiofrequency pulse is applied, which rotates the magnetization in the x-y plane. During the first τ period at time t_1 , a gradient pulse of time δ and magnitude g is applied and, due to the gradient field applied, the spin of the nuclei experiences a phase shift. At the end of the first time span τ , a 180° pulse is applied which reverses the sign of the precession and also reverses the sign of the applied field and the static field. At the time $t + \Delta$, another pulse of equal gradient and magnitude is applied. If the spins do not have any translational motion, the effect of the two gradient pulses cancel each other and thus, the spins refocus and show no change in the size of the observed peak. If there is a translational motion which moves the spins,

the extent of dephasing is directly proportional to the displacement in the direction of the gradient during the period Δ and the effects of the two gradient pulses do not cancel each other. The extent of the non-cancellation enhances due to increases in the phase shift or increasing displacement along the z-axis. The haphazard phase shifts are averaged all over the collection of nuclei that contribute to the NMR signal. Thus, the NMR signal does not shift phases but attenuates, and the greater the diffusion, the greater is the attenuation of the signal¹⁵.

The TMEDA-Monoglyme mixtures with different mole fraction of monoglyme in TMEDA with lithium triflate (80:1 = heteroatom:Li ratio) as a salt were investigated using the pulse field gradient NMR technique to measure the self diffusion coefficients. The results are summarized in Table:2.3.

Monoglyme %	TMEDA %	⁷ Li Diffusion Coefficients (m ² /s)	¹⁹ F Diffusion Coefficients (m ² /s)
0	100	6.93e-10	7.47e-10
20	80	7.43e-10	7.64e-10
40	60	8.46e-10	8.40e-10
50	50	8.53e-10	8.30e-10
60	40	8.93e-10	8.98e-10
80	20	9.21e-10	9.20e-10
90	10	1.07e-9	1.08e-9
100	0	1.23e-9	1.21e-9

Table 2.3 ⁷Li and ¹⁹F Self diffusion coefficients for TMEDA-MG/LiTf (80:1 = Heteroatom:Li) solutions. (Samples made with lithium triflate as salt with 80:1 heteroatom:Li ratio and measured at 25°C)

A plot of monoglyme mole fraction in TMEDA versus self diffusion coefficients for ^7Li and ^{19}F are plotted in Figure: 2.23.

The first and the foremost observation is that the ^7Li and ^{19}F have similar self diffusion coefficients. This could be due to ionic association of the lithium and triflate to form ion pairs or aggregates which causes the lithium and the triflate to diffuse together, thus resulting in the diffusion coefficients being similar for lithium and triflate.

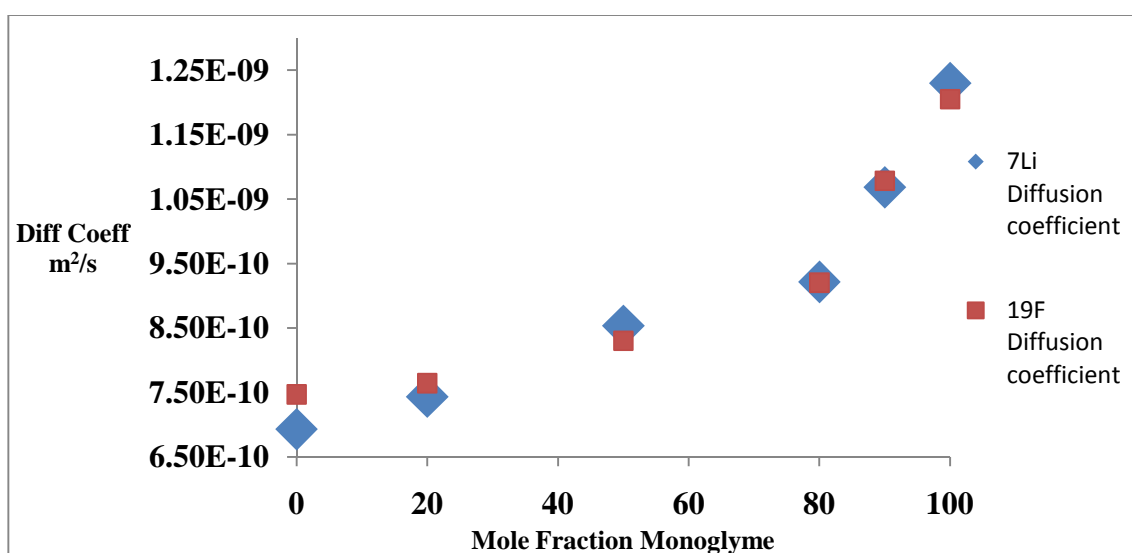


Figure 2.23 Plot of mole fraction of monoglyme in TMEDA versus self diffusion coefficients for ^7Li and ^{19}F . (Samples made with lithium triflate as salt with 80:1 heteroatom:Li ratio and measured at 25°C)

From the plot it can be seen that the ^7Li and the ^{19}F self diffusion coefficients values increase with an increase in the monoglyme mole fraction in TMEDA. The increase is not linear and the increase of self diffusion coefficients is slow up to ca. 80% monoglyme point, after which there is a sudden increase in the slope of the self diffusion coefficient. This observation is interesting as the ^7Li NMR shifts, the dielectric constant trend, and the specific conductivity show the same break at the ca. 80%

monoglyme point as discussed in the chapter earlier. As described earlier, at the 80% point, the speciation could be undergoing a drastic change so that relatively more lithium is less paired, thus exhibiting a break in the trend. As the dielectric constant shows the same trend (break at 80% monoglyme point), it hints that the same phenomena in which species form that orient better in the electric field and can be more polarized. Quantification of the ionic association from the self diffusion data follows.

The Nernst-Einstein equation establishes a relationship between ionic conductivity and diffusion coefficients.¹⁸ One of the assumptions made by the Nernst-Einstein equation is that when the salt is dissolved in the solvent, it is assumed to be completely dissociated. The Nernst-Einstein equation can be modified to Equation 2.10:

$$\sigma(\textit{calculated}) = \frac{nq^2}{kT} [D(\textit{Li}^+) + D(\textit{CF}_3\textit{SO}_3^-)] \quad (\textit{Equation 2.10})$$

It is also known from the literature that not all the salt is dissociated and there is ionic association seen in the solution. The actual measured conductivity ($\sigma_{\text{(measured)}}$) is lower than the calculated ionic conductivity. The difference in the measured ionic conductivity and the calculated ionic conductivity is due to ionic association and the formation of species which contribute to the diffusion and not to the ionic conductivity. A quantification of the ionic association can be given by Equation 2.11.^{18,19}

$$\sigma_{\text{(measured)}} = \sigma_{\text{(calculated)}} (1 - \Delta) \quad (\textit{Equation 2.11})$$

The equation gives the fraction of ions that are ionically associated and also the fraction of ions which are free. Table 2.4 summarizes the measured conductivity, calculated conductivity, and fractions of ionic associated species (Δ)

Mole fraction of Monoglyme in TMEDA with LiTf (80:1=Heteroatom:Li)	Measured conductivity σ_{measured}	Calculated conductivity $\sigma_{\text{calculated}}$	Fraction of Ionic associated species (Δ)	% of Ionic associated species (%) (Δ)
0	3.00e-6	0.907	0.999(99669)	99.9(99669)
20	7.80e-6	1.01	0.999(99227)	99.9(99227)
50	1.38e-5	1.25	0.999(98893)	99.9(98893)
80	8.19e-5	1.53	0.999(94656)	99.9(94656)
90	2.55e-4	1.86	0.999(86293)	99.9(86293)
100	4.59e-4	2.20	0.999(79148)	99.9(79148)

Table 2.4 Ionic associated species fraction in monoglyme and TMEDA mixtures with lithium triflate as salt (Numbers shown for three significant figures. Numbers in parentheses are shown to display the calculated small change in the ionic association on addition of TMEDA to monoglyme).

Figure 2.24 shows a plot for data of % fraction of ionic associated species is plotted against monoglyme mole fraction.

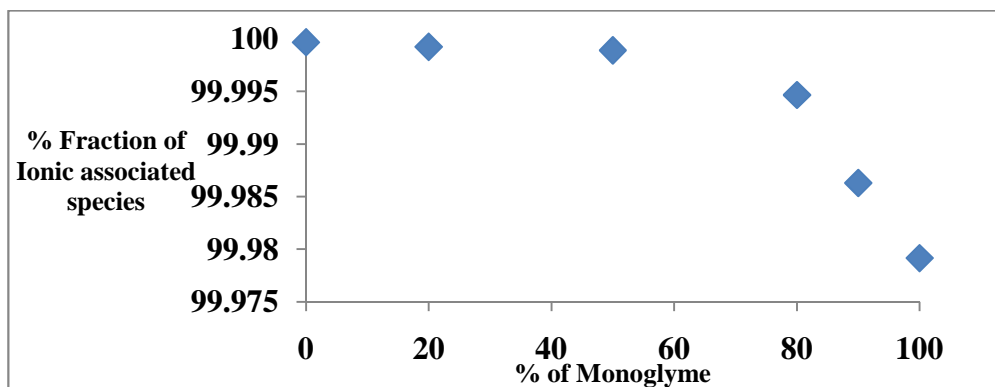


Figure 2.24 Plot of % Monoglyme in TMEDA versus % Fraction of Ionic associated species. (Samples made with lithium triflate as salt with 80:1 heteroatom:Li ratio and measured at 25°C)

As seen from the Figure: 2.24, considering the absolute fraction of ionic association, more than 99 % of the ions are ionically associated in either pure solvent and only a small amount of the ions tend to be free. But relatively, the amount of free ions increases on the addition of monoglyme. Although a decrease in the ionic association is observed, the change is not linear. The decrease in the fraction of species being ionically associated decreases initially at a slower rate until the ca. 80% monoglyme point. After the 80% monoglyme point, the decrease in the ionic association is fast and a break is seen in the trend at the 80% monoglyme point. This observation is important as the change in the dielectric constant follows the same trend. Comparing the dielectric constant data and the ionic association data, one can speculate that with the formation of different species of the lithium triflate in the TMEDA-monoglyme system, the change in the dielectric constant is responsible for the speciation and the mobility of the ions in the system.

An interesting observation can be made by comparing the self-diffusion data to the ionic association data, especially in the region from 0% monoglyme to 80% monoglyme. For the self diffusion data, the region from 0% monoglyme to 80% monoglyme shows a slow but steady increase in the self diffusion till the 80% monoglyme point. When the ionic association data is considered, the data shows not much of a change in the ionic association till the 80% monoglyme point which tracks the trend shown by the specific conductivity data. This is consistent with the specific conductivity depending largely on the “freer” ions present in the solution, whereas the self diffusion coefficient depends on all the species. After the 80% monoglyme point,

the speciation changes and more free ions are present which contribute to both the self diffusion coefficient and the specific conductivity.

As mentioned in Section 2.4, to carry out the investigation further on the systems which mimic the PEO/PEI systems, more solvents with nitrogens and oxygens were studied. The systems which were studied are given below;

- 1) Triethylamine (TEA) vs Monoglyme
- 2) TMEDA vs Diethylether (DEE)
- 3) G1 vs Monoglyme
- 4) G1 vs TMEDA

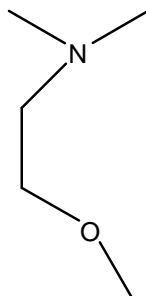


Figure 2.25 Structure of 2-methoxy-N,N-dimethylethanamine (G1)

To get a larger picture of the phenomena taking place in the competition between nitrogen and oxygen with the lithium and triflate, master plots for ^7Li , ^{19}F , specific conductivity and change in dielectric constant are plotted. In these master plots, ^7Li , ^{19}F , conductivity and change in dielectric constant data for TEA vs DEE, TMEDA vs Monoglyme, TEA vs Monoglyme, TMEDA vs DEE, G1 vs Monoglyme and G1 vs TMEDA are plotted on the same scale on a graph and will be compared.

2.12: Master Plots for ^7Li , ^{19}F and Specific Conductivity:

The ^7Li , ^{19}F , conductivity data and change in the dielectric constant for all the systems were plotted on the same chart. This will be helpful in comparing all the systems together on similar scale. Since all the systems involve mixed heteroatoms, nitrogen and oxygen, it will be easier to compare all the systems with % oxygen on the x-axis rather than having the mole fraction of a particular solvent in mixed nitrogen and oxygen solvents. When plotting on the same plot, the plotting of the G1 mole fraction becomes a problem as G1 molecule has one nitrogen and one oxygen. For the sake of simplicity, all the plots will be plotted against % oxygen versus ^7Li , ^{19}F , specific conductivity and change in dielectric constant.

Figure 2.26 shows a plot for % oxygen versus ^7Li NMR chemical shifts in ppm.

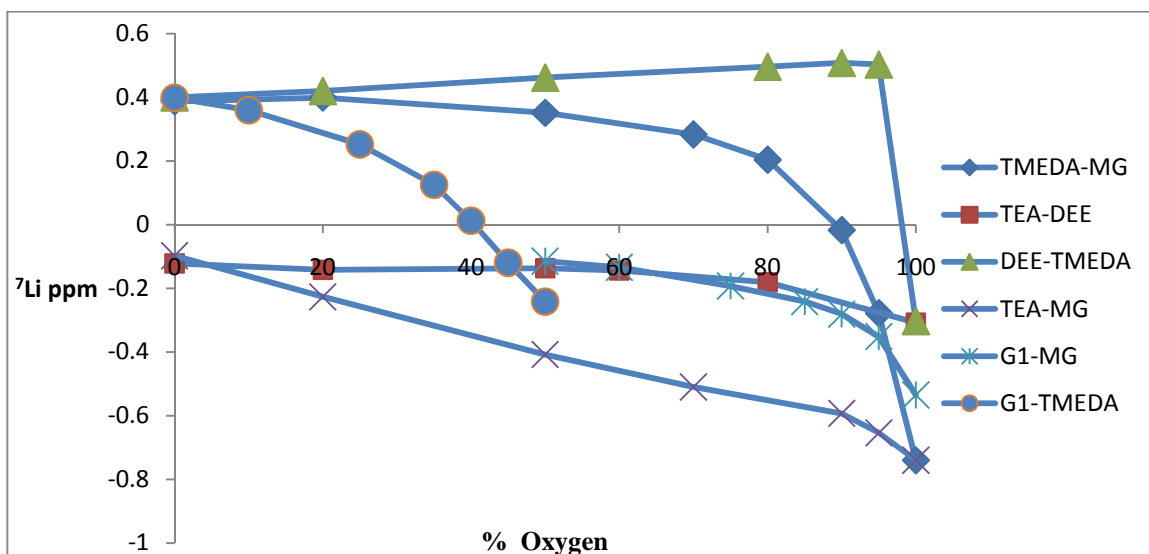


Figure 2.26 Plot of % Oxygen versus ^7Li NMR chemical shifts in ppm. (Samples made with lithium triflate as salt with 80:1 heteroatom:Li ratio and measured at 25°C)

The ^7Li shows significant changes with increasing % of oxygens in all the systems. The first observation to make here is the TMEDA-monoglyme system, covers the largest range of chemical shifts in the ^7Li NMR chemical shifts. Comparing the TMEDA-monoglyme to triethylamine-diethyl ether system, the triethylamine-diethyl ether curve does not show much of a change in the ^7Li NMR chemical shift. This suggests that chelation effect of the TMEDA and monoglyme shows a huge effect versus just the coordination effect of the triethylamine and diethyl ether.

One interesting observation is systems which have one chelating solvent and one coordinating solvent, i.e. triethylamine-monoglyme and TMEDA-diethyl ether. A large chelation effect can be seen triethylamine-monoglyme system and the TMEDA-diethyl ether system. In the TMEDA-diethyl ether system, on the addition of small amount of TMEDA to diethyl ether, the huge downfield shift suggests that the chelation effect of TMEDA competes strongly against the diethyl ether coordination effect. On the contrary, the coordination triethylamine appears to compete effectively with the monoglyme but not to the same extent as that of the chelation effect seen in the TMEDA-monoglyme system. The coordination of nitrogens of triethylamine competes and balances the chelation effects of the oxygens of monoglyme.

Another important effect is the comparison between G1-TMEDA, G1-Monoglyme and TMEDA-Monoglyme. Essentially, the G1-TMEDA and G1-monoglyme systems together should structurally represent the TMEDA-monoglyme. So the G1-TMEDA and G1-monoglyme should show similar chemical shifts and trends as the TMEDA-monglyme system. However, there is a big difference between the change in ^7Li NMR shifts for G1-monoglyme, G1-TMEDA and the TMEDA-monoglyme

system. The data suggests that the chelation effects of the G1 solvent are different than that of the TMEDA solvent. This can be explained by the fact that G1 has two different heteroatoms, nitrogen and oxygen, which have different coordinating tendencies.

Further, similar master curve was plotted for conductivity for all the systems. It would be of real interest to see any chelation effects and heteroatom effects discussed for the ^7Li NMR master plot have effect on the conductivity of the systems. The plot for % oxygen versus specific conductivity (S/cm) is given in Figure 2.27.

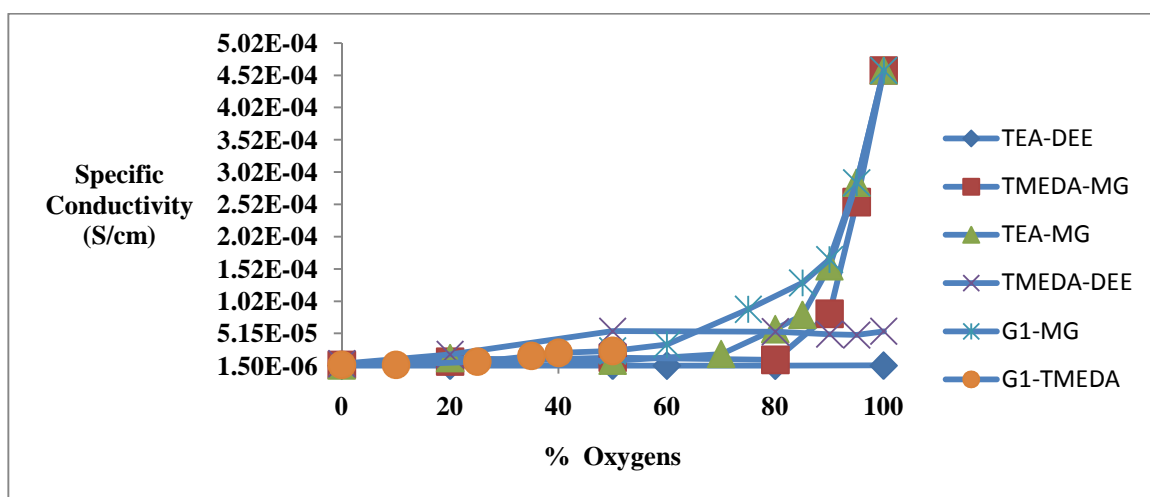


Figure 2.27 Plot of % Oxygen versus Specific conductivity (S/cm). (Samples made with lithium triflate as salt with 80:1 heteroatom:Li ratio and measured at 25°C)

The very first and important observation to make is the specific conductivity for triethylamine-diethyl ether. As compared to the other systems, the conductivity does not show any significant change and is low. This observation could be an effect of lower dielectric constant of both the solvents involved and no chelation effect. The lower dielectric constant could allow no dissociation of the salt species and thus cause formation of species (aggregates) which do not contribute towards conductivity.

The comparison of conductivity trends between TMEDA-monoglyme system, triethylamine-Monoglyme system and the G1-monoglyme system is also interesting. All these systems do show a decrease in the conductivity with the addition of the nitrogen based solvents (TEA, TMEDA and G1). However, the trend differs from solvent to solvent. In the TMEDA-monoglyme system with the addition of 20% nitrogens, the conductivity almost flattens out, whereas for the TEA-monoglyme system, on the addition of 30% nitrogens the conductivity flattens out. This behavior again could be attributed to the fact that TMEDA can form a chelate which is thermodynamically stable²⁹, thus affecting the transport of lithium ion which is responsible for conductivity whereas TEA does not form any chelates. However, the G1-monoglyme shows lower chelation effect when compared to the TMEDA-monoglyme and TEA-monoglyme system. In the G1-monoglyme system the conductivity does decrease on the addition of G1 to monoglyme but does not decrease as fast as seen with the TMEDA-monoglyme and TEA-monoglyme systems. The G1 solvent having two heteroatoms in a molecule can also form a chelate, then why does the conductivity decrease at a slower rate than the TEA-monoglyme system? This could be explained by the heteroatom effects. In the G1-monoglyme system, the chelation effect may be offset by the oxygen present in the G1 molecule. This could lead to slower decrease in the conductivity in the G1-monoglyme system.

Another system, where the heteroatom effects are strongly seen competing the chelation effect is the TMEDA-DEE system. Even with the addition of 40% TMEDA, no decrease of conductivity is seen which may suggest that the oxygens of diethyl ether strongly compete against the chelation effect of the TMEDA.

Since it was concluded from the data that the formation of triflate rich aggregates might be taking place in many of these systems, it will be of big interest to see all ^{19}F data for all the same systems plotted on the same scale. The master plot for ^{19}F is shown in Figure 2.28.

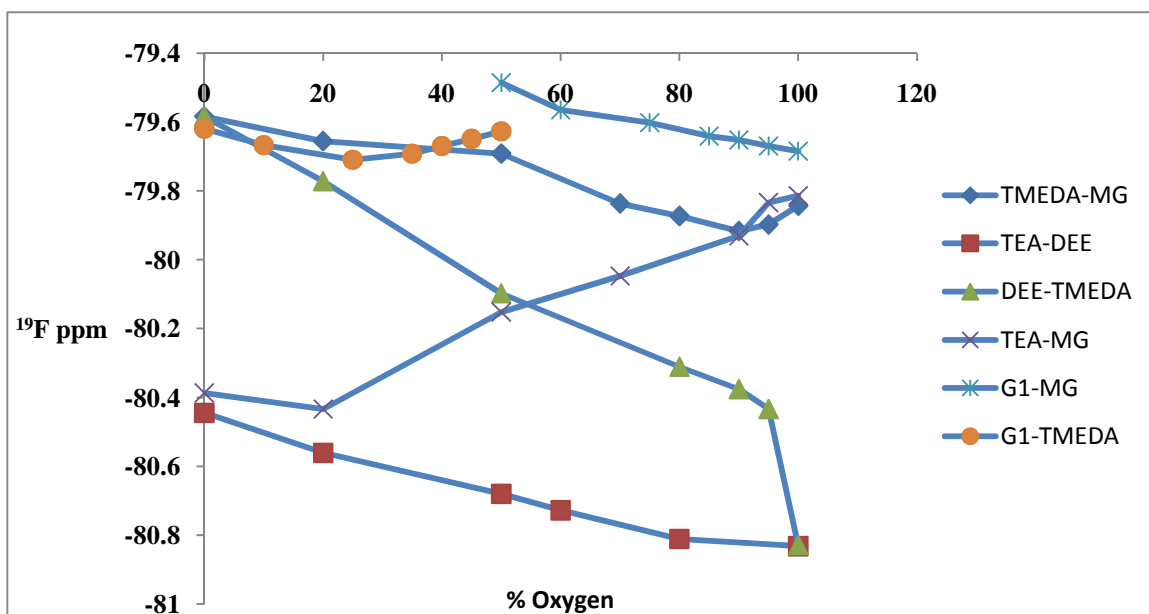


Figure 2.28 Plot of % oxygen versus ^{19}F NMR chemical shifts in ppm. (Samples made with lithium triflate as salt with 80:1 heteroatom:Li ratio and measured at 25°C)

The most important observation to make in the master curve for ^{19}F NMR is the difference in the chemical shifts for the TEA-DEE and the TMEDA-monoglyme system. The TMEDA-MG systems appear much downfield than that of the TEA-DEE system. This suggests that the triflate overall is more paired in the TMEDA-monoglyme system than the TEA-DEE system. This effect could explain the overall lower conductivity for TEA-DEE system than the TMEDA-monoglyme system. In the TMEDA-monoglyme system since tighter triflate rich aggregates are formed, the lithium could be chelated by the heteroatoms better than the TEA-DEE system which

lead to better conductivity. In the TEA-DEE system the triflate is less paired which means the lithium could be still loosely coordinated to the triflate anion which gives less sites for the heteroatom to coordinate, this lowering the conductivity.

Another surprising effect is the similarity between the TMEDA-Monoglyme system data and the G1-TMEDA and G1-monoglyme systems data. The G1-monoglyme and G1-TMEDA more or less show the same trend and chemical shift when compared to the TMEDA-monoglyme system. However, a significant change is seen in the ^7Li NMR chemical shift for the TMEDA-monoglyme, G1-monoglyme and G1-TMEDA systems. These comparisons of the chemical shift suggests that as far as the TMEDA-monoglyme, G1-monoglyme and G1-TMEDA systems are concerned, the triflate engages into similar speciation or aggregation, whereas the actual interaction of the lithium with the solvent heteroatoms governs the conductivity.

Another important observation is the big change in the ^{19}F NMR chemical shifts in the mixture of chelating and non-chelating solvents (TEA-monoglyme and TMEDA-DEE). The TEA-monoglyme and the TMEDA-DEE undergoes significant changes in chemical shift as compared to other systems. This could be again due to the chelating and the non-chelating effects competing which could lead to different speciations as far as the triflate anion is concerned. This is just a speculation and more investigation is required for these systems. It appears overall, that the triflate anion does not undergo big speciation changes in all the systems except a few and the lithium cation chelation or coordination to the solvents molecules is the limiting factor for these systems.

As mentioned in the TMEDA-monoglyme system section, the changes seen in the ^7Li NMR, conductivity and ^{19}F NMR data could be contribution of dielectric constant. Thus it was important to plot the changes in the dielectric constant of different systems on the same scale and make a master plot for changes in the dielectric constant against % Oxygen. Again, the EPR technique by which these changes in dielectric constant were measured will be discussed in chapter 3.

The plot of Intensity versus % Oxygen is given in Figure 2.29.

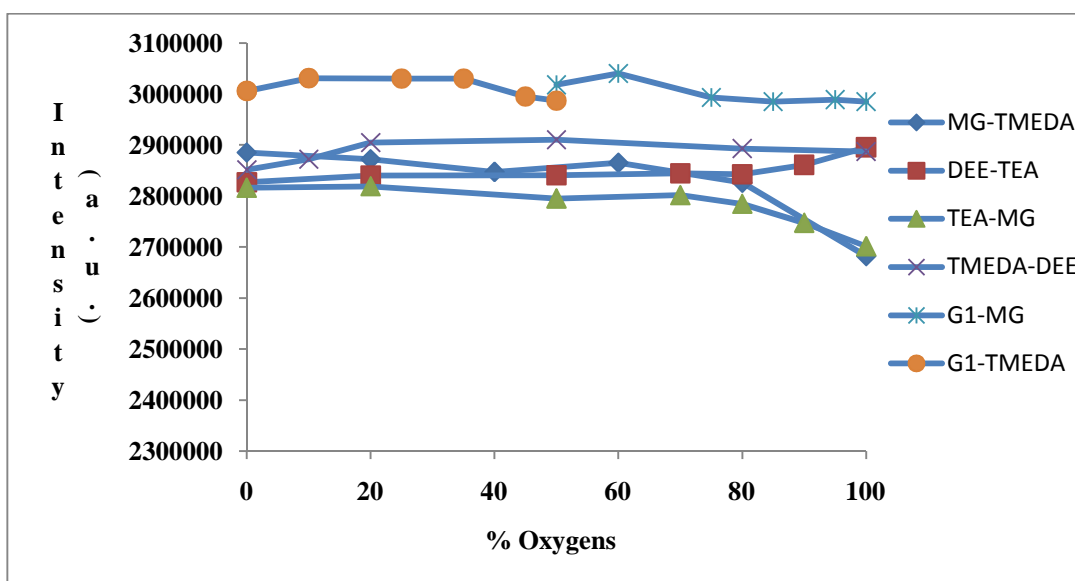


Figure 2.29 Plot of % oxygen versus EPR intensity in a.u. (Samples made with lithium triflate as salt with 80:1 heteroatom:Li ratio)

Figure 2.29 shows the changes in EPR intensity with varying % of oxygens to nitrogens. Intensity is inversely related to dielectric constant i.e. higher the intensity, lower is the dielectric constant. Since the measurements for different systems were made at different times, the intensities were corrected so that all the measured intensities could be in the same range.

From the plot it can be observed that there is no significant change in the dielectric constant of any of the systems investigated except for a small observable change in TMEDA - monoglyme and triethylamine - monoglyme system. Among all the systems studied, TMEDA-monoglyme and triethylamine - monoglyme has the relative biggest dielectric constant difference (TMEDA $\epsilon = 2.8$ and monoglyme $\epsilon = 7.2$ and triethylamine $\epsilon = 3.2$). However, overall the dielectric constant does not seem to change significantly and the data suggests that though dielectric constant of the solvents does play a role, it is not the only factor responsible for the different speciations of lithium triflate in mixed nitrogen and oxygen solvent systems.

In an attempt to see a complete picture of the phenomena taking place in the nitrogen versus oxygen competition, it is important to put together the master plots for ^7Li , ^{19}F and specific conductivity. From the ^7Li NMR plot it seems that for all the systems, the addition of nitrogen to oxygen makes the lithium cation less paired though the range of the chemical shifts is different for different systems from 100% oxygens to 100% nitrogens. However, similar to TMEDA-monoglyme system, the conductivity drops on the addition of nitrogen to oxygen even if the lithium cation is getting less paired in all the systems. This observation could be attributed to the aggregation phenomena where triflate rich aggregates are formed as explained in the TMEDA-monoglyme systems and also fits the ^{19}F NMR master curve. The observation suggests that the aggregation effect of lithium triflate outweighs the mere pairing effect of the lithium triflate in mixed nitrogen and oxygen involving solvents.

2.13: Conclusion and future studies:

The investigation of the competition between nitrogen and oxygen as a heteroatom to coordinate to the lithium cation in lithium triflate using ^7Li and ^{19}F NMR as a tool showed some complications in the analysis of the data. There are many factors which need to be considered when considering the mixed solvent systems with lithium triflate as the salt. Firstly, the change in the dielectric constant of the sample with the change in the mole fraction could cause changes in the salt speciation once placed in electric or magnetic field. The solvents used, mainly the amines have relatively low dielectric constant ($\epsilon_{\text{TMEDA}}=2.8$, $\epsilon_{\text{TEA}}=3.2$). The lower dielectric constant causes low separation of the cation and anion which may form aggregates without the coordination to the heteroatoms of the solvent. Thus the variation in the dielectric constant could be causing an effect on the dissociation of the ions in the electrolyte solution. Secondly, since the lithium triflate is added in the mixed solvent system on heteroatom basis (80:1=Heteroatom: Li) ratio, there is a change in the concentration (molarity) of the mixed solvent system. There is also a strong possibility that due to the change in the concentration, there could be change in speciation solely due to the concentration change. Thirdly, there is a chelation versus the coordination effect seen in the ^7Li and the specific conductivity.

The TMEDA-Monoglyme system being a good mimic for PEI-PEO system was investigated further by measuring the self diffusion coefficients and quantifying the ionic association of the ions (Lithium and Triflate) in the solution. The self diffusion and the quantification of the ionic species data gave an important insight into the amount of ionically associated species and could explain why we see a rise in the

conductivity increase at the 80% monoglyme point as there is a drastic change in the free ions after the 80% monoglyme point.

The actual purpose of the studies made in this chapter to investigate the nitrogen versus oxygen coordination to lithium cation was obstructed by the problems such as formation of aggregates in the mixtures of nitrogen and oxygen containing solvents. Since the NMR signal is an average of all the different species formed in the system, it was difficult to quantify and detect different species formed in the mixture of solvents with lithium triflate. Also, mixing of two different solvents with lithium triflate did alter the dielectric constant of the mixture and the alteration in the dielectric constant plays a major role in the speciation of the lithium triflate salt. The change in the dielectric constant which affects the speciation does affect the mobility of the ions.

Determination of the self diffusion constants for all the systems is necessary to give the quantification of how many of the species are actually contributing to the conductivity. The measurement of self diffusion coefficients will be important and will help many of the unexplained phenomena observed during this investigation. Siekierski et al has reported a bubble sort algorithm to quantify free, paired and aggregates formed by lithium triflate in mixtures of monoglyme and dioxane⁶. The same bubble sort algorithm could be used to quantify different species formed with the lithium triflate when mixed in different nitrogen and oxygen involving solvents.

Also, it will be interesting to actually investigate these studied systems in this chapter with computational calculations. It will be interesting to study and quantify different species formed with lithium triflate via computational calculation and match

the results to experimental results. On that note, Farid Ismail from my research group is actively involved in investigating the different nitrogen and oxygen involving systems with lithium triflate with computational chemistry.

2.14 Experimental

A: Solvents and reagents:

TMEDA, monoglyme, triethylamine, and diethyl ether were acquired from Sigma-Aldrich. The solvents were distilled from sodium and stored in a dried-air glove box over molecular sieves. Lithium triflate (reagent grade) was acquired from Sigma-Aldrich. Lithium triflate was stored in a dried-air glove box. All the samples for the mixtures of solvents were made in the dried-airglove box. The G1 model compound was acquired from Dr. Matthew Meredith in our lab and was stored in the glove box as well.

B: NMR Instrumentation:

Chemical shifts for all the samples and diffusion coefficients of TMEDA/monoglyme system, TEA/DEE system, TEA/monoglyme system, TMEDA/DEE system, G1/monoglyme system and G1/TMEDA system were measured using a Varian VNMRS 400 MHz NMR spectrometer with an AutoX-Dual Broadband probe. Temperature was regulated using an FTS sample cooler.

C: EPR Instrumentation:

All the measurements were carried out on Bruker EMX EPR spectrometer operating at the X band. The spectrometer has a Bruker 048T Microwave Bridge and

Bruker ER073 Magnet. The cavity used in all measurements was the standard rectangular configuration operating in the TE102 mode (Bruker 4102 ST cavity). The signal channel was kept constant at a magnetic field modulation frequency of 100 kHz. The microwave frequency is held constant at 9.725 GHz and the microwave power was held constant at 0.201 mW for all the measurements. The EPR cell set-up will be described in Ch. 3.

References:

- 1: Silverstein, R.M.; Webster, F.X.; Kiemle, D.J. *Spectroscopic Identification of Organic Compounds: 7th edition*, **2005**.
- 2: Rabi, I.I.; Zacharias, J.R.; Millman, S.; Kusch, P. *Physical Review Letter* 1938, 53, 318.
- 3: Edwards, J.C. *Principles of NMR*; URL: <http://www.processnmr.com/pdfs/NMR%20Overview.pdf>
- 4: *Basics of NMR*. URL: <http://www.chem.queensu.ca/facilities/NMR/nmr/webcourse/>
- 5: Bruice, P.Y. *Organic Chemistry: 5th Edition*, Chapter 13, p-569.
- 6: Plewa, A.; Kalita, M.; Solgala, A.; Siekierski, M. *ECS Transactions* **2007**, 2 (27), 117-124.
- 7: Plewa, A.; Kalita, M.; Solgala, A.; Zugowska, G.Z.; Siekierski, M. *ECS Transactions* **2006**, 3 (12), 59-66.
- 8: Gunther, H. Lithium NMR, *Encyclopedia of Magnetic Resonance* **2007**.

- 9: Gunther, H.; Moskau, D.; Bast, P.; Schmalz, D. *Angewandte Chemie International edition in English* **1987**, 26 (12), 1212-1220.
- 10: Dolbier, W.R. Jr. *Guide to Fluorine NMR for Organic Chemists* **2009**, p 9-14.
- 11: Petrowsky, M.; Frech, R.; Suarez, S.N.; Jayakody, J.R.P.; Greenbaum, S. *The Journal of Physical Chemistry: B* **2006**, 110, 23012-23021.
- 12: Electrolytic Conductivity Measurement: Theory and Application, Aquarius Technical Bulletin-No 88, URL: http://www.aquariustech.com.au/pdfs/tech-bulletins/Electrol_Conduct_Thery.pdf
- 13: Wu, Yung-Chi, Berezansky, P.A. *Journal of Research of the National Institute of Standards and Technology* **1995**, 100 (5), 521-527.
- 14: Price, W.S. *NMR Studies of Translational Motion: Principles and Applications* **2009**.
- 15: Price, W.S. *Concepts in Magnetic Resonance* **1997**, 9, 299-336.
- 16: Price, W.S. *Concepts in Magnetic Resonance* **1998**, 10, 197-237.
- 17: Vikhrenko, V.S.; Bokun, B.S. *Ionics* **1997**, 3, 44-51.
- 18: Williamson, M.J.; Hubbard, H.V.St.A.; Ward, I.M. *Polymer* **1999**, 40, 7177-7185.
- 19: Williamson, M.J. Southall, J.P.; Hubbard, H.V.St.A.; Johnston, S.F.; Davies, G.R.; Ward, I.M. *Electrochimica Acta* **1998**, 43, 1415-1420.

- 20: *Conductivities of Electrolytic Solutions*, URL:
http://wwwchem.uwimona.edu.jm:1104/lab_manuals/c10expt19.html
- 21: Theodore, S. *The Journal of American Chemical Society* **1932**, 54, 1411-1428.
- 22: Mohrig, J.R.; Hammond, C.S.; Schatz, P.F. *Techniques in Organic Chemistry, Second Edition*, p-273.
- 23: Plewa-Marczewska, A.; Kalita, M.; Marczewska, M.; Siekierski, M. *Electrochimica Acta* **2009**, 55, 1389-1395.
- 24: Gray, F.M. Armand, M. *Polymer Electrolytes; Handbook of Battery Materials*; Wiley-VCH Verlag **1999**.
- 25: Snow, A.; Sanders, R.; Frech, R.; Glatzhofer, D.T. *Electrochimica Acta* **2003**, 48, 2065-2069.
- 26: “*Electrochemistry Dictionary and Encyclopedia*”, URL:
<http://electrochem.cwru.edu/ed/dict.htm#d57>
- 27: Petrowsky, M.A; PhD Dissertation, The University of Oklahoma, **2008**.
- 28: Scibona, G.; Nathan, R.A.; Kertes, A.S.; Irvine, J.W. Jr. *Journal of Physical Chemistry* **1966**, 70, 375-379.
- 29: “Stability, chelation and the chelate effect” URL:
<http://wwwchem.uwimona.edu.jm:1104/courses/chelate.html>

Chapter 3

Electron Paramagnetic Resonance: A tool for studying dielectric properties of solutions

3.1 Introduction to dielectric constants

A dielectric is a material that is an electrical insulator and which may be polarized when an electric field is applied. When a dielectric material is placed in an electric field, electrical charges do not flow through the dielectric material as it does in a conductor, but only shifts from their normal equilibrium position causing a net polarization. The dielectric polarization causes the positive charges to align towards the field and the negative charges to align against the electric field. This creates an internal electric field. The internal electric field created by the polarization cancels out part of the external field. When put in an electric field, the molecules of a dielectric may reorient themselves to orient their axis of symmetry with the applied field¹.

The term dielectric is generally used to define materials with high polarizability. The extent to which a material is polarizable is given by a number which is generally referred to as “dielectric constant” and also known as the “relative permittivity” of the material. It is very important to distinguish between relative permittivity and another term referred to as “absolute permittivity”. The general concept of absolute permittivity is given by Equation 3.1^{2,3}:

$$\epsilon = \epsilon_r \epsilon_0 \quad \text{Equation 3.1}$$

Where ϵ = Absolute or actual permittivity or complex permittivity.

ϵ_r = Relative permittivity or dielectric constant.

ϵ_0 = Vacuum permittivity or permittivity of space or electric constant.

Vacuum Permittivity (ϵ_0) is generally given by the equation 3.2:

$$\epsilon_0 = 1/c_0^2 * \mu_0 = 8.8541878176 * 10^{-12} \text{ Farads/meter}^4. \quad \text{Equation 3.2}$$

Where, c_0 is the speed of light in free space.

μ_0 is the vacuum permeability.

The unit of vacuum permittivity is given by Farads/meter. The concept of absolute permittivity will not be discussed in detail here as it is out of the scope of this research dissertation.

As mentioned earlier, relative permittivity also known as the dielectric constant (ϵ_r) of a material, which is the measure of the extent to which it concentrates electrostatic lines of the flux. Although dielectric constant is the most commonly used term for relative permittivity in the literature, some other terms used are relative dielectric constant and static dielectric constant. While all these terms are common, they are sometimes ambiguous and have been used with great caution. The ambiguity arises for two different reasons. First, some older authors use the term “dielectric constant” for absolute permittivity rather than for relative permittivity. Second, the modern usage of dielectric constant refers to relative permittivity, which could be either static relative permittivity or frequency dependant relative permittivity. In this dissertation, “dielectric constant” mainly refers to “static relative permittivity”^{2,5}. Relative permittivity is generally given by the ratio of amount of electrical energy for a stored in a medium for

a given applied voltage, relative to the electrical energy stored by a vacuum. It is generally measured by measuring the capacitance of a cell with the medium of interest within it. It is also given by the ratio of the capacitance of the capacitor using the material as a dielectric to the similar capacitor with vacuum as the dielectric. It is given by the equation 3.3:

$$\epsilon_s = C_x / C_0 \quad \text{Equation 3.3}$$

where ϵ_s is the static relative permittivity (also known as the “dielectric constant”) of the sample, C_x is the capacitance of the capacitor with the material as the dielectric, and C_0 as the capacitance of the capacitor with vacuum as the dielectric.

Figure 3.1 shows a pair of parallel conducting plates of area A , separated by a distance “ h ”, connected to an ideal voltage source which generates constant voltage “ V ”. Connecting the plates to the voltage source, a surge of current flows to produce a charge $+Q_0$ on the inner surface of the upper plate and a charge of $-Q_0$ on the inner surface of the lower plate.

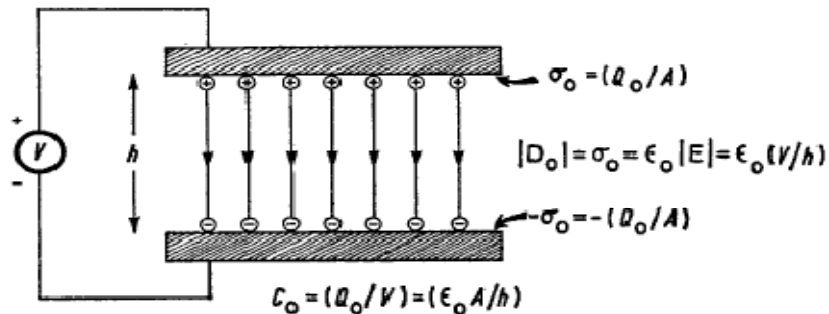


Figure 3.1. Sketch of parallel conducting plates at a distance of “ h ” and connected to a voltage source

The charges $+Q_0$ and $-Q_0$ are given by $+(\sigma_0 A)$ and $-(\sigma_0 A)$ respectively where σ_0 is the electric flux density produced due to the surface charge densities and “A” is the area of the plates. The ratio of the charge produced (Q_0) to the voltage (V) is given as the “capacitance” of the system and is denoted by C_0 .

$$C_0 = Q_0 / V \qquad \text{Equation 3.4}$$

The capacitance of a system is completely dependent on the geometry of the plates and is given by the equation (3.4).

$$C_0 = \epsilon_0 A / h \qquad \text{Equation 3.5}$$

where C_0 is the capacitance of the system, ϵ_0 is the electric constant, A is the area of the plates and h is the distance between the two plates.

When a dielectric material is inserted between the two plates, a further flow of charge takes place, increasing the charge ($+Q_0$) to $(+Q)$ and $(-Q_0)$ to $(-Q)$ (Figure 3.2). The total difference in charge ($Q - Q_0$), where Q is the total charge of the system when the dielectric material is inserted and Q_0 is the total charge of the system when the dielectric material is not placed in between the two plates, is due to the polarization of

the dielectric material due to the electric field.

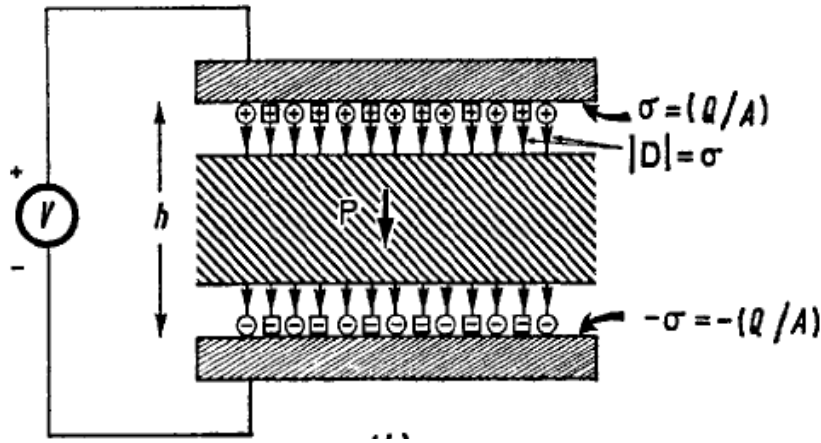


Figure 3.2

The new capacitance (C_x) for the system after the insertion of the dielectric material is given by the Equation 3.6⁶.

$$C_x = Q/V \quad \text{Equation 3.6}$$

The ratio for the new capacitance depends on only on the material from which the dielectric is made of. The “static relative permittivity” (static dielectric constant) can then be given as mentioned earlier in Equation 3.3, the ratio of the capacitance of the system with the dielectric material to the capacitance of the system with vacuum (without the dielectric material).

Some of the other (apart from capacitance) techniques used to determine dielectric constants include:

- 1) Microwave Dielectric Spectroscopy⁷,
- 2) Cavity Perturbation Methods⁸,
- 3) Ellipsometry⁹, and

4) Solvent Dichromatism^{10,11}

One of the biggest disadvantages of these methods is the volume of the sample used in these techniques. Each one of these techniques, including the capacitance method, uses at least 6-7 mL of sample (for weak dielectric solvents). Another problem of some of these techniques is the interaction of the probe with the material. Strong advantage of the EPR technique discussed here is that the volume of the sample used is less than 0.5 mL to study the dielectric properties of liquids.

B: Why are “dielectric” properties important?

As mentioned earlier, the science of dielectrics has been active for over a hundred years. This branch is one of the oldest branches in physics and is closely related to chemistry, materials, and electrical engineering. The term “dielectric” was first introduced by Faraday to suggest that there is something analogous to current which flows through a capacitor during the charging process when a current applied at one plate “flows” through the insulator to the other plate. The most important consequence of applying a static external field across the capacitor is that the positively and negatively charged features in the dielectric material become polarized. It is a well-established fact that dielectric materials reacts to an electric field differently compared to free space (vacuum) because the dielectric material has charged “features” that can be displaced. In Figure 3.3, some of the different configurations that undergo polarization when an external field is applied have been illustrated¹².

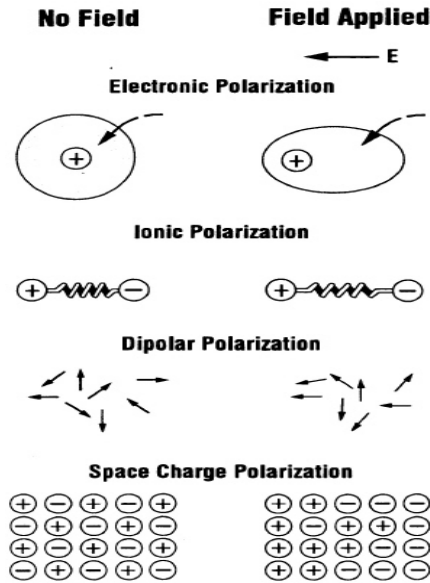


Figure 3.3

All material systems have such features and their collective effects can be quantified using dielectric constants.

In time, the focus in dielectric science and technology has broadened from materials used in traditional applications such as capacitors and semiconductors. Recently, materials with unique dielectric responses have been studied and utilized in novel ways. Some of the major fields and areas where dielectric science is involved are polarizability, relaxations, ions, phase transitions, bonding, crystal/ligand-fields, electronic correlations, interfaces, interphases and many more.

Figure 3.4 illustrates the different interactions among the many and diverse core areas of dielectric science and technology that present challenging possibilities for scientists, technologist and engineers in research development and manufacturing¹².

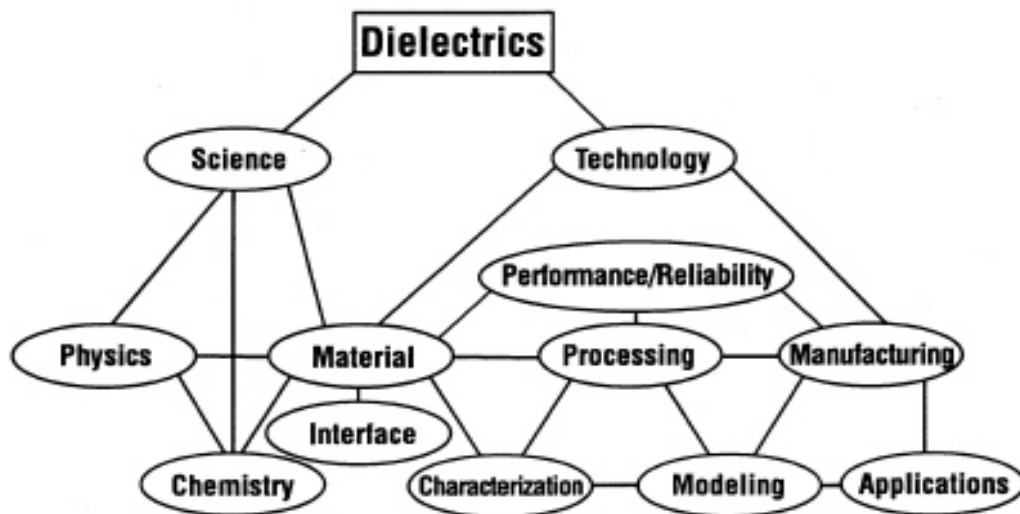


Figure 3.4 Figure reproduced from Dielectric Science and Technology: The Electrochemical Society Interface 2006, 28-31.

3.2 Electron Paramagnetic Resonance

A) Theory of EPR.

Earlier in this century when scientists began to apply quantum mechanics to understand atoms and molecules, they found that atoms have discrete states, each with a corresponding discrete energy. Spectroscopy is a tool for the measurement and interpretation of the energy differences between atomic, and molecular, states. Knowing this information, very detailed insight of the identity, structure and dynamics of a sample can be achieved^{13,14}.

The energy difference (ΔE) between states can be measured because of the important relationship between ΔE and the absorption of the electromagnetic radiation. According to Planck's law, when electromagnetic radiation is absorbed:

$$\Delta E = h\nu$$

Equation 3.7

Where h is the Planck's constant and ν is the frequency of the radiation^{13,14}.

Typically, the absorption of energy causes a transition from the lower energy state to a higher energy state. In conventional spectroscopy (NMR), the frequency is varied and the frequency at which the absorption takes place corresponds to the energy difference between the two energy levels. This record of the absorption at a particular frequency is called a spectrum. In electron paramagnetic resonance spectroscopy (EPR), the concept is slightly different. As mentioned earlier, in conventional NMR spectroscopy the magnetic field is kept constant and the frequency is scanned to achieve a spectra. On the contrary in EPR, the frequency of the electromagnetic radiation is kept constant and the magnetic field is varied across the field. Typically, the frequencies for spectroscopy vary from the megahertz range (radio waves) for NMR through those for visible light and ultraviolet light. Radiation in the gigahertz range (the same as used in our microwave oven) is used in the EPR spectroscopy^{13,14}.

B) The Zeeman effect:

EPR spectroscopy is a spectroscopic method which is applicable only for samples with unpaired electrons. The energy differences studied using the EPR technique are mainly due to the interactions of the unpaired electrons in the sample with the external applied magnetic field created by the magnet in the laboratory. This effect is called the Zeeman Effect. Electrons have a magnetic moment and when placed in external magnetic field (B_0); they act like tiny compasses or a bar magnets^{13,14}.

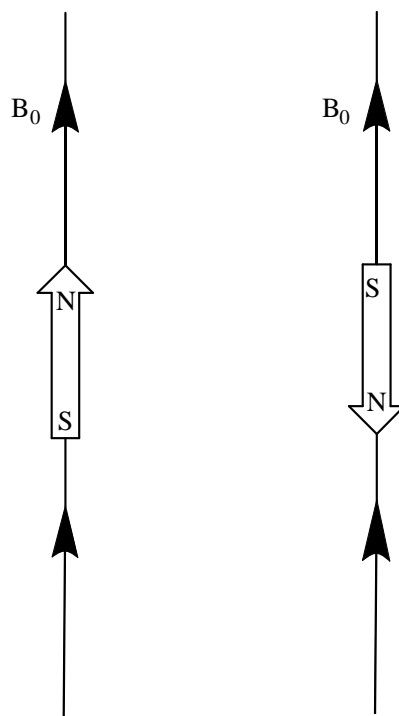


Figure 3.5

As shown in Figure 3.5, when the moment of the electron, μ , is aligned with the magnetic field, B_0 , it will have the state of lowest energy. Alternatively, when the moment of the electron, μ , is aligned against the magnetic field, B_0 , it will have the state of highest energy. The higher state and lower state of energy is designated by the projection of the electron spin, M_s , on the direction of the magnetic field. As the electron has spin number of $\frac{1}{2}$, the parallel state is labeled as $M_s = -1/2$ and the antiparallel state as $M_s = +1/2$.

From quantum mechanics, the most basic equation for EPR are given by:

$$\Delta E = h\nu = g\mu_B B_0 \quad \text{Equation 3.8}$$

Where g is the g-factor, which is a proportionality constant of ca. 2.0 for most samples, but can vary depending on the electronic configuration of the radical or ion. The Bohr magneton (μ_B) is the unit of electronic magnetic moment. When there is not a magnetic

field, there is no energy difference to measure (Figure 3.6). From Figure 3.6, it can be seen that the measured energy difference depends linearly on the magnetic field^{13,14}.

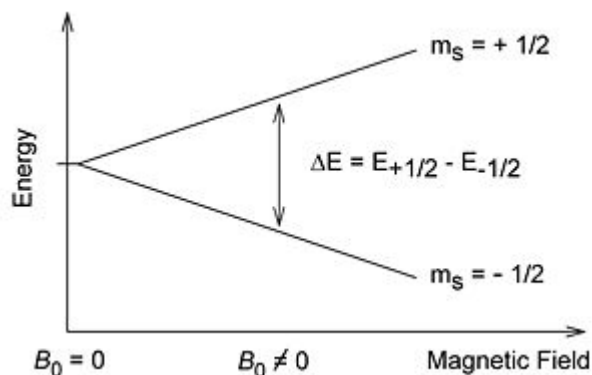


Figure 3.6

The energy difference between the two states can be changed by varying the magnetic field strength. In EPR spectroscopy, as mentioned earlier, the exciting electromagnetic radiation is kept at a constant frequency and the magnetic field is scanned. A peak in the absorption will occur when the magnetic field “tunes” the two spin states so that the energy difference between the two states matches with the energy of the electromagnetic radiation. This field is called as the “field of resonance”. The field of resonance is not a unique fingerprint for the identification of a compound as the spectra can be achieved at different frequencies. The “g-factor”, being independent of the microwave frequency, is much more unique parameter^{13,14}.

C) EPR signal intensity¹³

Along with the position of the signal, the size of the EPR signal also matters as far as the concentration of EPR active species in the sample goes. The size of the signal is generally defined as the integrated intensity, i.e. the area under the curve. In EPR signal intensity does not solely depend on the concentration of EPR active species in the

sample but also depends on the microwave power. The signal intensity increases as the square root of power until the saturation effect is reached, whereas at higher powers the signal diminishes and broadens¹³.

D) Basic EPR Instrumentation¹³

It was during World War II, during the development of radar, that the first EPR signal was detected by Zavoisky in 1945. The simplest possible spectrometer has three basic components:

- 1) A source of electromagnetic radiation,
- 2) A sample, and
- 3) A detector.

In an EPR spectrometer (Figure 3.7), the electromagnetic radiation source and the detector are in a box called the “microwave bridge”. The sample is inserted into the metal box, which is called a microwave cavity. The microwave cavity helps to amplify the weak signals from the sample. As mentioned earlier, the cavity is placed in a magnetic field to “tune” the electronic energy levels. In addition to the magnet, we have a “console” which controls the signal processing and electronics. A computer is used for analyzing the data as well as coordinating all the units for acquiring a spectrum.

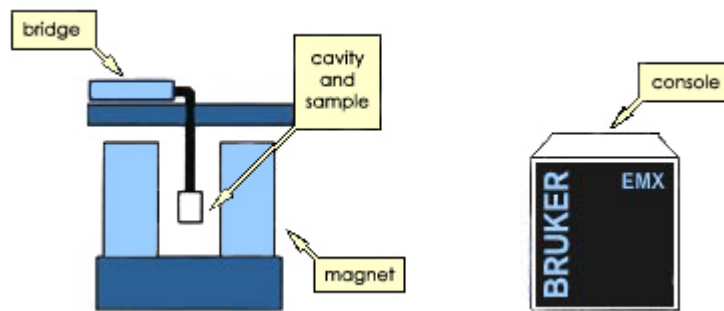


Figure 3.7 Sketch of the EPR Instrumentation

*E) The EPR cavity.*¹³

This section will highlight in brief the properties of microwave (EPR) cavities and how changes in these properties due to microwave absorption result in an EPR signal. As mentioned earlier, microwave cavities amplify the weak signals from the sample. A microwave cavity is simply a metal box which is generally rectangular or cylindrical in shape which “resonates” with the microwaves like an organ pipe resonates with sound waves. The word “resonance” as far as the EPR spectroscopy is concerned means that the cavity stores the microwave energy and at resonance frequency microwaves will not be reflected back, but will remain inside the cavity (Figure: 3.8).

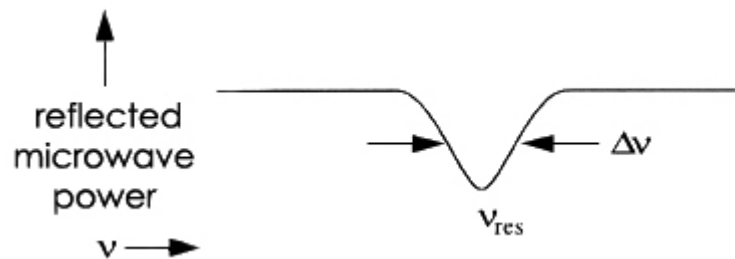


Figure 3.8

The EPR microwave cavities are characterized by their “Q” factor, which indicates how effective is the cavity in storing the microwaves. Higher the Q factor, the higher the sensitivity of the spectrometer. The Q factor is defined as:

$$Q = 2\pi (\text{energy stored}) / \text{energy dissipated per cycle} \quad \text{Equation 3.9}$$

The energy dissipated per cycle is the amount of energy lost during one microwave period. Energy loss can occur to the side walls of the cavity as the microwaves generate electrical currents in the side walls of the cavity which in turn generates heat.

As a consequence of the resonance achieved in the cavity there will be a standing wave inside the cavity. Standing electromagnetic waves have their electric and magnetic field components exactly out of phase, meaning when the electric field is minimum, the magnetic field is maximum and vice versa. The spatial distribution of the amplitudes of the electric and the magnetic field in the EPR cavity is shown in Figure 3.9.

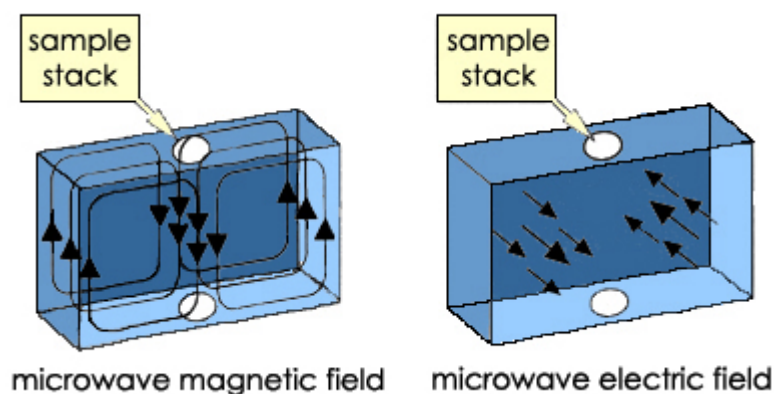


Figure 3.9

The spatial separation of the magnetic and the electrical components of the microwaves in the EPR cavity is taken advantage in the EPR technique. Most samples have a non-resonant absorption of the microwaves by the electrical field. Microwave ovens work on the principle of non-resonant absorption of the microwaves electrical field. The “Q factor” will be degraded by an increase in the dissipated energy. It is the magnetic field which is responsible for the absorption in the EPR. EPR samples are therefore placed in the cavity where the electric field is minimum and the magnetic field is maximum to achieve the maximum signal and the highest sensitivity.

The microwaves are coupled into the cavity using a hole called an iris. The size of the iris controls the amount of microwaves which will be reflected back from the cavity and how much will enter the cavity. The iris couples the microwaves by matching or transforming the impedances of the cavity and the waveguide (rectangular pipe used to carry the microwaves).

So how do all these different properties of the cavity give rise to an EPR signal? The sample in the cavity absorbs some microwave energy and there is a decrease in the “Q”. There is a decrease in the “Q” due to the increased losses and the coupling changes as the absorbing sample changes the impedance of the cavity. The microwave cavity is no longer critically coupled and the microwave is reflected back to the bridge thus giving rise to an EPR signal (Figure 3.10).

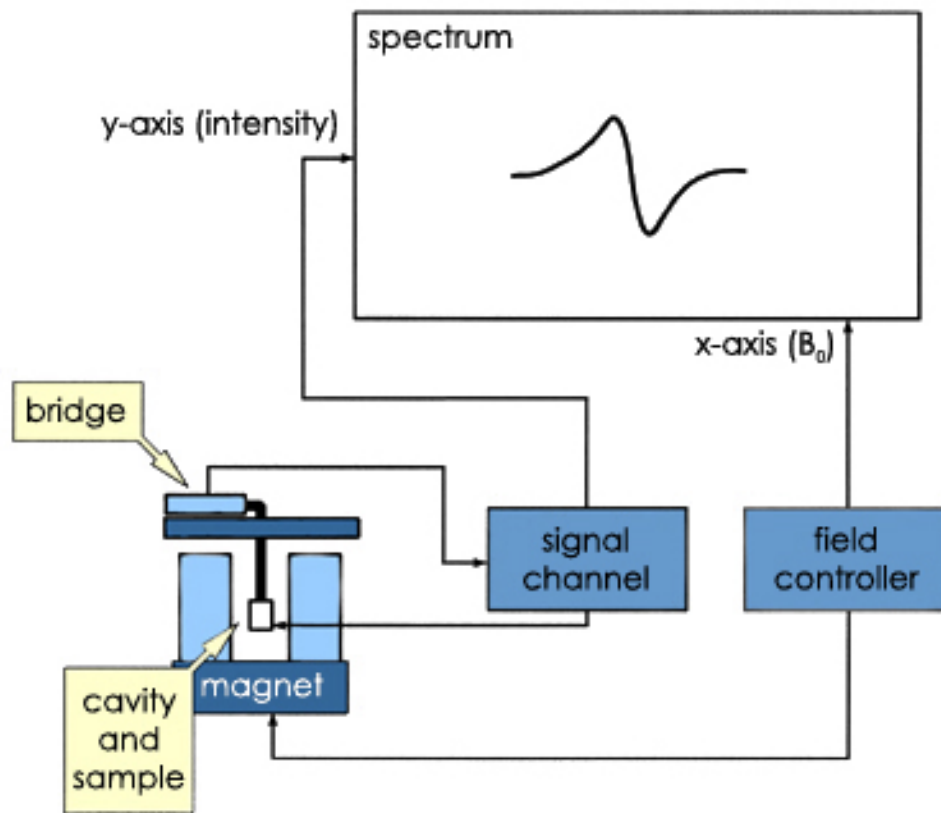


Figure 3.10

3.3 Relation between EPR (microwave radiation) and dielectric constant.

EPR signal responses depend on a lot of factors like sample and standard volume, sample and standard concentration, positioning of the sample in the EPR cavity, different cavities, and dielectric constants. There are a very few references in the literature which deal with the complicated effect of dielectric materials on the EPR signal.

In microwave electronics, relative permittivity is given by:¹⁵

$$\epsilon_r = \epsilon/\epsilon_0 \quad \text{Equation 3.10}$$

where relative permittivity (ϵ_r) is a dimensionless quantity.

The equation (3.10) can also be given as:

$$\epsilon_r = \epsilon/\epsilon_0 = [(\epsilon' - j\epsilon'')/\epsilon_0] = (\epsilon_r' - j\epsilon_r'') = \epsilon_r'(1 - j\tan\delta_e) \quad \text{Equation 3.11}$$

where ϵ = complex (absolute) permittivity, ϵ_r = relative permittivity, ϵ_0 = $8.8541878176 \times 10^{-12}$ Farads/meter, ϵ_r' = real part of the complex relative permittivity, ϵ_r'' = imaginary part of the complex relative permittivity, $\tan\delta_e$ = dielectric loss tangent, and δ_e = dielectric loss angle. As seen from the equation 3.11, the relative permittivity (dielectric constant) has two parts to it; energy storage and energy dissipation. Energy storage describes the lossless portion of the exchange of energy between the field and the material and energy dissipation occurs when the electromagnetic energy is absorbed by the material. So permittivity is generally expressed by complex numbers to describe the storage (real part = ϵ_r') and dissipation (imaginary part = ϵ_r'') effects^{13,15}.

Microwave fields interact with a dielectric sample in two different ways. Firstly, the electric component of the field is responsible for the movement of the electric dipoles in the sample. As a result of this phenomena, a part of the microwave energy is being lost. The amplitudes of both, the electric and the magnetic field, in the cavity decrease proportionally. As the “Q” factor decreases, the EPR signal intensity also diminishes. This interaction, due to the electric component penetration into the sample volume, depends on the imaginary part (ϵ_r'') of the sample dielectric constant. There are

different ways suggested by authors in the literature to normalize sample signals with a signal given by a standard permanently present in the cavity^{13,16,17}.

Unfortunately, there is a second effect, too. As mentioned above, along with the proportional decrease of the amplitudes because of the dielectric losses, there are some disproportionate changes in the amplitude in the cavity. This phenomena is known as the “sucking in” effect of the microwave field into the dielectric or the “lensing effect”. This effect of the field perturbation depends on the real part (ϵ_r') of the dielectric constant^{18,19,20}.

As shown in the literature in mathematical terms, the EPR signal intensity is a combination of the value of the microwave field amplitude in the sample and the different degrees of microwave field perturbation in the sample^{18,19,20}. Knowing all the parameters and establishing a relationship between the microwave radiation and dielectric constant, it is well established fact that the EPR signal intensity decreases as the dielectric constant of the material increases. As mentioned earlier, a correction method for this error has been given in the literature²¹.

N.D. Yordanov et al, has shown a direct relationship between the EPR signal intensity and the dielectric constant. A very unique coaxial geometric cell (Figure:3.11) was used to show the relationship between the EPR signal intensity and dielectric constant.

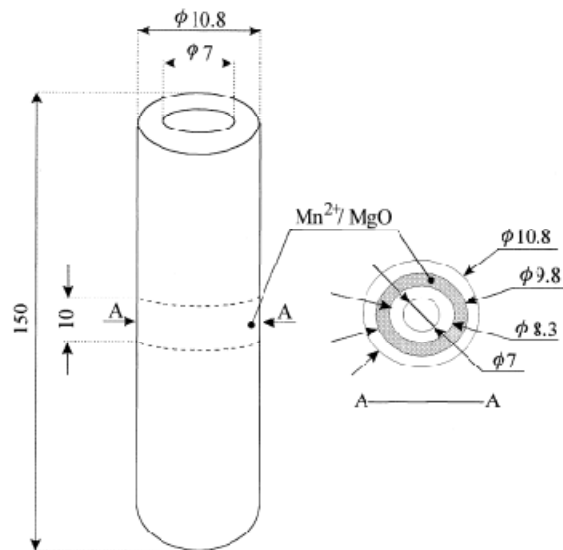


Figure 3.11. Construction of the holder for reference external to the unknown sample standard (dimensions in mm).

The reference standard used in this cell was external to the unknown sample in consideration. Its holder was made of a PTFE tube with a special hollow profile in the middle of its length in which the reference standard was pressed. The reference standard is a mixture of 90% (w/w) Mn^{+2} magnetically diluted in (1:500) in MgO and 10% (w/w) paraffin wax, which was used as a binder. The PTFE tube containing the standard is fixed in the EPR cavity and the different solvents to be studied were placed in the central tube. An internal reference, TEMPO ((2,2,6,6)-tetramethylpiperidine-1-oxy radical), was mixed with the solvent under study. The EPR signal intensity from the TEMPO radicals are then normalized against the EPR signal intensity from the external reference ($\text{Mn}^{+2}/\text{MgO}$) mixture²¹.

Yordanov et al, showed a relationship between the EPR signal intensity and dielectric constant and the sample diameter (Figure 3.12)²¹.

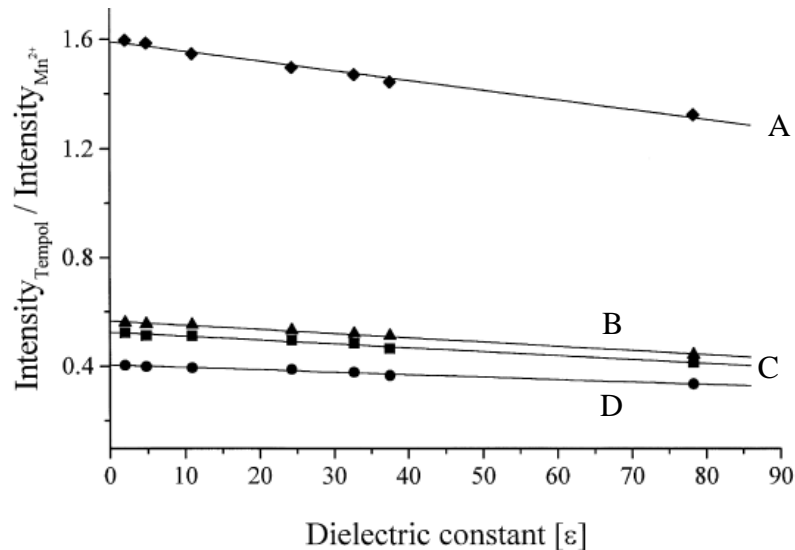


Figure 3.12. Magnitude relative to reference standard of EPR signal intensity of TEMPO dissolved in CCl_4 , $CHCl_3$, t -BuOH, EtOH, MeOH, CH_3CN and H_2O accommodated in sample container with $d = 1.0$ (D), 1.2(C), 1.5(B) mm and flat cell with 0.6 X 3.55mm (A).

As seen from Figure: 3.12, Yordanov et al showed a linear relationship between the EPR signal intensity and dielectric constant of different solvents (ϵ : 2.2-78). From Figure 3.12, it can also be concluded that the EPR signal intensity changes with the change in the diameter of the sample tube. Although the technique is excellent to show the relationship between the EPR signal intensity and dielectric constant, there are some disadvantages to this method if it were to be used to study or measure the dielectric properties of the solvents. Firstly, the cell assembly is intricate and the use of quartz tubes makes the assembly expensive. Secondly, it can only work with solvents which can dissolve TEMPO, the internal reference²¹. Thirdly, the TEMPO may interact with the solvent or other solutes in specific ways. Lastly, EPR is a sensitive technique where only a small amount of TEMPO is needed. Consistently weighing out and adding the

same amount of TEMPO to each solvent could introduce significant errors, especially if small amounts of sample are to be used.

In this chapter, the construction of a new and simpler cell assembly will be discussed for the EPR technique, where TEMPO dissolution in the solvents, weighing/addition errors, and the question of specific interactions would not be issues. The parameters (placement of the tube in the cavity, coaxial volume of the sample) for optimum signals with the new assembly will be discussed. The relationship between EPR signal intensity and dielectric constant will be employed to investigate the dielectric constant of an “unknown liquid” sample using a calibration curve from solvents with known dielectric constant values. The EPR technique was also used for some practical application like finding the concentration of water in a water/dioxane mixture, monitoring the kinetics of a reaction over a period of time, phase transition detection, measuring the dielectric constant of electrolyte solutions, and correlation with the “critical micelle concentration” of surfactant solutions will be discussed in the next chapter (Chapter 4). Studies of the changes in dielectric properties for lithium ion salts in mixtures of solvents (model compounds for solid polymer electrolytes) have been discussed in Chapter 2.

3.4 Construction of the coaxial assembly

A simple coaxial assembly (Figure 3.13) with different diameter NMR tubes (capillary, 3mm, 4mm and 5mm) was constructed taking into account the problems which may be encountered as far as the assembly discussed by Yordanov was concerned.

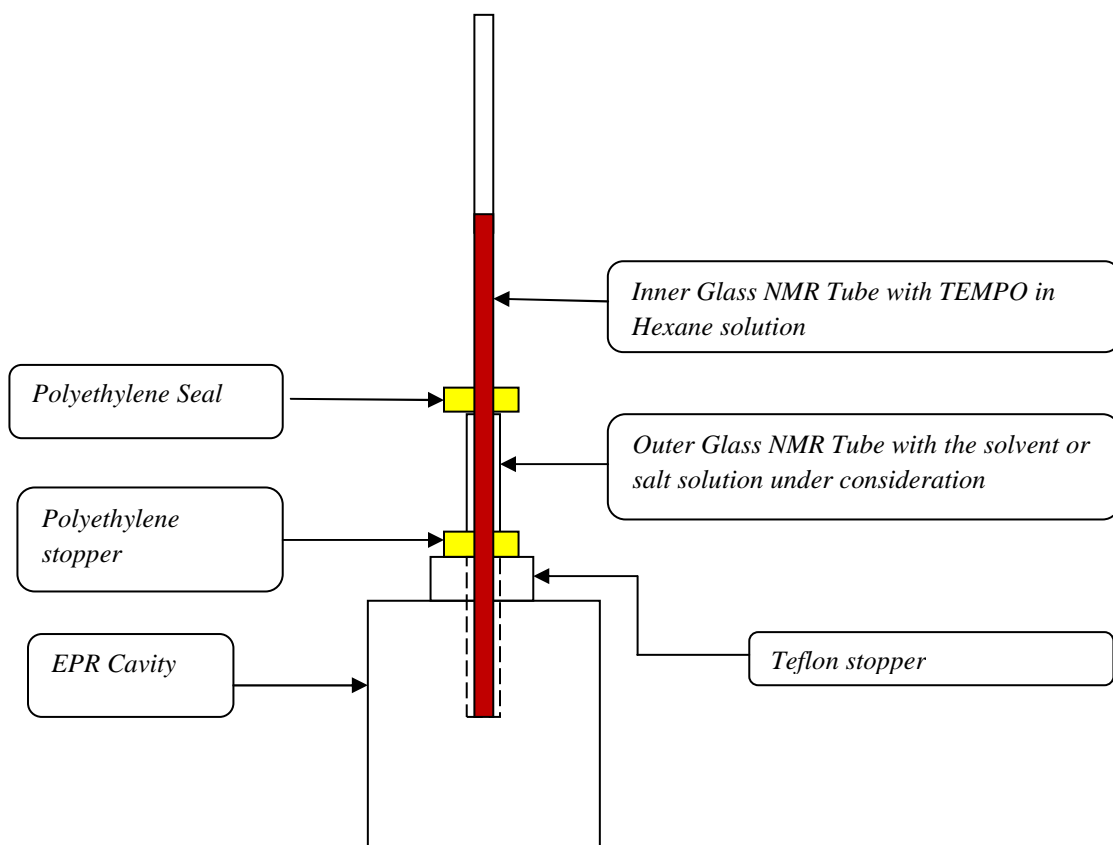


Figure 3.13 Sketch of the coaxial EPR cell assembly. (Note: The above sketch is not to scale.)

As seen in Figure 3.13, the assembly is made up of coaxial NMR glass tubes. The inner tube is filled with a solution of TEMPO in hexanes. TEMPO (2, 2, 6, 6-tetramethylpiperidine-1-oxy radical)²² is a very stable oxygen radical species which is EPR sensitive and gives a very clear spectra around 3480 Gauss. The structure of TEMPO is given in Figure: 3.14.

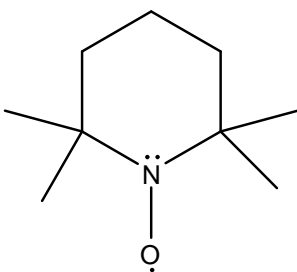


Figure 3.14. 2,2,6,6-tetramethylpiperidine-1-oxyl radical (TEMPO)

TEMPO is the most commonly used reference compound used as far as EPR spectroscopy is concerned.²² The stability of TEMPO can be attributed to delocalization of the radical from the oxygen to the nitrogen atom and steric protection by the methyl groups.

TEMPO gives EPR spectra as shown in Figure 3.15^{14,23}

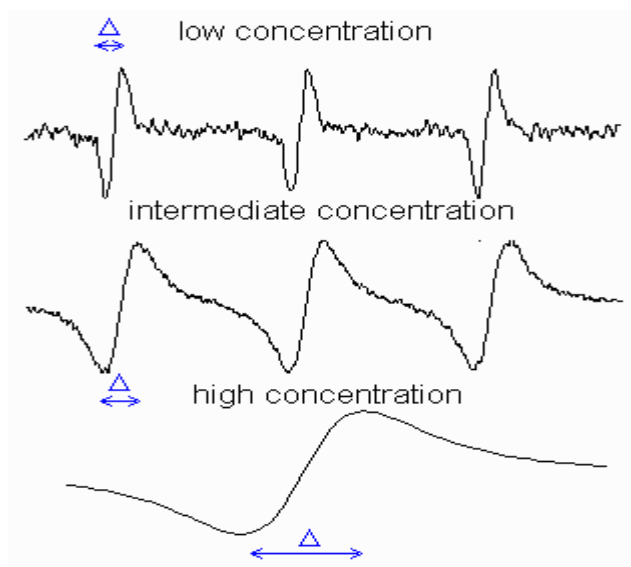


Figure 3.15 Signal Splitting for TEMPO in EPR at different concentrations

In EPR spectrum, the hyperfine splitting pattern is given by the equation $2nI+1$, where the “I” is the nuclear spin and “n” is the number of the equivalent nuclei interacting with the unpaired electron. As seen in Figure 3.15, the signal splits into a triplet which can be attributed to the nitrogen attached to the oxygen. Since for ^{16}O , $I = 0$, the splitting pattern could come from the nuclei bonded to the oxygen, i.e nitrogen. ^{14}N has spin number $I = 1$. Therefore according to the splitting pattern the signal should split into 3 lines as shown in Figure 3.15^{14,23}.

Figure 3.15 also shows the concentration effects of the TEMPO on the splitting pattern. At low concentrations, the signal for TEMPO is resolved due to heterogeneous broadening and as the concentration of the TEMPO increases, the spins do not remain localized to one molecule and exchanges with other radical species, thus giving the broadening effect of the signal²³. For this particular application, it is useful to have a concentrated solution of TEMPO, since a coaxial assembly is used and the concentrated TEMPO in the inner tube allows a larger range of dielectric constants to be studied for media in the outer volume.

Hexane is used as a solvent for the TEMPO as it is readily soluble and hexane is a non-polar, low dielectric constant ($\epsilon = 1.89$)²⁴ solvent. The lower dielectric constant of hexanes lessens attenuation of the TEMPO signal caused by high dielectric lossy samples. It is very important to minimize the loss occurring in the reference solution as it would be additive to the loss caused by the sample being studied. The inner tube is sealed under an inert argon atmosphere. The sealing of the reference inner tube serves two purposes, first, it prevents any evaporation of the TEMPO/hexane solution, preventing any change of concentration of the standard solution and second, the sealing of the reference tube under the argon inert atmosphere gets rid of any atmospheric oxygen present in the tube which might have some quenching effect on the TEMPO.

As a concentrated solution of TEMPO/hexane solution is used, spin exchange is fast and the EPR signal shows a single peak. To simplify the EPR signal intensity measurement, the derivative is taken of the signal. All the EPR signal intensities are reported as the first derivative of the EPR signal²³.

The polyethylene seal on the outer tube is designed so that it can seal the outer tube and prevent any evaporation from the tube. The polypropylene stopper on the outer tube can be moved up or down to adjust the depth of the tube in the microwave cavity.

In this chapter, some of the topics covered will include:

- ❖ The different diameters of the coaxial tubes used and their effects on studies will be discussed. The depth to which the cell is inserted in the cavity and its effects will also be investigated.
- ❖ The use of the EPR coaxial cell to record the EPR signal intensity of solvents with dielectric constants from 2.2 to 78²⁴ to plot a calibration curve, which can then be used to estimate a dielectric constant of an unknown solvent.
- ❖ The use of the EPR coaxial cell to measure the EPR signal intensity of a mixture of solvents (water/dioxane mixtures) with the dielectric constant range of 2.2-78 and use of a calibration curve to measure the dielectric constant, and therefore the composition of, an unknown mixture of solvents.

3.5 EPR as a tool to investigate dielectric constants of unknown liquid samples

Before discussing the actual experiments, some of the important rules need to be discussed for using EPR as a tool for applying the technique.

- ❖ It is very important that the settings of the instrument (frequency modulation, the position of the iris, the microwave power) remain the same for all the solvents used in a given set of experiments. Consistency of parameters throughout the measurements is really important to keep any errors arising from the instrument constant throughout the measurements.

- ❖ Though the thickness of the glass of the tubes seem even throughout the circumference of the tube, the tubes may have uneven thickness which may add some error. To keep the error constant throughout the measurements it is very important to put the tubes in the same position for each and every measurement.
- ❖ The depth to which the tubes are inserted in the cavity should be the same for each measurement of the solvents. The polyethylene stopper makes sure that the tubes stay at the same depth for each measurement. The depth to which the tubes are inserted should be optimum. In order to cover the entire range of dielectric constant from 2.2 to 78, the tubes were inserted only to the depth where the cell would give an EPR signal. If the tubes were inserted too deeply, the samples with higher dielectric constant (lossy samples) would be impossible to tune to the magnetic field. On the other hand, if the tubes were not inserted to a sufficient depth EPR signals were not observed.
- ❖ When known, all the measurements were done from lower dielectric constant to higher dielectric constant. The system worked optimally if the parameters were set so that the “Q” factor was around 1800-1900.

It was necessary that the practical guidelines were followed all the time if the method was used to measure dielectric constants.

As mentioned earlier, different diameters tubes were used as outer and inner tubes to investigate the EPR signal intensity of different solvents. The following Table 3.1 shows different outer and inner tube diameters used in the coaxial assembly.

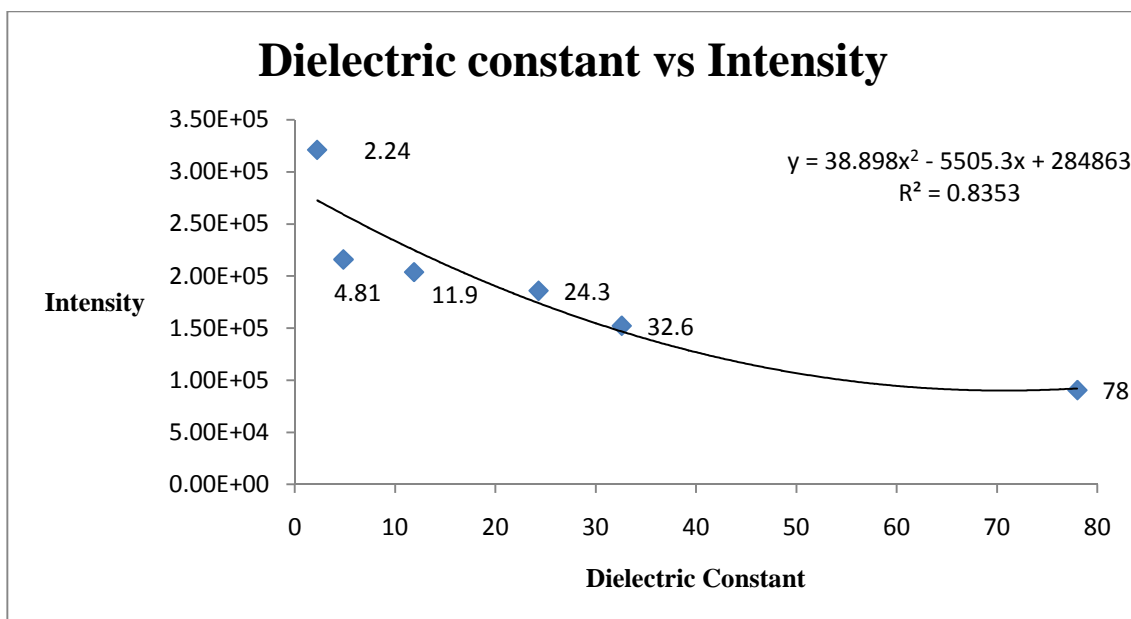
Outer tube diameter (mm)	Inner tube diameter (mm)
3	Capillary tube
4	Capillary tube
5	Capillary tube
5	3
5	4
4	3

Table 3.1. Inner and outer tube diameters in mm.

3 mm-capillary tube:

This coaxial cell was set up with 3mm outer tube and capillary as the inner tube.

The plot of “dielectric constant versus Intensity” is shown in Figure 3.16.



*Figure 3.16 Dielectric constant versus Intensity plot for 3 mm-capillary cell. ($\epsilon=2.24$ Carbon tetrachloride, $\epsilon=4.81$ chloroform, $\epsilon=11.9$ *t*-BuOH, $\epsilon=24.3$ ethanol, $\epsilon=32.6$, methanol, $\epsilon=78$ water)*

As seen from the plot, the EPR signal intensity is on the y-axis and the dielectric constant on the x-axis. The EPR signal intensity decreases with the increase in dielectric constant as expected. The EPR signal intensity is best fit by a polynomial equation. There were a few problems with using this assembly to get a calibration curve.

- ❖ The capillary (inner tube) does not sit in the middle of the outer tube and leans on an angle which gives a non-uniform distribution of the sample and the TEMPO in the coaxial volume of the cell. This uneven distribution causes a change in the parameters of the cell resulting in errors which change with every different solvent. Though it is possible to cover a large range of samples (solvents) with different dielectric constants, the leaning of the inner capillary tube towards one inner wall of the outer tube makes introduces significant errors which are reflected in the correlation coefficient (R as R^2) value of the plot. The

estimation of dielectric constant of an unknown sample (solvent) with this inner and outer diameter gave large error margins.

- ❖ The sealing of the capillary was done only with a Bunsen burner without any inert atmosphere. There is a possibility that the presence of atmospheric oxygen in the TEMPO solution may also cause errors.

4 mm NMR tube-Capillary tube:

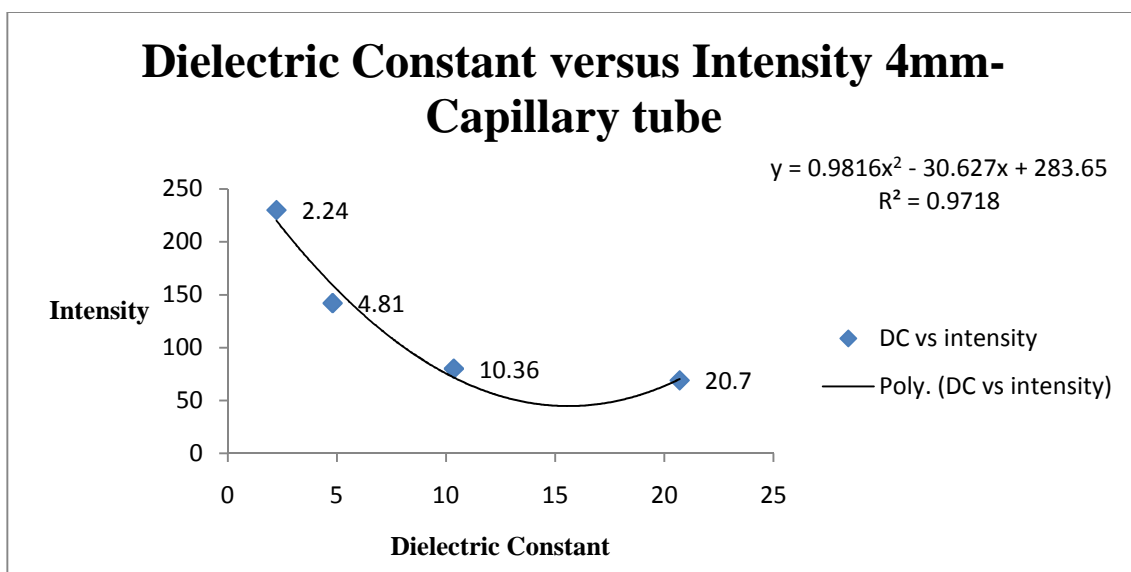


Figure 3.17 Dielectric constant versus Intensity plot for 4 mm-capillary cell. ($\epsilon=2.24$ Carbon tetrachloride, $\epsilon=4.86$ chloroform, $\epsilon=10.36$ dichloroethane, $\epsilon=20.7$ acetone,)

As seen from the plot of dielectric constant versus intensity for a 4 mm outer tube and capillary as the inner tube, only a short range of dielectric constants can be covered. Compared to the 3 mm-capillary tube assembly, the coaxial volume of the 4 mm-capillary assembly is much larger and accommodates more solvent than the 3 mm-capillary assembly. Therefore, having more volume of the solvent in the assembly causes more losses from the microwaves and, after a dielectric constant of ca. 21, it is

not possible to tune on the TEMO signal. When the absolute values for EPR signal intensity of the 3 mm-capillary assembly are compared to the 4 mm-capillary, the values for the 3 mm-capillary are higher by a factor of 3.

5 mm-Capillary tube:

The 5 mm-capillary assembly was also employed to get a trend with different solvents with different dielectric constants. The coaxial volume is so large in this assembly that it is not possible to tune the sample, even with a low dielectric constant solvents.

3 mm – 5 mm coaxial assembly:

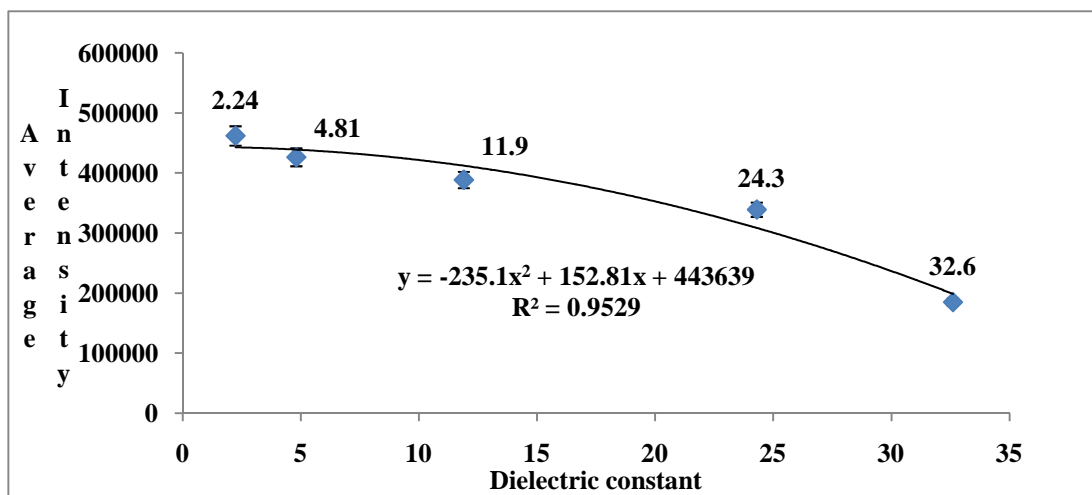


Figure 3.18 Dielectric constant versus Average Intensity plot for 3 mm – 5 mm cell. ($\epsilon=2.24$ Carbon tetrachloride, $\epsilon=4.86$ chloroform, $\epsilon=11.9$ t-BuOH, $\epsilon=24.3$ ethanol, $\epsilon=32.6$ methanol). The error bars represent a 3.5% error which was measured and will be discussed later in Section 3.7(B).

Figure 3.18 shows a plot of dielectric constant versus average intensity plot for 3 mm – 5 mm assembly. The diameter of the inner tube is 3 mm, whereas the diameter of the outer tube is 5 mm. As seen from the plot, the intensity is an average of two

different measurements taken on the same solvents with different dielectric constants at different times with the same assembly and keeping the parameters constant. With the 3 mm – 5 mm assembly it is still difficult to measure the larger range of dielectric constants (2 - 78). The problems (leaning against the outer tube and atmospheric oxygen) discussed in the capillary assembly section do not occur to the same extent in the 3 mm – 5 mm assembly. But again it is the large volume of the sample, as the difference in the tube diameters is 2 mm, which makes it impossible to tune the sample in the microwave cavity beyond a dielectric constant of ca. 33. Though only a certain range of dielectric constants are covered, the polynomial trend fits nicely on the data points giving the R^2 coefficient about 0.95. The high correlation coefficient is the reflection of the fact that the assembly is better in several ways than the capillary assemblies.

The data analysis for the data was done with two fits, linear and polynomial as shown in Table 3.2.

Fit for the data	Average Error (dielectric constant units)
Polynomial ($R^2 = 0.953$)	5.84
Linear ($R^2 = 0.910$)	6.47

Table 3.2 Average Errors for Polynomial and Linear fits for the 3mm-5mm coaxial assembly

As seen from the table, the polynomial fits better than the linear fit. An average error was calculated for each fit, which is a total average of the individual difference from known literature values. The average error for the polynomial fit is 5.84 dielectric constant units and is lower than the average error for linear fit (6.47 dielectric constant units). The cubic fit was also tried for the above data. Although the cubic fit was better, the average error is much higher than that for the polynomial fit.

The polynomial trend to fit the data from 3 mm – 5 mm assembly could be used to predict dielectric constant of an unknown sample only if the unknown has a dielectric constant in the range from 2 - 33. The other important observation made from the 3 mm – 5 mm plot is the polynomial equation's first variable is negative. As seen from the plot, the change in slope of the EPR signal intensity with the initial samples (solvents) is low and goes on increasing as the dielectric constant increases.

Since only a small dielectric range could be covered on the 3 mm – 5 mm coaxial assembly due to larger absorption, it would be helpful to have a 1 mm coaxial diameter difference. Two different coaxial assemblies were used for further investigation, the 4 mm – 5 mm and the 3 mm – 4 mm coaxial assemblies.

4 mm – 5 mm coaxial assembly:

The 4 mm – 5 mm assembly consisted of a 4 mm diameter inner tube which contains the reference solution, whereas the outer tube is 5 mm in diameter. The plot for the 4 mm – 5 mm assembly is shown in Figure 3.19.

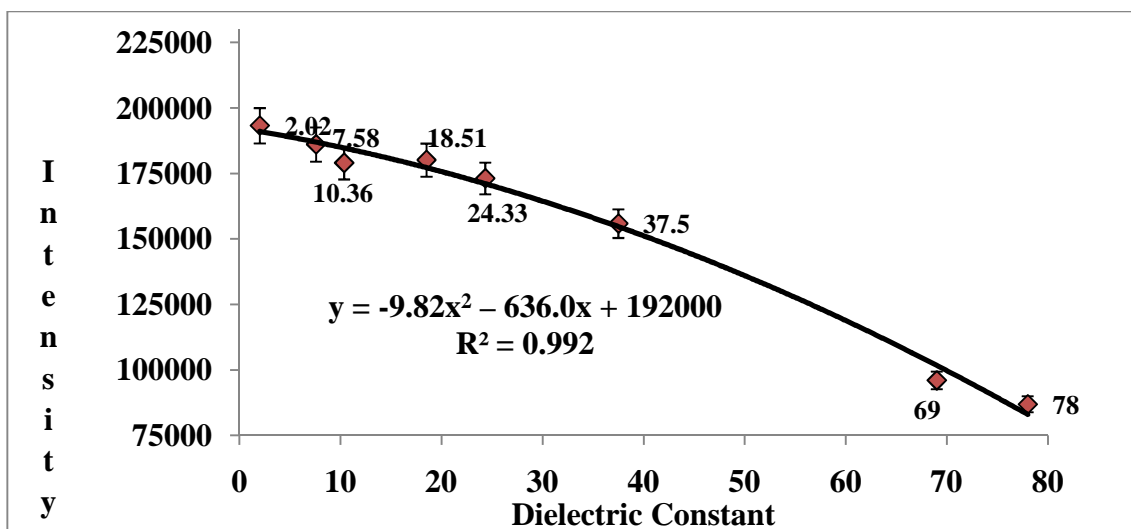


Figure 3.19 Literature values ($\epsilon=2.02$ Cyclohexane, $\epsilon=7.58$ THF, $\epsilon=10.4$ Dichloroethane, $\epsilon=18.5$ Methyl ethyl ketone, $\epsilon=24.3$ ethanol, $\epsilon=37.5$ acetonitrile, $\epsilon=69.0$ Propylene carbonate, $\epsilon=78.0$ water). The error bars represent a 3.5% error which was measured and will be discussed later in Section 3.7(B)

The difference in the diameters of the two coaxial tubes is only 1 mm. Thus the volume of sample required in the coaxial tubes is lower than the 3 mm – 5 mm assembly. Due to the smaller radial difference (0.5 mm) between the two tubes, a larger range of dielectric constants (2 - 78) can be measured. Compared to the capillary tube assembly or the 3 mm – 5 mm coaxial assembly, the errors found treating each solvent as an unknown using this assembly is lower as seen from Table 3.3.

Fit for the data	Average Error (dielectric constant units)
Polynomial $R^2 = 0.992$	3.85
Linear $R^2 = 0.991$	5.07

Table 3.3 Average Errors for Polynomial and Linear fits for the 4 mm – 5 mm coaxial assembly.

As seen from Table 3.3, the linear fit gives a correlation factor (R^2) of 0.991 and the polynomial fit gives a correlation factor (R^2) of 0.992. Thus, similar to the 3 mm – 5 mm assembly, the polynomial fit is better for the 4 mm – 5 mm assembly data. The average error calculated for the linear fit is 5.1 dielectric units, whereas the average error calculated for polynomial fit is 3.9 dielectric units.

Another important fact that needs to be considered is that the polynomial fit is not 100% fit to the data. Therefore the error involved in fitting the data could be carried forward in estimating the dielectric constant of the unknown sample from the quadratic equation.

3 mm – 4 mm coaxial assembly:

The 3 mm – 4 mm assembly consists of a 3 mm diameter inner tube which contains the reference solution, whereas the outer tube is 4 mm in diameter. The plot for the 3 mm – 4 mm assembly is shown in Figure 3.20.

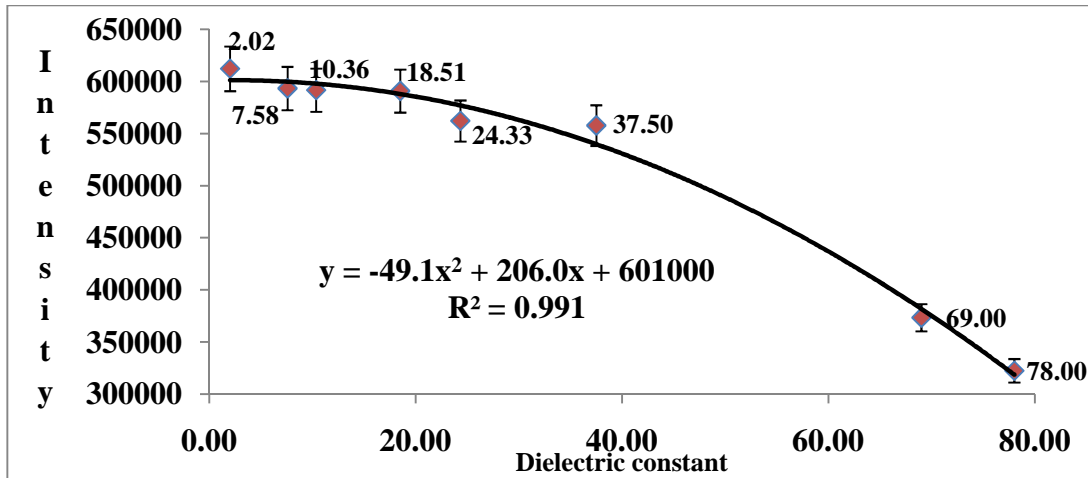


Figure 3.20 Literature Values ($\epsilon=2.02$ Cyclohexane, $\epsilon=7.58$ THF, $\epsilon=10.4$ Dichloroethane, $\epsilon=18.5$ Methyl ethyl ketone, $\epsilon=24.3$ ethanol, $\epsilon=37.5$ acetonitrile, $\epsilon=69.0$ Propylene carbonate, $\epsilon=78.0$ water). The error bars represent a 3.5% error which was measured and will be discussed later in Section 3.7(B)

The 3 mm – 4 mm assembly has a diameter difference of 1 mm which is, again, smaller than for the 3 mm - 5 mm coaxial assembly. The coaxial volume is less than the 4 mm - 5mm assembly. Table 3.4 shows the correlation factors and average errors for the linear and the polynomial fit.

Fit for the data	Average Error (Dielectric Constant Units)
Polynomial $R^2= 0.991$	5.66
Linear $R^2= 0.973$	7.91

Table 3.4 Average Errors for Polynomial and Linear fits for the 3mm-4mm coaxial assembly.

The correlation factor “ R^2 ” is 0.991 for the polynomial fit whereas it is 0.97 for the linear fit, which again suggests that a polynomial fit is better. The average error was calculated for both the fits and the average error for the polynomial fit is 5.66 dielectric constant units, whereas it is 7.91 dielectric constant units for the linear fit. Similar to that of the 4 mm – 5 mm coaxial assembly, the error caused due to the leaning effect of the inner tube on the inner side of the outer tube is lesser when compared to the capillary assemblies and the 3 mm – 5 mm coaxial assembly. The 3 mm – 4 mm assembly is similar to the 4 mm – 5 mm assembly as the difference in the radial diameters of the inner and outer tube is 1 mm in both cases and both the assemblies show similar results as far as trend of the data points is concerned. The comparison of the absolute values of the EPR signal intensity of the 3 mm - 4 mm and 4 mm – 5 mm assembly show that the EPR signal intensity for 4 mm – 5 mm are lower than those of the 3 mm – 4 mm assembly. This difference in the absolute intensity of the two assemblies is due to the fact that although the 4 mm – 5 mm and 3 mm – 4 mm assemblies both have 1 mm radial diameter differences, the coaxial volume of the 4 mm – 5 mm assembly is greater than for the 3 mm – 4 mm assembly. Thus, the greater the coaxial volume, the greater the energy losses to the solvent being measured.

Comparing the 4 mm – 5 mm assembly to the 3 mm – 4 mm assembly, it can be seen from the average error comparison that the 3 mm – 4 mm coaxial assembly gives a larger error than the 4 mm – 5 mm coaxial assembly. The reason for this could be due to the shrinking cross-sectional area of the entire assembly. Another important observation to be made is the fact that the data for every assembly fits better with a

polynomial fit than that for a linear fit. The reason for this observation could be a result of the circular geometry of the coaxial cell that could be causing a lensing effect.

As seen from all the data above, it can be concluded that the coaxial assemblies could be used on the EPR to estimate the dielectric constant of a unknown solvent, with some errors involved, by measuring the intensity of solvents with known dielectric constants to give a calibration curve and then interpolating the dielectric constant of the unknown solvent. The errors involved in these measurements may come from the geometry of the coaxial assembly, the water content in the solvents (the solvents are not distilled and measurements are made in open air) and the positioning of the tube.

3.6 EPR as a tool to investigate dielectric constant of unknown mixture of solvent samples

As the EPR coaxial assembly was effective in estimating the dielectric constant of solvents, it was of interest to see the application of the EPR coaxial assembly to measure dielectric constants of mixtures of solvents. The new system involves the measurement of the EPR signal intensity for different weight fractions of water in dioxane. The two reasons for the selection of these two solvents are;

- ❖ Dioxane has a dielectric constant of 2.24 and water has a dielectric constant of 78. By making mixtures of dioxane and water (w/w) it is possible to cover a large range of dielectric constants. Problems associated with trace water in the solvents are decreased since water is purposefully a part of the system.
- ❖ The dielectric constant values for different mixtures (w/w) are presented in the literature in 1936 by Gosta Akerlof and Oliver Short²⁵. A detailed chart for the

dielectric constant with the addition of water to dioxane (w/w) is given in Figure 3.21.

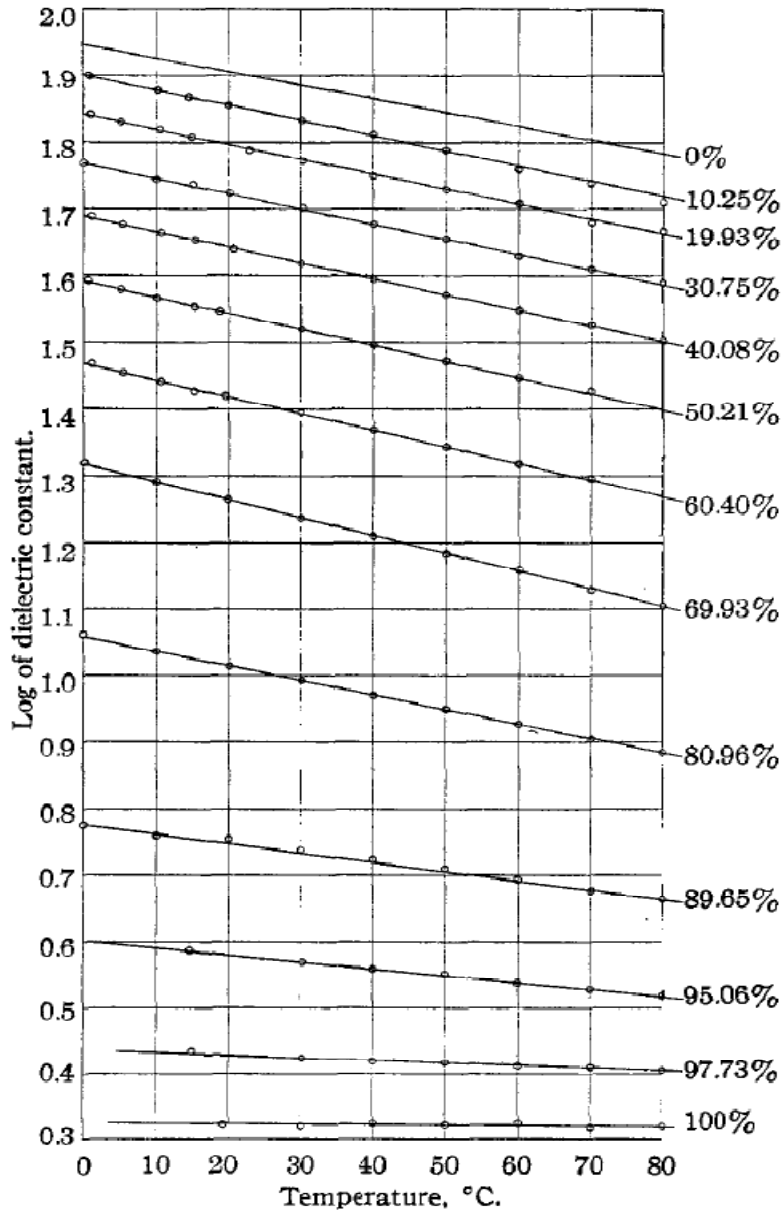


Figure 3.21. Curves for logarithm of the dielectric constant of dioxane-water mixtures of constant composition and varying temperature

Table 3.5 shows the weight fraction of the water-dioxane mixtures and their corresponding dielectric constants extrapolated from the data at 25 °C in Figure 3.21.

% Dioxane in water	Dielectric constant
0	81.28
10	72.44
20	63.09
30	53.7
40	43.7
50	35.48
60	26.3
70	18.62
80	12.58
90	5.62
100	2.14

Table 3.5 water-dioxane mixtures (w/w) and their dielectric constant at 25°C.

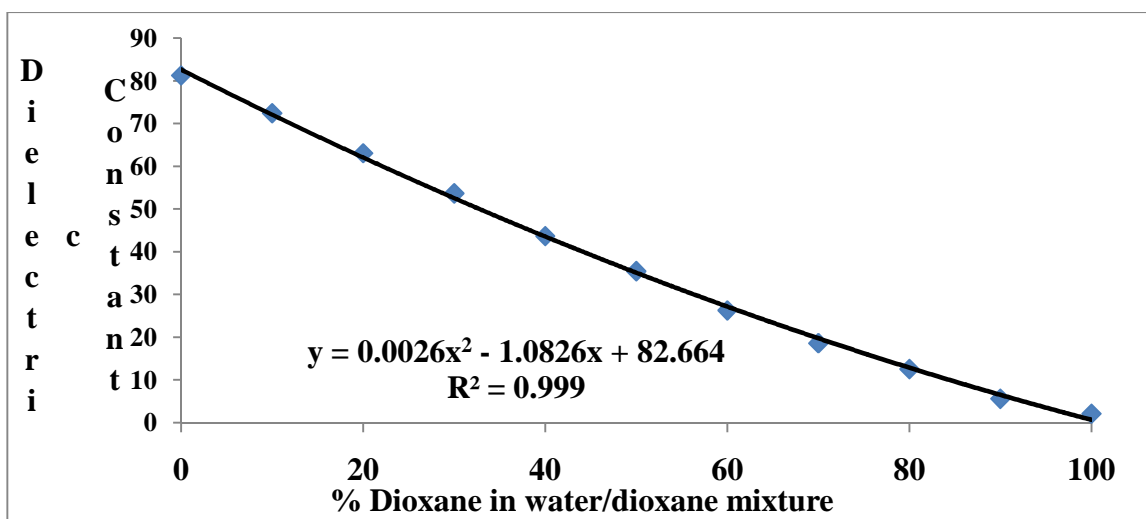


Figure 3.22 Plot of Dioxane % in water/dioxane mixture v/s Dielectric Constant at 25°C²⁵

As seen from Figure 3.22, the slope for the plot of dioxane % in water/dioxane mixture does not change exactly linearly and a polynomial fit gives a better correlation. The possible reason for this behavior will be discussed later in this chapter.

4 mm – 5 mm assembly-water/dioxane mixtures:

The 4 mm – 5 mm assembly was used to measure EPR signal intensities for different dioxane/water mixtures. Table 3.5 show the weight fraction of the water-dioxane mixtures and their corresponding dielectric constants.

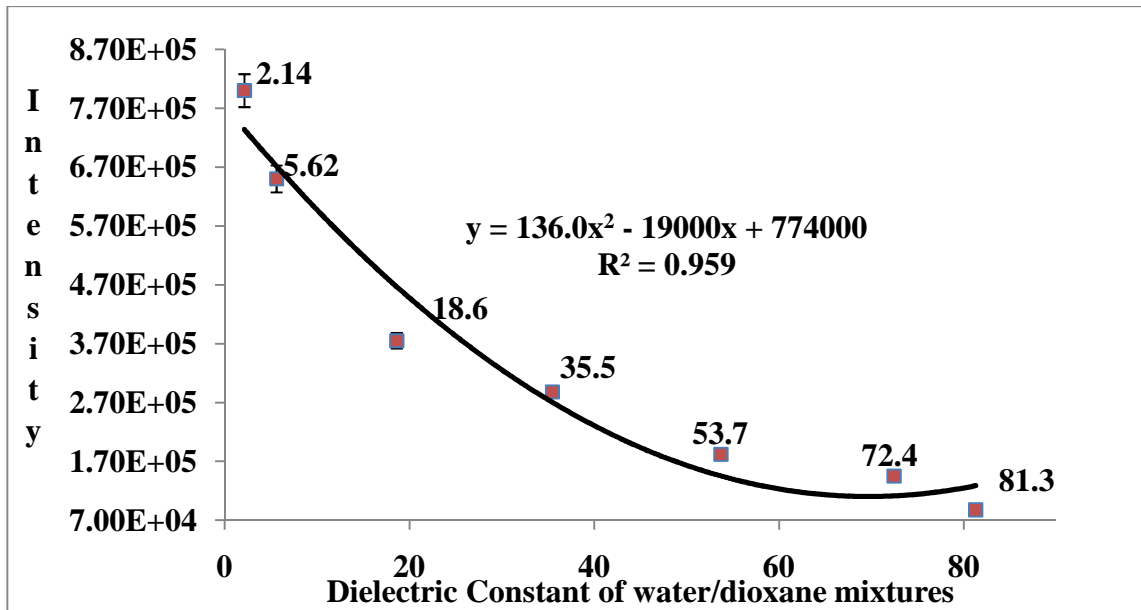


Figure 3.23 4 mm – 5 mm assembly. Plot of Dielectric constant for various water/dioxane mixtures versus EPR Intensity in a.u. The error bars represent a 3.5% error which was measured and will be discussed later in Section 3.7(B)

From Figure 3.23, it can be seen that a wide range of dielectric constants can be covered with the 4 mm – 5 mm assembly with the water-dioxane mixtures. The most important observation to be made here is the calibration curve fits best with a

polynomial fit as seen earlier with the solvent calibration curve. The polynomial fits the data with a correlation factor “R²” of 0.9553, which is satisfactory as far as the fitting of data is concerned.

Two unknown mixtures were prepared (w/w % not known during the measurement) to measure their EPR signal intensity and calculate their dielectric constant from the the calibration curve. Table 3.6 shows the data for the two unknown mixtures.

Water/dioxane (w/w) % 4mm-5mm coaxial assembly	Literature value²⁵ (ϵ) from Table 2	Calculated Value from the Polynomial fit
80% water/20% dioxane	63.1	61.3
40% water/60% dioxane	26.3	28.7

Table 3.6 4 mm – 5 mm coaxial assembly in measuring dielectric constant of water/dioxane mixtures

The first unknown mixture gave an EPR signal intensity of 120000 a.u. The calculated value for dielectric constant from the polynomial equation is 61.3. The unknown 1 was a (w/w) mixture of 20% dioxane-80% water. The corresponding dielectric constant for the 20% dioxane-80% water is 63.09 (Table 2). The EPR signal intensity for unknown mixture 2 was measured to be 340000 a.u. The value for the dielectric constant was calculated as 28.7. The unknown mixture 2 is (w/w) mixture of 60% dioxane and 40% water. The literature value of dielectric constant for 60% dioxane and 40% water is 26.3. The error of approximately 2 dielectric constant units is seen for

both the unknowns from the literature values. The errors could occur for various reasons. First, water content present in the “100% dioxane” could be responsible for some of the error. Secondly, weighing errors could add up to the total error to give deviations from the literature values. Since the same outer tube is used for all the measurements, the cleaning of the tube after every measurement is required. If the tube is not cleaned properly after every measurement, it could also add to the errors in the system.

Another issue with above data in specific is the fitting of the data. Since the data is fit to parabolic curve (polynomial of degree 2), at the higher end of the dielectric constant the intensity starts to go higher again which physically is impossible. Thus the data at the higher end of the dielectric constant axis will have higher error in the measurement of the EPR signal intensity. This problem could be addressed by trying to fit the data differently, and then interpolating the dielectric constant.

3mm-4mm assembly-water/dioxane mixtures:

The 3 mm – 4 mm assembly was also used to measure different mixtures (w/w) of water and dioxane. Figure 3.24 shows a plot of dielectric constant of dioxane-water mixtures versus the EPR signal intensity. Similar to the 4 mm – 5 mm assembly, the 3 mm – 4 mm assembly can also be used to cover a wide range of dielectric constants.

Similar to the 4 mm - 5 mm assembly, the data measured with 3 mm – 4 mm assembly also fits a polynomial equation well. The correlation factor “ R^2 ” is 0.983 is even better when compared to the 4 mm – 5 mm assembly.

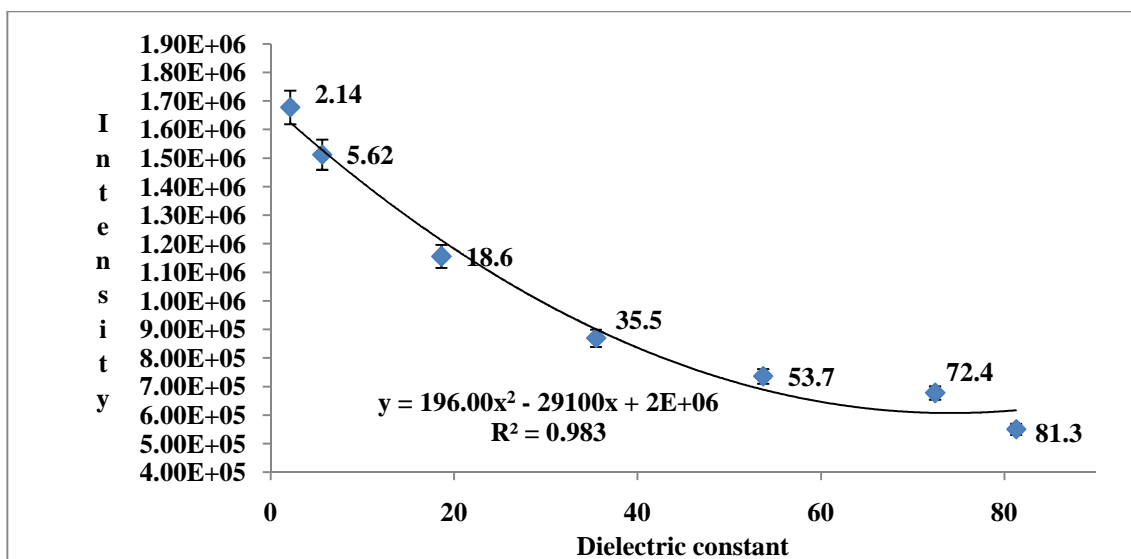


Figure 3.24 3 mm – 4 mm assembly. Plot of Dielectric constant versus Intensity for water-dioxane mixtures. The error bars represent a 3.5% error which was measured and will be discussed later in Section 3.7(B)

Two unknown mixtures (w/w) were prepared to check the EPR signal intensity and hence their dielectric constant could be calculated from the polynomial equation of the calibration curve. The data is shown in Table 3.7.

Water/dioxane (w/w) % 3 mm – 4 mm coaxial assembly	Literature value ²⁵ (ϵ) from Table 3.5	Calculated Value from the Polynomial fit
82% water/18% dioxane	63.2	61.8
58.3% water/41.7% dioxane	41.0	38.6

Table 3.7 3mm-4mm coaxial assembly in measuring dielectric constant of water/dioxane mixtures

Unknown mixture 1 gave an EPR signal intensity of 631200 a.u. The calculated value for dielectric constant from polynomial equation for unknown mixture 1 is 61.8.

Unknown mixture 1 was 18% dioxane-82% water. From the data in Table 3.5, the dielectric constant for 18% dioxane-82% water is 63.2. Similarly, unknown mixture 2 gave an EPR signal intensity of 846600 a.u. The calculated value of dielectric constant from the polynomial equation for unknown mixture 2 is 38.6. The unknown mixture 2 is a mixture of 41.7% dioxane-58.3% water. From the Table 3.5, the dielectric constant value for 41.7% dioxane-58.3% water is 41.0. Similar to the 4 mm – 5 mm assembly, the 3 mm – 4 mm assembly also shows an error of approximately 2 dielectric units.

The 4 mm – 5 mm assembly and the 3 mm – 4 mm assembly both seem to be reasonable assemblies to measure the dielectric constants of unknown liquids. The only difference in the 3 mm – 4 mm assembly and 4 mm – 5 mm assembly is the volume of solvent used in the measurements. The 4 mm – 5 mm uses slightly more sample (solvent) than the 3 mm – 4 mm assembly.

One very important observation made is in the way the slope changes in the mixture of solvents from that of the pure solvents. As mentioned earlier in Figure 3.22, the data plotted for dioxane% in water/dioxane mixture versus dielectric constant at 25°C, which is derived from Akerlof and Short, does not show a linear change but shows a same trend of change as seen in the plots for dielectric constant versus intensity. This observation could be attributed to the hydrogen-bonding tendency of the water. Dioxane, being an aprotic solvent, has no hydrogen bonding capability. On the addition of water, being a protic solvent, it starts to hydrogen bond (Figure 3.25) with the dioxane and with itself. Thus, on the addition of more water, the hydrogen bonding effect increases which could be the reason for the difference in the way the slope changes for dioxane/water mixture than seen in the regular solvents.

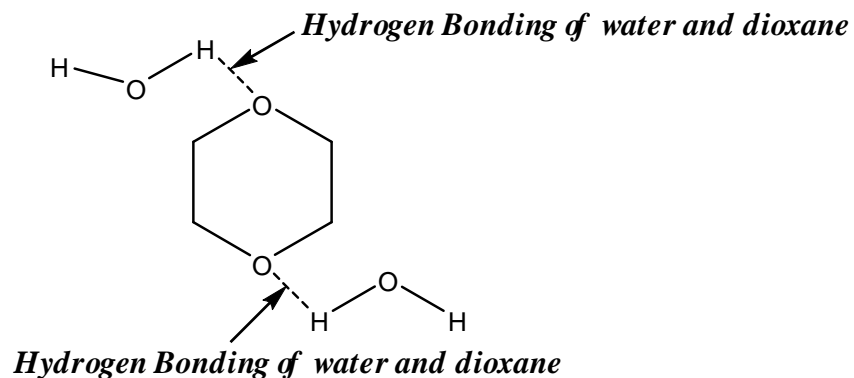


Figure 3.25 Hydrogen Bonding for water and Dioxane

The other related factor which could affect the way the slope changes as compared to the pure solvent data is the change in density. With the addition of every aliquot of water to dioxane or vice versa, there is a change in the density of the mixture. Thus along with the hydrogen bonding, changes in the density could be the reason that the slope for the dioxane/water mixture changes in a different (opposite) way.

3.7 Measurement of Errors

Different types of error were measured for the cell and the instrument. For all the error purposes 4mm-5mm coaxial assembly was used unless mentioned otherwise.

A: Placement Error without changing the aliquot of solvent for the coaxial assembly.

Placement error analysis was done with two different solvent with different dielectric constants. Methylene chloride (CH_2Cl_2 $\epsilon = 8.93$) and water (H_2O $\epsilon = 78$) were the two solvents measured. The coaxial assembly was filled with a solvent under consideration and the measurement of the EPR intensity for the solvent was taken. The coaxial assembly was then removed from the cavity and was placed back again in the

cavity without changing the aliquot of the solvent. This process was measured several (7-8) times for both the solvents.

An average for the measured EPR intensities was taken for both the solvents respectively. The difference between the individual intensities and the average intensity is calculated for each measurement. The value with the highest difference between the individual intensities and the average intensity is considered and divided by the average intensity. Table 3.8 shows the values for methylene chloride and water in percent.

Solvent	Dielectric Constant (ϵ)	Percent Error (%)
Methylene Chloride (CH ₂ Cl ₂)	8.98	0.79
Water (H ₂ O)	78	1.38

Table 3.8 Placement Errors for coaxial assembly without changing the aliquot of methylene chloride (CH₂Cl₂) and water (H₂O)

B: Placement Error with changing the aliquot of solvent for the coaxial assembly.

In this error measurement method, two different solvents were used with different dielectric constant. Methylene chloride (CH₂Cl₂ ϵ = 8.93) and water (H₂O ϵ = 78) were the two solvents measured. The coaxial assembly was filled with the solvent under investigation (water or methylene chloride). The coaxial assembly is then inserted in the cavity and EPR intensity is recorded. The coaxial assembly is then removed from the cavity, filled with another aliquot of the same solvent (water or methylene chloride),

inserted in the cavity and EPR intensity is recorded again. The process is continued several (7-8) times.

An average for the measured EPR intensities was taken for both the solvents respectively. The difference between the individual intensities and the average intensity is calculated for each measurement. The value with the highest difference between the individual intensities and the average intensity is considered and divided by the average intensity. Table 3.9 shows the values for methylene chloride and water in percent.

Solvent	Dielectric Constant (ϵ)	Percent Error (%)
Methylene Chloride (CH_2Cl_2)	8.98	0.88
Water (H_2O)	78	3.48

Table 3.9 Placement Errors for coaxial assembly with changing aliquots of methylene chloride (CH_2Cl_2) and water (H_2O)

Since most of the measurements discussed earlier with the 4mm-5mm coaxial assembly, 3mm-4mm coaxial assembly and 3mm-5mm coaxial assembly involves the changing of the solvent after every measurement an maximum error of 3.93 % (shown in Table 3.9) were applied to the systems.

C: Errors for drift in the Intensity over regular interval of time

In this error measurement method, two solvents with different dielectric constant were used. Methylene chloride (CH_2Cl_2 $\epsilon = 8.93$) and water (H_2O $\epsilon = 78$) were the two

solvents measured. The coaxial assembly was filled with the solvent under investigation (water or methylene chloride). The coaxial assembly is then inserted in the cavity and EPR intensity was recorded at regular intervals of time (every 15 mins). The solvents were measured over a span of 2 hours. During the measurement the coaxial assembly is not moved at all in the cavity. Precautions were taken to prevent any loss of solvent by evaporation by sealing the coaxial assembly with Teflon tape. During the measurement no visible evaporation was seen.

An average for the measured EPR intensities measured for methylene chloride and water was calculated respectively. The difference between the individual intensities measured at regular time intervals and the average intensity is calculated. The value with the highest difference between the measured intensities and the average intensity for a particular solvent is considered and divided by the average intensity for that solvent. Table 3.10 shows the values for methylene chloride and water in percent.

Solvent	Dielectric Constant (ϵ)	Percent Error (%)
1,2-dichloroethane ($C_2H_4Cl_2$)	10.36	1.35
Water (H_2O)	78	1.67

Table 3.10 Drift Errors for coaxial assembly for 1,2- dichloroethane ($C_2H_4Cl_2$)and water (H_2O)

D: Fluctuation in the Temperature of the Microwave Cavity of the EPR

A thermocouple was attached to the microwave cavity and the change in the temperature of the microwave cavity was measured at every 30 mins for 7.5 hours. The reaction of triethylamine with different concentration allyl chloride was studied and is discussed in detail in Chapter 4 using a 3mm-5mm coaxial assembly. Precautions were taken to prevent any loss of sample by evaporation by sealing the coaxial assembly with Teflon tape.

The starting temperature was 21.2 ° C of the microwave cavity which increased 22.4 ° C at the end of 7.5 hours. A difference of 1.2 ° C is seen in the temperature after 7.5 hours. Most of the measurements made on the EPR are done over a span of 2 hours and after 2 hours (120 minutes) the temperature was 21.2 ° C. Therefore after two hours no fluctuation in the temperature was observed. After 3 hours only an increase of 0.4 ° C was seen in the temperature from the starting temperature. Therefore, temperature fluctuation are not as significant in the microwave cavity.

3.8 Conclusion

From this chapter, it can be concluded that EPR as technique can be used for many other purposes than just the traditional purpose of EPR of detecting radical species. EPR can be used as tool to investigate the dielectric properties of different liquid media, including estimating dielectric constants from the calibration curve. Different types of coaxial assemblies were studied and optimum choice of the assemblies was made for further studies. The 3 mm – 4 mm coaxial and 4 mm – 5 mm coaxial assembly was the best choices for the assembly for further studies as a large

range of dielectric constants (2-78) could be covered with these two coaxial assemblies. Although the technique involves errors in determining the exact dielectric constant, with some precautions, this technique would be an apt technique to give a range of dielectric constant with an error of roughly (+) or (-) 5 dielectric constant units. With some further research, especially on the coaxial cell geometry, the errors may be able to be reduced more accurate values for the dielectric constant of an unknown sample (liquid) obtained. The circular geometry does account for some error due to the lens effect, which can be taken care of with a flat cell geometry.

This coaxial assembly EPR technique can also be used to study the dielectric properties of mixtures of solvents. The use of this technique to measure the dielectric constants of mixtures of dioxane-water was also discussed in this chapter. Again with the mixtures, a large range of dielectric constant was covered with different w/w mixtures of dioxane and water and the errors were lower than seen for the use of technique to determine the dielectric constants of single solvents. Some other practical uses of this EPR technique will be discussed in the next chapter.

3.9 Experimental

A: EPR instrumentation

All the measurements were carried out using a Bruker EMX EPR spectrometer operating at the X band. The spectrometer has Bruker 048T Microwave Bridge and Bruker ER073 Magnet. The cavity used in all measurements was the standard rectangular one operating in TE 102 mode (Bruker 4102 ST cavity). The signal channel was kept constant at a magnetic field modulation frequency of 100 kHz. The microwave

frequency was held constant at 9.725 GHz and the microwave power was held constant at 0.201 mW for all the measurements.

B: Coaxial assembly

The capillary tubes used in the capillary-3 mm, capillary-4 mm and capillary-5 mm assemblies were melting point capillaries. The NMR tubes (3 mm, 4 mm, 5 mm) were from Wilmad Lab Glass. The tubes were cut according to the required length of the tube. The inner tubes (3 mm and 4 mm) containing hexane and TEMPO were sealed under inert atmosphere using an acetylene torch.

C: Solvents and reagents.

All the solvents used for the calibration curves were reagent grade solvents used straight out of the containers. Distilled water was used for calibration curve estimation and for the dioxane-water mixtures.

References:

1: "Dielectric" Britannica Encyclopedia, URL:

<http://www.britannica.com/EBchecked/topic/162630/dielectric>

2: Jackson, J.D. Classical Electrodynamics (Third Edition), New York: Wiley, 1999, 154.

3: IEEE Standard definitions of Terms for Radiowaves Propagation **1997**, 30.

4: The NIST Reference on Constants, Units and Uncertainty, URL:

<http://physics.nist.gov/cgi-bin/cuu/Value?ep0>

- 5: King, R.W.P.; *Fundamental Electromagnetic Theory* **1963**, New York: Dover, 139.
- 6: Scaife, B.K.P.; *Dielectric and Related Molecular Processes*, Volume 1, Chapter 1, 9.
- 7: “Microwave Dielectric Spectroscopy Workshop: Measure the Difference” **2004**, Agilent Technologies.
- 8: Chao, Shuh-Han.; *IEEE Transactions on Microwave Theory and Techniques* **1985**, MTT 33, 6, 519-526.
- 9: Tsuzukiyama, K.; Sakai, T.; Yamazaki, T.; Hashimoto, O.; 33rd European Microwave Conference, Munich **2003**, 487-490.
- 10: Dhanya, R.; Kishore, V.C.; Kartha, C.S.; Sreekumar, K.; Joseph, R. *Spectrochimica Acta Part A* **2008**, 71, 1355-1359.
- 11: Paley, M.S.; Harris, J.M.; Looser, H.; Baumert, J.C. Bjorklund, D.J.; Twieg, R.J. *Journal of Organic Chemistry* **1989**, 54, 3774-3778.
- 12: Brown, B.; Hess, D.; Desai, V.; Deen, M.J. *Dielectric Science and Technology: The Electrochemical Society Interface* **2006**, 28-31.
- 13: Weber, R.T.; Jiang, J.; Barr, D.P.; EPR Division Bruker Instrument, Inc; Bellerica, MA, USA; *EMX User’s Manual* **1998**.
- 14: Weil, J.A.; Bolton, J.R.; Wertz, J.E. *Electron Paramagnetic Resonance, Elementary Theory and Practical Applications*: Wiley Interscience, New York **1994**.
- 15: Chen, L.F.; Ong, C.K.; Neo, C.P.; Varadan, V.V.; Varadan, V.K; *Microwave Electronics: Measurement and Materials Characterization* **2004**.

- 16: Stitch, M.L.; Microwave Interaction with Matter, Proceedings of The IRE **1962**, 1225-1231.
- 17: Jacob, J.; Chia, L.H.L.; Boey, F.Y.C. Journal of Material Science **1995**, 30, 5321-5327.
- 18: Nagy, V. Applied Magnetic Resonance **1994**, 6, 259-285.
- 19: Ito, T.; Yokoyama, H.; Sato, T.; Ogata, T. Applied Magnetic Resonance **2001**, 21, 97-103.
- 20: Dalal, D.P.; Eaton, S.S.; Eaton, G.R. Journal of Magnetic Resonance **1981**, 44, 415-428.
- 21: Yordanov, N.D.; Lubenova, S. Analytica Chimica Acta **2000**, 403, 305-313.
- 22: Barriga, S. Synlett (4) **2001**, 563.
- 23: EPR Spectroscopy: Introduction,
URL:<http://web.nmsu.edu/~snsm/classes/chem435/Lab7/>
- 24: Dielectric Constant Values, URL:
<https://www.clippercontrols.com/pages/dielectric-constant-values>
- 25: Akerlof, G.; Short, O.A. Journal of the American Chemical Society **1936**, 58 (7), 1241-1243.

Chapter 4

Practical applications of the coaxial EPR assemblies to study dielectric properties of liquid media

The coaxial assemblies, especially the 4 mm – 5 mm and 3 mm – 4 mm could be very useful in several practical applications like measuring the amount of water in a solvent, monitoring the rate of a reaction etc. In this section, these practical applications of the EPR technique for studying dielectric properties will be discussed. The applications discussed in this chapter are listed below:

- 1) Determining the water content in water-dioxane mixture,
- 2) Studying changes in the dielectric constant of electrolyte solutions as a function of salt concentration,
- 3) Detecting phase transitions,
- 4) Monitoring the rate of a reaction, and
- 5: Correlation of changes in the dielectric properties of surfactant solutions to their critical micelle concentrations (CMC).

4.1 Application to measuring % water in water/dioxane mixtures

In synthetic chemistry, the presence of water in solvents can cause major differences in reaction pathways and the yield of desired products. In synthetic laboratories, great effort is often made to exclude water from solvents. Dehydration techniques are usually used to make sure of the removal of water and the reproducibility

of the experimental results. Also, in analytical chemistry the presence of water can be a major concern as it may have adverse effect on measurements where water interferes. Analytical chemists have come up various techniques to detect the amount of water in solvents.

In this section of the chapter, the application of the EPR technique to study dielectric properties was used to determine the weight % of water present in water-dioxane mixtures. The the 3 mm – 4 mm and the 4 mm – 5 mm coaxial assemblies were used to measure the weight % of water in water/dioxane mixtures.

4 mm – 5 mm assembly in measurement of % water in water-dioxane mixtures

The measurement of % water in water/dioxane mixtures can be derived from the dielectric constant data plot which is presented in Ch. 3. The plot for dielectric constant versus Intensity is shown in Figure:4.1.

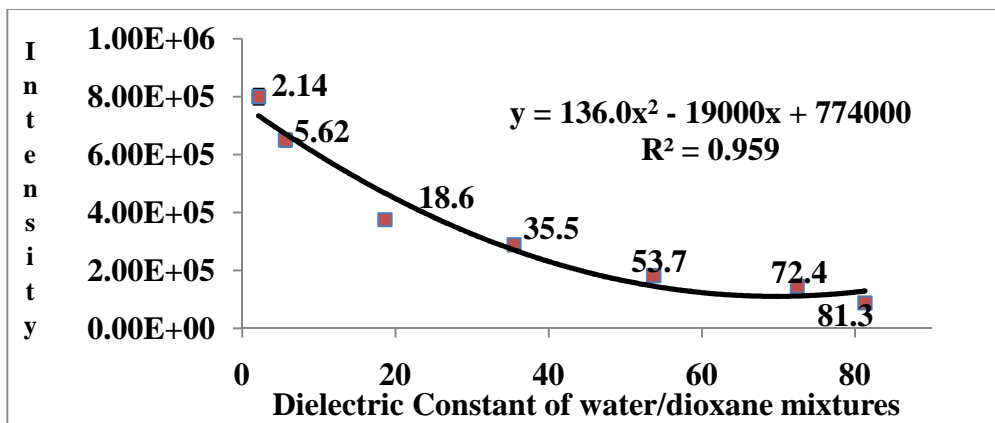


Figure 4.1. Plot of Dielectric constants for % Dioxane mixture versus EPR signal intensity. (4 mm - 5 mm assembly) The error bars represent a 3.5% error, measured and discussed in Section 3.7(B)

The determined dielectric constant is related to the weight % by the correlation plot of dioxane % in water/dioxane mixture versus intensity at 25°C derived from the data of Akerlof and Short (Figure 3.21, chapter 3). The calculated % water in the unknown water/dioxane mixtures is shown in Table:4.1.

Dioxane/water Mixture (w/w) Actual weight %	Literature Value¹ (ε)	Calculated Value from the fit (ε)	% Water in dioxane value from literature
20% Dioxane 80% Water	63.1	61.3	20.8% Dioxane 79.2% Water
60% Dioxane 40% Water	26.3	28.7	58.0% Dioxane 42.0% Water

Table 4.1 Values for Weight % of water in water/dioxane mixtures from Akerlof and Short correlation chart for 4 mm – 5 mm assembly.

As seen from the Table 4.1, the unknown water/dioxane mixture which had a calculated value of 61.3 as the dielectric constant, shows a % water value of 79.2%. The actual weight % of water in the unknown water/dioxane mixture was 80%. Similarly for the other unknown water/dioxane mixture, which had a calculated value of 28.7 as the dielectric constant, shows 58% of water in the mixture. The unknown water/dioxane

mixture contained 60% water. Both the unknown water/dioxane mixtures are in agreement with the actual water % (weight %) in the water/dioxane mixtures. There is an error of ca. 2% water content involved which could be due to weighing errors during the making of these samples. The above results prove that the 4 mm – 5 mm assembly can be used to measure the % water % in solvent mixtures with a relatively small error involved.

3 mm – 4 mm assembly in measurement of % water in water-dioxane mixtures

Figure 4.2 shows a plot of dielectric constant of water/dioxane mixtures versus the EPR signal intensity.

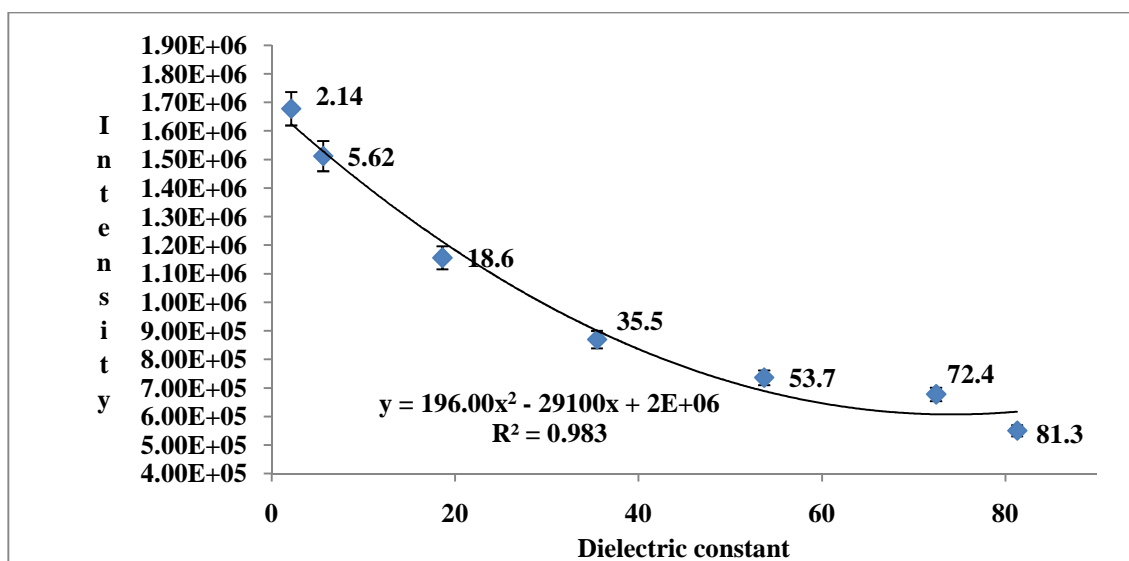


Figure 4.2. Plot of Dielectric Constant for water/dioxane mixtures versus EPR signal intensity. (3 mm – 4 mm assembly) The error bars represent a 3.5% error, measured and discussed in Section 3.7(B)

The plot is the same plot as shown in Chapter 3. The dielectric constant calculated from this plot were correlated to the % water from plot of dioxane % in

water/dioxane mixtures derived from the correlation chart shown by Akerlof and Short in the literature.

The correlated % water from the calculated dielectric constant data from the literature is given in the Table 4.2.

Dioxane/water Mixture (w/w) Actual weight %	Literature Value¹ (ϵ)	Calculated Value from the fit (ϵ)	Calculated value from literature for Dioxane and water %
18% Dioxane 82% Water	63.2	61.8	20.2% Dioxane 79.8% Water
41.7% Dioxane 58.3% Water	41.0	38.6	45.7% Dioxane 54.3% Water

Table 4.2 Values for Weight % of water in water/dioxane mixtures from Akerlof and Short correlation chart for 3 mm – 4 mm assembly.

The dielectric constant for the first unknown water/dioxane mixture was calculated as 61.8 in the previous chapter. The corresponding water content was 79.8%. The actual % water in the water/dioxane mixture was 82%. The error in the calculated and the predicted value is again ca. 2% water. Similarly, the dielectric constant for the

second unknown water/dioxane mixture was calculated to be 38.6. The corresponding % water was 54.3%. The actual % water in the second unknown water/dioxane mixture was 58.3%. The error was ca. 4% water.

There are likely various sources of errors for the measurements. As the amount of dioxane changes, the relationship between instrumental signal error and dielectric constant (and thus composition) becomes complex with regard to the composition values. There could also be some amount of water present in the dioxane solvent already on top of weighing error. Third, the cell errors discussed in Chapter 3 during measurement of the dielectric constant could be carried forward to this application. The 4 mm – 5mm assembly appears to give less error, likely stemming from an increased sensitivity due to its larger sampling within the dielectric window volume. All error sources considered, the method works remarkably well.

To summarize, the use of these coaxial assemblies (3mm - 4mm and 4 mm – 5 mm) with the EPR technique can be applied to detect the % water in solvents. A double calibration technique has to be used to measure the % water and any other solvent mixture whose information has not been investigated in the literature. First, the dielectric constants of the various water/solvent mixtures can be measured using the calibration technique with solvents of known dielectric constants as shown in Chapter 3. Second, a second calibration curve can be plotted to with the % water in the mixtures versus the measured dielectric constants determined from the first calibration curve. The dielectric constant of the unknown can be then correlated to the % water from the second calibration curve.

4.2 Application in studying the dielectric properties of electrolyte solutions

The relationship between ionic transport in liquids and polymer electrolytes and the static dielectric constant of the solution has been widely discussed in the literature^{2,3,4,5}. According to Walden's rule, the size, charge of the ions and viscosity of the medium are responsible for ionic mobilities. However, ionic mobilities often do not simply depend on the above mentioned parameters and it becomes important to measure other properties of electrolyte solutions, such as dielectric constants^{6,7}.

In an earlier chapter, the dependence of ionic conductivity on the static dielectric constants of the solution was discussed. In 2008, Petrowsky and Frech showed the importance of measuring the static dielectric constant of salt solutions in different solvents to explain the ionic mobilities of ions in the system and the impact the change in the dielectric constant can have on molar conductivities. Figure 4.3 shows the molar conductivities of tetrabutylammonium triflate solutions in solvents with different dielectric constants⁷.

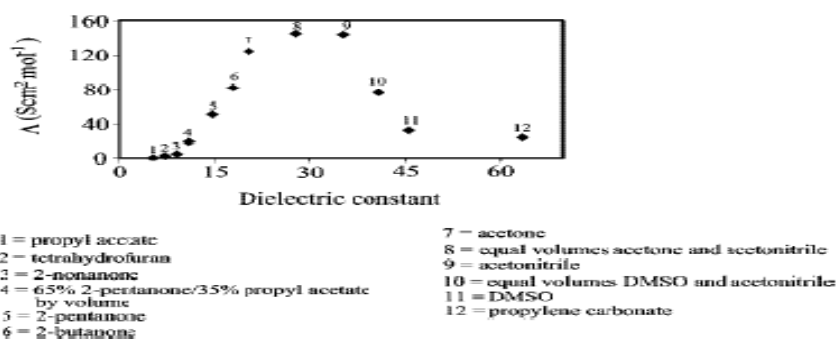


Figure 4.3 Dependence of molar conductivity of electrolyte solutions on dielectric constant of different solvents.

It is well known that the addition of salts to solvents will decrease or increase the dielectric constant of the electrolyte solution depending on the solvent the salt is dissolved in. A good example of this is the addition of alkali and alkaline earth metal halides to water and methanol, which decreases the dielectric constant of the solution. The decrease in the dielectric constant with the increase in the concentration of the salt continues up to a certain point, after which the dielectric constant levels off (stays constant). Initially, the addition of the salt to water or methanol results in ion solvation by the solvent molecules which causes the rotation or the orientation of the solvent molecules in the electric field to become more difficult, reducing the dielectric constant. After a certain concentration, with the addition of more salt there is a deficit of solvent molecules in the solution, resulting in a reorganization of the solvation layers, which then causes the leveling effect on the dielectric constant. On the other hand, in low dielectric constant solvents such as benzene and acetone, ions tend to form ion pairs. The ion pairs formed in the solution have a higher dipole moment than that of the solvent alone. Therefore, upon the addition of more salt, more ion pairs are formed and the dielectric constant goes up. At higher concentration the dielectric constant stays constant. This observation has been attributed to aggregation of the salts. Once the aggregates are formed, they have negligible dipole moments which keep the dielectric constant steady⁷.

In this section initial studies of the use of the EPR technique to study dielectric properties will be applied to salt solutions. Two different solvents, ethyl acetate and tetrahydrofuran, with different concentrations of lithium perchlorate (LiClO_4) will be investigated and discussed⁸. Since the dielectric constants of both these solvents are

pretty low (THF = 7.8, Ethyl acetate = 6.02), the dielectric constant is expected to increase as the concentration of LiClO₄ increases.

Ethyl acetate and LiClO₄

Figure 4.4 shows the calibration plot with regular solvents versus intensity.

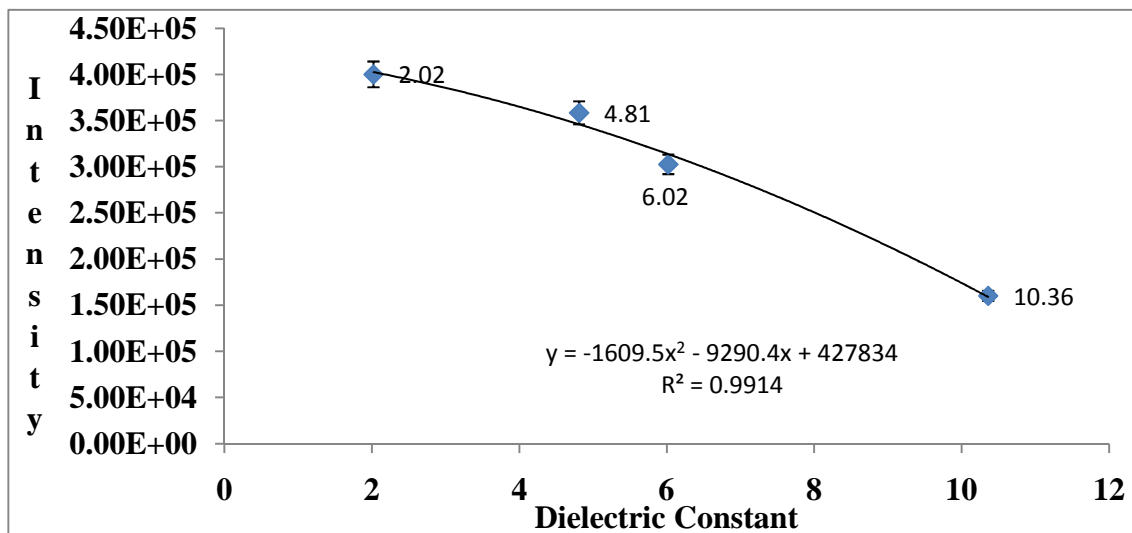


Figure 4.4 Calibration curve with solvents. (cyclohexane=2.02, chloroform=4.81, ethyl acetate=6.02, ethylene dichloride=10.36). Error bars represent +/- 3.5% error in the intensity

Three different concentrations of LiClO₄ in ethyl acetate were measured. The data is summarized in Table 4.3. As seen from the plot, with increasing salt concentration there is a decrease in the intensity of the EPR signal. This observation suggests that the dielectric constant of the solution increases with the increase in the concentration of LiClO₄. The observation is in agreement with that of the trend shown in the literature.

LiClO₄ concentration in ethyl acetate (M)	Dielectric constant from the Literature⁸	Intensity*10³ (a.u) measured on the EPR	Dielectric Constant calculated from the calibration curve (Figure:)
0.1	7.57	242	8.23
0.2	9.4	230	8.57
0.4	12.7	180	9.85

Table 4.3 Measured Intensity and calculated Dielectric constant from the calibration curve for different ethyl acetate/LiClO₄. The error bars represent a 3.5% error, measured and discussed in Section 3.7(B)

The average error from the literature value is calculated as explained earlier in Ch. 3. The average error was 1.4 dielectric units. The deviation from the literature value could be a result of various factors such as the errors in the calibration curve as discussed earlier. It is also possible that the static dielectric constants measured using this method may actually be more appropriate than those obtained using ac techniques as they are carried out at higher frequencies (GHz) and there is no electrode polarization.

THF and LiClO₄

Similar to the ethyl acetate-LiClO₄ system, different concentrations of LiClO₄ in THF were measured. Solvents with different known dielectric constants were employed for the calibration curve.

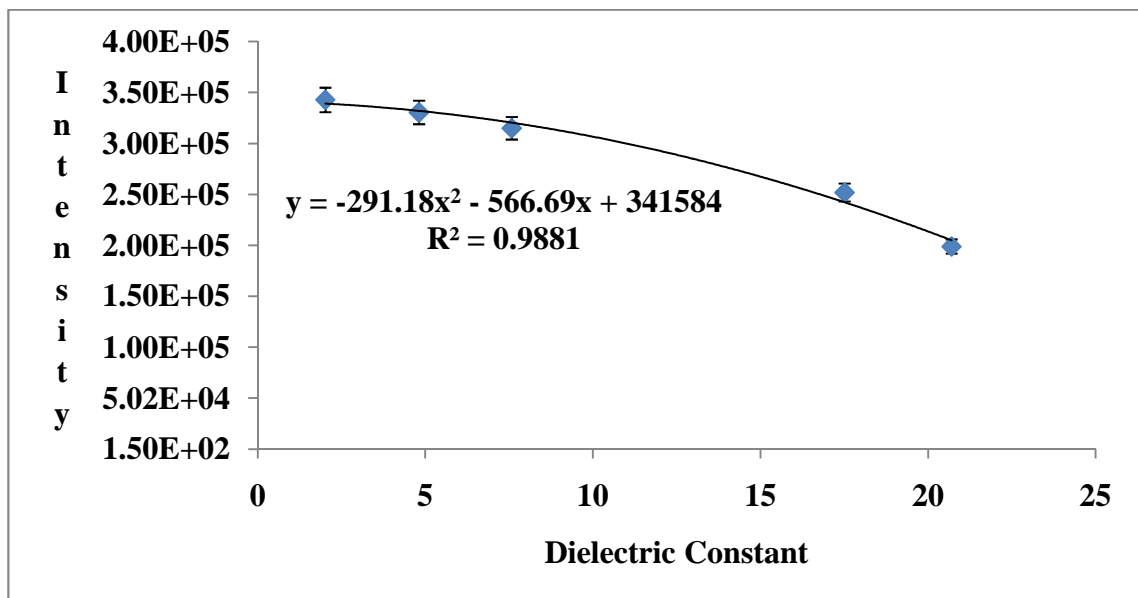


Figure 4.5 Calibration curve with solvents. (cyclohexane=2.02, chloroform=4.81, THF=7.58, 1-butanol=17.51, acetone=20.7).The error bars represent a 3.5% error, measured and discussed in Section 3.7(B)

The intensity of 5 different concentrations of LiClO₄ in THF were measured and are summarized in Table 4.4. As seen from the data, the dielectric constant of the solution goes up higher with the increase in the concentration of LiClO₄ as expected.

LiClO₄ concentration in THF (M)	Dielectric constant from the Literature⁸	Intensity * 10³(a.u) measured on the EPR	Dielectric Constant calculated from the calibration curve (Figure:)
0.1	8.81	294	11.84
0.25	11.95	242	17.54
0.4	13.9	235	18.18
0.6	16.2	228	18.8
0.8	18.2	206.7	20.57

Table 4.4 Measured intensity and calculated dielectric constant from the calibration curve for different THF/LiClO₄

The average error was calculated for the THF/LiClO₄ system as explained in Chapter 3. The average error was calculated to be 3.6 dielectric units.

The error seen in the THF/ is higher than those for the ethyl acetate/ LiClO₄ by approximately 2 dielectric units. In addition to the error carried over from the calibration curve and the coaxial assembly geometrical errors, the THF likely has some amount of water in it, which would increase the dielectric constant of the solution. This supposition can be supported by the fact that the measured dielectric constant is always higher than its literature dielectric constant value for the THF/LiClO₄ by roughly the same amount for each sample. Such a behavior is not seen with the ethyl acetate/LiClO₄ system.

4.3 Application in monitoring phase transitions

The EPR technique for studying dielectric properties can be used as a tool to monitor a phase change in the reaction. In spite of magnitude errors, the technique is quite sensitive to changes in dielectric constant. When a reaction takes place, with time more and more of the reactants are converted to product and if the product formation involves a phase change (liquid to solid), there should be a change in the dielectric constant of the entire system. As we have shown that the EPR technique is sensitive to the change in dielectric constant of a liquid, therefore it is possible to monitor a phase change in the system. It is worthwhile to mention that the application of this technique to monitor phase changes was an accidental discovery. A reaction was initially set up to evaluate if the technique could be used to monitor the rate of the reaction, but the reaction chosen was too fast and the product formed crystallized and the solution solidified, resulting in an abrupt change in the signal intensity and thus the dielectric constant.

It is known from the literature that when a salt is added to a solvent, the dielectric constant of that sample generally increases. The salt dissociation causes the polarization of the cation and anion in the solvent, increasing the dielectric constant of the sample. With increasing salt concentration more and more polarization occurs to give further increases in the dielectric constant. The dielectric constant increases up to a certain concentration, after which saturation is reached and the cation and anion are forced to be ion paired. The ion pairing brings the positive and negative charges together and thus the dielectric constant starts to decrease.

With the intent to investigate whether the EPR technique can be used as a tool to monitor the rate of product formation during a reaction, a reaction was chosen where the reactants will react to form a quaternary ammonium salt. The idea is that as the reaction proceeds more and more quaternary ammonium salt is formed in the system and the dielectric constant would go up⁷. As the dielectric constant of the system goes up, the EPR signal intensity should decrease. The rate of decrease in the EPR signal intensity should be directly proportional to the rate of formation of the quaternary ammonium salt. The reaction chosen for study was triethylamine/allyl bromide, reaction of which gives a quaternary ammonium salt.

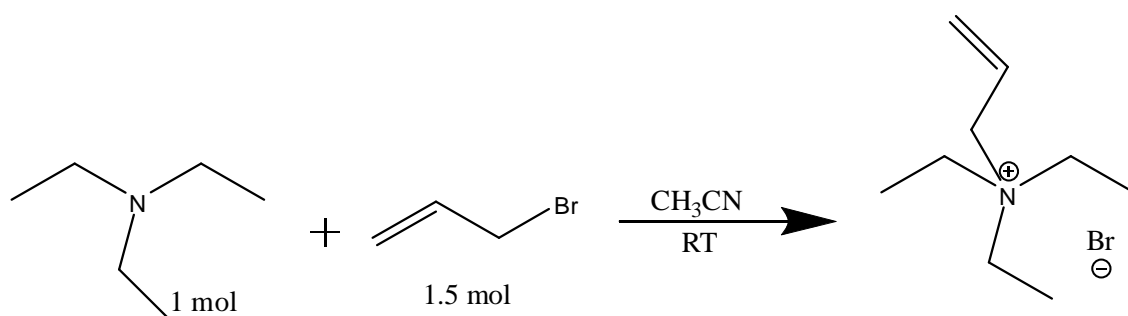


Figure 4.6. Reaction scheme for triethylamine (1 mol) and allyl bromide (1.5 mol) to form a quaternary ammonium bromide.

In Figure 4.6, the reaction scheme for triethylamine with allyl bromide to give the quaternary ammonium bromide salt is shown. In the reaction, triethylamine is the limiting reagent and allyl bromide is the excess reagent. The reaction is carried out in acetonitrile that is 2.5 M with respect to triethylamine. The reason for using acetonitrile as a solvent for the reaction is that acetonitrile is polar solvent⁹ and will help the quaternary ammonium bromide salt to stay in solution. The reactants were mixed and put in the 3 mm – 4 mm coaxial assembly. The coaxial tubes were put into the EPR

cavity and the signal intensity was measured every 30 minutes. It is expected for the EPR intensity to decrease with the increase in the product.

Figure 4.7 shows the plot of time (in minutes) for the reaction versus the EPR signal intensity.

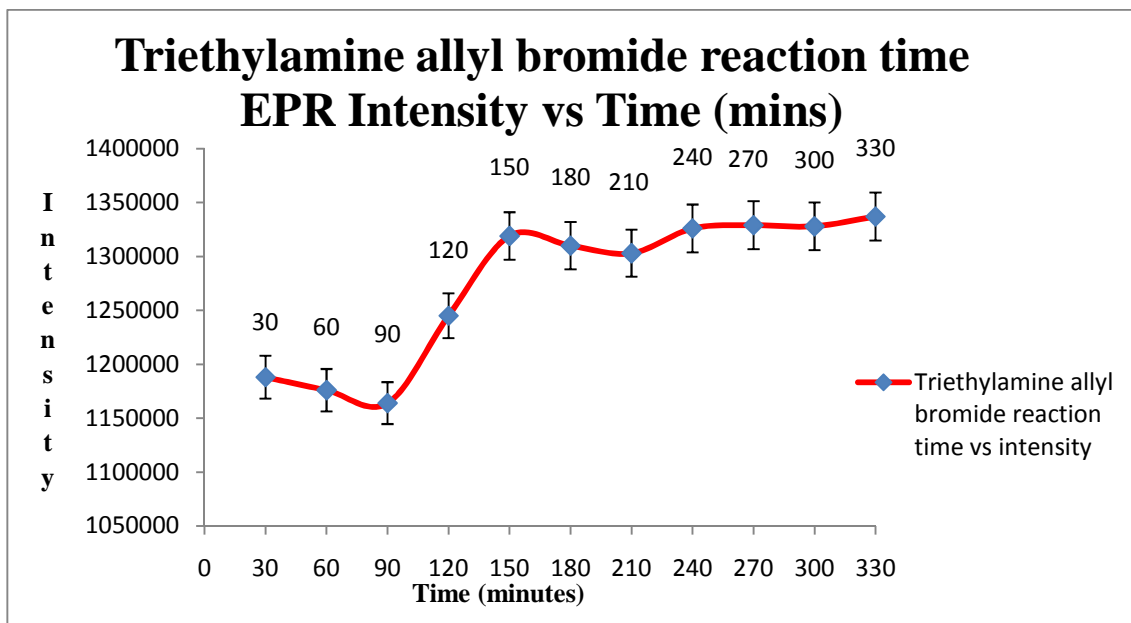


Figure 4.7. Plot of time (minutes) versus EPR signal intensity. (3mm-4mm assembly). The error bars represent a 1.67% error, measured and discussed in Section 3.7(C).

The reaction of triethylamine and allyl bromide showed a different behavior than expected. As seen from the plot, the EPR signal intensity decreased somewhat, as expected, for the first 90 minutes and then there was a sudden increase in the EPR signal intensity significantly, then the EPR signal intensity plateaus somewhat. This unexpected behavior can be explained. The reaction of triethylamine and allyl bromide occurs quickly, and solid product crystallizes in the tube at ca. 90 minutes. As the reaction proceeds, the product concentration increases and thus more and more solid is

crystallized out of the solution which explains the increase in the intensity up to the 150 minute point. After the 150 minute point, the reaction slows and the rate of change attenuates.

A parallel study for the same reaction was done using $^1\text{H-NMR}$. The reaction was monitored every 15 minutes and the spectra are shown in Figure 4.8.

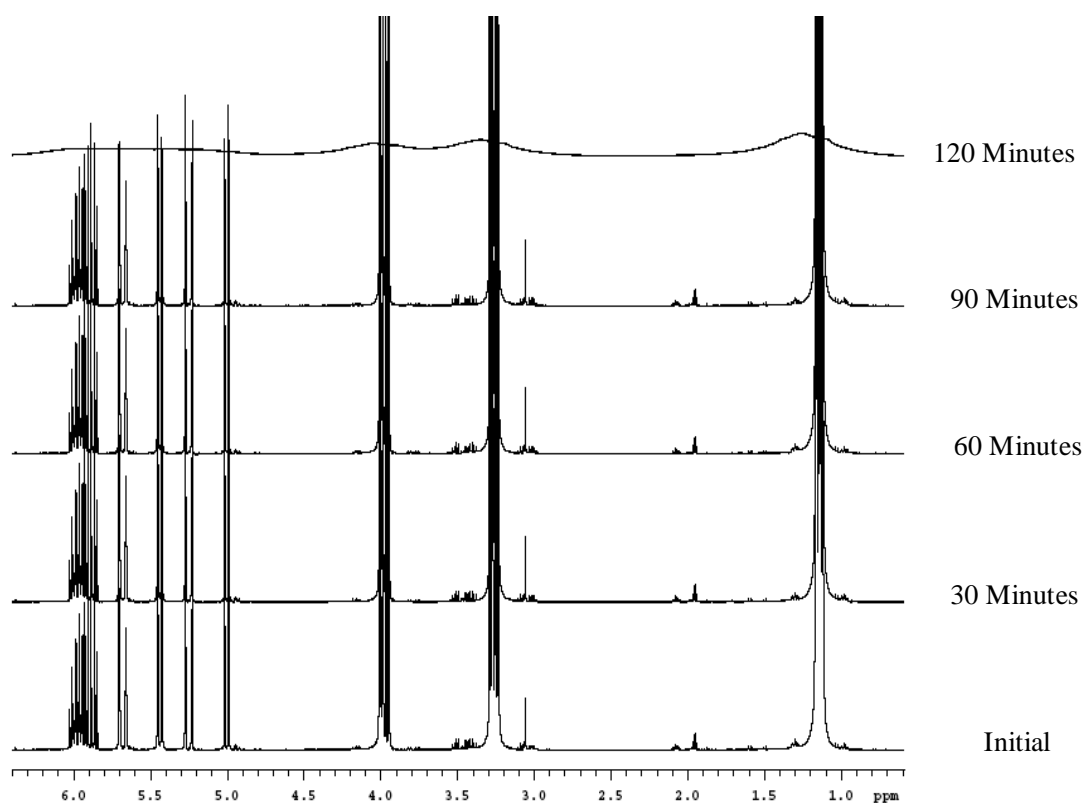


Figure 4.8 NMR spectra every 30 minutes for the triethylamine and allyl bromide reaction.

It can be seen from the NMR spectra that the reaction proceeds and gives sharp peaks and continues to form the product until the 90 minute point. At the 120 minute point the peaks become unusually broad and no splitting of the peaks can be seen anymore. The most interesting part this parallel NMR experiment is the time at which

the peaks start to become broader and less resolved. Comparing the NMR and the EPR data, the reaction shows no crystallization until the 90 minutes point in both the cases, after which there is a sudden change in the intensity due to crystallization, resulting broadening of the peaks in the NMR. These observations show that the EPR technique on the EPR can be used for the monitoring of phase changes.

4.4 Application to study relative kinetics for the triethylamine-allylchloride reaction

As seen from the earlier section, the triethylamine-allyl bromide reaction was too fast to monitor well using the EPR technique. To investigate further, allyl chloride was chosen to replace allyl bromide. Since the reaction likely proceeds mainly by a nucleophilic substitution mechanism, chloride is not as good a leaving group as bromide.

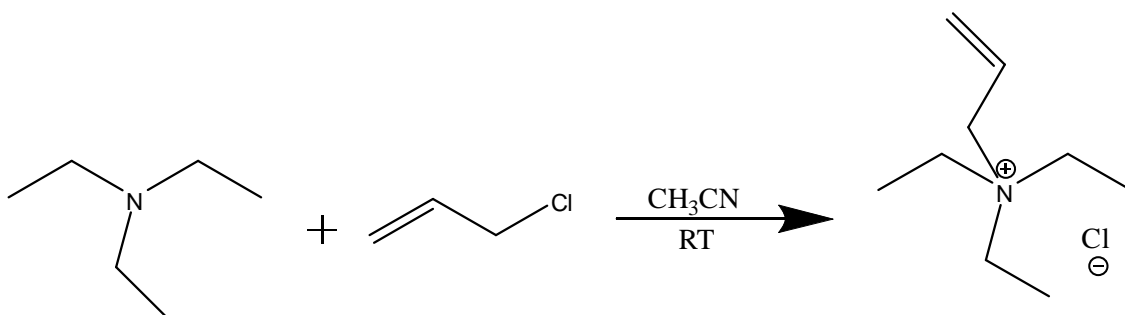


Figure 4.9. Reaction scheme for triethylamine and allyl chloride to form quaternary ammonium chloride.

Figure 4.9 show the reaction scheme for the reaction of triethylamine with allyl chloride. The reaction was monitored using the EPR technique for two different stoichiometric ratios. The two different stoichiometric ratios are 1 mole triethylamine:1.5 moles allyl bromide and 1 mole triethylamine:1 mole allyl bromide. The rate of the

reaction with 1.5 moles allyl bromide should be ca.1.5 times faster than that of the reaction with 1 mole allyl bromide. Both the reactions (1 mole allyl bromide and 1.5 moles allyl bromide) are carried out under the same conditions as for the triethylamine-allyl bromide reaction. The reactants are mixed and put in the 3 mm – 4 mm assembly and placed in the EPR cavity. Both the reactions are monitored every 30 minutes by measuring the EPR signal intensity every 30 minutes.

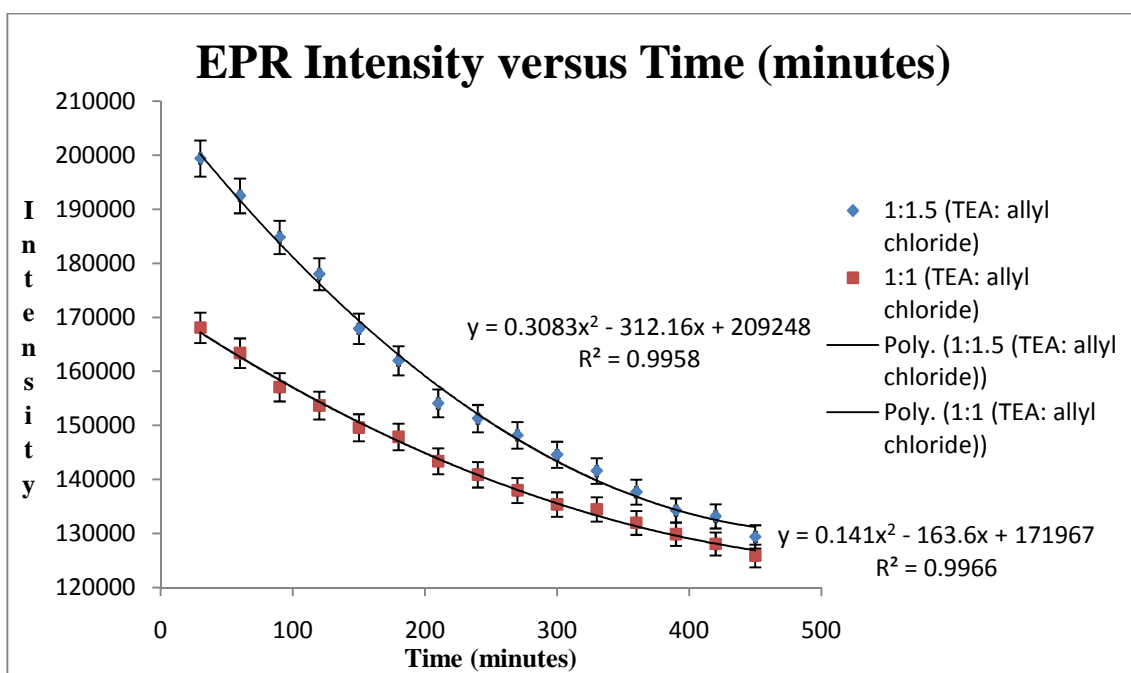


Figure 4.10. Time versus intensity plot for triethylamine and allyl chloride reaction in acetonitrile at room temperature. (3 mm – 4 mm assembly). The error bars represent a 1.67% error, measured and discussed in Section 3.7(C)

Figure 4.10 shows the progress of the triethylamine and allyl chloride reactions. It can be seen that rate of the reaction with 1:1.5 (triethylamine:allyl chloride) stoichiometry is faster compared to the 1:1 (triethylamine:allyl chloride). As seen from

the plot, the reaction is slower with allyl chloride than with the bromide and is not complete after 450 minutes.

The reaction of triethylamine and allyl chloride goes through a nucleophilic substitution mechanism to give the product. Therefore the rate of the reaction is given by Equation(s) 4.1.

$$\text{Rate} = k[\text{Allylchloride}] \text{ or } \text{Rate} = k[\text{Triethylamine}][\text{Allylchloride}]^{10} \quad \text{Equation(s) 4.1}$$

In Equation(s) 4.1 k = rate constant for the reaction, [triethylamine] = concentration of triethylamine, and [allyl chloride] = concentration of allyl chloride. Since the reaction can go through either an S_N1 or S_N2 reaction, we chose to vary the amount of allyl chloride as the rate of the reaction depends on its concentration in any event.

Using the first several data points (low conversion) for each reaction to approximate constant reactant concentrations, the EPR signal intensity, which changes ca. linearly, could be used to monitor the relative rates of the reaction (Figure 4.12). The set of 5 points in the data cover 150 minutes.

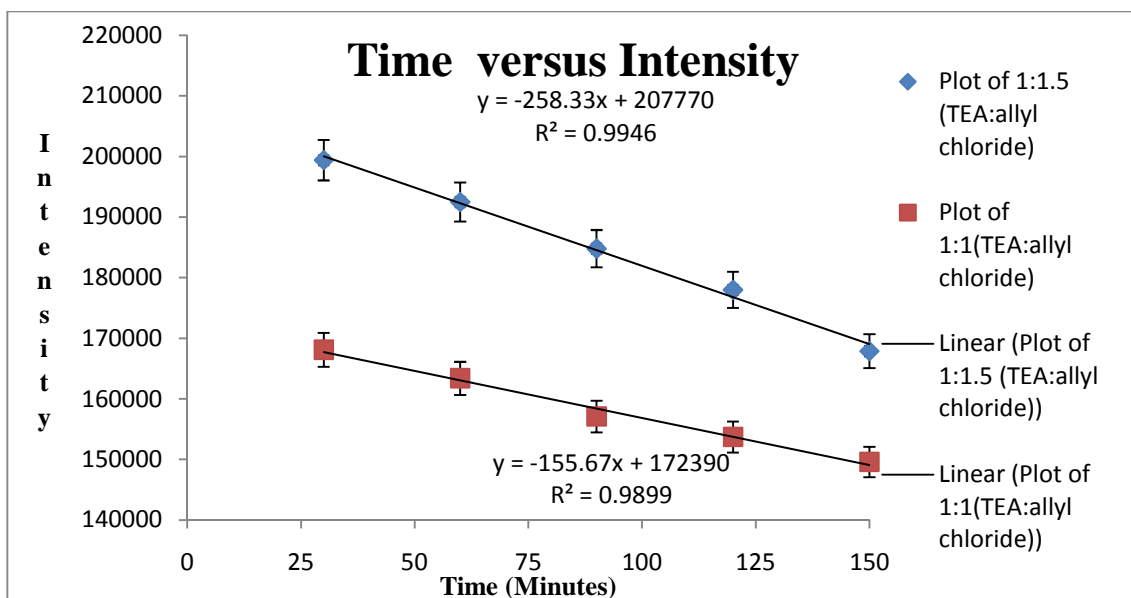


Figure 4.12. Plot of EPR intensity versus time (minutes)(the first 5 points). The error bars represent a 1.67% error, measured and discussed in Section 3.7(C)

As seen from Figure 4.12, both the sets of data show the rate of change of EPR signal intensity which in turn reflects the rate at which the product is formed. The slope for the first line, 1:1.5 (triethylamine:allyl chloride), is 258.33. The slope for the second line, 1:1 (triethylamine:allyl chloride), is 155.67. Comparing the two slopes, the rate formation of product is faster in 1:1.5 (triethylamine: allyl chloride) reaction since it has a higher slope than that of the 1:1 (triethylamine:allyl chloride). Theoretically speaking, initial rate of formation of product in the 1:1.5 (triethylamine:allyl chloride) reaction should be 1.5 times faster than the 1:1 (triethylamine:allyl chloride). From the comparison of the two slopes, it shows that the 1:1.5 (triethylamine:allyl chloride) reaction forms the product 1.66 times faster than the 1:1 (triethylamine:allyl chloride) reaction, agreeing reasonably well with the theoretical value of 1.5.

4.5 Application in studying the dielectric properties of surfactant solutions

The property of the surface of a liquid to resist any external force is known as “surface tension”^{11,12,13}. Surface tension has the dimension of force per unit length or energy per unit area^{11,12,13}. Surface tension is also known as “surface energy”, which is a more general term that includes solids as well as liquids. Surface tension in the literature is denoted as “ γ ”¹³. It is well known that short-range forces of attraction exist between molecules. The phenomenon of surface tension (and interfacial tension) is explained by these forces of attraction. For example, in the liquid/air interface, the molecules in the bulk of the liquid experience an equal force from directions whereas the molecules on the surface experience unbalanced attractive force which leads to a net inward pull (Figure 4.13)¹³.

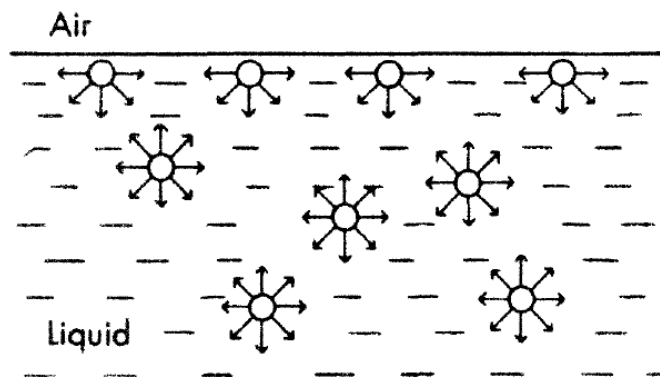


Figure 4.13 Attractive forces at the surface and in the interior of the liquid.

Due to the uneven forces at the surface, as many molecules as possible leave the surface and go into the bulk. This phenomenon causes the surface to contract inward. This is the reason that droplets of liquids and gas tend to attain spherical shape¹³.

Surface active agents (surfactants) are molecules which reduce the surface tension of a liquid. Surface active agents consist of molecules having both polar and non-polar groups and are called amphiphilic molecules. On the addition of a surfactant to a liquid, a strong

adsorption of the surfactants on the surface of the liquid takes place to form an oriented monomolecular layer on the surface of the liquid. This observed phenomenon is termed “surface activity”. For example, a surfactant molecule in water first adsorbs to form a monolayer in such a way that the hydrophilic group is in the aqueous phase and the hydrophobic part sticks out in the air (Figure 4.14). Surface activity is a dynamic phenomenon, which establishes an equilibrium between the adsorption and complete mixing of the molecules in the liquid due to the thermal motion of the molecules at the surface or the interface¹³.

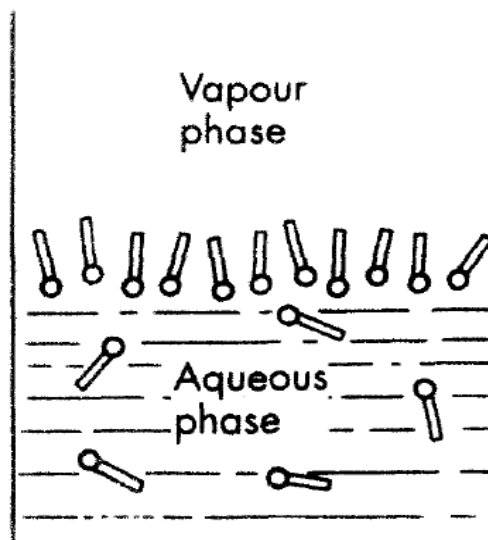


Figure 4.14 Adsorption of the surfactant molecules on the water surface.

The tendency of the surfactants to pack at the interface favors the expansion of the interface, which in turn balances out the tendency of the interface to contract under normal surface tension forces. If π is the surface pressure exerted by the adsorbed layer of surfactants, the surface tension will be lowered to the value given by equation 4.4¹³.

$$\gamma = (\gamma_0 - \pi)$$

Equation 4.4

It is worthwhile to take a note of the fact that longer the hydrophobic (hydrocarbon chain) part of the chain, the greater the number of surfactant molecules at the surface, and hence the lower the surface tension.

Surfactants are generally classified as anionic, cationic, non-ionic or ampholytic depending on the charge carried by the surface active part of the molecule. Anionic surfactants are the most used surfactants as they are cheap and have good performance. Cationics, although expensive, have some germicidal action that makes them useful for some applications. The advantage of non-ionics is that the chain length of both the hydrophobic and hydrophilic groups can be varied.

Micelle formation^{13,16}

Solutions with highly surface-active agents (surfactants) display unusual physical properties. In a dilute solution of surfactant, the surfactant behaves as a normal solute which means in the case of ionic surfactants a normal electrolytic behavior is observed. At some concentration of the surfactant, an abrupt change in the physical properties (osmotic pressure, electrical conductivity, turbidity etc) of the solution is observed. McBain explained this phenomenon by change in the speciation of the surfactant molecules. At the point of abrupt change, there is formation of reasonably well-defined aggregates also known as “micelles” (Figure 4.15).

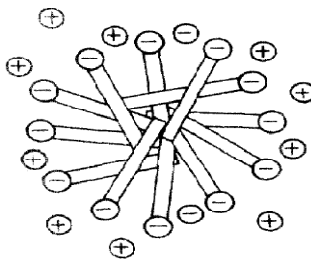


Figure 4.15 A generic micelle structure

The micelles have the hydrophobic part (hydrocarbon chain) oriented inwards, leaving the hydrophilic part (charged part) forming the outer surface of the micelle which is in contact with the polar aqueous phase. The concentration above which the micelles are formed in appreciable amounts is called as the “critical micelle concentration” or the “CMC” of the surfactant.

One of the several applications for surfactants in solutions above the CMC is solubilization of non-polar organic materials in aqueous media that would not be solubilized media otherwise. The organic material is incorporated in the interior of the micelle where there is the presence of the hydrophobic (organic) part of the surfactants. Solubilization is a very important phenomenon, including in the pharmaceutical industry where many organic compounds have to be solubilized in aqueous media, for detergents where it removes dirt and oil, emulsion polymerization, and organic reactions involving micellar catalysis. Due to these wide applications mentioned above, the CMC of a surfactant is an important parameter.

Measurement of the CMC Point

In the literature, electrical impedance spectroscopy can be used to measure the CMC of a surfactant solution. Although the change in conductivity is widely used to measure the CMC, many other techniques such as UV-Vis spectroscopy¹⁹, luminescence spectroscopy²⁰, light scattering, potentiometry¹⁸, and Nuclear Magnetic spectroscopy¹⁷ are also used as tools to measure CMC's. Some of the other physical properties that can be measured to determine the CMC are surface tension, turbidity, osmotic pressure, etc. The point where an abrupt change is seen shows the CMC point for the surfactant. A plot of molar concentration versus the change in these properties is shown in Figure 4.16.

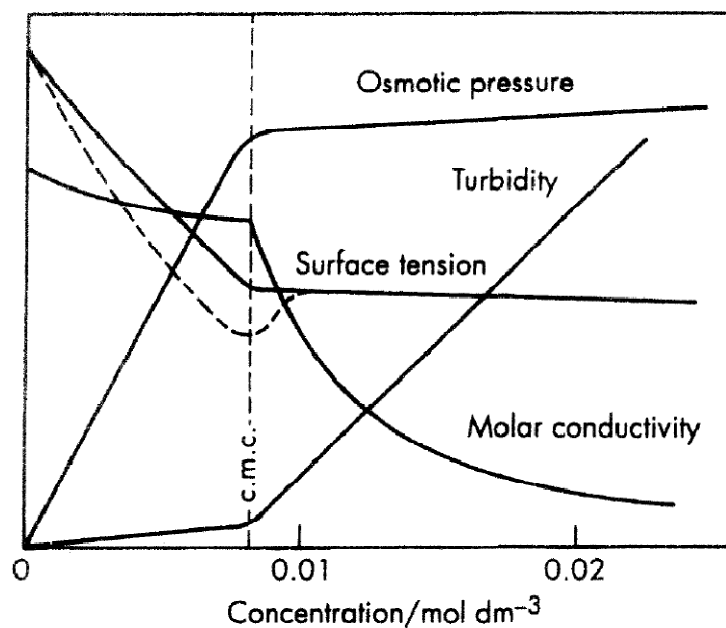


Figure 4.16 Changes in physical properties of the surfactant solution with change in molar concentration

From Figure 4.16, it can be seen that there is a sudden change in many of the properties of the surfactant solution at a certain concentration that is considered to be the specific CMC of the surfactant¹³.

Apart from the physical properties of the surfactant solutions used to measure CMC's, it has been reported in the literature by Neto et al that dielectric constant can be used to measure the CMC point¹⁴ (Figure 4.17).

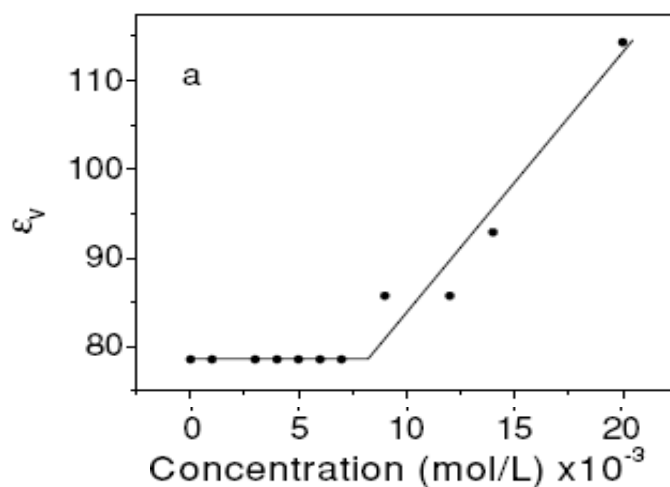


Figure 4.17 Dependence of concentration of sodium dodecyl sulfate (SDS) on bulk dielectric constant

Figure 4.17 shows the change in the bulk dielectric constant changes in the concentration of sodium dodecyl sulfate (SDS). It seems from the plot that with the addition of SDS to water the bulk dielectric constant changes little and is the same as that for water ($\epsilon = 78$) until the CMC. After the CMC point (8×10^{-3} moles/Liter) for SDS, the dielectric constant begins to increase approximately 10% with further addition of the surfactants to water. The authors suggest that, after the CMC, counter ions present at the micelles surface become more easily polarized and results in an increase in the dielectric constant¹⁴.

Most of the dielectric constant investigations made on surfactant solutions in the literature are highly frequency dependent and are carried out in the range of $1-10^7$ Hz^{14,15}. At lower frequencies, the electrode polarization occurs but at higher frequency, the electric field changes direction before the dipole of the molecule orients to the field, thus at higher frequency the dielectric constant is smaller.

Since in the earlier sections it has been shown that EPR technique can be used to measure changes in dielectric constants, including phase changes, and the literature shows that the dielectric constant of the solution changes past the CMC point, this section addresses the question of whether the EPR signal intensity as a function of surfactant concentration correlates with the CMC for different surfactants. Three different kinds of surfactants were taken under investigation.

A) Sodium dodecylsulfate (SDS) ----- Anionic Surfactant

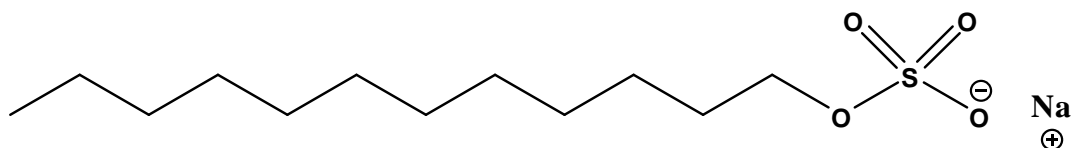


Figure 4.18 Structure of sodium dodecylsulfate (SDS)

B: Cetyltrimethylammonium bromide. (CTAB) ----- Cationic Surfactant

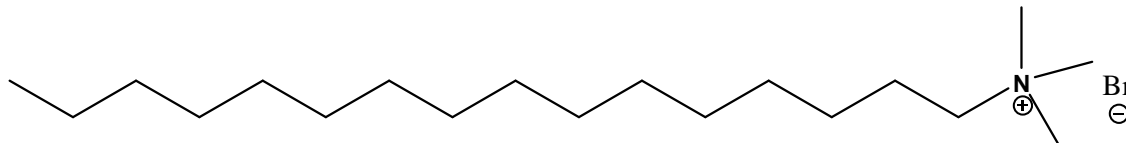


Figure: 4.19 Structure of cetyltrimethylammonium Bromide (CTAB)

C: Pluronic F127----- Non-ionic Surfactant



Figure 4.20 Structure of Pluronic F127

The Pluronic F127 is a triblock copolymer with the repeat unit structure of ca. -[EO₉₉PO₆₅EO₉₉]_n-, where EO are ethylene oxide units and PO are propylene oxide units.

Solutions of different concentrations were made by the dilution method, where a concentrated surfactant solution was prepared by dissolving the required amount of surfactant in water, sonicating the solution for 30 mins, diluting as needed to achieve desired concentration, and then studied using the EPR technique.

A) Application to sodium dodecylsulfate solutions

Large Concentration Range.

SDS solutions were made with concentrations ranging from 0.0001 M to 0.1 M. The plot of concentration of SDS versus Intensity (a.u) is shown in Figure 4.21.

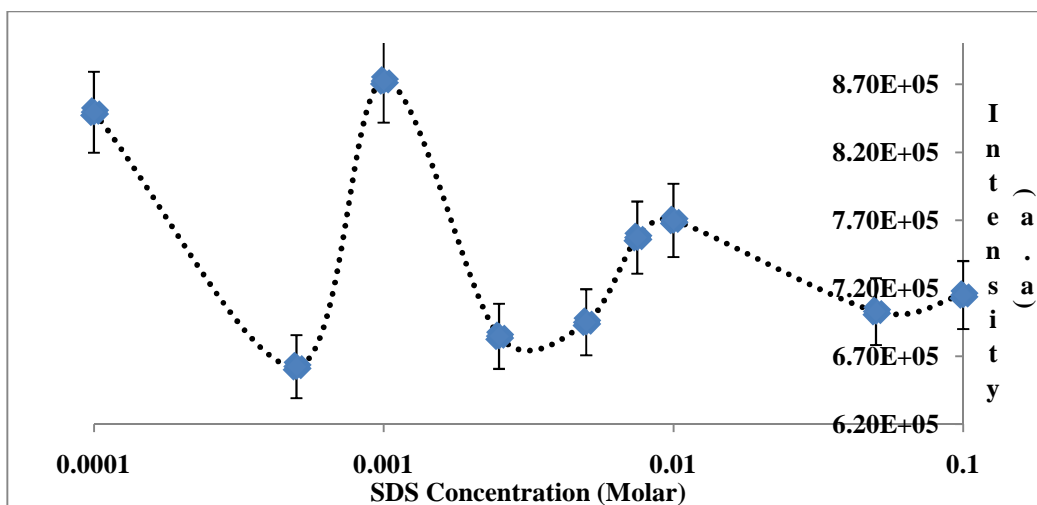


Figure 4.21 Plot of SDS concentration versus EPR signal intensity (a.u). The error bars represent a 3.5% error, measured and discussed in Section 3.7(B)

It can be seen from the plot that the intensity does not remain constant and breaks at several concentrations. The literature value for the CMC of SDS is around $0.0082 \text{ M}^{21,22}$. As seen from the plot, a peak around 0.008 M is seen which correlates to the CMC of SDS. The explanation to this phenomenon could be complex. There could be various transition phases between the surfactant monomer and the micelle formation that result in several intensity changes or breaks and hence in the dielectric constant of the surfactant solutions. The features are reproducible. These are initial studies and further investigation in this area is required to interpret the behavior seen over the large range of concentrations.

The goal of this section was to investigate whether the EPR could be used to study surfactant solutions and correlate the data to the CMC point of the surfactant. Therefore, the investigation was focused more on the region where the CMC of SDS occurs, as reported in the literature i.e 0.0082 M .

Small Concentration Range for SDS (Close to the CMC point)

Figure: 4.22 shows a plot of SDS concentration versus Intensity.

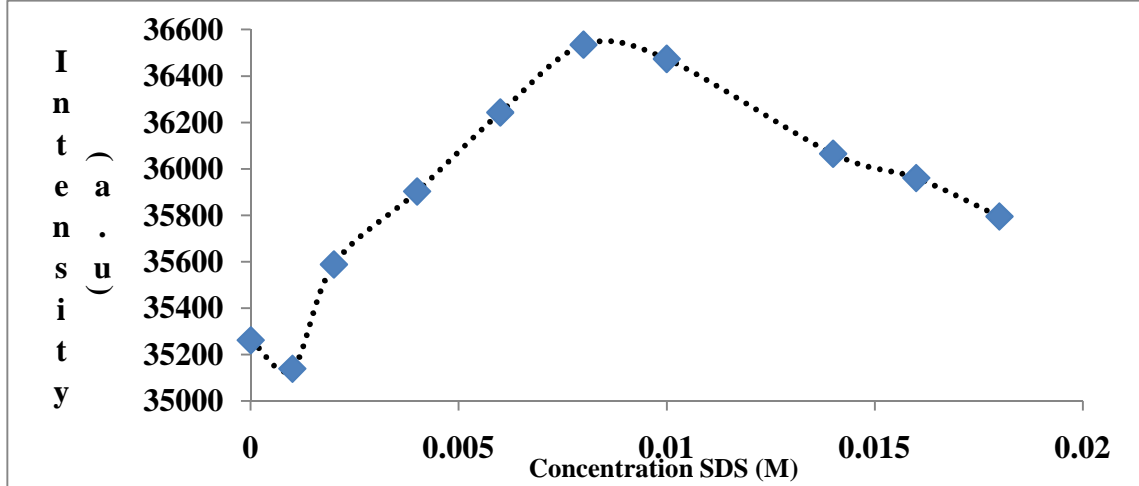


Figure 4.22 Plot of SDS concentration (small concentration range) versus intensity (a.u)

As seen from the plot, the concentration range has been attenuated and the range where the CMC for SDS has been reported has been investigated thoroughly by taking some more measurements in the attenuated range. The plot shows a transition peak at around 0.008 M concentration of SDS. The peak corresponds to the CMC value for SDS in water. Looking at the data from dielectric point of view, the dielectric constant decreases (increasing signal intensity) with the increase in the concentration until the CMC point, after which the dielectric constant starts to increase again. Before the CMC point, addition of the hydrophobic part of the surfactant dominates changes in the bulk dielectric constant and thus on the increase in the concentration, a decrease in the dielectric constant is seen until the CMC point is reached. At the CMC, due to the micelle formation that involves the conversion of the hydrophobic parts of the surfactant molecules into the micellar interior and exposure of the polarizable charged

surface to the aqueous media, an increase in the dielectric constant is seen. As the hydrophobic effect from the hydrophobic part of the surfactant molecule is no longer prominent, the polarization of the counter ion near the micelle surface takes over to give an increase in the dielectric constant¹⁴ as additional surfactant forms more micelles.

Thus intensity data from the EPR technique can be correlated to the CMC of SDS but the other features of the plots remain to be explained. Since the coaxial assembly could be used to measure the CMC of SDS, which is an anionic surfactant, the next obvious step would be to investigate a cationic surfactant.

B) Application to cetyltrimethylammonium bromide (CTAB) solutions

Large range concentration for CTAB

CTAB solutions were investigated over a broad range of concentration from 0.00001 M to 0.01 M. Since the CMC value for CTAB reported in the literature is 0.00093 M^{21,22,23}, the range under investigation is dilute by a factor of 10 compared to the SDS concentration range. A plot of concentration of CTAB versus the EPR intensity in arbitrary units (a.u) is shown in Figure 4.23.

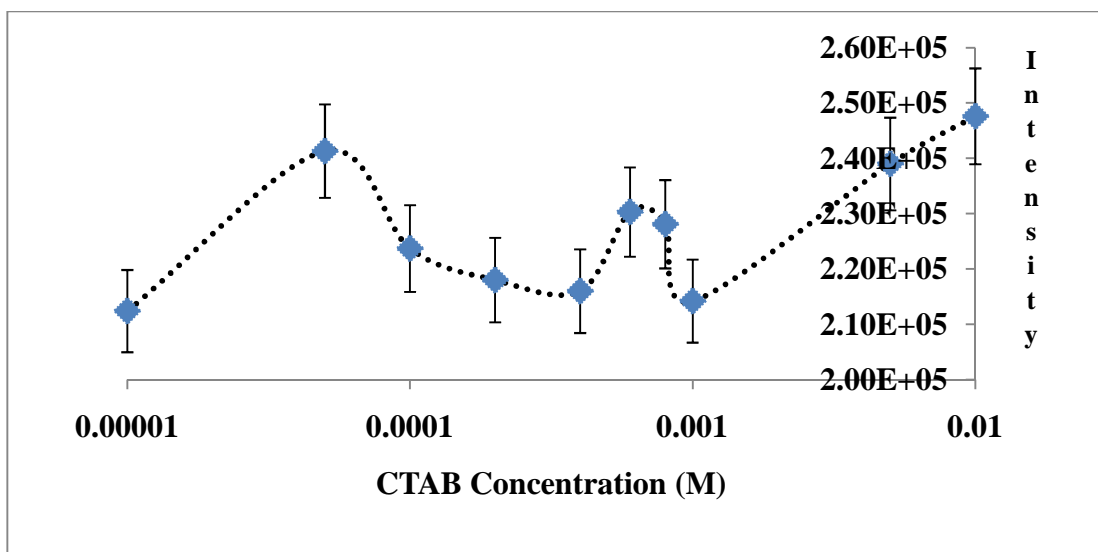


Figure 4.23 Plot of CTAB concentration (M) versus Intensity (a.u). The error bars represent a 3.5% error, measured and discussed in Section 3.7(B)

Similar to the SDS, a wide range was covered with the CTAB cationic surfactant. There is a similar kind of behavior where there are at least two transition points before the CMC point. As mentioned before, in depth investigations are needed to resolve or to explain these transitions seen before the CMC.

Small Concentration Range for CTAB (Close to the CMC point)

The plot of concentration of SDS versus EPR intensity for the smaller range of concentrations is given in Figure 4.24.

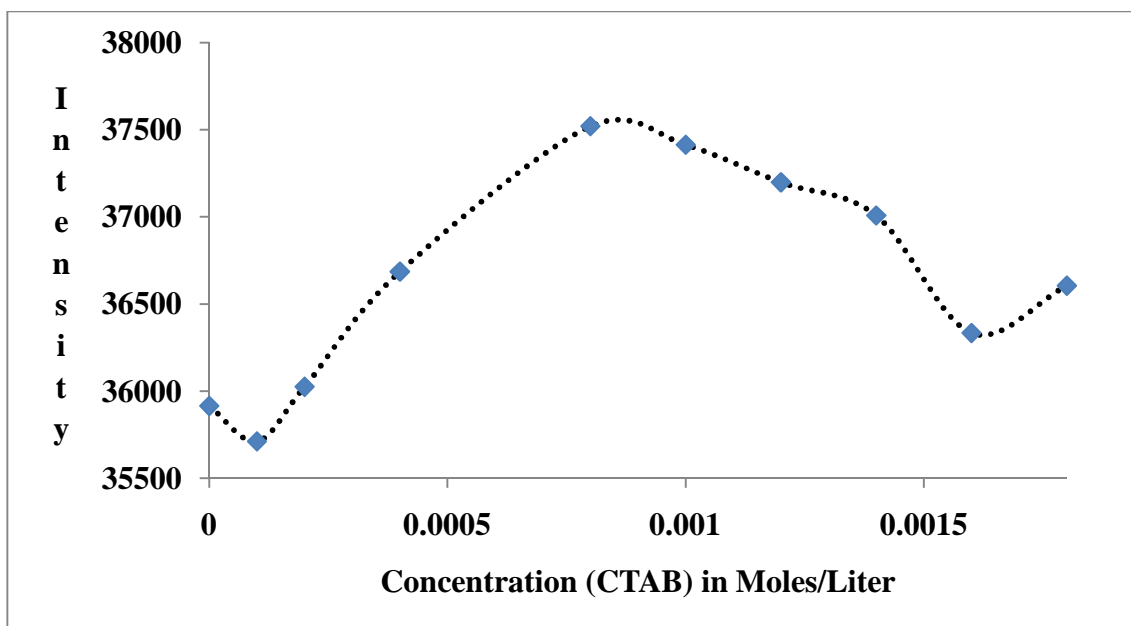


Figure 4.24 Plot of SDS concentration (M) versus EPR intensity (a.u)

CTAB was investigated over a short range of concentrations from 0.0001M to 0.0018M. Since the CMC of CTAB is reported to be 0.00093 in the literature, the range would allow investigating the CMC with much clarity and depth. The CTAB shows a similar behavior as seen with SDS as would be expected

C) Comparison of the large-range data for CTAB and SDS

While it is gratifying that local features in the signal intensity-concentration plots for SDS and CTAB can be correlated to their respective CMC's, the other features are perplexing. As mentioned earlier, it becomes essential to investigate the various transitions seen throughout the entire concentration range. Some speculative causes for these other features include changes in microwave absorption due to interfacial surfactant absorption/concentration (glass-liquid or gas-liquid). Since glass of the coaxial assembly cell can be charged (depending on the pH of the medium and the point

of zero charge of the glass), the other features, especially those at concentrations below the CMC's, may be related to such interfacial phenomena. Above the CMC's, transitions to other surfactant phases (e. g. micelle to rod) may be occurring. More study is needed in any event to elucidate the nature of the observed phenomena.

To investigate these phenomenon a bit further, a non-ionic surfactant, Pluronic F127, was investigated over a range of concentrations (Figure 4.25). Pluronic F127 is non-ionic surfactant that is uncharged. As described earlier Pluronic F127 is a tri-co-block polymer with PEO and PPO repeat units. As the non-ionic surfactant is uncharged, it should not show strong solid-liquid adsorption phenomena as speculated upon with the SDS and CTAB surfactants.

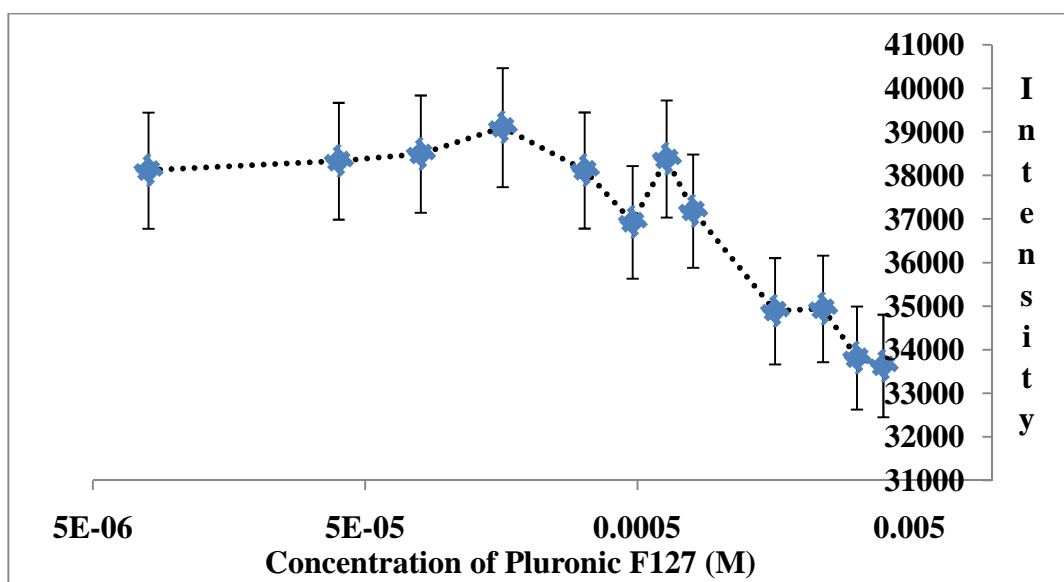


Figure 4.25 Plot of Pluronic F127 concentration (M) versus EPR intensity. The error bars represent a 3.5% error, measured and discussed in Section 3.7(B)

The plot of Pluronic F127 concentration versus EPR signal intensity is shown in Figure 4.25. As expected, there were no strong transitions seen at the lower

concentration until the reported CMC point was reached which is $0.00056 \text{ M}^{24,25}$. At around 0.0006 M there is a peak which again correlates to the CMC. After the CMC point, there is decrease in the intensity, from which it can be inferred that there is an increase in the dielectric constant. The micelle core is made up of PPO and the exterior is made up of PEO which could be more polarizable through interaction with water or micellization diminishes the effectiveness of the non-polar portions of the molecule at keeping the dielectric constant lower.

Figure 4.26 shows a plot of concentration (M) of SDS, CTAB and Pluronic F127 versus the normalized EPR intensity to get all the 3 plots for SDS, CTAB and Pluronic F127 on the same scale. The concentration is divided by a factor of 12 so that the CMC for all the three surfactants, SDS, CTAB and Pluronic F127 can be plotted approximately on the same scale.

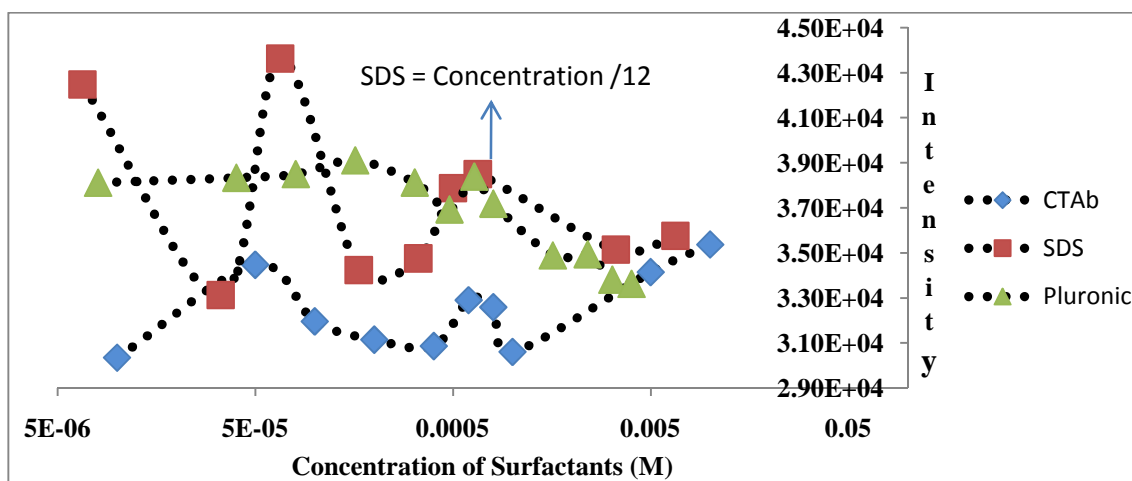


Figure 4.26 Plot of Concentration of Surfactants (SDS, CTAB and Pluronic F127) versus EPR Intensity

4.6 Conclusions

In this chapter, it can be seen that the EPR technique for studying dielectric properties can potentially be applied to the study of many types of systems. Some examples included estimating the water content in solvents, monitoring of a phase transition during a reaction, measurement of the relative rate of a reaction and the study of surfactant solutions.

At this point the technique appears to be quite sensitive to detecting change in dielectric properties but suffers from two drawbacks: 1) the need to do a calibration curve using the same cell every time it is desired to measure or estimate the actual value of the dielectric constant of the medium and 2) the significant amount of error for the calibration curves, most likely largely due to impure standards. As the technique is developed further, it is anticipated that improvements in cell design and use of better standards will decrease measurement errors and enhance the utility of the technique.

4.7 Experimental Section

A) EPR instrumentation

All the measurements were carried out using a Bruker EMX EPR spectrometer operating at the X band. The spectrometer has a Bruker 048T Microwave Bridge and Bruker ER073 Magnet. The cavity used in all measurements was the standard rectangular one operating in TE 102 mode (Bruker 4102 ST cavity). The signal channel was kept constant at a magnetic field modulation frequency of 100 kHz. The microwave frequency was held constant at 9.725 GHz and the microwave power was held constant at 0.201 mW for all the measurements.

B) NMR instrumentation

The monitoring of the allyl bromide and triethylamine reaction was done using a Varian VNMRS 400 MHz NMR with an AutoX-Dual Broadband probe. Temperature was regulated using a FTS sample cooler.

C) Coaxial assemblies

The NMR tubes (3 mm, 4 mm, 5 mm) were commercially acquired from Wilmad Lab Glass. The tubes were cut according to the required length of the tube. The inner tubes (3 mm and 4 mm) containing hexane/TEMPO were sealed under an argon atmosphere using an acetylene torch.

D) Solvents and reagents.

All the solvents used for the calibration curve were reagent grade solvents used straight out of the containers. Distilled water was used for the dioxane-water mixtures. Lithium perchlorate was acquired from Sigma-Aldrich and stored and weighed in a continuous air-purge drybox.

Triethylamine, allyl chloride and allyl bromide were from Sigma-Aldrich and were used as-is.

The surfactants sodium dodecylsulfate (electrophoretic grade) was acquired from Sigma-Aldrich, cetyltrimethylammonium bromide was acquired from ?? and Pluronic F127 was acquired from BASF. All surfactants were used as-is.

References

- 1: Akerlof, G.; Short, O.A. *Journal of the American Chemical Society* **1936**, 58 (7), 1241-1243.
- 2: Sigvarsten, T.; Gestblom, B.; Noreland, E.; Songstad, J. *Acta Chimica Scandinavica* **1989**, 43,103-115.
- 3: Berns, D. S.; Fuoss, R. M. *Journal of the American Chemical Society* **1961**, 83, 1321.
- 4: Barthel, J.; Buchner, R. *Pure and Applied Chemistry* **1986**, 58, 1077.
- 5: Wang, M.; Weifang, J.; Ziyu, L.; Jiaotong, X.; Shaanxi, X. *Proceedings of the 3rd International Conference on Properties and Applications of Dielectric Materials* **1991**, 77-80.
- 6: Walden, P. Z. *Elektrochem. Angew. Phys. Chem.* **1906**, 12, 77.
- 7: Petrowsky, M.; Frech, R. *The Journal of Physical Chemistry B* **2008**, 112, 8285-8290.
- 8: Cachet, H.; Cyrot, A.; Fekir, M.; Lestrade, Jean-Claude. *The Journal of Physical Chemistry* **1979**, 83 (18), 2419-2429.
- 9: *Dielectric Constant Values*, URL:
<https://www.clippercontrols.com/pages/dielectric-constant-values>
- 10: Pavia, D.L.; Lampman, G.M.; Kriz, G.S. *Introduction to Organic Laboratory Techniques: A contemporary approach*, p-198.
- 11: *Surface Tension*, URL: <http://hyperphysics.phy-astr.gsu.edu/hbase/surten.html>
- 12: Bush, J.W.M. *Surface Tension Module*, URL: <http://web.mit.edu/1.63/www/LectureNotes/Surfacetension/Lecture1.pdf>

- 13: Shaw, D.J. *Introduction to Colloid and Surface Chemistry*, 4th Edition, p-64-96.
- 14: Neto, J.M.Z.; Da Cunha, H.N.; Neto, J.M.M.; Ferreira, G.F.L *Journal of Sol-Gel Science and Technology* **2006**, 38, 191-195.
- 15: Abe, M.; Ogino, K. *Journal of colloid and Interface Science* 1981, 80(1), 58-66.
- 16: Singh H.N.; Saleem, S.M.; Singh, R.P. *The Journal of Physical Chemistry* **1980**, 84, 2191-2194.
- 17: Inoue, H.; Nakagawa, T. *The Journal of Physical Chemistry* **1966**, 70 (4), 1108-1113.
- 18: Reis, S.; Moutinho, C.G.; Matos, C.; Baltazar de Castro.; Gameiro, P.; Lima, J.L.F.C. *Analytical Biochemistry* **2004**, 334, 117-126.
- 19: Guo, Q.; Zhu, X.; Ren, Tan.; Liu, Y. *Journal of Inclusion Phenomena and Molecular Recognition in Chemistry* **1994**, 17, 37-44.
- 20: Sahyun, M.R.V. *The Journal of Physical Chemistry* **1988**, 92, 6028-6032.
- 21: Mukerjee, P.; Mysels, K. J. *Critical Micelle Concentration of Aqueous Surfactant Systems* **1970**; National Bureau of Standards: Washington, DC.
- 22: Cifuentes, A.; Bernal, J.L.; Diez-Masa, J.C. *Analytical Chemistry* 1997, 69, 4271-4274.
- 23: Li, F.; Li, G.; Wang, H.; Xue, Q. *Colloids and Surfaces A: Physicochemical and Engineering Aspects* **1997**, 127, 89-96.
- 24: Desai, P.R.; Jain, N.J.; Sharma, R.K.; Bahadur, P. *Colloids and Surfaces A: Physicochemical and Engineering Aspects* **2001**, 178, 57-69.
- 25: Alexandridis, P.; Holzwarth, J.F.; Hatton, T. *Macromolecules* **1994**, 27, 2414-2425.

Chapter 5

Investigation and modification of Linear and Branched poly(ethylenimine)as Solid Polymer Electrolyte

5.1 Introduction:

In this chapter different polymers have been investigated with regard to their application as solid polymer electrolytes. Several different polymers have been investigated with the final goal of achieving batteries that are leak-free. A lot of these polymers are modified to enhance their performance. With this goal in mind, poly(ethyleneimine) (PEI) based polymers have been investigated and discussed in this chapter. Modification of PEI by substituting different groups on the polymer backbone and cross-linking to make the films more physically and chemically stable will be discussed in this chapter. In the first part of this chapter, modification of branched PEI and the ionic conductivity of the resulting films will be investigated. In the second part of this chapter, linear PEI synthesis, modification, and the ionic conductivity of the films will be discussed.

5.2) Branched poly(ethyleneimine) (BPEI) and Branched poly(allylethyleneimine) (BPAEI):

BPEI is an inexpensive and commercially available polymer. The structure of BPEI is shown in Figure 5.1^{1,2}

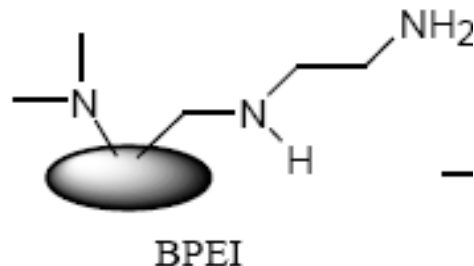


Figure 5.1 BPEI (The structure does not represent the actual structure of BPEI)

Figure 5.1 does not show the exact structure of BPEI. The actual structure is more complicated but the above structure helps in displaying the basic structure of BPEI. BPEI has three different types of nitrogens; primary, secondary and tertiary. The ratio of primary:secondary:tertiary nitrogens is 1:2:1. BPEI is viscous and clear polymer. BPEI has a low T_g , glass transition temperature, of -50°C . BPEI and some of its simple chemical modifications do not have the physical integrity to be applied as a solid polymer electrolyte material. There have been reports in the literature where the physical properties of BPEI are improved by cross-linking. Lieyu Hu successfully substituted the nitrogens of BPAEI with allyl groups that were then cross-linked radically. The modification of the BPEI is shown in Figure 5.2.^{1,2}

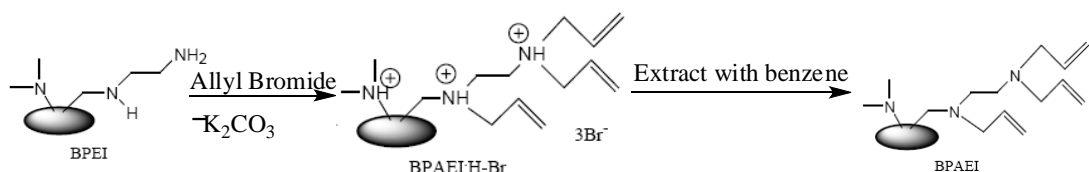


Figure 5.2 Scheme for synthesis of BPAEI (Branched Poly(allyl-ethyleneimine)).

The BPEI is treated with allyl bromide in the presence of a base (potassium carbonate). The nitrogens of the BPEI backbone do a nucleophilic attack on the electrophilic carbon next to the bromide on the allyl bromide. The base, potassium

carbonate help in deprotonation of the quaternary ammonium species to give neutral nitrogen based polymer. The salt and the polymer are separated using the solvent extraction technique using benzene. Benzene, being a non-polar solvent, dissolves the polymer and the salt is precipitated out of the solvent, which can be separated by filtration. The NMR spectrum for BPAEI is shown in Figure 5.3. The spectrum matches perfectly with that shown as by Dr Hu for BPAEI².

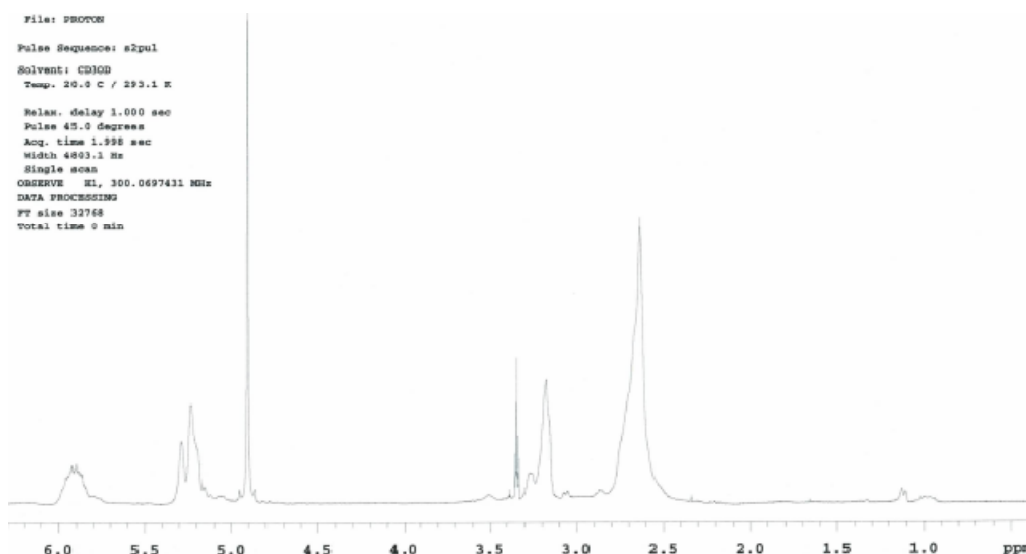


Figure:5.3 NMR spectra of BPAEI

The resulting BPAEI was cross-linked with different radical initiators with the intention of application of these films as solid polymer electrolytes in fuel cells or lithium ion batteries.

Dr Lieyu Hu investigated the cross-linking of BPAEI with different amounts of lithium triflate and different cross-linking radical initiators and investigated the cross-linked films for their ionic conductivity². Based on the results given in his dissertation, it was shown that cross-linking of allylated PEI-based polymers is a practical strategy

for the improvement of the physical properties of solid polymer electrolytes (SPE). Dr Hu studied several cross-linking radical initiators and found 2,2-azobis(2-amidinopropane)dihydrochloride (V-50) the optimum initiator for the cross-linking of BPAEI. A possible cross-linking mechanism described by Dr Hu is shown in Figure 5.4².

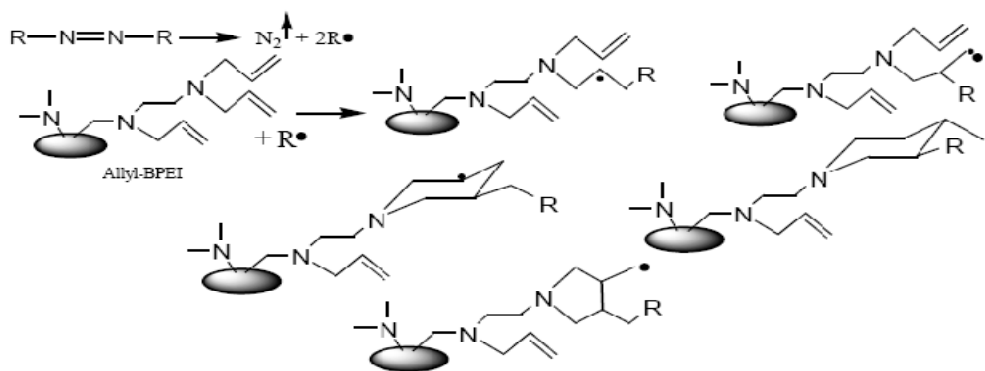


Figure 5.4 Different possible species formed during the cross-linking of the allyl groups.

The highest ionic conductivity was obtained with 20:1 (N:Li) ratio and 60:1 (N:initiator) ratio. The ionic conductivity was on the order of 10^{-7} S/cm at 20°C which increases to 10^{-5} S/cm at 80°C. Dr Hu speculated that the chloride ions from the initiator V-50 could seriously hinder the ionic conductivity in BPAEI SPEs². The chloride ions could migrate under the influence of electric field to the electrode-electrolyte interface and deposit on the electrode in the form of LiCl. The formation of lithium chloride on the surface of the chloride can block and hinder the ionic transport^{1,2}.

To investigate the matter further and to verify if the chloride anion interferes with the ionic transport phenomena in the SPE, cross-linking of the allyl groups without any initiators was taken under consideration. It is well known that double bonds can be

polymerized with UV (ultra-violet) light. Therefore to eliminate the possibility of the chloride ions interfering in the ion transport mechanism, the allyl groups were subjected to cross-linking using UV light. BPAEI with 20:1 (N:Li triflate) ratio was cast from methanol and subjected to UV radiation for 3 days. A self-standing BPAEI/LiTf film was obtained which was brown and opaque in appearance after 3 days under the UV light. The ionic conductivity for the film was tested on the impedance analyzer. The ionic conductivity for the film was measured to be on the order of 10^{-10} S/cm at 22°C which increased to the order of 10^{-8} S/cm at 41°C and was 1.12×10^{-7} at 53°C. The conductivity after this was difficult to measure as the film broke in the cell and cell short-circuited. Comparing the data to Dr Hu's data, it shows that ionic conductivity is significantly lower. The lower mechanical stability of the film could be due to the fact that UV light does not provide optimum cross-linking. This gives indirect evidence that the chloride anion may not be interfering with the ion transport mechanism when the thermal initiator is used and/or the lower values of conductivity could be a morphological in nature.

An attempt to cross-link BPAEI with a different initiator that does not involve chloride anions was also tried. An attempt was made to use compounds like $\text{Li}_2\text{S}_2\text{O}_8$ and $\text{K}_2\text{S}_2\text{O}_8$ to cross-link the allyl groups under UV light. Though the films did cross-link, the films were not physically robust enough to measure the ionic conductivity.

5.3 Linear poly(ethyleneimine) (LPEI) and linear poly(allylethyleneimine) (LPAEI)

BPAEI showed lower conductivities and the conductivities did not change even when the cross-linking was done using UV light. This suggests that the chloride ion

plays little role in the conductivity of the polymer electrolyte. As mentioned earlier, the lower conductivities could be due to the morphological changes of BPAEI on addition of Lithium Triflate. It would be of interest to study LPAEI which has a linear backbone as opposed to the branched backbone of BPAEI.

LPEI is synthesized by hydrolyzing PEOz (poly(N-ethyl oxazoline)) under acidic conditions (Figure 5.5). The hydrolysis forms a polyammonium salt that is further neutralized with NaOH to give neutral LPEI^{3,4}. The formation of LPEI was analyzed by proton NMR spectroscopy. The spectrum is shown in Figure 5.6. The NMR spectrum shows a singlet peak at 3.3 ppm for the CH₂ groups (2H) on the backbone. It has been shown that LPEI has low conductivities with added lithium triflate due to the extensive hydrogen bonding of the N-H's in LPEI. Therefore substitution of nitrogen with a functional group to avoid hydrogen bonding is a good strategy to avoid hydrogen bonding.

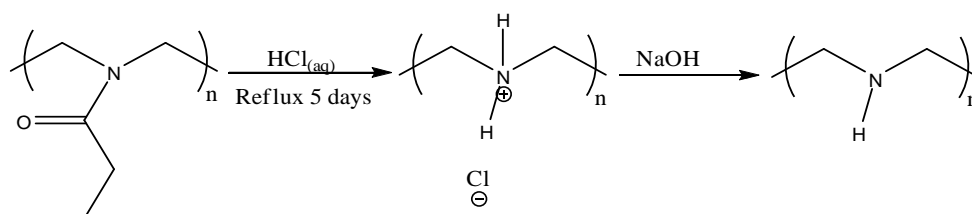


Figure 5.5 Schematic representation for synthesis of LPEI.⁸

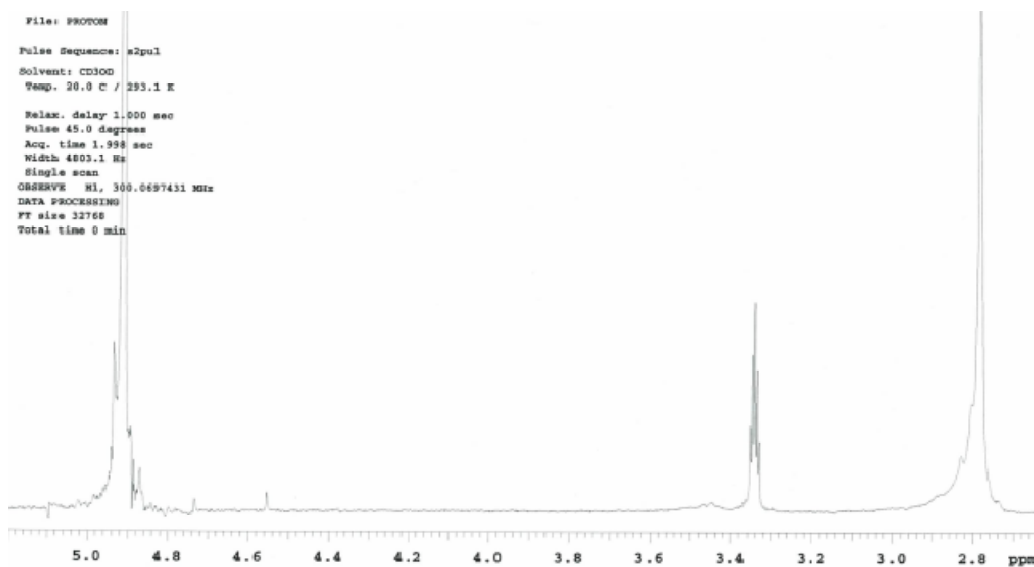


Figure 5.6 NMR spectrum of LPEI.

100% LPAEI was synthesized by reacting allyl bromide with LPEI in the presence of a base such as K_2CO_3 . The scheme of the reaction is given in Figure 5.7. The LPAEI product was analyzed by using NMR spectroscopy. The spectrum for LPAEI is shown in Figure 5.8.²

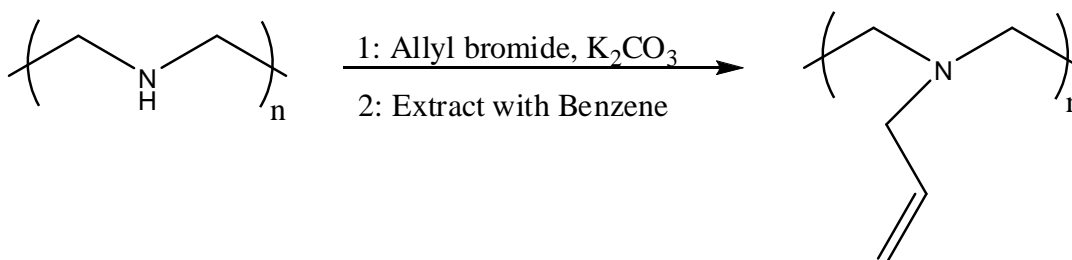


Figure 5.7 Schematic representation for conversion of LPEI to LPAEI

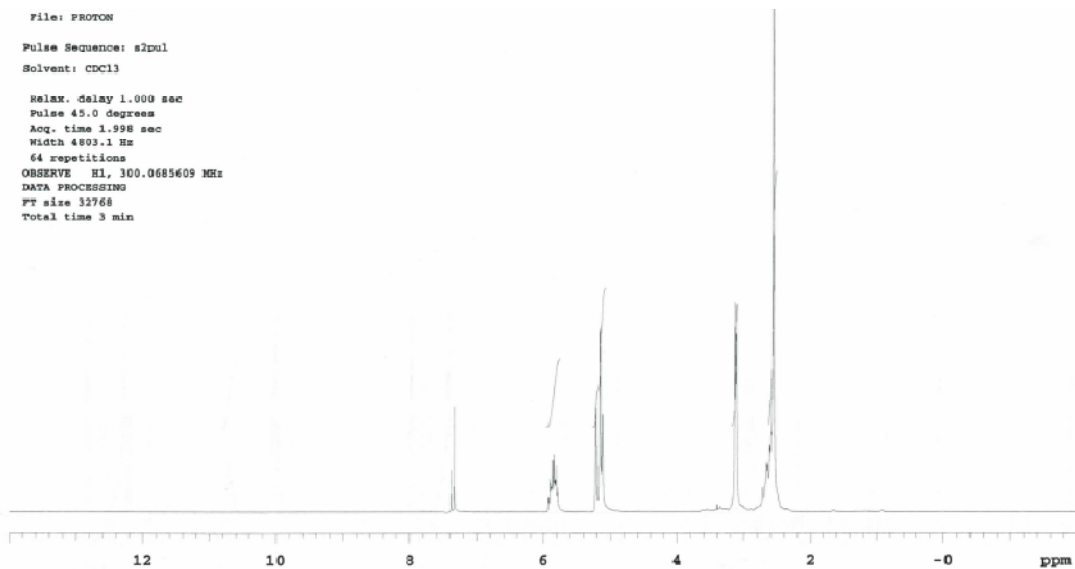


Figure 5.8 NMR spectrum of LPAEI

The 100% LPAEI shows a multiplet at 5.9 ppm (vinyl methine proton, 1 H), a doublet at 5.2 ppm (vinyl methylene protons, 2H), a broadened singlet at 3.1 ppm (N-methylene proton on the side chain, 2H), and a singlet 2.5 ppm (backbone methylene 4H). LPAEI is whitish viscous polymer. The substitution of nitrogen in LPEI with allyl groups serves dual purpose. First, there are no more hydrogens on the nitrogens in the backbone, which eliminates hydrogen bonding and secondly, the cross-linking of allyl group gives physical and mechanical stability to the films formed.

Dr Hu showed that BPAEI gave good conductivities with 20:1 (N:Li triflate) ratio and V-50 as an initiator with 60:1 (N:initiator) ratio². LPAEI was cross-linked under the same conditions with the same concentration of lithium triflate and initiator (V-50) at 80°C in a vacuum oven. Ionic conductivity measurements were done on the films at different temperatures. The data is summarized in Table 5.1

Temperature (°C)	Ionic Conductivity (S/cm)
22	1.98×10^{-10}
41	2.04×10^{-10}
61	4.52×10^{-10}
86	1.17×10^{-9}
100	5.17×10^{-10}

Table 5.1 Ionic Conductivity data for LPAEI 20:1 (N:Li) ratio of lithium triflate and 60:1 (N:initiator) ratio.

The LPAEI with 20:1 (N:Li) ratio and V-50 as the initiator with 60:1 (N:Li) ratio showed ionic conductivities even lower than that for BPAEI with 20:1 (N:Li) ratio and V-50 as the initiator with 60:1 (N:Li) ratio. Attempts were also made to cross-link LPAEI using UV light in combination with different initiators such as $K_2S_2O_8$, V-50 and $Li_2S_2O_8$ with the N:initiator ratio 60:1. The films were exposed to UV radiation for 3 days, and turned into viscous solutions but did not form films which could be useful to measure ionic conductivity. Out of the three initiators, $Li_2S_2O_8$ showed better cross-linking (less free flowing) of the allyl groups in LPAEI. Since LPAEI did not cross-link under UV light, LPAEI was tried with higher concentration of $Li_2S_2O_8$. Different films were tried with different N:Li ratio such as 5:1, 10:1, 15:1, 20:1, 25:1 (N:Li) ratios with 30:1 (N:initiator) of $Li_2S_2O_8$ at 80°C under vacuum. The data is summarized in Table 5.2.

Temperature °C	5:1 (N:Li) σ (S/cm)	10:1 (N:Li) σ (S/cm)	15:1 (N:Li) σ (S/cm)	20:1 (N:Li) σ (S/cm)
25	5.61×10^{-10}	No Fit to the Data	No Fit to the Data	2.20×10^{-8}
45	8.67×10^{-10}	1.55×10^{-11}	2.27×10^{-10}	8.70×10^{-8}
65	3.68×10^{-9}	6.20×10^{-11}	4.39×10^{-8}	5.87×10^{-8}
85	1.03×10^{-8}	7.75×10^{-11}	1.58×10^{-8}	3.44×10^{-8}
100	1.90×10^{-8}	1.23×10^{-10}	1.61×10^{-8}	5.82×10^{-9}

Table 5.2 Ionic conductivity data for LPAEI with different concentration of LiTf with 30:1 (N:Li) ratio

LPAEI was also cross-linked with a 25:1 (N:Li) ratio of lithium triflate with $\text{Li}_2\text{S}_2\text{O}_8$ at 30:1 (N:initiator). The data is shown in Table: 5.3.

Temperature °C	25:1 (N:Li) σ (S/cm)
22	3.50×10^{-9}
50	9.14×10^{-9}
74	2.04×10^{-8}
97	3.59×10^{-9}

Table 5.2 Ionic conductivity data for LPAEI with 25:1 (N:Li) ratio of LiTf with 30:1 (N:Li) ratio

The ionic conductivity for LPAEI shows that ionic conductivity ranges from the factor of 10^{-11} to 10^{-8} S/cm. The ionic conductivities are exceedingly low and are not close to the benchmark (Approx on the order of 10^{-4} S/cm)^{4,5} required for a Solid Polymer Electrolyte for a battery. A possible reason for the low conductivity in LPAEI with lithium triflate could be a high degree of cross-linking which could be limiting the polymer segmental motion. It is well known from the literature that the segmental motion allows the ion transport to occur in the solid polymer electrolyte. Another possibility is that the lithium cation could be coordinating to the nitrogens, which locks the backbone in a conformation(s) which could, again, limit the segmental motion that could lead to decreases in the ionic conductivity^{1,2}.

5.4 Linear Poly(N-allylethyleneimine-co-(N-(2-methoxyethyl)ethyleneimine))

(LPAG₁EI), Linear Poly(N-allylethyleneimine-co-(N-(2-(2-methoxyethoxy)ethyl)ethyleneimine)) (LPAG₂EI), Linear Poly(N-allylethyleneimine-co-N-(2-(2-(2-(methoxyethoxy)ethoxy)ethyl)ethyleneimine)) (LPAG₃EI) and their model compounds.(LPAG_xEI series: x = 1,2,3)

As seen from earlier sections, the linear and branched poly(ethyleneimine)-based SPE's gave low ionic conductivities. The main issue is the optimization of the SPE's where they are physically and mechanically stable, along with good ionic conductivities. The polymer electrolytes which give good conductivities like MEEP^{5,6} are not physically stable to incorporate in a battery, whereas PEI based polymer electrolytes as described earlier have good mechanical properties but do not have high ionic conductivities^{1,2}.

As described in Chapter 1, polymers having PEO like tethers have given good ionic conductivities. For example Poly(bis-methoxyethoxyethoxyphosphazene) (MEEP), a liquid polymer with a T_g of -84°C , has been investigated in depth by Allcock et al^{5,6}. Also, Snow et al has investigated polyamine electrolytes with PEO-like tethers, such as poly(N-(2-(2-methoxyethoxy)-ethyl)ethylenimine) (LPEI-G2). LPEI-G2 is a viscous liquid with a T_g of -76°C . LPEI-G2 with lithium triflate in a 10:1 (N:Li) ratio has shown an ionic conductivity of 5×10^{-6} S/cm at 25°C which increases to 7×10^{-5} S/cm at 60°C ^{7,8}. Though, the conductivities for LPEI-G2 and MEEP are high, the mechanical stability of these polymers restricts the use of these polymers as SPE's.

Since LPEI-G2 was mechanically unstable, Hu et al substituted 50% of the nitrogens on LPEI with allyl groups and 50% were substituted with the G2 tether as shown in Figure 5.9².

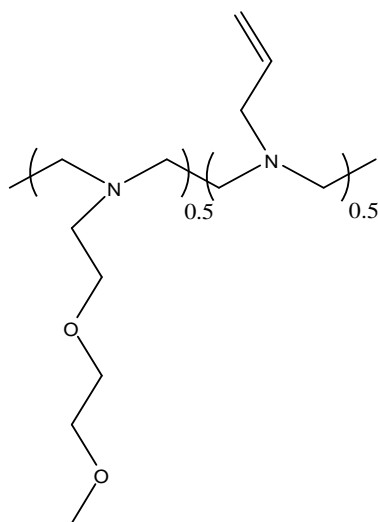


Figure 5.9 Repeat Unit for LPAG₂EI

Dr Hu also showed that the conductivity of LPAG₂EI with lithium triflate at 20:1 (N:Li) ratio and 30:1 (N:V-50) cross-linker ratio was 1.3×10^{-6} S/cm at room

temperature which increase to 7.1×10^{-4} S/cm at 100°C^2 . When compared to PEO based electrolytes, which shows ionic conductivity on the order of 10^{-5} S/cm, LPAG₂EI shows exceptional ionic conductivity².

Dr Hu's synthetic scheme is shown in Figure 5.10².

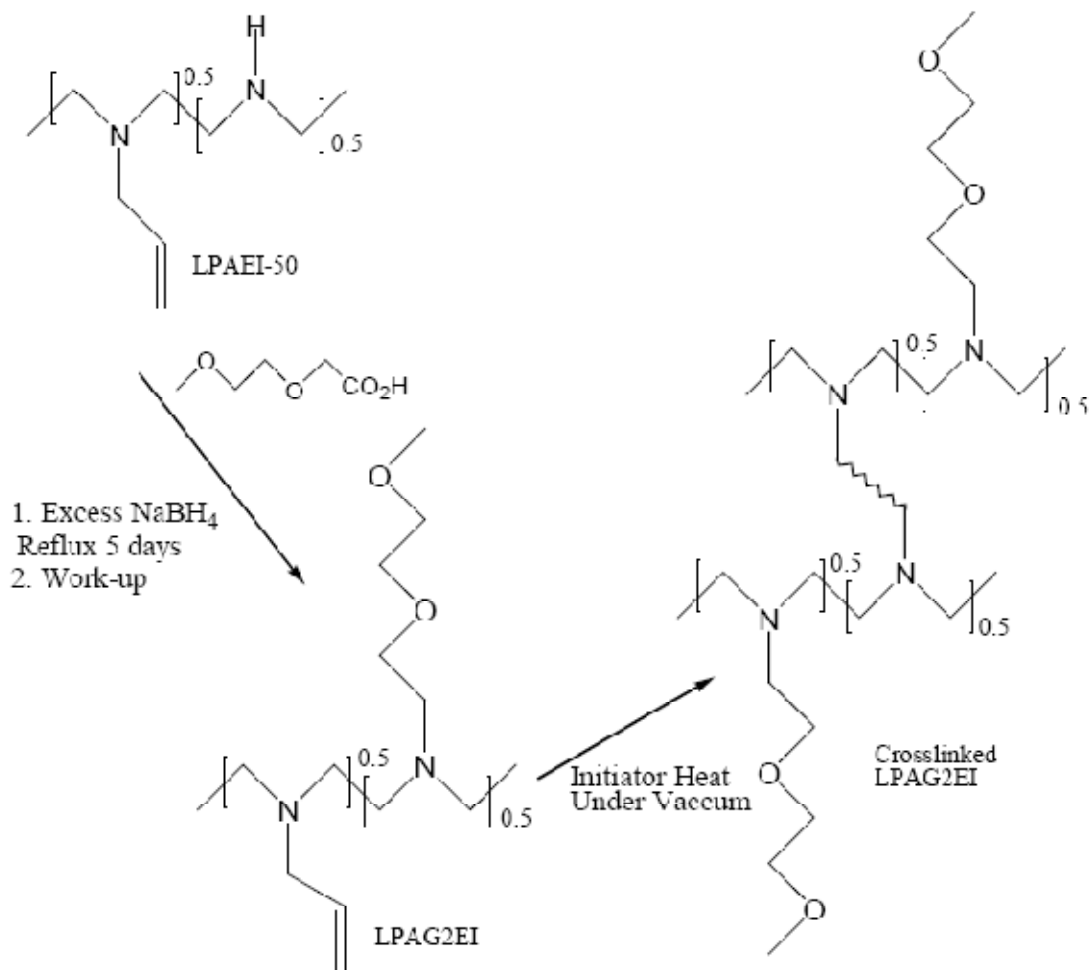


Figure 5.10 Scheme of synthesis of LPAG₂EI from LPAEI as reported by Hu (Scheme reproduced from Dr. Lieyu Hu thesis)

As seen from the Figure 5.7, the substitution of the ethylene oxide-like tether on the nitrogen of the backbone of PEI was done using a reductive alkylation method by reacting the PEI with acid analog of the ethylene oxide ether. The reaction took 5 days.

The goal of this section was to use a different strategy in substitution of the ethylene oxide-like tether on the nitrogen of the backbone of PEI. Instead of the reductive alkylation as reported by Dr Hu², a simple substitution reaction (S_N2 reaction) between the nucleophilic nitrogen in the backbone of the LPAEI and the electrophilic halide derivative of different lengths of ethylene glycol tethers (G1-Cl, G2-Cl, G3-Cl) was carried out (Figure 5.11).

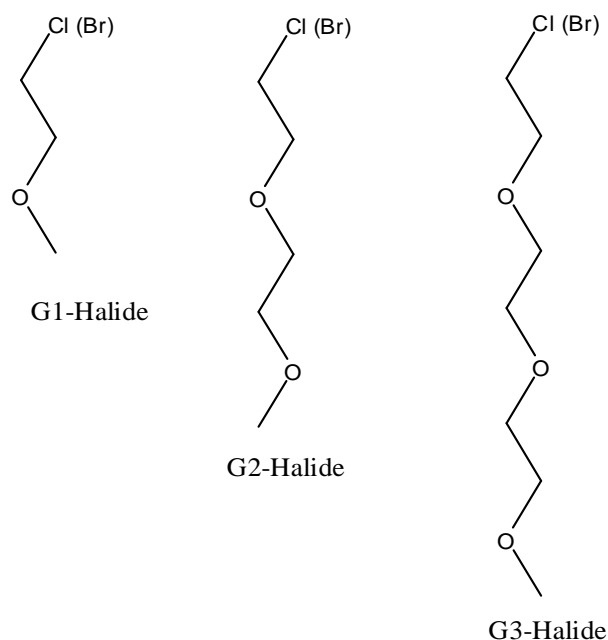


Figure 5.11 Structure of G1-Halide, G2-Halide, G3-Halide.

Since the G1-, G2-, and G3-Halide were synthesized by analogous means, the tethers will be referred to as $\text{CH}_3\text{-(O-CH}_2\text{-CH}_2\text{)}_n\text{-Cl (Br)}$, where $n = 1, 2$ or 3 depending on the tether. The scheme for synthesizing $\text{CH}_3\text{-(O-CH}_2\text{-CH}_2\text{)}_n\text{-Cl (Br)}$ is shown in

Figure 5.12. As seen from the scheme, the G_x series alcohols are easily available and can be converted to halide G_x analog in good yields. The $G1\text{-Cl}$ is available commercially and was not synthesized in the laboratory. The $G2\text{-Cl}$ and $G3\text{-Cl}$ is synthesized from $G2\text{-OH}$ and $G3\text{-OH}$ by reacting it with SOCl_2 ⁹. The $G1$, $G2$, $G3$ chlorides were then reacted with 50% substituted LPAEI in the presence of a base. The resulting polymer was extracted using benzene. All the polymers were characterized using $^1\text{H-NMR}$ spectroscopy.

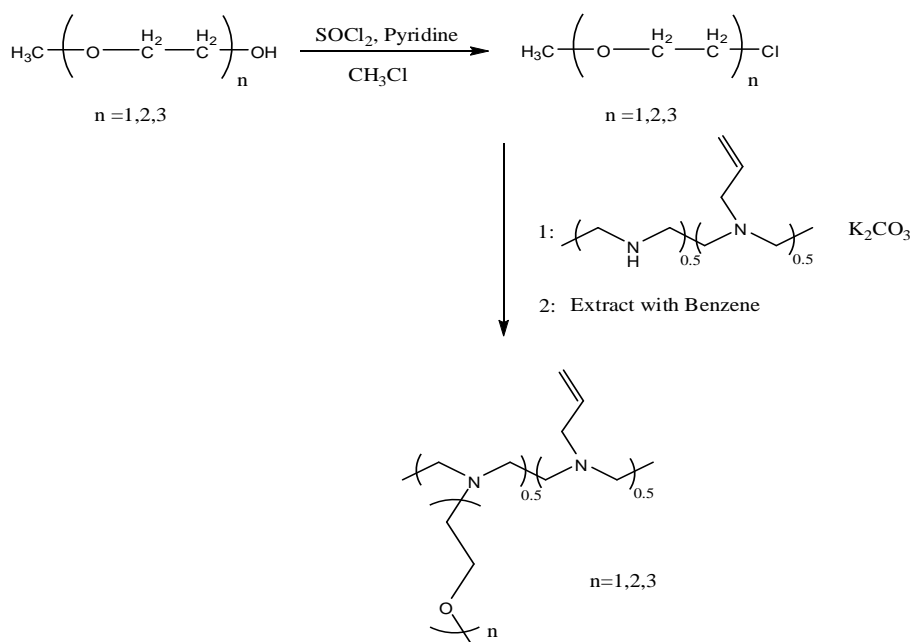


Figure 5.12 Synthetic scheme for synthesizing LPAG_xEI

A) LPAG_1EI

The NMR for LPAG_1EI is shown below in Figure 5.13. The respective signals for the different protons are assigned in Figure 5.13. The NMR shows a multiplet at 5.83 ppm (vinyl methine proton, 1H), a triplet at 5.21 ppm (vinyl methylene protons, 2H), a broad multiplet from 3.41 ppm to 3.58 ppm (side chain O-methylene protons,

2H), a singlet at 3.31 ppm (O-methyl protons, 3H), a doublet at 3.10 ppm (allyl group side chain N-methylene protons, 2H), a triplet at 2.65 ppm (G₁ side chain N-methylene protons, 2H) and 2 overlapping singlets from 2.48 to 2.62 (backbone methylene protons, 8H). The integrations show that the allyl:G₁ group substitution was approximately 1:1. While one set of peaks is likely due to residual solvent, the nature of the small but non-negligible absorptions at ca. 2.0 ppm is unclear. The whole purpose of studying this system was to measure the conductivity of films formed by cross-linking the film under the reaction conditions as described by Hu, i.e. 20:1 (N:Li) ratio of lithium triflate and 30:1 (N:Initiator) ratio of the V-50².

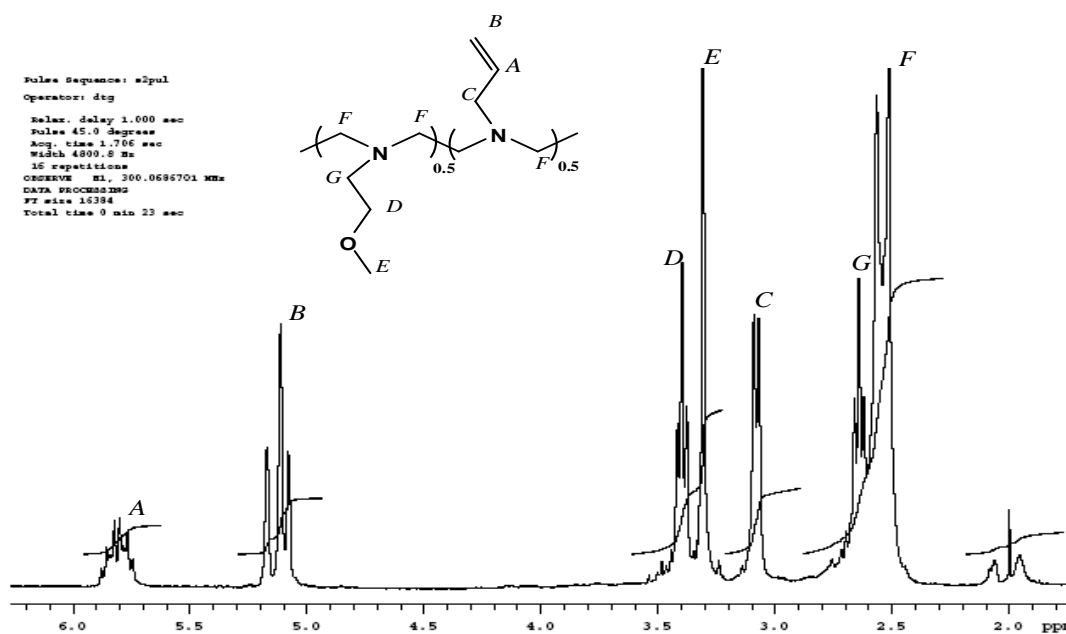


Figure 5.13 ¹H NMR spectra for LPAG₇EI

The films were cast and were cross-linked at 80°C under vacuum. The ionic conductivity for the films was measured and is summarized in Table 5.3.

Temperature (°C)	Specific Conductivity (σ) S/cm
25	8.71×10^{-8}
60	1.09×10^{-7}
80	1.41×10^{-7}
100	2.73×10^{-7}

Table 5.3 Conductivity data for LPAG₁EI with 20:1 (N:Li) ratio and 30:1 (N:Initiator) ratio.

The conductivity for LPAG₂EI is 8.71×10^{-8} S/cm at 25°C, which increases up to 2.73×10^{-7} S/cm at 100°C. It is seen from the liquid electrolyte studies earlier that the N:O ratio governs the conductivity of the electrolyte. This could be the reason for the low conductivity where the N:O ratio in the polymer is not optimum.

B) LPAG₂EI

To study the G_x series further, LPAG₂EI polymer was synthesized using the same scheme as shown in Figure 5.12. The NMR spectrum for LPAG₂EI is shown in Figure: 5.14. The respective signals for the different protons are assigned in Figure 5.14. The NMR shows a multiplet at 5.83 ppm (vinyl methine proton, 1H), a triplet at 5.15 ppm (vinyl methylene protons, 2H), a broad multiplet from 3.41 ppm to 3.62 ppm (side chain O-methylene protons, 6H), a singlet at 3.31 ppm (O-methyl protons, 3H), a doublet at 3.10 ppm (allyl group side chain N-methylene protons, 2H), a triplet at 2.65 ppm (G₂ side chain N-methylene protons, 2H) and 2 overlapping singlets from 2.48 to 2.72 (backbone methylene protons, 8H). The integrations show that the allyl:G₂ group

substitution was approximately 1:1. Again the origin of the small peaks seen from 2.0 to 2.3 ppm is unknown, although they are consistent with those seen for the LPAG₁EI, suggesting they are a feature of the polymer, perhaps associated with non-substituted segments. One important observation to be mentioned is that although the substitution of the G₂-side chain was done using a different synthetic strategy, the NMR spectrum was consistent with that reported by Hu².

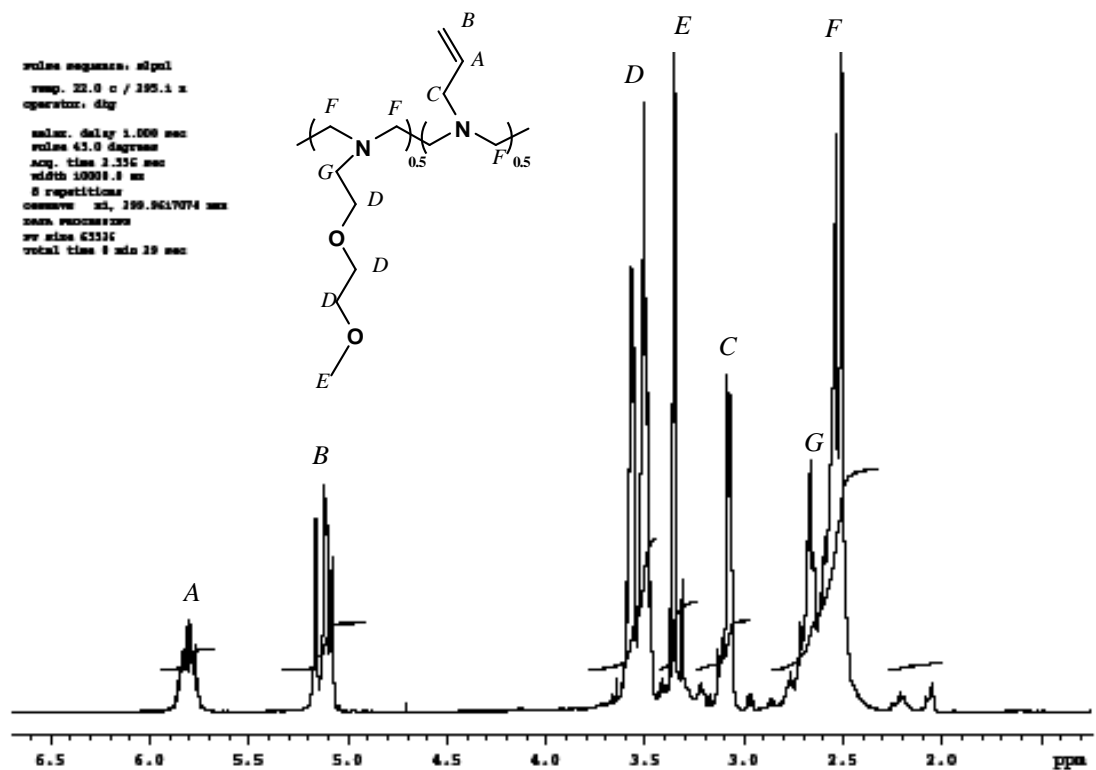


Figure 5.14 ¹H NMR spectrum for LPAG₂EI

The polymer was cast into films with a 20:1 (N:Li) ratio of lithium triflate and 30:1 (N:Initiator) ratio of V-50. The conductivity was measured at different temperatures and the data is summarized in Table 5.4.

Temperature (°C)	Specific Conductivity (σ) S/cm
25	1.96×10^{-8}
60	3.96×10^{-7}
80	1.24×10^{-6}
100	4.43×10^{-6}

Table 5.4 Conductivity data for LPAG₂EI with 20:1 (N:Li) ratio and 30:1 (N:Initiator) ratio.

When the ionic conductivity for the LPAG₂EI is compared to the values reported by Hu for LPAG₂EI (1.3×10^{-6} S/cm at room temperature which increase to 7.1×10^{-4} S/cm at 100°C)², the conductivity shown in the table is low by a factor of 2. This decrease could again be due a lower degree of substitution or some small amount of quaternization which does not show clearly in the spectrum. The substitution of the G₂-side chain is done using a different synthetic strategy, so different reaction conditions such as temperature and reagents may lead to small structural changes in the polymer, which in turn could impact the conductivity.

C) LPAG₃EI

Since the LPAG₂EI did not show as high conductivity as reported by Dr Hu², an attempt to put G₃-side chains on 50% substituted LPAEI was made. A similar synthetic strategy was used to substitute the G₃-sidechain on the LPAEI backbone. The NMR spectrum for LPAG₃EI is shown in Figure 5.15.

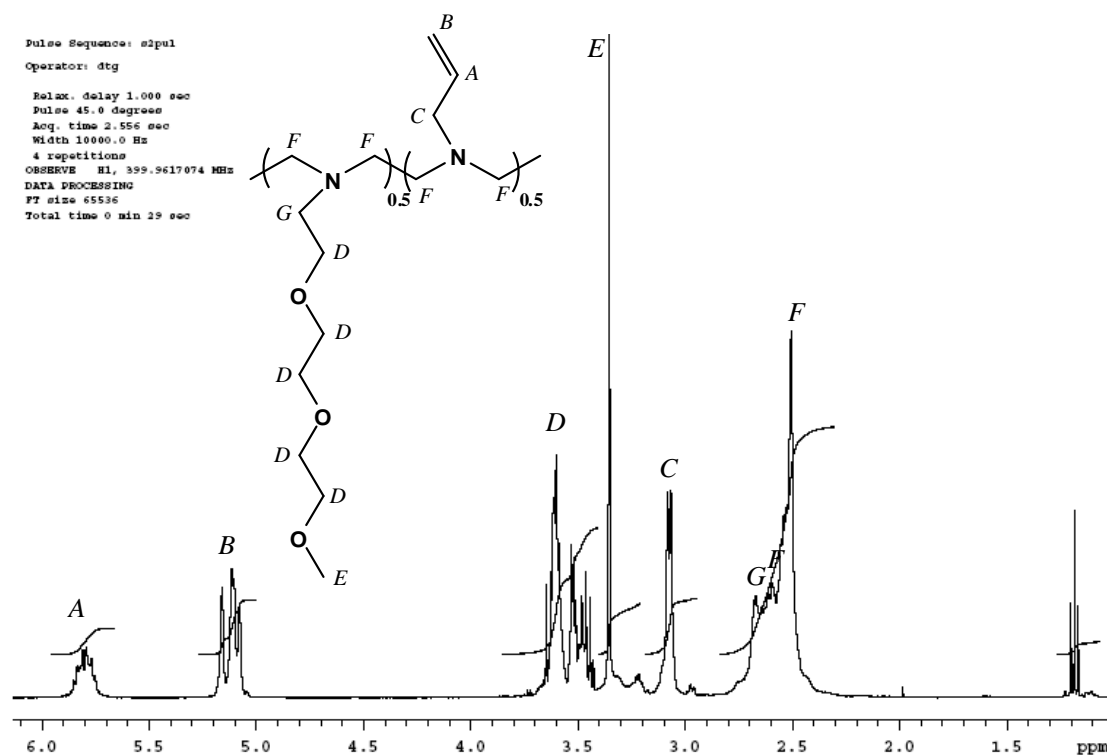


Figure 5.15 ^1H NMR spectrum for LPAG₃EI

The respective signals for the different protons are assigned in Figure 5.14. The NMR shows a multiplet at 5.83 ppm (vinyl methine proton, 1H), a triplet at 5.15 ppm (vinyl methylene protons, 2H), a broad multiplet from 3.41 ppm to 3.62 ppm (side chain O-methylene protons, 10H), a singlet at 3.31 ppm (O-methyl protons, 3H), a doublet at 3.10 ppm (allyl group side chain N-methylene protons, 2H), a triplet at 2.65 ppm (G₂ side chain N-methylene protons, 2H) and 2 overlapping singlets from 2.48 to 2.72 (backbone methylene protons, 8H). From the integration it can be seen that the substitution of the LPAEI with G₃-side chains was far from complete. The reaction was run for more than 24 hours and no increase in the G₃-side chains substitution was seen. The integration shows that less than 25% of the nitrogens are G₃-substituted. Nonetheless the polymer

was cross-linked with a 20:1 (N:Li) ratio of lithium triflate and 30:1 (N:Initiator) of V-50.

The ionic conductivity data for LPAG₃EI is summarized in Table: 5.5.

Temperature (°C)	Specific Conductivity (σ) S/cm
25	1.77×10^{-8}
40	2.50×10^{-8}
60	5.47×10^{-8}
80	5.73×10^{-8}
100	7.43×10^{-8}

Table 5.5 Conductivity data for LPAG₃EI with 20:1 (N:Li) ratio and 30:1 (N:Initiator) ratio.

The ionic conductivity shown by the LPAG₃EI is low and with temperature it does not show much rise in the conductivity. The ionic conductivity data suggest that even with increase in temperature there is not much of an increase in the ion transport. The low conductivity may be attributed to the non-substituted nitrogens, which could be involved in hydrogen bonding, either restricting segmental motion or interacting with triflate ions.

Among the LPAG_xEI series, the LPAG₂EI looked the most promising as a polymer electrolyte. Although LPAG₂EI showed somewhat lower conductivity than that reported by Dr Hu, it was higher than any of the LPAG₁EI or LPAG₃EI. The use of a nucleophilic substitution strategy, rather than the reductive amination method of Dr Hu, to put G_x-side chains on the LPAEI backbone clearly has some problems. To be used effectively, reaction would need to be controlled to give more complete G_x-substitution

while completely prohibiting quaternization; specifications that may be impossible to achieve using this synthetic methodology.

5.5 LPG_xEI model compounds

In an attempt to understand the G_x series polymer in detail, LPG_xEI model compounds were synthesized. Similar synthetic strategy as used in $LPAG_xEI$ polymers, was used to synthesize the LPG_xEI model compounds. The reaction scheme for these compounds is reported in Figure 5.16. Diethylamine was reacted with G_x halides using acetonitrile as solvent to give the DEA- G_x salt; which was neutralized with base, and extracted with benzene to give the LPG_xEI model compound.

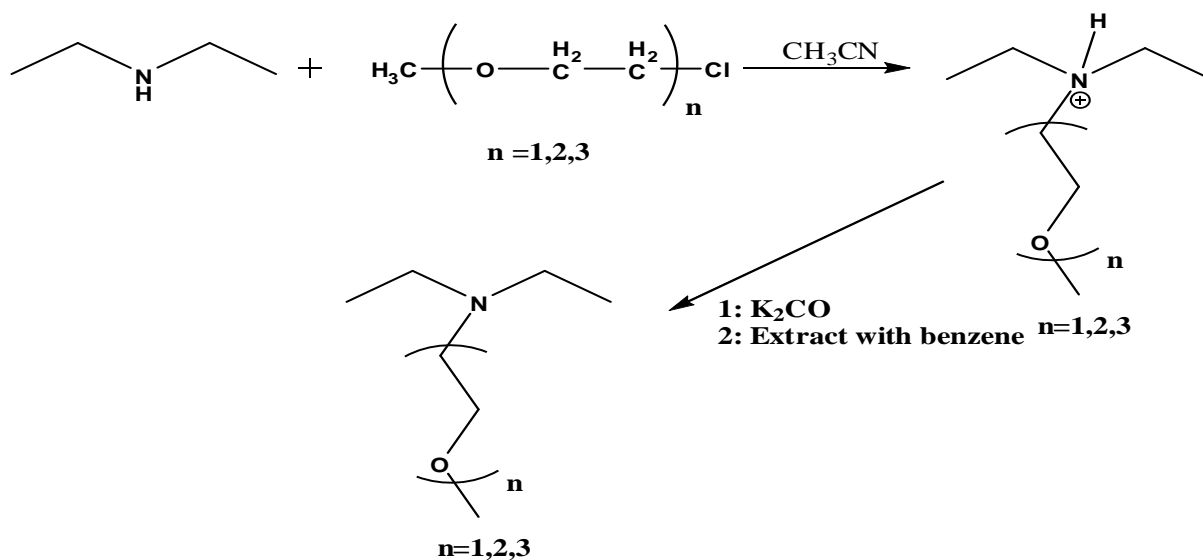


Figure 5.16 Reaction scheme to synthesize LPG_xEI model compound.

The LPG_xEI model compounds were analyzed using 1H NMR spectroscopy. Diethylamine was the limiting reagent in the synthesis of LPG_xEI model compounds. The

procedure for the synthesis of LPG_xEI model compounds is discussed in detail in the experimental section (Section 5.8).

A) LPG_1EI model compound

The LPG_1EI model compound was synthesized as shown in Figure 5.16. The product was analyzed stepwise using the ^1H NMR. The ^1H NMR spectrum is shown in Figure 5.17.

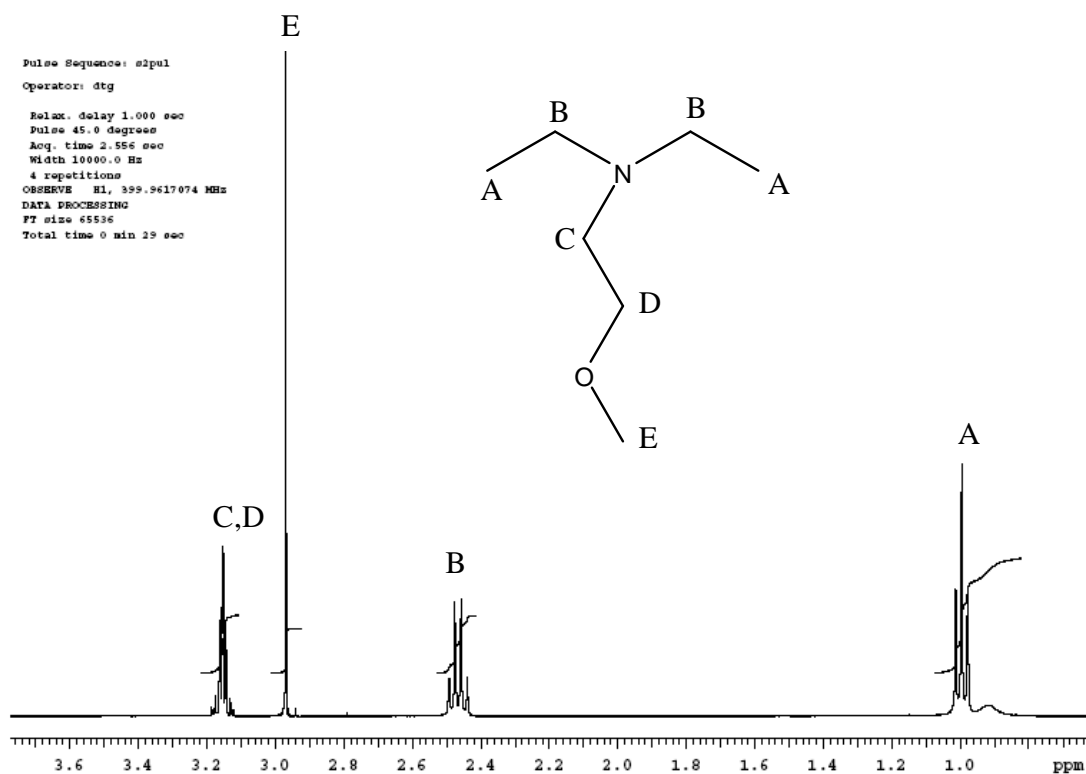


Figure 5.17 ^1H NMR spectrum for LPG_1EI model compound.

The ^1H NMR spectrum shows that there are four different signals for different hydrogens. Two signals overlap at ca. 3.5 ppm. The ^1H NMR assignments are labeled in Figure 5.18 (a) (triplet at 1.0 ppm (methyl group in the diethylamine part, 6H), a quartet at 2.46 ppm (methylene in the diethylamine part, 4H), a singlet 2.90 ppm (methyl group

on the G1 tether, 3H) and a multiplet from 3.12 ppm to 3.2 ppm (methylene groups in the G1 tether, 4H)).

B) *LPG₂EI* model compound

The *LPG₂EI* model compound was synthesized as shown in Figure 5.16. The product was characterized using ¹H NMR. The ¹H NMR in Figure 5.18.

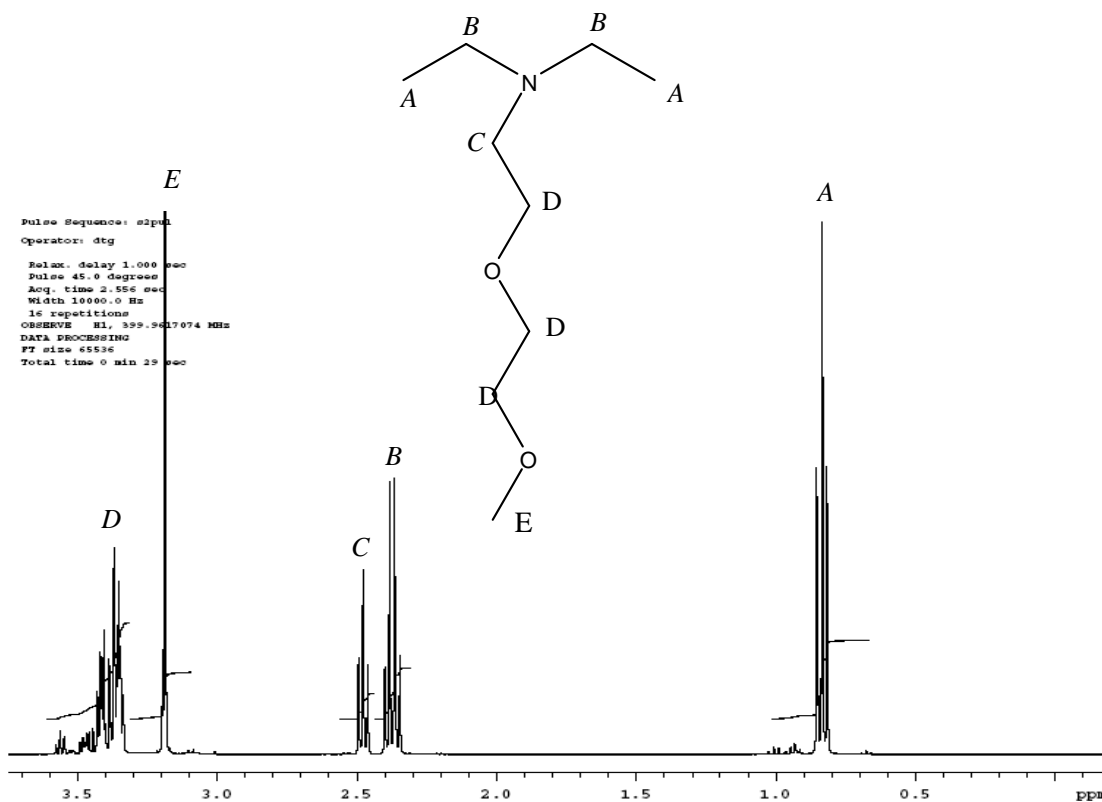


Figure 5.18 ¹H NMR spectrum for *LPG₂EI*

The ¹H NMR spectrum shows that there are five different signals for different hydrogens. The ¹H NMR spectra the assignments can be made for the *LPG₂EI* model compound structure. The assignments are shown in Figure: 5.18 (a): (triplet at 0.82 ppm (methyl group in the diethylamine part 6H), a quartet at 2.38 ppm (methylene in the

diethylamine part 4H), a triplet at 2.5 ppm (N-methylene group 2H), a singlet 3.2 ppm (methyl group on the G1 tether 3H) and a multiplet from 3.3 ppm to 3.5 ppm (methylene groups in the G1 tether 6H)).

C) *LPG₃EI* model compound

Similar to the *LPG₁EI* and *LPG₂EI* model compounds, the *LPG₃EI* model compound was also synthesized as mentioned in Figure: 5.16. The product obtained isolated and purified by distillation technique. The *LPG₃EI* was also analyzed by ¹H NMR in Figure: 5.19.

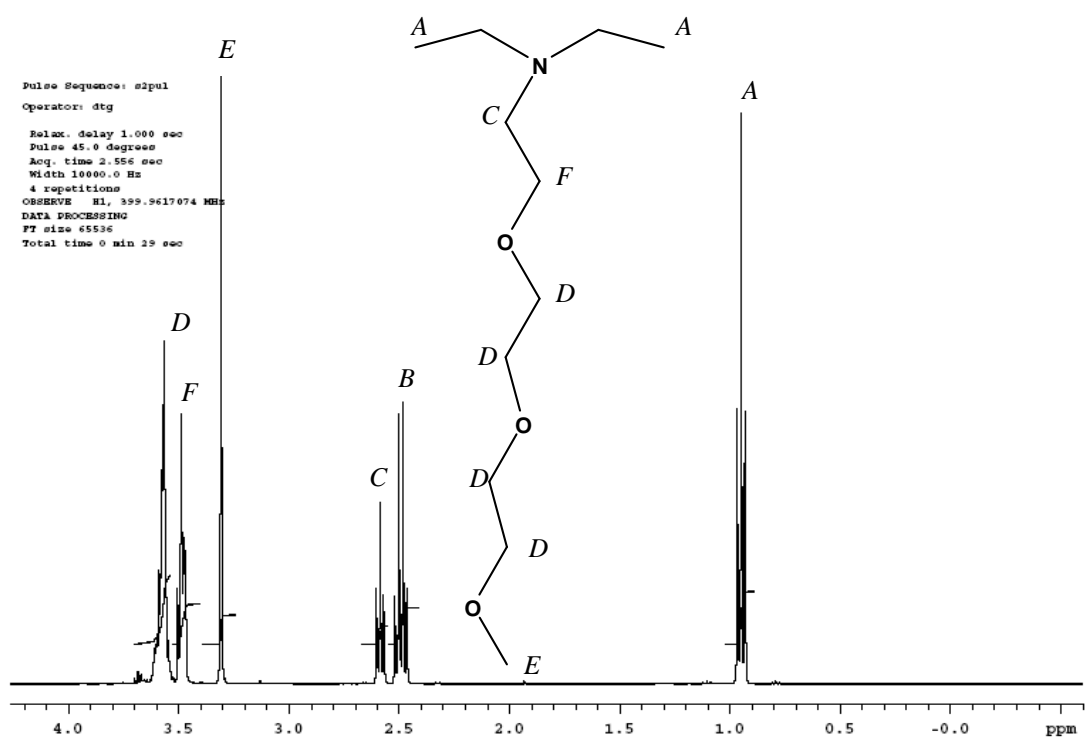


Figure 5.19 ¹H NMR spectrum for *LPG₃EI*

The ^1H NMR spectrum shows that there are six different signals for different hydrogens. The ^1H NMR spectra the assignments can be made for the LPG_3EI model compound structure. The assignments are shown in Figure: 5.19 (a): (triplet at 0.96 ppm (methyl group in the diethylamine part 6H), a quartet at 2.50 ppm (methylene in the diethylamine part 4H), a triplet at 2.60 ppm (N-methylene group 2H), a singlet 3.3 ppm (methyl group on the G1 tether 3H), a triplet at 3.50 ppm (N- CH_2 -methylene group 2H) and a multiplet from 3.3 ppm to 3.5 ppm (methylene groups in the G1 tether 8H)). The intention was to investigate the model compound further with lithium triflate salts in it and see the speciation of lithium triflate in the model compound. This work is still pending and can be insightful project to investigate the N vs O coordination issue (Chapter 2).

The LPG_xEI model compounds were successfully synthesized and were analyzed by ^1H NMR technique. As these compounds are model compounds for the LPAG_xEI polymer series, they will help providing some more insight in to the issue of the effects of nitrogen and oxygen containing solvents on the ionic transport mechanism of lithium triflate. The detailed ^7Li and ^{19}F study on these solvents as liquid lithium triflate electrolytes should be done. Also it will be helpful to measure the dielectric constant of these solvents neat and with lithium triflate in them.

5.6) BPAEI as a proton exchange membrane (PEM's)

A proton exchange membrane or polymer electrolyte membrane is a semi-permeable film or membrane that is designed to conduct protons and has low permeability to gases¹⁰. Glatzhofer *et al* has reported that linear poly(ethyleneimine)

hydrochloride/phosphoric acid could be crosslinked from 1,1,3,3-tetramethoxypropane¹¹. The material displays good conductivity and mechanical stability. Since LPEI displayed good conductivity and mechanical stability, it would be of great interest to apply BPEI as a proton exchange membrane.

Allyl substituted BPEI (BPAEI), as mentioned earlier, has allyl groups substituted on the nitrogens of the BPEI which can be cross-linked with initiators. In this section the scope of cross-linking of BPAEI with different initiators with 1:1 (N:H₃PO₄) will be discussed. An attempt was made to cross-link BPAEI from methanol with 1:1 (N:H₃PO₄) and 2,2-azobis(2-amidinopropane)dihydrochloride (V-50)^{1,2} and (2,2'-azobis [2-methyl-N-(2-hydroxyethyl) propionamide]) (VA-086)² as initiators with 30:1 (N:Initiator) ratio. The polymer was then subjected to heat at 80°C under vacuum. The films formed from methanol did cross-link but the cross-linking was too fast and the films foamed up. This foaming could be a result of the methanol boiling or the initiator releasing N₂ gas. A V-50 initiator with similar concentration was used to cross-link a sample under UV light. It did cross-link but once again the cross-linked film showed a lot of foam (air bubbles) trapped in it. This again could be due to the release of N₂ gas.

To avoid the foaming effect, the films were cast from water instead of methanol. The cross-linking conditions were the same (1:1 (N:H₃PO₄) and 30:1 (N:Initiator) ratio. Though the films cross-linked, the cross-linking was too fast. The cross-linked films were mechanically friable. Since the cross-linking was too fast, a different initiator was chosen, i.e AIBN (azobisisobutyronitrile). AIBN did not dissolve in methanol and caused the whole polymer to crash out of the system.

Potassium persulfate ($K_2S_2O_8$) (30:1 = N:initiator ratio) was also tried several times under heat and vacuum to use as a cross-linking agent to cross-link BPAEI in the presence of H_3PO_4 but each time the cross-linking was too fast and the film would turn out brittle. To investigate further, different concentrations of $K_2S_2O_8$ were employed with different concentrations of BPAEI in water. The polymer (30% concentration in water, 40% concentration in water, 50% concentration in water) with different concentration of $K_2S_2O_8$ (3 mol % and 4 mol %) was subjected to heat at about $45^\circ C$. The 50% polymer in water with 4 mol % initiator cross-linked, but the others did not. Cross-linking was attempted using $K_2S_2O_8$ at higher temperatures but the resulting films were too brittle.

Potassium persulfate ($K_2S_2O_8$) (30:1 = N:initiator ratio) was used to cross-link LPAEI under UV exposure and it did cross-link and gave a stable film. Lithium and ammonium persulfate ($Li_2S_2O_8$ and $(NH_4)_2S_2O_8$) (30:1 = N:Initiator ratio) were tried as initiators. Where $Li_2S_2O_8$ gave a stable film, $(NH_4)_2S_2O_8$ did not cross-link the film at all.

5.7) Conclusion:

BPAEI was synthesized using BPEI and allyl chloride. The synthesized BPAEI was cross-linked with lithium triflate present under UV light and in the absence of initiator. Conductivities were similar to those reported by Hu with a cross-linker. The cross-linking under UV light of BPAEI indicates that the chloride ions from the V-50 initiator do not interfere with the ion transport mechanism and do not decrease the ionic conductivity. The low ionic conductivity for both systems is likely due to

morphological characteristics resulting from a high degree of cross-linking, reducing the segmental motion of the polymer chains.

Fully allyl-substituted LPAEI was also cross-linked under similar conditions (20:1 = N:Li ratio and 60:1 = N:Initiator ratio). The conductivities of these films were low (on the order of 10^{-10} S/cm). UV light gave poor cross-linking results. Lithium persulfate as an initiator worked better and showed some promising results as far as the cross-linking was concerned. LPAEI (100% substituted) was tried with 30:1 (N:Initiator) ratio and different concentrations of lithium triflate. The highest conductivity achieved was on the order of 10^{-8} S/cm at 100°C, which is much lower than needed for battery applications.

Since the solely nitrogen-based SPE's gave lower conductivities, the substitution of oxygen-containing tethers on the nitrogens of the backbone (LPG₁EI and LPAG₂EI) did increase the ionic conductivity as reported by Hu. The synthetic strategy was altered to make the syntheses easier but the ionic conductivities of the resulting systems were lower than those reported by Hu.

The G1, G2 and G3 polymers made by the new synthetic strategy should be investigated with regard to their T_g 's and the data compared to those of Hu. IR studies on the polymer electrolyte systems on the G1, G2 and G3 systems should also be done. Model compounds should also be investigated with lithium triflate using IR and NMR techniques to understand the speciation of lithium triflate and give a better understanding of the speciation in the polymers.

5.8) Experimental

A) Synthesis of LPEI

LPEI was synthesized by acid hydrolysis of linear poly(2-ethyl-oxazoline) which was acquired from Aldrich (MW 200,000) as reported in Dr Albert Snow Thesis (Procedure reported on Page number 52 in Dr Albert Snow PhD Thesis)⁸.

B) Synthesis of BPAEI

BPAEI was synthesized from BPEI which was acquired from Aldrich and allyl bromide as described by Dr Lieyu Hu².

C) Casting BPAEI films

BPAEI (0.5 gm) was dissolved in a minimal amount of methanol. The required amount of lithium triflate and initiator (if required) was added with stirring until the lithium triflate completely dissolved. The films were cast onto glass plates and put in a vacuum at 80° C for 12 hours oven or under UV lamp till a film was formed, depending the method chosen for cross-linking. The cross-linked films were carefully removed from the glass plate using a razor blade. The films were used for ionic conductivity measurements.

D) Synthesis of LPAEI

LPAEI was synthesized from LPEI as reported by Dr Lieyu Hu in his PhD dissertation².

E) Casting LPAEI films

LPAEI (0.5 g) was dissolved in a minimal amount of methanol and the required amount of lithium triflate and initiator (if required) was added to the LPAEI/methanol solution and stirred until all solid dissolved. The viscous solution was then cast onto glass plates and put in a vacuum oven at 80° C for 12 hours or under UV light until it forms a film,

depending on the method chosen for cross-linking. The cross-linked films were removed with a razor blade from the glass plate. The films were used for ionic conductivity measurements.

F) Synthesis of LPAG_xEI series

LPAEI 50% substituted with allyl groups was synthesized as reported by Hu². The substituted LPAEI (3 g) was dissolved in acetonitrile in a 250 mL round bottom flask. K₂CO₃ (1 equivalent) was added to the round bottom flask along with G_x-Cl (x = 1,2,3) (0.5 equivalent). The reaction was refluxed for 12 hours at 50° C - 60° C. After completion of the reaction, the acetonitrile was removed under reduced pressure on the rotavap. It should be noted that the G_x-Cl should not be added in excess as it is difficult to remove. Any excess G_x-Cl was removed by adding methanesulfonic acid in ether to the round bottom flask. On the addition of methanesulfonic acid, the polymer is protonated and forms a salt which can be easily separated by filtration. The protonated polymer is mixed with methanol and treated with NaOH until neutral to pH paper. The resulting polymer is then extracted with benzene and filtered. Benzene is then removed under reduced pressure on the rotavap.

H) Casting LPAG_xEI films:

0.5 gms of LPAG_xEI polymer was dissolved in minimum amount of methanol. Lithium triflate is added to the LPAG_xEI/methanol solution so that the heteroatom: lithium ratio is 20:1. V-50 initiator (N:Initiator = 30:1) is added to LPAG_xEI/methanol solution. The polymer solution is then stirred till the lithium triflate and the initiator is completely dissolved. The viscous LPAG_xEI/methanol solution is cast on a glass plate and is put in a vacuum oven and is heated to 80° C for 12 hours. The cross-linked films were

removed with a razor blade from the glass plate. The films were used for ionic conductivity measurements.

G) Synthesis of LPG_xEI model compounds:

Diethylamine (5 g) in acetonitrile was added to a round bottom flask. G_x-Cl (1.5 equivalent) was added to the round bottom flask. The reaction was refluxed with a reflux condenser for 12 hours at 60° C. The reaction was cooled and the mixture was treated with methanesulfonic acid. The protonated product is isolated by filtration, thus removing the excess of G_x-Cl. The protonated model compound is dissolved in methanol and treated with NaOH till neutral to pH paper. The methanol is removed under reduced pressure on the rotavap. The LPG_xEI model compound is then extracted with benzene. The resulting polymer is then extracted with benzene and filtered. Benzene is then removed under reduced pressure on the rotavap. The model compound was distilled to give pure G_x model compound over NaOH pellets to give pure model compound.

H) Conductivity Measurements by Complex Impedance

Films of the cross-linked polymer/lithium triflate were sandwiched between 12.5 mm stainless steel electrodes in an airtight conductivity cell. The temperature was maintained by using a vacuum oven. A thermocouple was used to monitor the temperature. Complex impedance is measured over a frequency range of 10Hz to 10,000 Hz using an HP 4192 LF impedance analyzer and over a range of temperature from room temperature to 100°C. The data achieved from impedance analyzer was analyzed by fitting the data to an ellipse equation by using the LEVM 7.1 software.

References

- 1: Hu, L.; Frech, R.; Glatzhofer, D.T. *Polymer* **2006**, 47, 2099-2105.
- 2: Hu, L.; PhD Dissertation, University of Oklahoma, **2005**.
- 3: Tanaka, R.; Ueoka, I.; Takaki, K.; Kataoka, K.; Saito, S. *Macromolecules* **1983**, 16, 849.
- 4: Dillon, R.E.A.; Shriver, D.F. *Chem. Mater.* **2001**, 13, 1369-1373.
- 5: Blonsky, P.M.; Shriver, D.F.; Austin, P.; Allcock, H.R. *Solid State Ionics* **1986**, 18 & 19, 258-264.
- 6: York, S.; Kelam III, E.C.; Allcock, H.R.; Frech, R. *Electrochimica Acta* **2001**, 46, 1553-1557.
- 7: Snow, A.G.; Sanders, R.A.; Frech, R.; Glatzhofer, D.T. *Electrochimica Acta* **2003**, 48, 2065-2069.
- 8: Snow, A.G.; PhD Dissertation, University of Oklahoma, **2002**.
- 9: Gudipati, V.; Curran, D.P.; Wilcox, C.S.; *Journal of Organic Chemistry* **2006**, 71, 3599-3607.
- 10: "Alternative electrochemical systems for ozonation of water", NASA Tech Briefs, 2003-07. URL: http://findarticles.com/p/articles/mi_qa3957/is_200307/ai_n9239603/
- 11: Giffin, G.A.; Yopez, F.C.; Frech, R.; Glatzhofer, D.T.; Burba, C.M. *Polymer* **2009**, 50, 171-176.

Chapter 6

6.1 Conclusions and Future Work

A) Investigation of liquid and polymer electrolytes

Detailed investigation of the TMEDA-Monoglyme system using ^7Li and ^{19}F NMR spectroscopy, self-diffusion measurements, dielectric constant trend measurements, and ionic conductivity measurements gave evidence consistent with lithium triflate existing mostly in aggregates in TMEDA. With the addition of monoglyme, the aggregates start to de-aggregate somewhat. The most interesting part of the investigation was the change in the trend seen in the ^7Li NMR chemical shift data. The ^7Li NMR chemical shift suggested that after 80 mole% monoglyme is added there is a significant change in the speciation of the lithium ion. The data is strongly supported by the ^{19}F NMR data, conductivity data, self-diffusion coefficient data and the dielectric constant data. Applying the Stokes-Einstein equation¹, it was also shown quantitatively that after 80 mole% monoglyme was added, significant deaggregation occurred. It will be of great interest to also measure self-diffusion coefficients of lithium and fluorine in the triethylamine-diethylether system. Since the triethylamine-diethylamine system non-chelating, it would give greater insight into the lithium coordination and speciation. It would be of interest to measure the self-diffusion coefficients for the other systems, especially the G1 model compound mixed with monoglyme and TMEDA. The G2 and the G3 model compounds have also been synthesized and analyzed with ^1H NMR. The investigation and comparison of the self-diffusion coefficients of lithium and fluorine in the G1, G2 and G3 compounds with

lithium triflate will also give a better understanding of the role the nitrogen and oxygen plays in the speciation and ion transport of lithium and the triflate ion. Based on the observations made in the mixed solvent (N and O) electrolytes, it would be very informative to apply the observations to the polymer system. It would be interesting to synthesize and investigate polymer system with the ratio of N:O = 15:85 such that the polymer has 15% of the nitrogens and 85% of oxygens to be applied as SPE. This idea is conceived from the observation made from the mixed liquid electrolyte system, TMEDA-Monoglyme with lithium triflate, where the conductivity shows a significant rise.

Since Dr Hu has compared poly(propyleneimine) with lithium triflate to PEI^{2,3}, it would be investigate model compounds of PPI which would be the 3-carbon analog of TMEDA. 3-Carbon analogs of TMEDA and monoglyme were synthesized but only initial investigations were made. The ⁷Li NMR, ¹⁹F NMR, ionic conductivity and dielectric data for the 3-carbon analog of TMEDA and monoglyme can be compared to the ⁷Li, ¹⁹F, ionic conductivity and dielectric constant trend of TMEDA-Monoglyme system. It would be also interesting to synthesize and investigate polymer systems with PPI (polypropyleneimine) substituted with ethylene glycol-like tethers.

B) Investigation and application of coaxial assembly in measuring dielectric constants and properties affected by dielectric constant

As shown in Chapter 3 and 4, the use of a coaxial cell assembly for EPR can be used to measure dielectric constants of a solvent as well as solvent mixture. The dielectric constant was measured by using the calibration curve technique, where signal

intensities for jacket solvents with known dielectric constants are measured and a calibration curve was plotted. The dielectric constant of an unknown solvent is estimated from the calibration curve. The coaxial assembly was tried with different inner and outer tubes. The 3 mm-4 mm and the 4 mm-5 mm coaxial assembly gave the best dielectric constant measurements among all the assemblies tried. Though the 3 mm-4 mm and the 4 mm-5 mm assemblies gave good measurements of the dielectric constants, there are several errors involved with the measurements using the coaxial assemblies. Some errors arise from the alignment of the inner tube in the outer tube. Though an attempt is made to align the inner tube by holding it in the center of the outer tube with a laboratory made holder, there is always a possibility of alignment on one side of the inner wall of the outer tube that results in a “*wicking effect*” that gives an error in the measurement of the dielectric constant. One way to eliminate the wicking effect is to have the inner tube bottom sealed to the bottom of the outer tube which will hold the inner tube in place.

Another error involved with the circular coaxial assembly is the lensing effect that is caused by the circular geometry. A flat coaxial assembly could be used to minimize the error caused by the lensing effect.

More serious errors likely involve trace water content present in the solvents, which could be causing errors in the measurement. Investigation of some of the solvents used for calibration curve should be performed after distilling the solvents to remove water.

The solvents used in the measurement for calibration solvents were all non-aromatic. It would be very interesting to actually measure aromatic solvents. Because of the polarizability of the aromatic system, it may be necessary to investigate the aromatic solvents as a different class.

The coaxial assembly can be used to measure the dielectric constant of mixtures of solvents. The trend of the intensity seen for water-dioxane mixtures follows a different trend than seen with the regular solvents. Hydrogen bonding between the molecules of water and dioxane, as well as significant change in the volume fraction of the total sample upon mixing, gives a different curvature to the data. It would also be of great interest to investigate mixture of solvents that would cover a large dielectric constant range with no interaction between the molecules and investigate the trend. The trend was investigated for closer dielectric constant range (TMEDA ($\epsilon = 2.8$) and monoglyme ($\epsilon = 7.2$)). The trend shown for these two solvents was approximately linear.

The coaxial assembly was also used to determine the amount of water in water-dioxane mixtures. The amount of water was predicted from literature values that were measured by a completely different independent method. Values for mixtures treated as unknowns were measured using the EPR method for the amount of water and were in close agreement with actual values.

The coaxial assembly was also used for the EPR method to measure the dielectric constants of lithium electrolyte solutions. Only two different solvents, THF ($\epsilon = 7.8$) and ethyl acetate ($\epsilon = 6.2$), were investigated with a few concentrations of lithium

triflate. While trends were in reasonable agreement with literature values the magnitudes of the dielectric constants did not match. To carry out the investigations in detail, more concentrations should be investigated on both the ends of concentrations, low and high. It would be also interesting to investigate solvents with high dielectric constants with lithium triflate dissolved in them.

The EPR method was used to study phase transitions as well as the relative rates of a reaction. The reaction between triethylamine and allyl chloride in acetonitrile at room temperature was monitored with different concentrations of allyl chloride. It would also be interesting to monitor a different reaction with the EPR method.

The EPR method was also used in studying the behavior of surfactant solutions. Three different types of surfactants (anionic (SDS), cationic (CTAB) and non ionic (Pluronic F 127)) were used to demonstrate the correlation of the EPR intensity data with the CMC of the surfactants. The surfactant showed different types of transitions before the CMC point of the cationic and anionic surfactants. It was shown by the non-ionic surfactant measurements that the transitions seen with the cationic and anionic surfactant were not an EPR instrument artifact. Some of the non-CMC transitions could be due to adsorption phenomena occurring at the solid-liquid interface of the glass and the water containing the surfactant. A change in the dielectric constant is seen before and after the CMC point for the surfactants. It would be useful to investigate more concentrations before and after the CMC point.

Coaxial assemblies can be used to measure the dielectric constant of some other materials, like ionic liquids and liquid crystals. The EPR intensity of a few ionic liquids

were measured but not enough is known in the literature to compare with the data. It would also be interesting to measure the dielectric constant of liquid crystals using the EPR technique. Measurement of dielectric constant of liquid crystals is a problem by the traditional methods due to their anisotropic nature.

References:

- 1: Williamson, M.J.; Hubbard, H.V.St.A.; Ward, I.M. *Polymer* **1999**, 40, 7177-7185
- 2: Hu, L.; PhD Dissertation, University of Oklahoma, 2005.
- 3: Hu, L.; Frech, R.; Glatzhofer, D.T.; Mason, R.; York, S.S. *Solid State Ionics* **2008**, 179, 401-408.